Metal-Based Dithiocarbamato Glycoconjugates: a Suitable Strategy to Target Tumour Glycolysis?

Andrea Pettenuzzo, M.Chem.

School of Chemistry

Presented to

The National University of Ireland, Galway

For the degree of

Doctor of Philosophy

Supervisor: Dr. Luca Ronconi

Head of School: Dr. Patrick O'Leary

March 2019

Declaration

This thesis has not been submitted before, in whole or in part, to this or any other university for any degree, and is, except where otherwise stated, the original work of the author.

Signature _____ (Andrea Pettenuzzo)

This thesis is based on the collaborative research work of various groups. The contribution of the candidate represents the majority of the work (> 80%) although, where otherwise stated, the contribution of other groups is described.

Signature _____ (Andrea Pettenuzzo)

Abstract

Rapidly dividing tumour cells require higher amounts of nutrients and energy for their fast proliferation, and glucose is no exception (the so-called "Warburg effect"). Consequently, such increased demand of glucose by cancer cells makes it very attractive to selectively target tumour sites. In particular, tailored glucose-like substrates can be conjugated to chemotherapeutics (including metal-containing anticancer agents) to attain the site-specific delivery of drugs into the affected tissues. Accordingly, we have been focusing on the design of metal-dithiocarbamato glycoconjugates which can combine the antitumor properties and the favourable toxicological profile of the metal-dithiocarbamato scaffold, along with an improved selectivity and cellular uptake provided by the glucose-containing ligands coordinated to the metal center, through the exploitation of the glucose-mediated cellular internalization facilitated by glucose transporters (GLUTs).

In this thesis, the generation of novel gold(I/III)-, manganese(I)-, and platinum(II)-dithiocarbamato glycoconjugates *via* an innovative synthetic approach is reported. Starting from the rationale behind our research work, the main results achieved to date concerning the development of the aforementioned metal-based bioconjugates, solution studies and preliminary *in vitro* biological studies are here illustrated and discussed. In particular, gold(I)-carbene and gold(III)-organometallic dithiocarbamato derivatives showed promising cytotoxicity towards cancer cells making them interesting candidates for further studies. Interestingly, gold(I)-carbene derivatives do not seem to be internalized inside the cells, suggesting an extracellular mode of action. Finally, a concluding section will briefly describe some side-projects generated during this PhD research projects, in collaboration with other academic research group, regarding the design and obtainment of novel ruthenium(II)-arene dithiocarbamato glycoconjugates, heterometallic platinum(IV)-gold(III) adducts, and innovative methods for intracellular delivery of cytotoxic agents *via* encapsulation with nucleic acid nanoparticles (NANs) or mesoporous silica nanoparticles (MSNs).

Table of Contents

Contributions

Publications

A. Pettenuzzo, D. Montagner, P. McArdle, L. Ronconi, "An innovative and efficient route to the synthesis of metal-based glycoconjugates: proof-of-concept and potential applications", *Dalton Trans.* **2018**, *47*, 10721–10736.

A. Pettenuzzo, R. Pigot, L. Ronconi, "Vitamin B_{12}-Metal Conjugates for Targeted Chemotherapy and Diagnosis: Current Status and Future Prospects", *Eur. J. Inorg. Chem*. **2016**, 1625–1638.

A. Pettenuzzo, R. Pigot, L. Ronconi, "Metal-Based Glycoconjugates and Their Potential in Targeted Anticancer Chemotherapy", *Metallodrugs*, **2015**, *1*, 36–61.

Conference Proceedings

A. Pettenuzzo, J. Wölker, A. Terenzi, I. Ott, L.Ronconi, Gold-based glycoconjugates for the targeted anticancer chemotherapy, 2nd Symposium of the Irish Biological Inorganic Chemistry Society IBICS-2, November 2nd, 2018, Galway, Ireland (oral presentation).

A. Pettenuzzo, L. Ronconi, Targeting the "Warburg effect" with gold-based glycoconjugate anticancer agents, 5th RSC Early Career Symposium, August 30th–31th, 2018, Liverpool, UK (poster).

A. Pettenuzzo, J. Wölker, A. Terenzi, I. Ott, L.Ronconi, A "sweet approach" to the targeted anticancer chemotherapy: gold-based glycoconjugates, 1st Symposium of the Irish Biological Inorganic Chemistry Society IBICS-1, November 3rd, 2017, Maynooth, Ireland (oral presentation).

A. Pettenuzzo, J. Wölker, A. Terenzi, I. Ott, L. Ronconi, A "sweet approach" to the targeted anticancer chemotherapy: gold-based glycoconjugates, 14th International Symposium on Applied Bioinorganic Chemistry ISABC13, June 7th–10th, 2017, Toulouse, France (poster).

A. Pettenuzzo, E. Fotopoulou, L. Ronconi, Gold: not just jewelry…, NUI Galway Career Day, January 20th, 2017, Galway, Ireland (poster).

A. Pettenuzzo, A "sweet" approach to the targeted anticancer chemotherapy: gold-based glycoconjugates, Eli Lilly Postgraduate Symposium Prize, January 20th, 2017, Galway, Ireland (oral presentation).

A. Pettenuzzo, L. Ronconi, Recent developments of gold(III)-dithiocarbamato glycoconjugates for the targeted metal-based anticancer chemotherapy, 68th Irish

Universities Chemistry Research Colloquium, June 23th–24th, 2016, Cork, Ireland (flash presentation + poster).

A. Pettenuzzo, L. Ronconi, Recent developments of gold(III)-dithiocarbamato glycoconjugates for the targeted metal-based anticancer chemotherapy, 3rd International Symposium on Functional Metal Complexes that Bind to Biomolecules – 4th Whole Action Meeting of the COST Action CM1105, April 28th–29th, 2016, Palma de Mallorca, Spain (poster presentation).

A. Pettenuzzo, R. Pigot, M. Sonnay, R. Alberto, F. Zelder, L. Ronconi, Fancy a lift? Vitamin B12 and glucose as carriers for the site-specific delivery of gold-based chemotherapeutics into tumor cells, COST Action CM1105 Meeting WG3, September 1st–2nd, 2015, Warsaw, Poland (oral presentation).

A. Pettenuzzo, R. Pigot, L. Ronconi, A Trojan Horse approach to the targeted metal-based anticancer chemotherapy, 13th International Symposium on Applied Bioinorganic Chemistry ISABC13, June 12th–15th, 2015, Galway, Ireland (poster presentation).

Awards

Eli Lilly Postgraduate Symposium Prize, NUI Galway, 20th January 2017

Modules Attended (for Structured PhD Programme)

Teaching and Learning (GS506)

Technical Writing (PH6022_UL)

Core Skills for Chemistry Research (CH506)

Seminar Programme (GS501)

Masterclass in Process Development and Scale-Up in the Pharmaceutical Industry (CH510)

Masterclass in Carbohydrate Chemistry (CH503)

Symbols and abbreviations

δ	Bending (IR)
δ	Chemical shift (NMR)
ε	Molar extinction coefficient
μM	Micromolar, μmol L^{-1}
ν	Stretching
A2780	Human ovarian carcinoma (wild type)
A2780cis	Human ovarian carcinoma (cisplatin resistant variant)
BIm	Benzimidazole
Bnpy	2-benzylpyridine
cm^{-1}	$Centimeter^{-1}$ (wavenumber)
CORM	CO-releasing molecule
COSY	Correlation spectroscopy
CS_2	Carbon disulfide
d	Doublet
dd	Doublet of doublets
ddd	Doublet of doublets of doublets
DEPT	Distortionless enhancement by polarization transfer
DFT	Density functional theory
DIPEA	*N*,*N*-diisopropylethylamine
DLS	Dynamic light scattering
DMDT	*N*,*N*-dimethyl dithiocarbamate
DMF	*N*,*N*-dimethylformamide
DMSO	Dimethyl sulfoxide
DUB	Deubiquitinase
dtc	Dithiocarbamate
ESDT	Ethyl sarcosine dithiocarbamate
ESI	Electrospray ionization
Et	Ethyl
FT-IR	Fourier transform infrared
GLUT	Glucose transporter
GSH	Glutathione
HeLa	Human cervix epitheloid carcinoma
HMBC	Heteronuclear multiple bond correlation
HSQC	Heteronuclear single quantum correlation
HT-29	Human colorectal adenocarcinoma
IC_{50}	Inhibitory concentration (at 50%)
ICP-MS	Inductively coupled plasma mass spectrometry
Inp	Isonipecotic
Ip	In-plane
J	Coupling constant (NMR)
Log*D*	Partition (or distribution) coefficient *n*-octanol/water
m	Medium (IR)
m	Multiplet (NMR)
M.p.	Melting point
Mb	Myoglobin
MbCO	Carboxymyoglobin
MCF7	Human breast adenocarcinoma
MDA-MB-231	Human breast adenocarcinoma
MHz	Megahertz

MS	Mass spectrometry
MSN	Mesoporous silica nanoparticle
NAN	Nucleic acid nanoparticle
NHC	*N*-heterocyclic carbene
nm	Nanometers
NMR	Nuclear magnetic resonance (spectroscopy)
oop	Out-of-plane
OSu	*O*-succinimide
PBS	Phosphate buffer saline
PDT	Pyrrolidine dithiocarbamate
PET	Positron emission tomography
ppm	Parts per million
q	Quartet
RC124	Human kidney epithelial cells
R_f	Retention factor
s	Singlet (NMR)
s	Strong (IR)
Sar	Sarcosine (*N*-methyl glycine)
SCM	Surface crosslinked micelles
SEM	Scanning electron microscope
SGLT	Sodium-glucose co-transporter
sh	Shoulder
SNAP	*S*-nitroso-*N*-acetylpenicillamine
Succ	Succinimidyl (or Su)
t	Triplet
TEA	Triethylamine
TEM	Transmission electron microscopy
TLC	Thin layer chromatography
Trx	Thioredoxin
TrxR	Thioredoxin reductase
TSTU	*N,N,N',N'*-tetramethyl-*O*-(*N*-succinimidyl)uronium tetrafluoroborate
tt	Triplet of triplets
U2OS	Human osteosarcoma
UV-Vis	Ultraviolet-visible (spectroscopy)
vs	Very strong
w	Weak
XRD	X-ray diffraction
Z-	Carbobenzyloxy-

Chapter 1

Introduction

Chapter 1. Introduction

1.1 The global burden of cancer

The generic term cancer (or tumour or neoplasm) is used to define a group of diseases which can affect any part of the body, arising from the transformation of normal cells into tumour cells in a multistage process. A distinctive aspect of cancer is the rapid abnormal generation and proliferation of cells, which can culminate with the invasion of contiguous parts of the body and spread to other organs. This phenomenon, also known as metastasis, represents the major cause of death from cancer.[1]

Cancer is the second leading cause of mortality globally after heart-related diseases. The WHO (World Health Organization) reports that 8.8 million people died in 2015 from cancer, the most common being lung, liver, colorectal, stomach, prostate and breast cancers.[2,3] Around 14.1 million new cases worldwide have been estimated in 2012, but the number is expected to dramatically rise by about 70% in the next two decades, with over 20 million new cancer cases diagnosed annually by 2025.[4,5] The global economic burden of cancer in 2010 was estimated at approximately US$ 1.16 trillion.

Approximately one-third of deaths from cancer are due to the four leading behavioural and dietary risks: tobacco consumption, alcohol abuse, unhealthy diet and lack of physical activity. Other risks are associated with radiation exposure, smog or inhalation of carcinogenic chemicals, infection from certain viruses (e.g. human papillomavirus, hepatitis B and hepatitis C, HIV type 1), bacteria or parasites (e.g. *Helicobacter pilori*) and, in rare cases, with genetic factors.[6,7]

It has been also observed that cancer incidence is dramatically correlated with age, growing exponentially from 40 years age onwards. This is most likely due to a combination of build-up of risks for specific cancers and a tendency for cellular repair mechanisms to be less effective with ageing (**Figure 1.1**).[8]

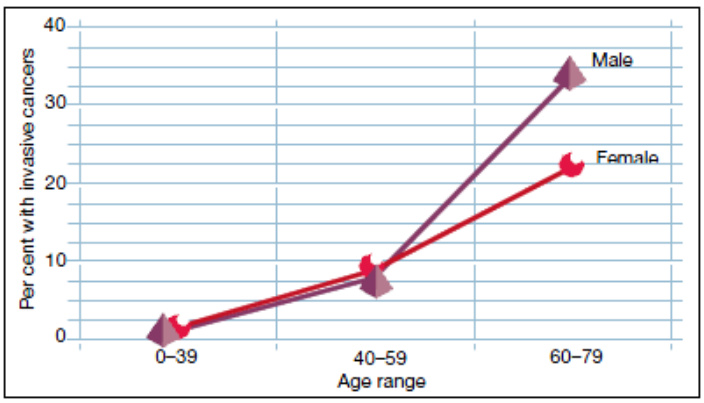

Figure 1.1. Tumour incidence with ageing. The curve shows a dramatic increase of the incidence in the range 40-80 years age (adapted from [8]).

Antitumour therapies, together with early diagnosis, can significantly prolong patient life expectations and may encompass one or more of the following modalities: surgery, radiotherapy and chemotherapy. Other types of therapies developed recently include hormone therapy, immunotherapy, photodynamic therapy and targeted therapy.[9]

Surgery consists in the surgical removal of the tumour and the surrounding tissues, if the tumour is still in an early stage and has not generated metastasis.[10,11] Although being the first and most common way exploited to treat cancer, surgery presents some limitations, such as: inability to fully remove microscopic tumours, failure to prevent metastasis, inefficiency towards non-solid tumours (e.g. leukemia), inability to remove damage to nearby normal tissues, ablation of an organ which can affect patient's quality of life.[11] Usually surgical removal is adjuvated by radiotherapy or chemotherapy.

Radiotherapy relies on the administration of high-energy radiation (X-rays, γ-rays) or charged particles (α, β^+, β^-) to the patient in order to destroy the tumour mass by damaging the tumour cell DNA, thus inhibiting cancer cell replication and proliferation.[12,13] Radiation can be delivered by either a machine outside the body (external-beam radiation therapy) or *via* a radioactive compound which is administered into the tumour site (internal radiation therapy or brachytherapy).[14] Radiotherapy is more effective than surgery in removing localized diseases, even microscopic, and to safely preserve organs. However some limitations and side-effects would occur such as inability to kill cancer cells that are not visualized and/or have migrated in nearby lymph nodes or in metastasis, infertility, insurgence of radiation-induced secondary tumours, weariness and fatigue.[15]

Chemotherapy consists in the administration of chemical substances in order to inhibit the tumour growth and ease cancer-related symptoms.[16] It can be very effective in killing systematically microscopic diseased cells, also in conjunction with radiotherapy, throughout the entire body, preserving at the same time the organs and improving patient's quality of life. Its effectiveness and high versatility, that can also be tailored depending on the patient and the type of tumour to be treated, have made chemotherapy the most common way for cancer treatment nowadays in high-income countries. However, systemic toxicity which may affect normal tissues, lack of tumour selectivity and the potential development of intrinsic or acquired resistance to the treatment regimen are some of the drawbacks which may arise from this kind of therapy.[17,18]

1.2 Cisplatin and platinum-based chemotherapeutics

Metals have been widely used for their putative medicinal properties throughout the history of humanity. Ancient Chinese documents traced back to 2500 B.C. the first uses of gold preparations.[19] Copper was employed by ancient Egyptians to sterilize water and wounds; antimony was used as antiparasitic agents while mercury salts were used as diuretics.[20–22]

Nevertheless, it is only since the 20th century that metal derivatives gained considerable attention in clinical practices. Salvarsan (**Figure 1.2**), also known as arsphenamine, is a mixture consisting of trimeric and pentameric arsenic-based species that has been long used to treat syphilis and trypanosomiasis.[23,24] Gold(I)-based compounds, such as potassium dicyanoaurate ($K[Au(CN)_2]$), were used to treat tubercolosis, whereas aurothiomalate, aurothioglucose and auranofin were used to treat tuberculosis or rheumatoid arthritis (see Chapter 1.4.1).[19]

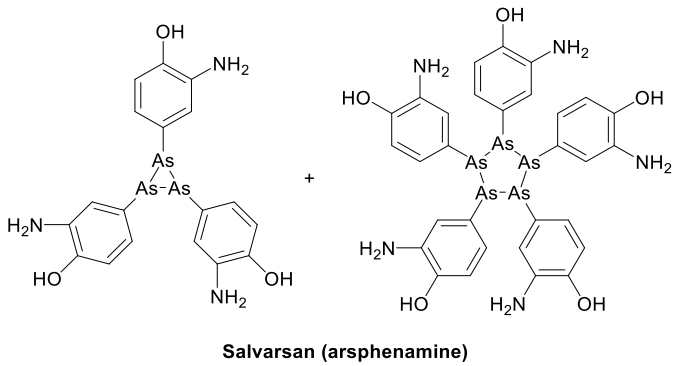

Figure 1.2. Chemical drawing of the arsenic-based species contained in Salvarsan.

The exploitation of inorganic chemistry for biomedical applications represents an innovative and ever-increasing research area. It offers a great potential to design novel therapeutics and diagnostic agents for the treatment and understanding of a number of pathologies. Compared with the common drugs based on organic compounds, coordination compounds may offer several advantages that have been somewhat underestimated by either academic or industrial drug research so far. Among all, a variety of accessible coordination numbers, geometries and redox states, and the possibility to modulate the thermodynamics and the kinetics of ligand substitution can be accounted for.[25]

The development of metal derivatives in chemotherapy received a great impulse towards the end of 1960s following the serendipitous discovery by Sir Barnett Rosenberg of the anticancer properties of cisplatin (*cis*-diamminedichloroplatinum(II), *cis*-$[PtCl_2(NH_3)_2]$

or *cis*-DDP, **Figure 1.3a**), a square-planar platinum(II) complex already known since the mid-19th century with the name of "Peyrone salt".[26–28]

In the attempt to study the influence of electric fields applied through platinum electrodes on the cell replication of *E. Coli*, Rosenberg observed that they assumed the shape of long filaments rather than the common short rods. After further investigations he came up with the conclusion that the alleged inert platinum electrode, in the presence of chlorides from the electrolytic solution, generated two bioactive complexes, namely cisplatin and *cis*-diamminetetrachloroplatinum(IV).[29]

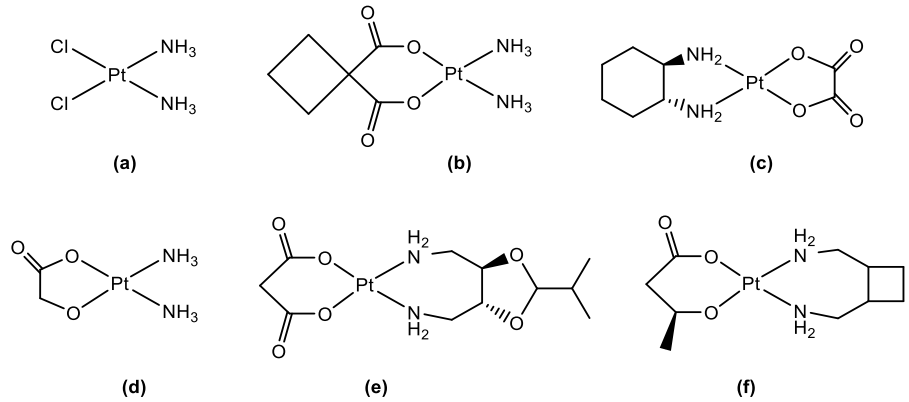

Figure 1.3. Chemical drawing of the platinum-based anticancer complexes in clinical use: cisplatin (**a**), carboplatin (**b**), oxaliplatin (**c**), nedaplatin (**d**), heptaplatin (**e**) and lobaplatin (**f**).

After Rosenberg's groundbreaking discovery, cisplatin quickly entered clinical trials and it was granted approval by the Food and Drug Administration (FDA) in 1978.[29,30] Cisplatin is mainly administered for the treatment of advanced testicular, ovarian and bladder cancers, as well as in combination with other antineoplastic agents for the treatment of cervical, head and neck, oesophageal, small-cell lung cancers and paediatric malignancies among others.[30,31]

The acknowledged biological target of cisplatin and its analogues is cellular DNA. Cisplatin undergoes hydrolysis after crossing the cell membrane and entering the cytoplasm, favoured by the lower concentration of chlorides in the cytosol (3-20 mM), compared with the extracellular environment (~100 mM). Aquation favours the formation of Pt(II) mono- and di-aquo species *cis*-$[PtCl(NH_3)_2(H_2O)]^+$ and *cis*-$[Pt(NH_3)_2(H_2O)_2]^{2+}$ (**Figure 1.4**). [32]

Hydrolyzed cisplatin species form adducts with N-containing nucleobases in the double strand of the DNA, in particular in the N-7 sites of contiguous guanines.[33] Double strand platination generates different kinds of lesions to the DNA such as mono- or bis-adducts (intrastrand, interstrand or DNA-protein crosslink).

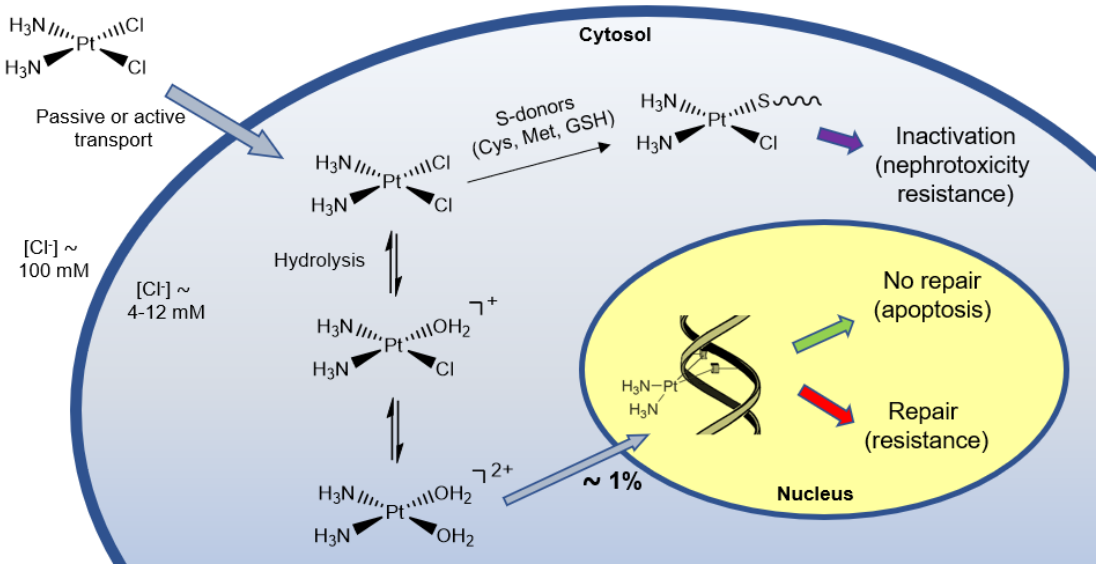

Figure 1.4. Mechanism of cisplatin cell internalization, hydrolysis, inactivation by interaction with S-donor ligands and DNA platination (adapted from R.J. Browning, P.J.T. Reardon, M. Parhizkar, R.B. Pedley, M. Edirisinghe, J.C. Knowles, E. Stride, *ACS Nano*, **2017**, *11*, 8560–8578).

Intrastrand crosslinks are the most common type of DNA platination induced by cisplatin (around 96%) and they generate a distortion of the DNA double helix. Such distortion dramatically impairs cell functions by blocking DNA-polymerase activity, an enzyme involved in cell replication, and, consequently, DNA-transcription and the mechanisms of DNA repairing.[34] The inhibition of such functions would lead to programmed cell death, also known as apoptosis.

However, the unquestionable clinical success of cisplatin is accompanied by numerous side-effects displayed during the treatment, especially the relatively high toxicity of cisplatin, causing nephrotoxicity, neurotoxicity, ototoxicity, nausea, alopecia, vomiting.[35–37] An additional major issue is represented by the intrinsic resistance shown by some specific neoplasias, or the resistance acquired during the cycles of chemotherapy.[38,39]

In order to mitigate the undesired cisplatin-induced side-effects, new platinum-based compounds with anticancer properties were designed by varying the amino or anionic ligands coordinated to the metal centre. Among all, carboplatin and, more recently, oxaliplatin (**Figure 1.3b**,**c**), reached the spotlight for their promising pharmacological profile, sharing with cisplatin the status of metal-based drugs currently in clinical use.[30] Carboplatin (**Figure 1.3b**) is used primarily to treat ovarian cancer but has also found use in treating retinoblastomas, neuroblastomas, nephroblastomas, and brain tumors, as well as cancers of the head and neck, endometrium, cervix, testes, breast, lung, and bladder. Oxaliplatin (**Figure 1.3c**), although originally proposed in the late 1970s as a potential

anticancer agent, is the most recent platinum-based drug gaining FDA approval in 2002. Nowadays it is a component of the front-line combination chemotherapy treatment for colon cancers that do not respond to cisplatin.[30] In fact, it proved very effective in combination with 5-fluorouracil and leucovorin for the treatment of metastatic colon cancers.[31]

In addition to the clinically-established cisplatin, carboplatin and oxaliplatin, nedaplatin, lobaplatin and heptaplatin (**Figure 1.3d**,**e**,**f**) received clinical approval in Japan, China and South Korea, respectively. Nedaplatin is approved primarily for the treatment of head, neck and esophagus cancers, but is also used in patients suffering from small-cell and non-small-cell lung cancer. Lobaplatin is used mainly to treat chronic myelogenous leukemia, as well as small cell lung cancer and metastatic breast cancer. Finally, heptaplatin is approved for the treatment of gastric cancer.[40]

In the attempt to increase the antitumour efficiency and, at the same time, to reduce the toxicity still present in some first-generation platinum(II)-based analogues, second- and third-generation derivatives were designed (**Figure 1.5**). Among all, platinum(IV)-based complexes, such as JM216/satraplatin (**Figure 1.5a**), platinum(II) complexes with aromatic ligands (e.g. pyridines or picolines such as AMD473/picoplatin, **Figure 1.4b**), or polinuclear complexes (e.g. BBR3464/triplatin, **Figure 1.5c**) have been studied in-depth.[41] However, although each of these compounds represented an important milestone towards the development of metal-based anticancer chemotherapy, none has shown so far in clinical trials an actual improvement in terms of better antitumour activity and reduced toxicity compared to cisplatin.[40]

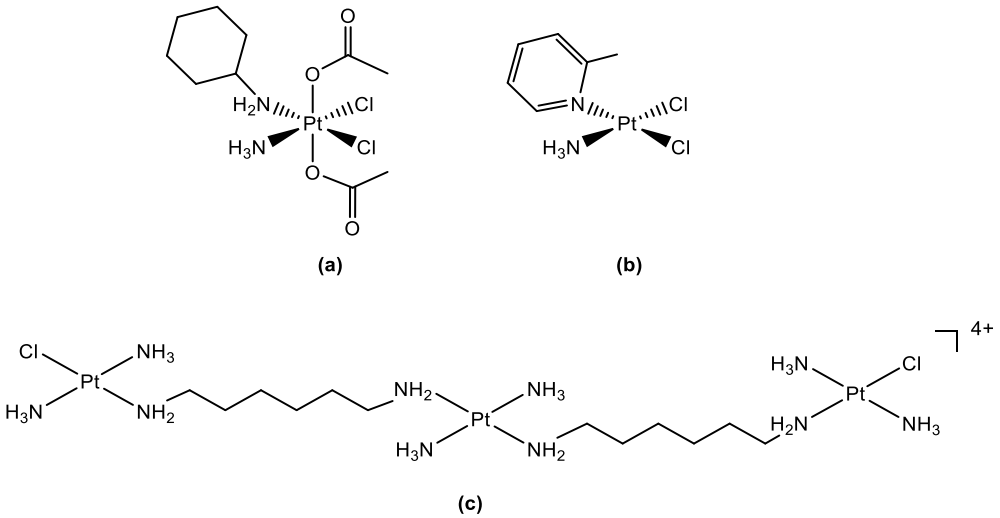

Figure 1.5. Chemical drawing of JM216/satraplatin (**a**), AMD473/picoplatin (**b**), BBR3464/triplatin (**c**).

As previously mentioned, the clinical success of cisplatin and its platinum-based analogues is hindered by several drawbacks, such as nausea, alopecia, nephrotoxicity, ototoxicity, neurotoxicity, and myelosuppresion.[42–45] Moreover, resistance, either intrinsic in/for certain types of tumor or acquired during repeated cycles of therapy, represents another relevant major issue.[46,47]

Among all, nephrotoxicity (*i.e*. kidney toxicity) is the major downside correlated to cisplatin treatment. The effect was observed since the early preclinical studies in 1969, and it typically manifests several days after the administration of cisplatin in 20-30% of patients, enduring for 2-4 weeks.[35] Research efforts in the last decades aimed at clarifying the complex mechanisms of cisplatin-induced nephrotoxicity which involve multiple pathways and, eventually, lead to renal failure. This seems to be caused by the accumulation of platinum in the kidneys, due to the mediated uptake operated by two membrane transporters: Ctr1 (copper transporter 1) and OTC2 (organic cation transporter 2).[48,49]

The interaction between sulfur-containing biomolecules (such as glutathione, metallothionein, albumin, cysteine and methionine residues of renal enzymes) and platinum-based drugs is believed to play a significant role in their mechanism of action, leading to negative effects on their therapeutic effectiveness. This non-beneficial interaction is commonly associated with drug detoxification, nephrotoxicity and resistance. Cisplatin, but also other compounds containing Pt(II) "soft" metal centers, have high affinity for "soft" sulfur-donor ligands, and may readily react with, for example, glutathione (GSH) in aqueous solution under physiological conditions (**Figure 1.4**).[50–52] In the cytoplasm, glutathione concentration is in great excess compared with cisplatin (mM vs. μM).[53,54] It can thus be assumed that GSH is a major cellular target of cisplatin, leading to the formation of stable GS-platinum(II) adducts which prevent platinum from binding to cellular DNA.[55,56]

Moreover, the strong and irreversible binding of platinum to intracellular sulfur donors present in proteins and enzymes is considered another major inactivation step, which alters the conformation of the proteins themselves. This invariably disrupts and changes the normal biological functions, especially when enzymatic processes are involved.[57]

1.3 Dithiocarbamates

As previously mentioned, nephrotoxicity severely hinders the efficacy of cisplatin and related platinum-based derivatives in the clinical treatment. In order to modulate

cisplatin-induced nephrotoxicity, several thiol- and sulfur-based compounds were tested in coadministration as chemoprotectant agents (**Figure 1.6**). Platinum(II) centers ("soft" Lewis acid) have strong affinity with sulfur-containing molecules ("soft" Lewis bases). Although Pt–S interactions are kinetically favoured, it has been demonstrated that they can be reverted and changed slowly to thermodynamically favoured Pt–N7 interactions of guanine.[56] Nevertheless, the Pt-N7(guanine) bond appears to have a higher thermodynamic stability than Pt–N7(adenine). Thus, this should remove the platinum from thiol molecules, acting as a "reservoir of bioactive platinum", without affecting the cisplatin-DNA adducts responsible of the anticancer activity. However, a selective protection of normal tissues without inhibition of the anticancer activity proved challenging.[58]

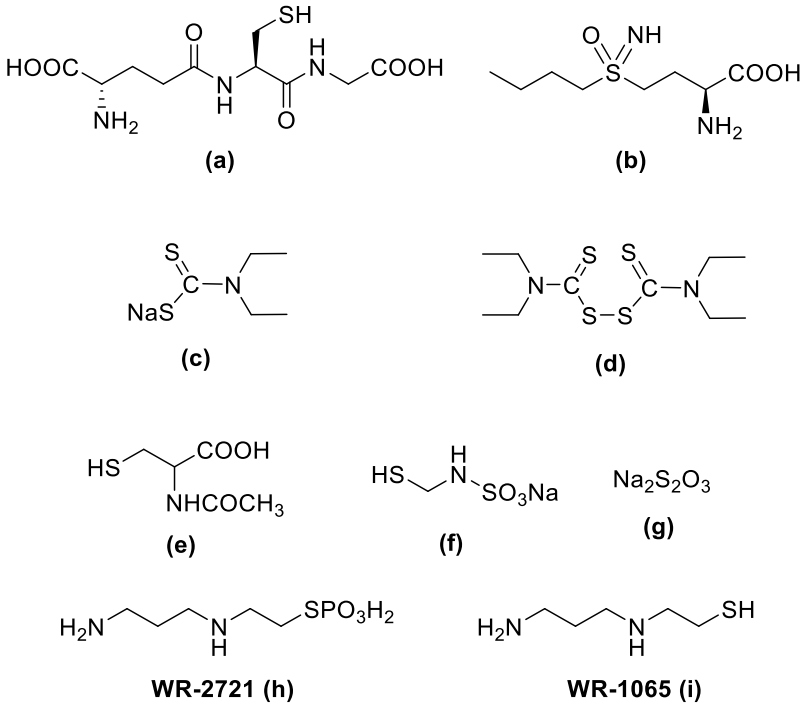

Figure 1.6. Cisplatin sulfur-based modulators: glutathione (GSH, (**a**)), the GSH-depleting antimetabolite L-buthionine sulfoximine (L-BSO, (**b**)), the sulfydryl metabolite of disulfiram diethyldithiocarbamate (DEDT, (**c**)), the parent disulfide disulfiram (antabuse, (**d**)), *N*-acetyl-L-cysteine (L-NAC, (**e**)), *S*-mercaptoethane sulfonate sodium salt (mesna, (**f**)), sodium thiosulfate (**g**), the phosphothiolamifostine (WR-2721, (**h**)) and its active metabolite actifostine (WR-1065, (**i**)) formed by alkaline phosphatase activity).

Among all the chemoprotectants tested, sodium *N*,*N*-diethyldithiocarbamate (DEDTNa, **Figure 1.6c**) showed positive outcomes providing protection from renal, gastrointestinal and bone marrow toxicity without altering the therapeutic effect of cisplatin.[59] When administered 1-4 h after cisplatin, DEDTNa does not interfere with the antitumour properties of cisplatin. This behaviour is consistent with the observation that DEDTNa can reverse certain Pt-DNA adducts, but not the chelate Pt-adducts with guanosines

responsible for DNA lesions.[60] DEDTNa is also capable to reverse Pt-methionine bonds but not Pt-cysteine ones.[61] It thus appears that DEDTNa acts as a real rescue agent preventing not only protein inactivation but also repairing cisplatin-induced damage by dissociating Pt-protein adducts.[62] Therefore DEDT can chelate and cleave the platinum from all the other sulfur-containing molecules.[56] However, DEDTNa was not widely exploited in the clinical practice, mainly due to the acute toxicity profile, especially geno- and neurotoxicity, of non-coordinated dithiocarbamates, together with their ability to chelate and remove other metals essential for biological functions.[63,64]

The dithiocarbamato scaffold (–NCSS) acts mainly as a bidentate ligand (although monodentate coordination is also reported) and it is thought to stabilize the metal centre through the so-called "chelate effect". Moreover, the solubility and other properties (e.g. fluorescence, interaction with certain receptors, etc.) may be modulated by ligand tailoring of the substituents bound to the N atom of the –NCSS moiety. For what concerns square-planar metal complexes, the presence of the bidentate dithiocarbamato ligand should, in principle, prevent the further coordination of S-containing biomolecules *trans* to the dithiocarbamato sulfur donor atoms due to their rather strong *trans*-influencing effect.[65] This phenomenon would potentially avoid the interaction of the metal centre with the thiol-containing renal enzymes and, thus, reduce the nephrotoxic side-effects.

On account of these considerations, over the last two decades several dithiocarbamato complexes of different transition metals, such as Pt(II), Pd(II), Au(I/III), Zn(II), Cu(II), Ru(II/III), have been investigated as promising alternative to clinically-established platinum-based drugs.[66–69]

The first compounds to be obtained and studied were palladium(II) and platinum(II) derivatives of the type [MCl(ESDT)(Am/Py)] (M: Pd(II), Pt(II); ESDT: ethylsarcosinedithiocarbamate; Am/Py: various aliphatic amines or pyridines, **Figure 1.7**).[70–74]

Figure 1.7. General structure of platinum(II)/palladium(II) complexes with the ESDT dithiocarbamato ligand.

There are a number of reasons as to the choice of the ligands. Firstly, cisplatin analogues of *n*-propylamine are being evaluated for their antitumor activity.[41] Sterically hindered Pt(II)-complexes coordinated to pyridine and substituted pyridines showed a reduction of the deactivation rate induced by sulphydryl groups, without interfering with DNA binding

or cytotoxicity. For instance, the complex [$PtCl_2$(2-pic)(NH_3)] (2-pic: 2-methylpyridine or 2-picoline, also named picoplatin or AMD473, **Figure 1.5b**) entered various clinical trials (Phase I or II) for the treatment of carboplatin-resistant solid tumours such as lung, ovarian, breast, bladder, and colorectal tumours.[40,75,76] Additionally, sarcosinedithiocarbamate was shown to increase the therapeutic effectiveness of the clinically established drugs doxorubicin, methotrexate, teniposide and mitoxontrone when used in pretreatment against leukemia L1210.[77] The ester group was preferred instead of the carboxylic acid function in order to avoid unwanted coordination of the free carboxylate with the metal centre, as well as to modulate the physico-chemical properties of the final derivatives.

Among all the complexes studied, the pyridine derivative [PtCl(ESDT)(Py)], named PTL1, performed best in terms of anticancer activity.[74] In fact, the complex displayed a broader spectrum of activity than the reference drug cisplatin towards a number of intrinsically resistant human tumour cell lines. Moreover, the complex was active also against C13 cisplatin-resistant tumour cells, with a reduced resistant factor of about 14-fold when compared with cisplatin.[78]

The promising *in vitro* outcomes of PTL1 were confirmed by *in vivo* studies on mice bearing inoculated Ehrlich ascitic carcinomas. Animal treatment with PTL1 caused a tumour size reduction comparable to cisplatin of ca. 70%, while increasing the life span with %T/C (i.e. survival time of treated animals *vs*. control) of 190% (versus 129% for cisplatin). Moreover, treatment with PTL1 was better tolerated by the tested animals showing less signs of prostration, such as body weight loss, anorexia and dehydration than cisplatin-treated counterparts.[79] Finally, further studies on urinary and renal cortical biomarkers showed the lack of nephrotoxicity induced by PTL1, thus confirming the effectiveness of the strategy to coordinate a dithiocarbamic ligand in order to reduce the nephrotoxic side-effects.[80,81]

However, despite these promising results, further evaluation as potential anticancer agents was abandoned owing to poor water solubility and low stability under physiological conditions (essential prerequisites for pharmacological application), together with lengthy synthetic routes.[65]

1.4 Gold-containing anticancer compounds

1.4.1 Gold in medicine and chemotherapy

As previously mentioned, gold-based compounds were amongst the first metal-based drugs to be introduced for the treatment of tuberculosis and rheumatoid arthritis. The latter in particular is a long-term and chronic autoimmune disease that affects joints, by causing painful inflammatory conditions accompanied with progressive joint erosions. The causes of this disabling disease are still unknown, and since there is no definite cure for rheumatoid arthritis, the current therapy consists only on alleviating the symptoms rather than eradicating the disease itself.[82]

Gold-based drugs are still used in the treatment regimen aimed at reducing the inflammation as well as disease progression with the so-called "crysotherapy", that is the treatment with gold salts. These compounds include the gold(I) derivatives solganal, myocrisin, sanocrysin, allocrysin, and auranofin (**Figure 1.8**). In contrast with the other gold derivatives, which have to be injected, auranofin ([(2,3,4,6-tetra-O-acetyl-1-thio-β-D-glucopyranosato-S)(triethylphosphino)]gold(I), **Figure 1.8e**), currently marketed as Ridaura™, is of special interest since it can be orally administered.[83]

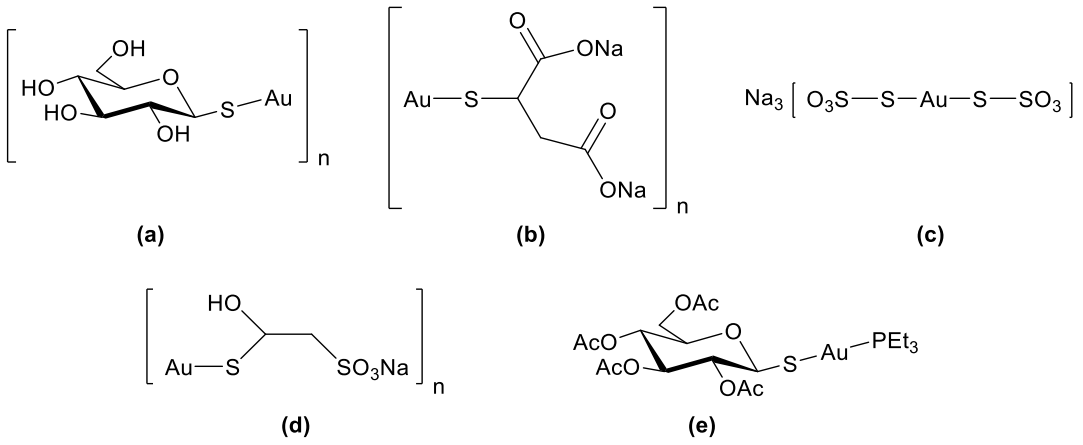

Figure 1.8. Clinically-established gold(I) antiarthritic drugs: solganal (**a**), myocrisin (**b**), sanocrysin (**c**), allocrysin (**d**), and auranofin (**e**).

Beside its anti-inflammatory activity, auranofin possesses also tumour growth inhibiting properties *in vitro* and, as such, was extensively studied.[84] In fact, it proved cytotoxic toward several human tumour cell lines, including cisplatin-sensitive and -resistant ovarian,[85,86] multiple myeloma,[87] colorectal,[88] and leukemia cells.[89] Unfortunately, antitumour activity was confirmed *in vivo* only against murine P388 lymphoma.[90,91] Nevertheless, auranofin has completed Phase II clinical trials for the treatment of chronic lymphocytic leukemia, small lymphocytic lymphoma and prolymphocytic lymphoma,

while it is entering in Phase II for the treatment of ovarian cancers and in Phase I for the treatment of recurrent or advanced non-small cell lung cancer or small cell lung cancer.[92,93] As to its mechanism of action, the antiarthritic activity seems to arise from the inhibition of enzymes such as cyclooxygenases,[84] whereas the inactivation of the seleno-enzyme thioredoxin reductase is likely to account for its anticancer properties.[86] As a consequence, thanks to the discovery of their tumour growth inhibiting effects, gold-based compounds received more and more attention in recent years, fostering research efforts on repurposing them for anticancer applications.[94]

1.4.2 First-generation gold(III)-dithiocarbamato complexes

With the aim to explore alternatives to platinum(II)- and palladium(II)-dithiocarbamato derivatives with improved pharmacological profiles and, at the same time, to overcome the issues displayed by such compounds, Ronconi and coworkers reported on a series of square-planar gold(III) complexes of the type [AuX_2(DMDT)], [AuX_2(PDT)], [AuX_2(RSDT)] (X: Cl, Br; DMDT: *N,N*-dimethyldithiocarbamate; PDT: pyrrolidinedithiocarbamate; RSDT: methyl-, ethyl-, or *ter*-butyl sarcosineditiocarbamate) (**Figure 1.9**).[59,95–97]

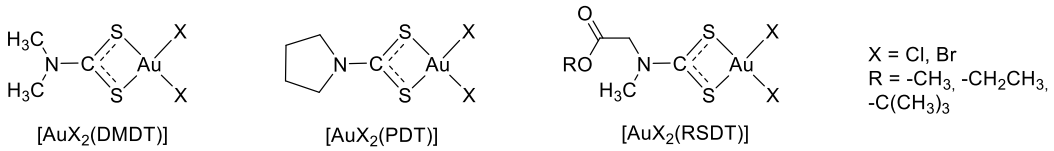

Figure 1.9. General structure of first-generation gold(III)-dithiocarbamato complexes reported by Ronconi and co-workers.

The choice of the metal centre was not accidental. In fact, as already mentioned, gold compounds have found a number of applications in medicine, especially in the treatment of rheumatoid arthritis with the so-called "chrysotherapy". Secondly, gold(III) is isoelectronic to platinum(II) (d^8 electron configuration), and it is expected to form square-planar metal complexes with close structural similarities to the bioactive platinum(II) metallodrugs. Nevertheless, the presence of a dithiocarbamato ligand facilitates the stabilization of the complex in the +3 oxidation state and limits the reduction to gold(I) under physiological conditions by lowering its reduction potential.[77,98] Finally, it is foreseen that the dithiocarbamato ligand should, in principle, protect the metal center from thiol-induced inactivation (see paragraph 1.3), thus reducing the occurrence of toxic side-effects and maintaining the therapeutic effectiveness.

Crystal structures obtained by single crystal XRD confirmed the square-planar coordination fashion of the bidentate dithiocarbamato scaffold (–NCSS) and the two *cis*

halogenido ligands (Cl, Br) bound to the gold(III) centre.[99] Furthermore, potentiometric and UV-Vis studies elucidated a possible hydrolytic behaviour of substitution of the halogenides by one or two molecules of water to form mono- and di-aquo species, respectively, in a similar manner to cisplatin.[98]

In vitro cytotoxicity studies showed that the object compounds possessed a remarkably higher antiproliferative activity than cisplatin (IC_{50} values in the lower micromolar range), even against human tumour cells intrinsically resistant to platinum-based chemotherapy.[95]

It was also observed that such gold(III)-dithiocarbamato complexes differ from cisplatin in their mechanism of action. In fact, once in the cytoplasm they would target mitochondria rather than causing lesions to the nuclear DNA. In this regard, a common biological target for gold(III)-dithiocarbamato derivatives is known to be the thioredoxin reductase enzyme (TrxR).[100] The thioredoxin system plays a key role in the maintainment of the intracellular redox status. The TrxR enzyme is a complex homodimeric selenoenzyme that controls the redox balance of thioredoxin and is the only enzyme known to reduce thioredoxin. It was proved that many gold compounds inhibit TrxR activity, thus triggering an impairment of the mitochondrial functions and inducing oxidative stress accompanied by the production of reactive oxygen species (ROS) that subsequently lead to cell death. All the gold(III)-dithiocarbamato derivatives have shown to inhibit TrxR activity and to induce tumour cell death either via apoptotic and non-apoptotic pathways.[99]

Together with mitochondria, another important biological target of such compounds is the ubiquitine-proteasome system (**Figure 1.10**).[101] The ubiquitine-proteasome system has a fundamental role in the degradation of damaged and/or mutated proteins with major consequences on the cell cycle, proliferation and apoptosis.[102] The 26S proteasome is a complex multienzymatic system, localized in the nucleus and in the cytosol, with proteolytic functions. The proteasome degrades intracellular proteins previously tagged with ubiquitin (a 76 amino acid protein), and involving three different subunits contained in the proteolytic core (also known as proteasome 20S) showing chymotrypsin-, trypsin- and caspase-like activity.[103]

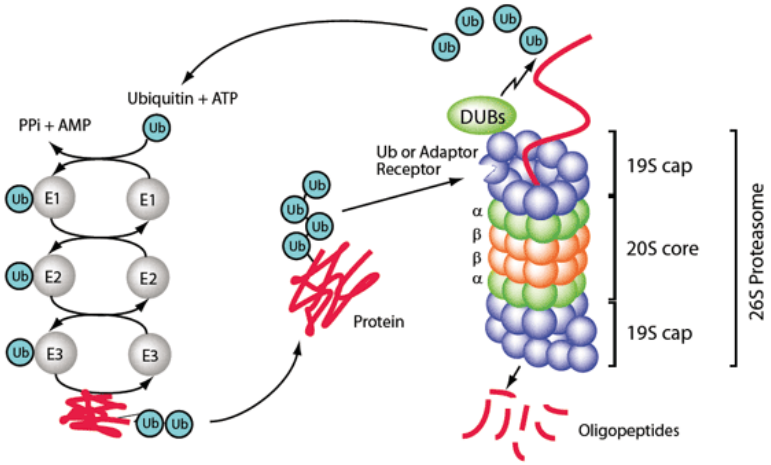

Figure 1.10. Schematic overview of the ubiquitine-proteasome system (adapted from https://www.biomol.com/ubiquitin-and-proteasome-research.html?id=1374).

An abnormal overexpressed proteasome activity seems to be associated with some malignancies, making it an intriguing target for the design and development of novel anticancer agents specifically targeting and inhibiting proteasome. For instance, it was demonstrated that the complex AUL14, [$AuBr_2$(DMDT)], can strongly inhibit the chymotrypsin-like activity of the 20S proteasome purified from rabbit and from MDA-MB-231 cell extract.[104]

Further *in vivo* studies were carried out on three different murine tumour models: Ehrlich solid carcinoma, Ehrlich ascite, and Lewis lung carcinoma.[105] For all these cases, the complex [$AuBr_2$(ESDT)] (AUL12), selected for its favourable features in terms of solubility, stability in physiological medium and *in vitro* cytotoxicity, revealed a much greater capability to shrink tumours than cisplatin. In addition, contrary to cisplatin-treated mice, animals treated with AUL12 did not show, after an initial loss of body weight, further signs of prostration and anorexia. Interestingly, intravenous acute toxicity was also very low (LD_{50} 30 mg Kg^{-1} *vs*. 11 mg Kg^{-1} cisplatin) and the nephrotoxicity side-effects were negligible.[105]

1.4.3 Towards the "golden magic bullet": gold(III)-dithiocarbamato peptidomimetics

Notwithstanding the excellent outcomes obtained by the first-generation gold(III)-dithiocarbamato complexes, the lack of selectivity still represents a considerable challenge. In fact, the design of a more selective anticancer drug is desirable in order to: i) improve the therapeutic effectiveness due to a reduced amount of administered drug; ii) decrease the systemic and/or specific toxicity arising from the interaction of the drug

with healthy cells. In this regard, a major challenge is to design compounds capable of crossing the cell membrane of tumour cells to enter the cytosol. One of the objectives of the research in pharmacology is aimed at enhancing the selective cellular uptake of chemotherapeutics in cancerous tissues.

In the '90s two new membrane proteins were identified, namely PEPT1 and PEPT2. These proteins are localized in the epithelial cells of small intestine, kidneys, lungs, mammary glands and several other tissues, and they are devoted to the internalization of di- and tri-peptides in the cell.[106] PEPTs are overexpressed in some tumour cells, making them an interesting pharmacological target since they mediate cellular internalization of oligopeptides and favour the absorption of peptidomimetic drugs, such as β-lactam antibiotics (penicillin and its derivatives and aminocephalosporine).[107]

With this in mind, a second-generation series of gold(III)-dithiocarbamato complexes functionalized with oligopeptides was synthesized by Ronconi and coworkers. Different di- and tri-peptides were designed and attached to the anticancer gold(III)-dithiocarbamato scaffold in order to exploit the interaction with PEPTs.[108,109] All complexes were tested against a number of human tumour cell lines. Among all, the complexes named AUD6 and AUD8 ([AuX_2(dtc-Sar-Aib-O*t*Bu)], X: Cl, Br; dtc: dithiocarbamato moiety, –NCSS; Sar: sarcosine, *N*-methylglycine; Aib: α-amminoisobutyrric acid; *t*Bu: *ter*-butyl, **Figure 1.11**) performed best in terms of cytotoxicity on human prostate cisplatin-sensitive (PC3 and DU145) and cisplatin-resistant (PC3-R and DU145-R) cell lines, with IC_{50} values in the range 1-2 μM (lower than cisplatin). In addition, AUD6 and AUD8 induced cell death *via* apoptotic pathways in PC3, DU145, and cisplatin-resistant C13 cells.[108]

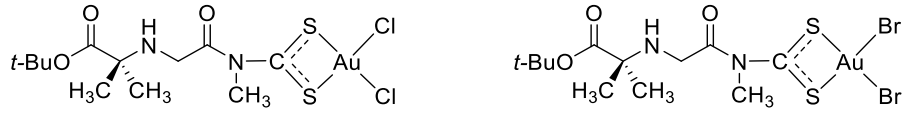

AUD6 **AUD8**

Figure 1.11. Structure of the gold(III)-dithiocarbamato peptidomimetics AUD6 and AUD8.

AUD6 and AUD8 were also selected for further *in vitro* interaction studies with the proteasome 20S, showing that the latter is inhibited in PC3 cells by this type of compounds, as already observed for the first-generation complexes.[110] The compound AUD8 showed also a significative anticancer activity *in vivo* on a xenografic prostate tumour PC3 implanted in mice, with tumour growth reduction of about 70% after 19 days of treatment. Remarkably, the treated animals did not possess histologically detectable

cytotoxicity involving lungs, kidneys, liver or spleen, nor show signs of body weight loss.[110]

1.5 Glycoconjugation strategy for the targeted delivery of metallodrugs

1.5.1 Tumour glycolysis

All cells require glucose for the generation of adenosine triphosphate (ATP) as energy source to drive a number of subsequent biochemical processes. Once internalized into the cell through the transmembrane glucose transporters (GLUTs), one molecule of glucose undergoes a multistep enzyme-catalyzed metabolic process (termed glycolysis) eventually devoted to its oxidation to pyruvate (**Fig. 1.12**).[111]

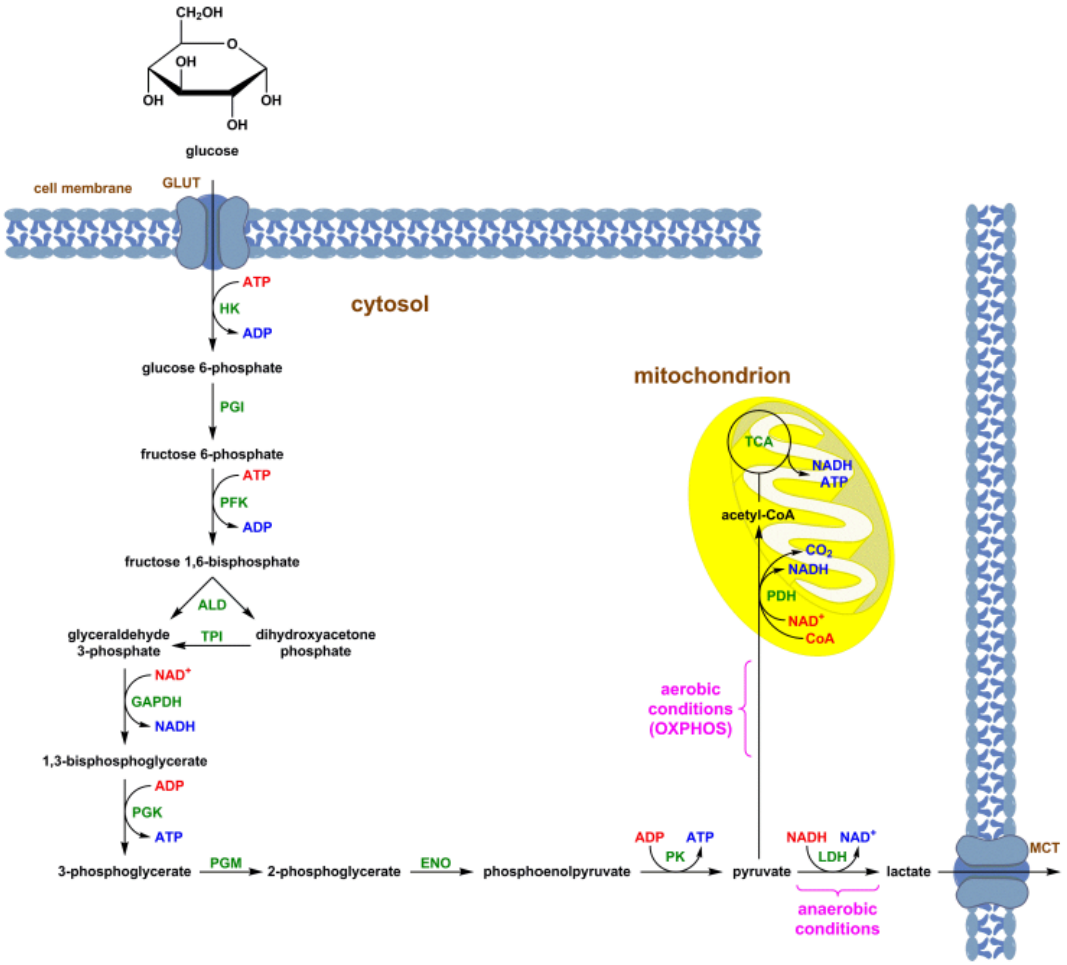

Figure 1.12. Schematic overview of the glycolytic pathway (GLUT: glucose transporter; ATP: adenosine-5'-triphosphate; HK: hexokinase; ADP: adenosine-5'-diphosphate; PGI: phosphoglucoseisomerase; PFK: phosphofructokinase; ALD: aldolase; TPI: triosephosphate isomerase; NAD_+: nicotinamide adenine dinucleotide - oxidized form; GAPDH: glyceraldehyde-3-phosphate dehydrogenase; NADH: nicotinamide adenine dinucleotide - reduced form; PGK: phosphoglycerate kinase; PGM: phosphoglycerate mutase; ENO: enolase; PK: pyruvate kinase; LDH: lactate dehydrogenase; MCT: monocarboxylate transporter; OXPHOS: oxidative phosphorylation; CoA: coenzyme A; PDH: pyruvate dehydrogenase; TCA: tricarboxylic acid (Krebs) cycle (adapted from [112]).

Typically, normal cells metabolize glucose under aerobic conditions and, as such, the glycolytic pathway is coupled with the mitochondrial oxidative phosphorylation (OXPHOS) process. Therefore, pyruvate produced *via* glycolysis enters mitochondria and is used to generate acetyl-coenzyme A (acetyl-CoA) which then enters the tricarboxylic acid (TCA) cycle. As a result, reduced adenine dinucleotide (NADH) is formed which is needed to maximize ATP production, and up to 36 molecules of ATP may be produced by 1 molecule of glucose. Alternatively, under anaerobic conditions, OXPHOS is unlikely to occur and pyruvate is converted to lactate which is excreted from the cell through the monocarboxylate transporter (MCT).[112]

There is compelling evidence due to altered glucose metabolism in cancer cells for hypoxia in tumor tissues. In 1924, the German biochemist Otto Heinrich Warburg (**Figure 1.13**) first postulated "anaerobic" glycolysis as the major glucose metabolism in tumors, a phenomenon known as "the Warburg effect".[113] In particular, he showed that pyruvate resulting from the glycolytic process, under anaerobic conditions induced by the hypoxic tumour intracellular environment, is more likely converted to lactate rather than undergoing mitochondrial OXPHOS. Such high excretion of lactic acid is consistent with increased extracellular acidosis compared with normal cells.[114] Although the anaerobic glycolytic pathway is less efficient than OXPHOS in generating ATP (2 *vs.* 36 ATPs per one glucose molecule), it produces ATP at a faster rate.[115] This accounts for Warburg's observation that tumour cells are generally characterized by exaggerated demand and consumption of glucose to sustain their abnormal proliferation rates.[116,117] Thanks to these discoveries, Warburg was awarded the Nobel Prize in Physiology or Medicine in 1931.[118]

Figure 1.13. Otto Warburg (photography from the Archives of the Max Planck Society, Berlin, Germany).

Hypoxia-inducible factor 1 (HIF-1) plays a key role in promoting glycolysis in hypoxic tumor cells, leading to the Warburg effect. Such metabolic reprogramming responds to

the greater demand of energy and glycolysis-related anabolites, as well as to the decreased effectiveness of the overall glycolytic flux preferentially forming lactate.

Specifically, HIF-1 promotes: a) the overexpression of glucose transporters 1 and 3 (GLUT1 and GLUT3); b) the enhanced transcription of hexokinases 1 and 2 (HK1, HK2), phosphofructokinases 1 and 2 (PFK1, PFK2), aldolases A and C (ALDA, ALDC), phosphoglycerate kinase 1 (PGK1), enolase 1 (ENO1), pyruvate kinase M2 (PKM2); c) the expression of pyruvate dehydrogenase kinases 1 and 2 (PDK1, PDK2); d) enhanced production of monocarboxylate transporter 4 (MCT4).[119]

Owing to the abnormal demand of glucose in tumour cells, the overexpression of GLUT1 and GLUT3 facilitates its uptake, whereas its conversion to pyruvate is favoured by the enhanced transcription of the enzymes directly involved in the whole process (that is, HK1, HK2, PFK1, PFK2, ALDA, ALDC, PGK1, ENO1, PKM2). Furthermore, the expression of PDK1 and PDK2 inhibits pyruvate dehydrogenase (PDH) and, consequently, the conversion of pyruvate to acetyl-CoA, thus preventing it to undergo the OXPHOS process in the mithocondria. In turn, the expression of lactate dehydrogenase 5 (LDH5) is promoted, thus favouring the conversion of pyruvate to lactate. Finally, the overexpression of MCT4 allows lactate to be effectively sent out of the cell.

Owing to its role in promoting tumour glycolysis and its low activity in normal tissues, HIF-1 is an attractive target in cancer chemotherapy so as to achieve selectivity toward tumour cells with minimal side-effects.[120–122] In a broader sense, any effector of tumour glycolysis, in particular those whose overexpression is promoted by the activation of HIF-1, may be regarded as suitable targets for the development of anticancer agents. To date, a few potential anticancer agents aiming at counteracting tumour glycolysis have entered Phase I-III clinical trials, and many others are undergoing preclinical evaluation.[123,124]

1.5.2 Targeting glucose transporters

Among all, a suitable strategy is based on the development of chemotherapeutics specifically targeting glucose transporters (GLUTs). GLUTs are devoted to the recognition and cellular internalization of glucose, subsequently entering the glycolytic flux to provide energy and nutrients for cell growth and sustenance.

There are 14 isoforms of GLUTs, categorized into three classes based on their primary sequence and specific affinity for glucose or other carbohydrates.[125] GLUT1-GLUT4 belong to Class 1 and are selective for glucose transport, whereas Class 2 (GLUT5) and Class 3 (GLUT6, GLUT8, GLUT10) show preference for other sugars. Remarkably, all

GLUTs consist of 12 transmembrane domains characterized by similar amino acid sequences and tertiary structures.[126]

In order to support the abnormal proliferation rates, the activity of GLUTs in tumours is 10 to 12-fold higher than in normal tissues, thus indicating the strong dependence of cancer cells on such transporters for their survival and growth.[126,127]

In particular, the activation of HIF-1 under hypoxic conditions induces the overexpression of GLUT1 and GLUT3 in a wide range of human tumours, thus providing cancers with the capability to take up and internalize glucose even when its supply is limited.[128] Accordingly, tumours tendency to upregulate glucose uptake and the linkage between the overexpression of GLUT1/GLUT3 and poor prognosis of a number of human tumours have become, in recent years, hallmarks of cancer.[129,130]

Such avidity of glucose by fast-proliferating cancer cells has been already exploited in the clinics for the detection of primary tumours and metastases, as well as their progression. In this regard, the positron emission tomography (PET) tracer [^{18}F]-fluorodeoxyglucose (FDG, **Figure 1.14**) was developed as diagnostic probe owing to its increased preferential uptake in a number of tumours.[131] Nevertheless, from a therapeutic point of view, the overexpression of GLUTs in tumours provides the rationale to design GLUTs inhibitors capable of depleting cancer cells of a major nutrient by blocking glucose uptake, thus thwarting the glycolytic flux and, eventually, inducing cell death by starvation.

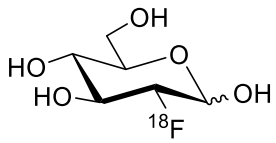

[^{18}F]-fluorodeoxyglucose
(^{18}F-FDG)

Figure 1.14. Chemical structure of [^{18}F]-fluorodeoxyglucose.

In this context, some natural products belonging to the family of flavonoids were found to exert anticancer activity by inhibiting GLUTs, the most promising being silybin[132] and phloretin (**Figure 1.15**).[133] However, owing to the varied biological features of flavonoids, including the well-known antioxidant properties,[134] it seems daring to assume that their anticancer effectiveness is only associated with their inhibitory effect of GLUTs. Direct inhibition of GLUTs was linked to the cytotoxic activity of glucose-like or glucose-mimicking agents (**Figure 1.15**). For example, 6-glucosechlorambucil, STF-31 and fasentin were shown to exert their anticancer activity by binding directly to

GLUT1 (and also GLUT4 for the latter) leading to its inactivation.[135–137]

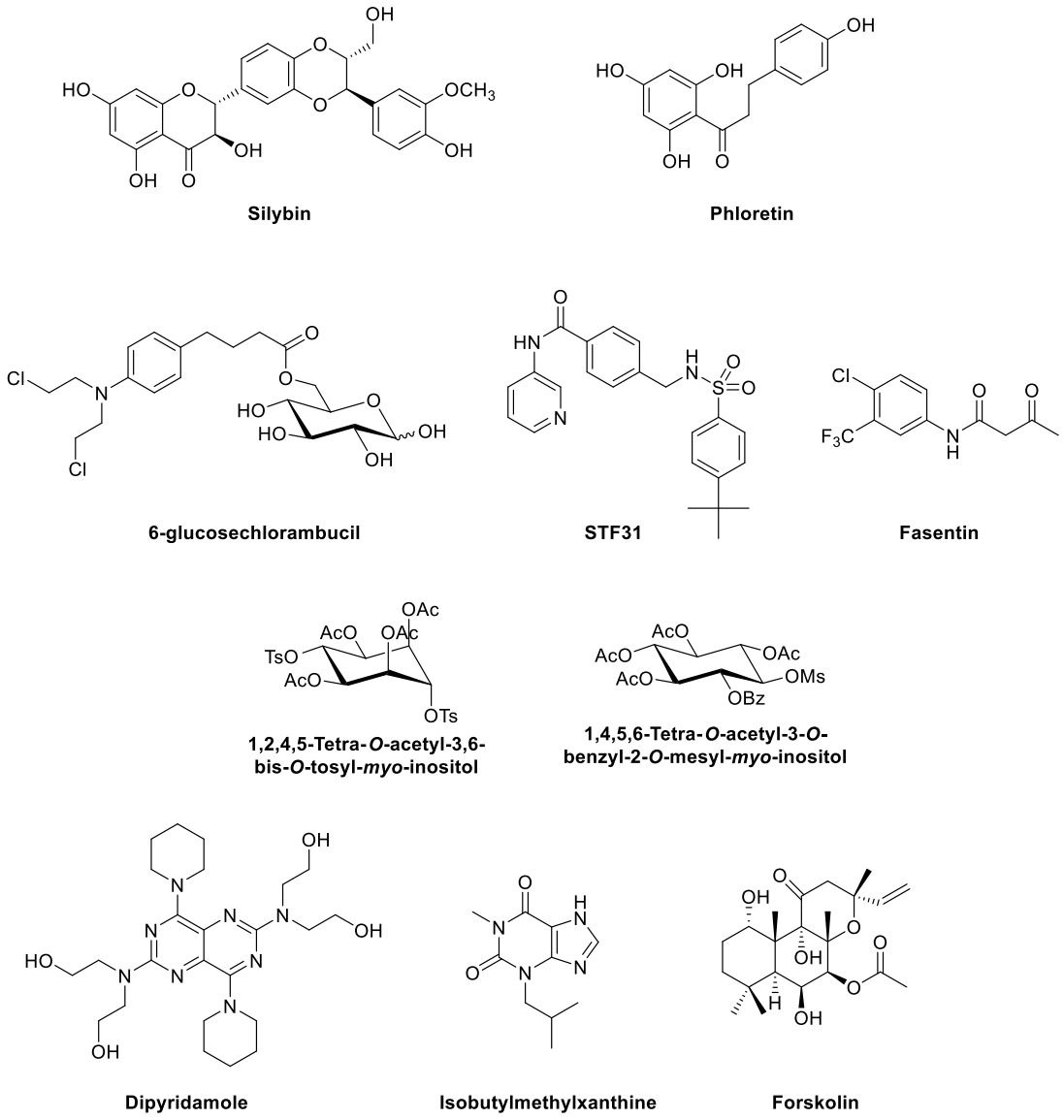

Figure 1.15. GLUTs inhibitors and glycoconjugates currently under preclinical evaluation.

Additionally, two *O*-protected derivatives of the pseudo-sugar *myo*-inositol proved cytotoxic toward cancer cells *in vitro* upon inhibition of GLUTs in a dose-dependent way,[138] whereas dipyridamole, isobutylmethylxanthine and forskolin were reported to selectively inhibit GLUT4 activity.[139] Notwithstanding the potential of such inhibition as a suitable strategy to block tumour glycolysis, only a few substances have GLUTs inhibition undoubtedly identified as the primary anticancer mechanism of action.

1.5.3 GLUT-interacting glycoconjugates

1.5.3.1 Organic molecules

An alternative approach is to target GLUTs not to inhibit them but to exploit their overexpression in tumours for the GLUT-mediated site-specific delivery of therapeutics.

This is based on the conjugation of a therapeutic agent to glucose-like or glycomimetic substrates acting as carriers of a pharmaceutically-active core.[140] The rationale of such designing strategy relies on the assumption that the glucose-like scaffold (anchored to a bioactive molecule) should be recognized by GLUTs and, if this is the case, the glycoconjugate would be internalized as a whole. Eventually, once taken up, the cytotoxic/diagnostic species would exert its anticancer/diagnostic activity directly inside the tumour cell, thus acting as a "Trojan Horse". These glycoconjugates may be regarded as pro-drugs in which the structural features of the glucose-like scaffold conceal the attached active drug. Remarkably, they have the potential to combine the antitumor properties of the drug with an enhanced uptake and tumour selectivity provided by the glucose-like tail-mediated cell internalization upon exploitation of the GLUTs overexpressed in cancer cells, therefore increasing the therapeutic effectiveness without affecting healthy tissues.

As already stated, among the various facilitative sugar transporters, GLUT1 represents the most well-known target for GLUT-exploiting glycoconjugates. Recent publications of the crystal structure of GLUT1, GLUT3, GLUT5 and XylE, an *Escherichia coli* homologue of GLUT1-4, provided an important framework for the mechanistic understanding of glucose transporters and sugar transporters in general.[141–144]

A successful application of this targeting strategy was reported for the glycoconjugate obtained by linking the nitric oxide releasing agent *S*-nitroso-*N*-acetylpenicillamine (SNAP) to the C-2 position of a glucosamine molecule to generate 2-glucose-SNAP (**Figure 1.16**).

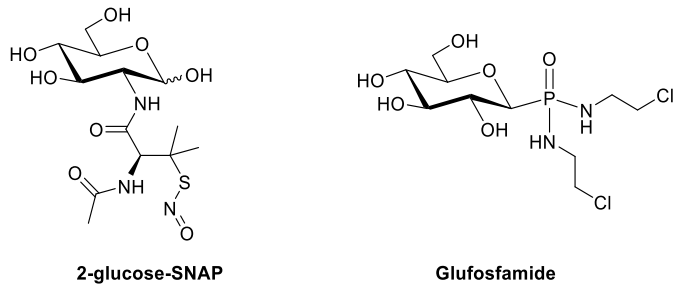

Figure 1.16. Chemical structures of 2-glucose-SNAP and glufosfamide.

Remarkably, it was observed that the conjugate had up to 5000-fold higher cytotoxicity toward ovarian carcinomas *in vitro* compared with the non-conjugated SNAP precursor, and such impressive enhanced activity was linked to the capability of 2-glucose-SNAP to target GLUT1.[145] Similar outcomes were also reported for glufosfamide, a glycoconjugate of the nitrogen mustard alkylating agent ifosfamide (**Figure 1.16**), which is currently undergoing Phase III clinical trials. In particular, enhancement in anticancer

activity upon glycoconjugation was observed in tumour cells overexpressing GLUTs.[146] Remarkably, in both cases, no evidence of GLUT inhibition was observed.

1.5.3.2 Platinum glycoconjugates

Despite a large number of organic glycoconjugates with proven tumour-targeting properties arising from GLUT-mediated internalization, only a scarce amount of metal-based conjugates with the same properties has been investigated so far. Over the last two decades, many metal complexes functionalized with carbohydrates have been synthesized with the aim to increase water-solubility and GLUT-targeting properties. However, apart from a patent dated back to 2006,[147] in most cases GLUT-mediated internalization was only postulated without proven experimental evidence.[112]

On the other hand, the resolution in 2014 of the first crystal structure of a human glucose transporter ever reported, GLUT1, followed by the publication of the crystal structures of GLUT3 and GLUT5, have been fostering research on novel GLUT-interacting glycoderivatives.[141–144] Lippard and Gao groups have independently reported on carbohydrate-appended analogues of oxaliplatin with such properties.

Lippard and coworkers investigated the effect of the functionalization of different positions of D-glucose, as well as of length of the spacer arm, on the biological activity of platinum glycoconjugates.[148,149] All possible positional isomers (C1α, C1β, C2, C3, C4 and C6) of a glucose-platinum derivative were synthesized (**Figure 1.17**).[149]

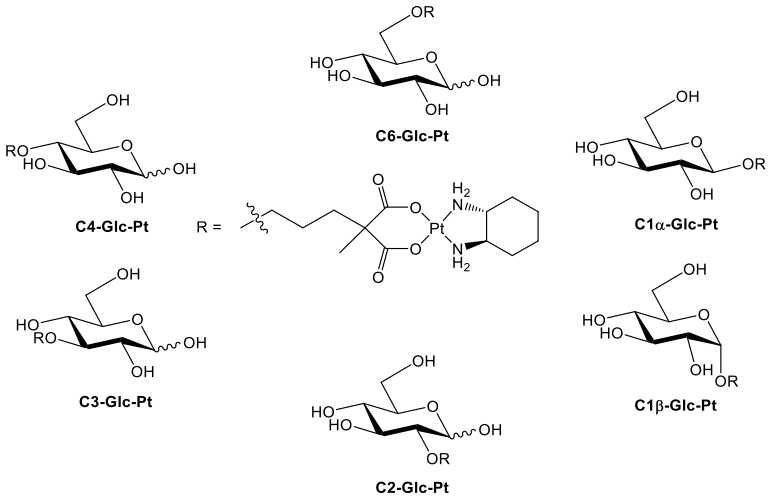

Figure 1.17. Structures of C1−C6-substituted positional isomers of a glucose−platinum conjugate reported by Lippard et al.[149]

The biological activity of the compounds was evaluated both *in vitro* and *in vivo*. The variation of the conjugation site of D-glucose affected not only cell uptake and cytotoxicity profile but also the GLUT1-targeting specificity of the resulting

glycoconjugates. Results from this study revealed that the C2-substituted derivative (**Figure 1.17**, C2-Glc-Pt) has the highest GLUT1-specific internalization, consistent with the greatest cancer-targeting capability. In a syngeneic breast cancer mouse model overexpressing GLUT1, C2-Glc-Pt showed excellent antitumour efficacy and selective uptake in tumours with no observable toxicity. In addition, docking studies of C6-functionalized glycoconjugates (**Figure 1.18**) with GLUT1 revealed no potential sterical constraints of the substrate into the binding pocket of the transporter.[148] Moreover, it was observed that the *in vitro* cytotoxic activity and cell uptake decreases by increasing the length of the spacer arm.

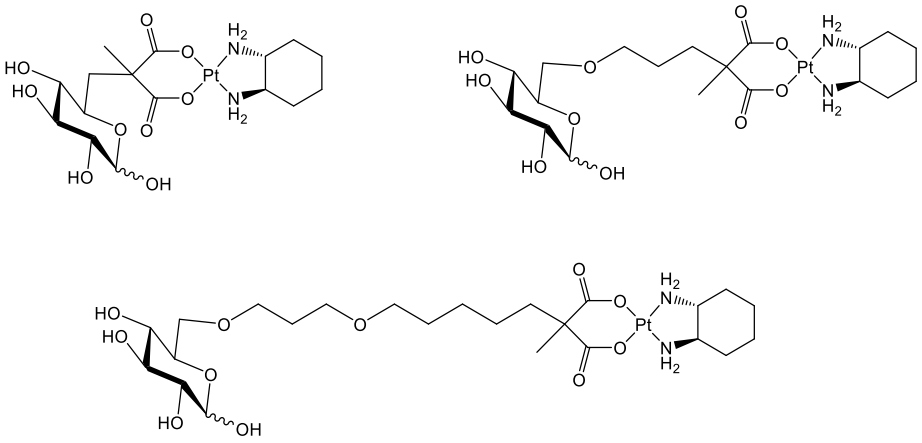

Figure 1.18. Structures of C6-substituted glucose-platinum conjugates appended *via* a space arm with different lenghts reported by Lippard et al.[148]

Gao and coworkers reported on a number of platinum derivatives functionalized with glucose, mannose, galactose and 2-deoxyglucose, either at the C1 or C6 position.[150–157] Interestingly, such complexes display much higher water-solubility, increased *in vitro* anticancer activity, and better therapeutic index compared to the reference drug oxaliplatin. In addition, they showed diminished *in vitro* anticancer activity in the presence of different GLUT-inhibitors, thus confirming that internalization is mediated by glucose transporters.[150]

More recently, some bioactive platinum(IV) glycoconjugates as suitable substrates for targeting GLUTs and OCTs (organic cation transporters) were reported for the first time and showed great potential (**Figure 1.19**).[158] As expected, the glycosylated platinum(IV) counterparts protected by acetyl groups did not have such properties.[159,160] In particular, all such metal glycoconjugates displayed increased (up to nearly 150-fold) *in vitro* anticancer activity towards various tumour cell lines compared to the reference drugs cisplatin, oxaliplatin and satraplatin.[158] The C1-substituted gluco- (**Figure 1.19a**), manno- and galactoside platinum(IV) derivatives showed better anticancer activity than

the C6-substituted pyranoside acids (**Figure 1.19b**). All the glycoconjugates possessed tumour-targeting properties, with the C1-substituted analogues revealing a fast GLUT1- and OCT2-mediated intracellular accumulation in tumour tissues. The presence of exadecanoic acid allowed the binding with human serum albumin (HSA) for drug delivery, increasing the stability of the conjugates in the biological media.

In vivo studies carried out on a mouse model of GLUT1-overexpressing breast cancer (MCF-7) in Balb/c mice, revealed that one of these glycosylated platinum(IV) complexes exhibited significant antitumour activity by reducing tumour volume and, at the same time, showing reduced toxicity compared to oxaliplatin.

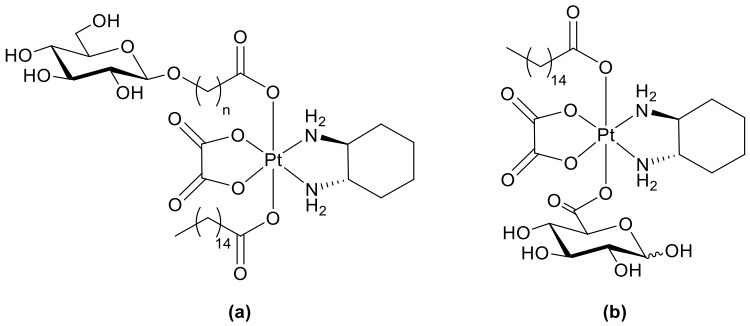

Figure 1.19. Structures of the GLUT-interacting Pt(IV) glycoconjugates.

1.5.3.3 Other metal-based glycoconjugates

Owing to its suitability for *in vivo* applications, the radioactive element technetium-99m (γ, $t_{1/2}$ = 6.0 h) has become the most commonly used radionuclide in diagnostic nuclear medicine, with 67 imaging agents approved by the U.S. Food and Drug Administration and 17 currently marketed. In particular, a ^{99m}Tc-DTPA (DTPA = diethylenetriamine-*N,N,N',N'',N''*-pentaacetic acid) complex is marketed as Techneplex® and has gained approval for renal, brain, and lung SPECT imaging.[161] Owing to the enhanced accumulation of glucose in tumour cells, ^{99m}Tc-labeled glycoconjugates have attracted increasing interest as tumour imaging agents.[162] Alberto and coworkers significantly advanced research into new radiopharmaceuticals by proposing an alternative strategy for labelling of biomolecules such as carbohydrates through the introduction of the organometallic {*fac*-$^{99m}Tc^{I}(CO)_3$} core.[163,164] Owing to the low-spin d^6 electron configuration of technetium(I), the resulting complexes possess great robustness in water, especially towards oxidation or carbonyl ligand substitution. The precursor *fac*-$[^{99m}Tc^{I}(CO)_3(H_2O)_3]^+$ can be conveniently prepared from $[Tc^{VII}O_4]^-$ and, given the small size of the metal core, labelling of biomolecules can be achieved with retention of activity and specificity.[165] Moreover, the three coordinated water molecules in the complex ion *fac*-$[^{99m}Tc^{I}(CO)_3(H_2O)_3]^+$ can be replaced by mono-, bi-, or tridentate ligands.[164]

Therefore, carboxylato pendants of biomolecules would act as anchoring sites for labelling once appropriately derivatized. Over the past decade, the so-called single amino acid chelate (SAAC) strategy has been introduced as a new approach for the preparation of labelled amino acid-containing bioconjugates.[166] This approach exploits the modification of an amino acid to incorporate both a tridentate terminus and a terminus to be attached to biomolecules at different positions within the backbone. Thus, Schibli and coworkers synthesized various glucose-appended complexes bearing the *fac*-$\{^{99m}Tc^{I}(CO)_3\}$ motif (**Figure 1.20**).[167] Uptake studies showed a relatively low accumulation in tumour cells and the uptake was not dose-dependent and did not vary in the presence of cytochalasin B, a potent GLUT1 inhibitor. The authors therefore speculated that alternative uptake mechanisms would take place (*e.g.* passive diffusion).

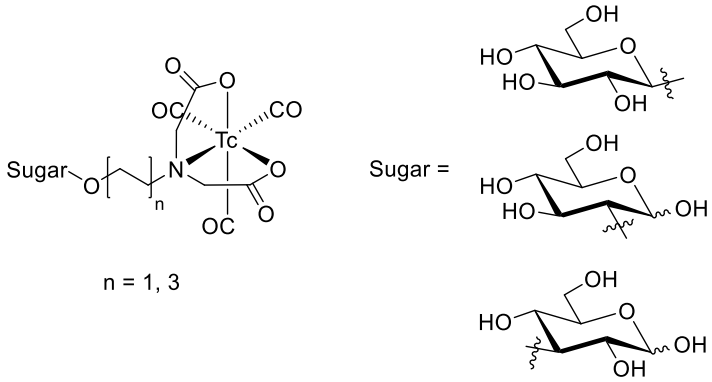

Figure 1.20. Chemical structures of the technetium(I) glucose-appended glycoconjugates reported by Schibli and coworkers.[167]

Over the last few years, Lo and coworkers focused on the design of luminescent rhenium(I) and iridium(III) polypyridine complexes. In particular, a number of theranostic complexes functionalized with carbohydrate pendants were described. Some iridium(III) complexes appended *via* an *N*-methylaminooxy group, $[Ir(N^{\wedge}C)_2(bipy\text{-}ONHCH_3)]^+$ and $[Ir(N^{\wedge}C)_2(bipy\text{-}TEG\text{-}ONHCH_3\text{-}\beta\text{-}D\text{-}sugar)]^+$ (N^C: various phenylpyridine ligands; bipy: bipyridine; TEG: triethylene glycol; sugar: glucose, galactose), were designed and used to functionalize monosaccharides (D-glucose and D-galactose, **Figure 1.21a**,**b**) and disaccharides (D-lactose and D-maltose). The uptake of the β-glucose conjugate by human cervical cancer (HeLa) cells is higher than the other glyconjugated analogues, suggesting the involvement of GLUTs in its cellular internalization.[168] Temperature-dependent and chemical inhibition experiments indicated that the uptake of the glucose-conjugate bearing the 2-((1,1′-biphenyl)-4-yl)benzothiazole) occurs *via* an energy-dependent process, such as endocytosis, along with a GLUT-mediated pathway.[169] Rhenium(I) complexes with different polypyridine

ligands bearing an α-D-glucose pendant, such as that depicted in **Figure 1.21c**, showed efficient intracellular internalization by exploitation of GLUTs.[170] One of these compounds is taken up more effectively in the tumourigenic cell lines HeLa and MCF7 than in the non-tumourigenic cell lines human embryonic kidney cells (HEK293T) and mouse embryonic fibroblasts (NIH/3T3). This suggested a GLUT-mediated uptake since the transformed cell lines are known to overexpress these transporters. The cell uptake of these compounds was also inhibited in presence of D-glucose and 2-deoxy-D-glucose, but not L-glucose. Finally, confocal microscopy studies revealed that such derivatives are localized in the mitochondria.

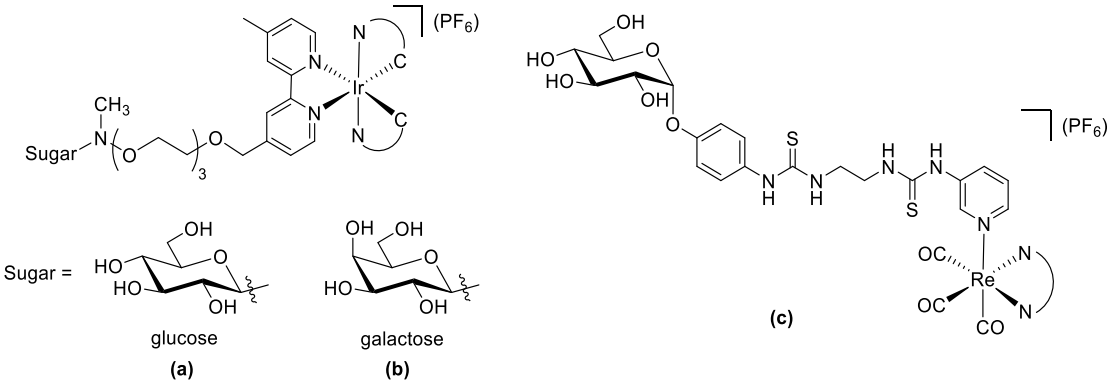

Figure 1.21. Chemical structures of the iridium(III)- (**a**,**b**) and rhenium(I)-glycoconjugates (**c**) reported by Lo and coworkers.

GLUTs-mediated uptake is not limited to glucose; fructose, for example, is a substrate for GLUT5. This transporter is overexpressed in breast cancer tissues, although its expression in other cancer tissues and in normal breast tissues is very limited.[171] With the aim to target GLUT5, the fructose-functionalized luminescent iridium(III) $[Ir(N^{\wedge}C)_2(bipy\text{-}fructose)](PF_6)$ (**Figure 1.22a**,**b**, N^C: various phenylpyridine ligands; bipy-fructose: fructose-functionalized bipyridine),[172] and rhenium(I) $[Re(Ph_2phen)(CO)_3(py\text{-}fructose)](TfO)$ (**Figure 1.22c**, Ph_2phen: 4,9-diphenyl-phenantroline; py-fructose: fructose-functionalized pyridine)[173] complexes were generated.

Notably, competitive experiments performed against breast adenocarcinoma cell lines (MCF-7 and MDA-MB-231), two non-breast cancer cell lines (A549 and HepG2), and two non-tumourigenic cell lines (NIH/3T3 and HEK293T) indicate that the uptake of the complexes is much more efficient in breast cancer cells, and that the uptake is inhibited upon addition of unmodified fructose. This highlights the possible use of such fructose derivatives as imaging reagents for breast cancer cells, as well as luminescent fructose-uptake indicators.

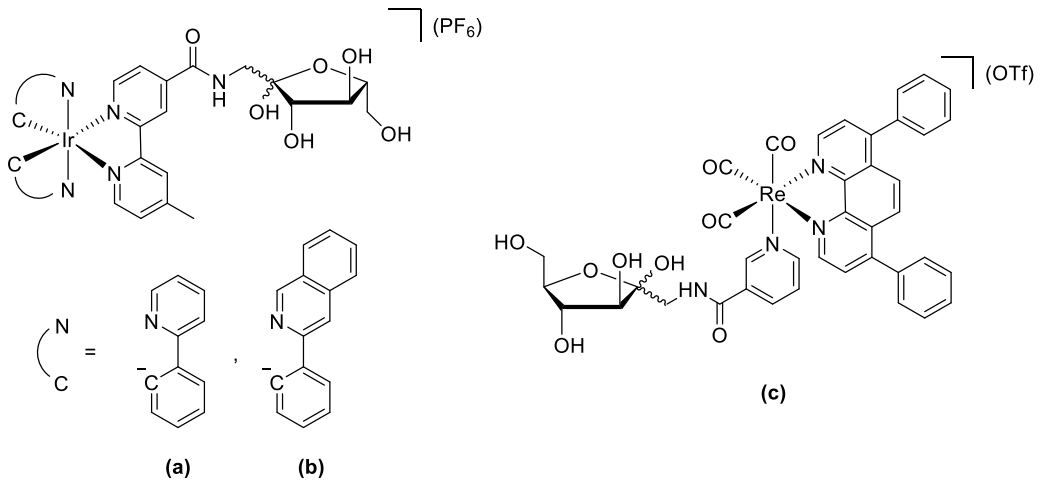

Figure 1.22. Chemical structures of the iridium(III)- (**a**,**b**) and rhenium(I)-glycoconjugates (**c**) of fructose reported by Lo and coworkers.[172,173]

Finally, Bonnet and coworkers generated some octahedral ruthenium(II) derivatives by coordinating D- or L-glucose thioether ligands to the highly lipophilic ruthenium complex $[Ru(tpy)(dppn)(H_2O)]^{2+}$ (**Figure 1.23**, dppn = benzo[*i*]dipyrido-[3,2-*a*:2′,3′-*c*]phenazine; tpy = 2,2′:6′,2″-terpyridine).[174]

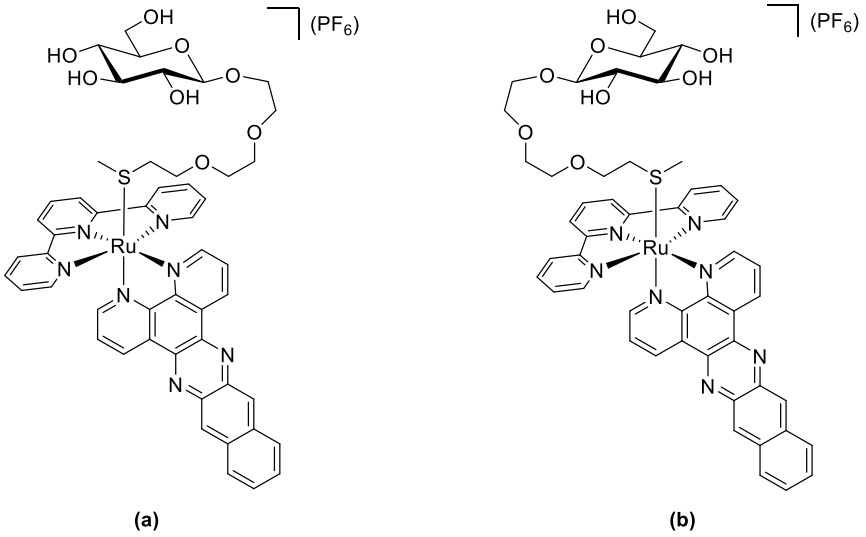

Figure 1.23. Chemical structures of the D- (**a**) and L-glucose (**b**) appended Ru(II) conjugates reported by Bonnet and coworkers.[174]

Both compounds were slightly emissive and showed moderate cytotoxicity in the dark, but potent cytotoxicity upon irradiation. *In vitro* emission imaging studies showed that the compounds were localized in the mitochondria. Coincubation with sodium azide, an inhibitor of energy-dependent uptake mechanisms, did not affect emission and localization of the compounds. This revealed that an energy-independent uptake mechanism would take place. This finding seems to rule out an energy-dependent uptake

mechanism (such as involving the sodium-glucose cotransporter, SGLT), whereas it cannot exclude the involvement of an energy-independent GLUT-mediated mechanism.

1.6 Mechanistic considerations for the rational design of GLUT-interacting glycoconjugates

The development of cytotoxic metal-based compounds capable of interacting with the glucose transporters, aiming at increasing their intracellular uptake and tumour selectivity, is the core question of the research here reported. However, in order to rationally design metal-glycoconjugates with effective GLUT-targeting properties, several considerations should be addressed. These features have been highlighted by numerous structural studies, and the recent resolution of the crystal structure of some glucose transporters has pointed out the importance of some structural requirements.

(a) What position(s) of glucose can be metal-functionalized?

Although glucose-conjugated anticancer drugs have been reported for nearly 20 years, there has been no systematic assessment of the influence of functionalizing different sites of the glucose scaffold on the biological activity of metal glycoconjugates. Only in a recent publication by Lippard and coworkers an extensive structure-activity relationship (SAR) study has been carried out on some platinum(II) glycoconjugates, by taking into account the functionalization site and/or the length of the spacer between the carbohydrate and the metal-containing core (**Figures 1.17,18**).[148,149]

The insulin-independent glucose transporter GLUT1 has been selected as the major target to study the interaction with glycoconjugates *via* kinetic or computational modeling. GLUT1 is a facilitative glucose uniporter protein of 492 amino acidic residues (55 kDa) constituted of 12 transmembrane helical domains,[142] and is widely overexpressed in various solid tumours.[175–177]

With reference to **Figure 1.24**, conjugation at the various sites of glucose can be rationalized as follows.

- The C1 and C3 hydroxyl groups and the oxygen of the pyran ring of glucose in the chair-shaped cyclic conformation are known to be involved in hydrogen bonding interactions with the amino acid residues within the binding pocket of the transporter. Thus, modifications of such positions reducing their capability to form hydrogen bonds may reduce affinity for GLUT1.[178,179] Nevertheless, conjugation at C1 and C3 may be tolerated, even with bulky substituents, as long as the hydrogen bonding interaction with the transporter can still take place.[180]

The type of anomeric conformation is also believed to play an important role in terms of recognition of glucose-like moieties by the transporter, albeit the preferred conformation of glycoconjugates is still subject to debate. Contrasting results have been obtained, since glucose conjugates in the β conformation should be preferred for GLUT1 transport, owing to its prevalence in aqueous solution.[181,182] However, the recent report of a crystal structures of both the α- and β-anomers of D-glucose bound to human GLUT3 suggest that also the α conformation may be recognized by GLUTs.[143]

- The C2, C4, and C6 hydroxyl groups of glucose are not involved in hydrogen bonding interactions with GLUT1 and, thus, inclusion of substituents in these positions may be tolerated. For example, the PET tracer 2-^{18}F-fluoro-2-deoxyglucose (^{18}F-FDG, **Figure 1.14**) is known to retain affinity towards GLUT1 and GLUT3. Also 2-NBDG (2-(*N*-(7-nitrobenz-2-oxa-1,3-diazol-4-yl)amino)-2-deoxylucose), where the C2 hydroxyl group is replaced by a fluorescent probe via an amino linkage, was shown to enter cells *via* a GLUT-mediated mechanism.[183,184] Conjugation at the C4 site is also reported not to reduce significantly affinity towards GLUTs. However, the lengthy synthetic routes required to functionalize such position of glucose have severely hampered the development of C4 conjugates so far.
- Experimental evidences indicate that functionalization at C6 may only slightly reduce the affinity to GLUT1.[135,178] In addition, the primary hydroxyl group possesses a different chemical reactivity compared to the other hydroxyl moieties of glucose. These two aspects contribute to make this position an intriguing site for conjugation of bioactive substrates.

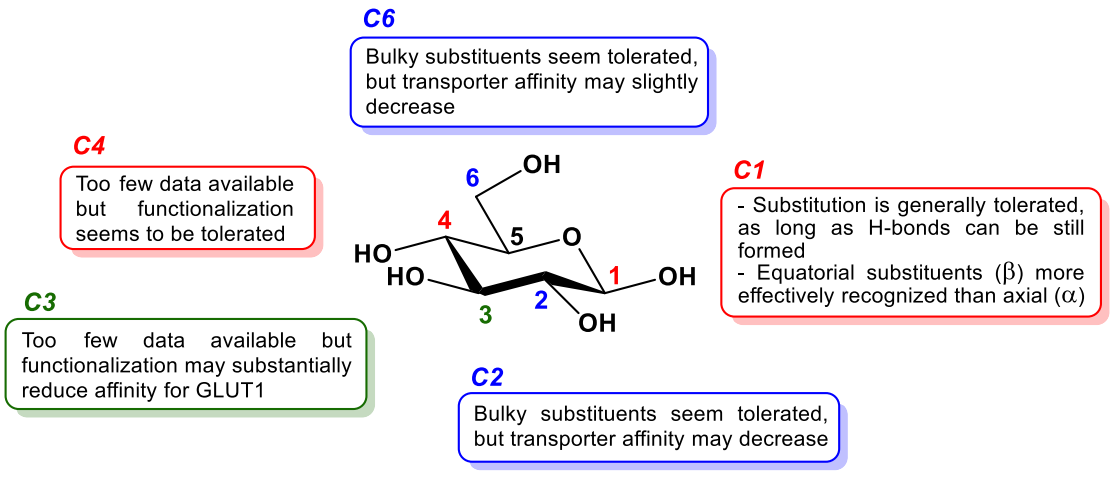

Figure 1.24. Rationalization of the structure-affinity relationship of D-glucose scaffolds as substrates for recognition by GLUT1.

(b) Can other sugars be efficient substrates to target GLUT1?

Carbohydrates other than glucose can be used as alternative substrates for recognition by glucose transporters. For example, GLUT1 has highest affinity for D-glucose, but can transport 2-deoxy-D-glucose, D-mannose, D-galactose and D-glucosamine, albeit with different binding affinities.[185,186] Different GLUTs proved selective for carbohydrates other than D-glucose; for instance, GLUT5 is specific for D-fructose, whereas GLUT13 is specific for *myo*-inositol.[187] Therefore, advantage can be taken from these diverse affinities, for example by designing a prodrug which may be specifically released by enzymatic cleavage inside the target. However, targeting only one glucose transporter among the others is a challenging task which goes beyond the scope of the work of this project. Therefore, as a first attempt to glycoconjugate metal-dithiocarbamato scaffolds, only selected derivatives of D-glucose were considered.

In order to achieve GLUTs targeting, protection of the glucose substrate (*e.g*. acetylation) should be avoided. In fact, it has been demonstrated that acetylated glucose gold(I) analogues of auranofin and platinum(IV) are internalized inside the cells but not through GLUT1 (although the involvement of other isoforms cannot be ruled out).[159,188] This is in contrast with what initially postulated for aminoglycoside antibiotics (also known as neoglycosides) and peracetylated glucose conjugates which were originally regarded as substrates targeting GLUT1.[189]

(c) Are linkers tolerated and, if so, what type of linker can be used?

Special attention should be paid to conjugating the metal scaffold to the glucose moiety in such a way that the capability of the latter to be recognized and taken up by GLUTs is not impaired. In this regard, the compound 2-glucose-SNAP (**Figure 1.15**), in which a glucosamine unit is bound to *S*-nitroso-*N*-acetylpenicillamine (SNAP) *via* an amide bond, is known to be a substrate recognized by GLUT1.[145] Consequently, the idea of functionalizing the carbohydrate with an amino acidic linker (e.g. pyperidine carboxamide) through the formation of an amide bond may be tolerated.

Alternatively, conjugation of linkers to sugars *via* formation of an ether linkage should maintain the H-bond acceptor character of oxygen atoms and, thus, retain affinity for the transporters. This principle has been widely exploited in the past, especially to functionalize the anomeric position, and proved successful to generate substrates with high affinity for GLUT1.

In this project, both linkage types, amide or ether bonds, have been explored to attach the carbohydrates to the metal scaffolds.

In summary, functionalization at C1, C2, and C6 position of the glucose ring have been most explored to date, demonstrating that some substitutions can be made with the resulting conjugate retaining affinity for GLUT1. Substitutions at C3 and C4 have been less explored, but contrasting data on their capability to retain affinity for GLUT1 are reported. Finally, linkers can be used, provided that the glucose scaffold can still form hydrogen bonds in specific sites, and that the length/bulkiness of the spacer arm do not interfere with the recognition of the substrate by GLUTs. These structural considerations provided the structural rationale for the design of the glycoconjugates here reported.

1.7 General aims of the research work and thesis outline

The present PhD research work has involved the preparation of a number of novel dithiocarbamato-containing metal-based glycoconjugates. On account of the aforementioned considerations, such derivatives have been rationally designed in order to meet the following requirements (**Figure 1.25**).

- A bioactive metal centre (i.e. anticancer core): different metal ions whose anticancer activity is well-known were used, such as gold(I/III), platinum(II) and manganese(I).
- A dithiocarbamato (–NCSS) motif. This scaffold provides chemoprotection against the further coordination of sulfur-containing biomolecules, thus protecting from drug inactivation. The ligand can coordinate either in a mono- or bidentate fashion, depending on the metal centre, its oxidation number, and the coordination sphere.
- Other ligands can saturate the coordination sphere. These ligands can be not only ancillary, but they can also play an active role (e.g. by tuning stability/kinetic of ligand release, lipophilicity, biological activity, etc.). In this project several ligands were exploited, such as halides (Cl^-, Br^-) and 2-benzylpyridine for gold(III), triphenylphosphine and *N*-heterocyclic carbene (NHC) ligands for gold(I), carbon monoxide (CO) for manganese(I).
- A linker can act as a spacer, by preventing the glucose moiety to not being recognized by the GLUTs. In fact, the presence of a close bulky non-glucose moiety may hamper the affinity/recognition with the transporter. In addition, the linker or the type of linkage with the sugar may be designed in a way to be cleaved once in the intracellular environment, thus releasing the bioactive part. This strategy is called prodrug approach.

- Finally, a glucose-like scaffold could act as a proper "Trojan Horse", being recognized, as already discussed in **chapter 1.8**, by the glucose transporter and thus internalizing the cytotoxic smart bomb.

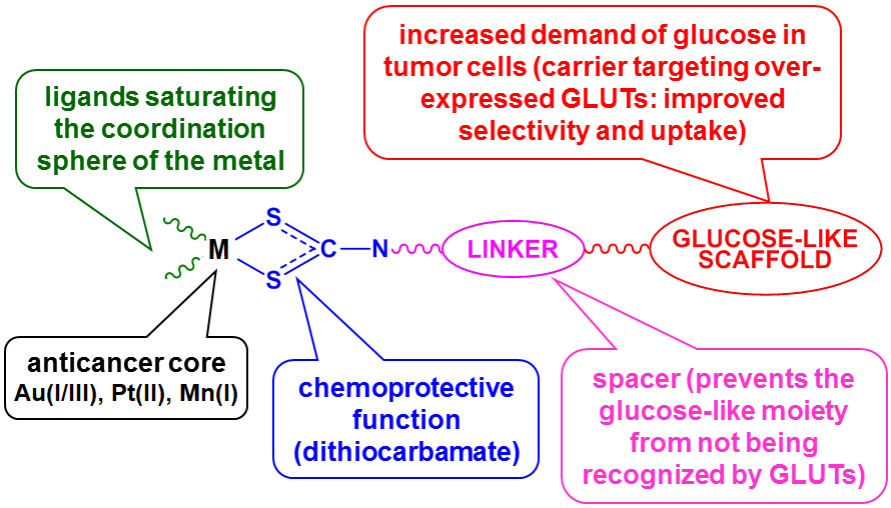

Figure 1.25. Schematic overview of the general structure of the compounds designed in this research project.

Here below a general outline of the aims are listed, which will be developed in the next sections:

i. Synthesis and characterization of the carbohydrates to be used as biomolecule for coupling reaction with preformed dithiocarbamato metal derivatives (Chapter 2).

ii. Synthesis and characterization of the zinc(II)-dithiocarbamato precursors and subsequent glycoconjugation with the obtained carbohydrates (Chapter 2).

iii. Synthesis, characterization, solution and biological activity studies of gold(III)-dithiocarbamato glycoconjugates (Chapter 3).

iv. Synthesis, characterization, solution and biological activity studies of gold(III)-dithiocarbamato organometallic glycoconjugates (Chapter 4).

v. Synthesis, characterization, solution and biological activity studies of gold(I)-dithiocarbamato glycoconjugates containing carbene and organophosphino ligands (Chapter 5).

vi. Synthesis, characterization and solution studies of novel carbonyl manganese(I)-dithiocarbamato glycoconjugates as potential carbon monoxide-releasing agents (Chapter 6).

vii. Finally, a concluding section will briefly describe some side-projects generated during this PhD research projects, in collaboration with other academic research group, regarding the design and obtainment of novel Pt(II)- and Ru(II)-arene dithiocarbamato glyconjugates, heterometallic Pt(IV)-Au(III) adducts, and

innovative methods for intracellular delivery of cytotoxic agents *via* encapsulation with nucleic acid nanoparticles (NANs) or mesoporous silica nanoparticles (MSNs) (Chapter 7).

1.8 References

[1] A. Mantovani, *Nature* **2009**, *457*, 36–37.
[2] L. A. Torre, F. Bray, R. L. Siegel, J. Ferlay, J. Lortet-Tieulent, A. Jemal, *CA Cancer J. Clin.* **2015**, *65*, 87–108.
[3] "Key facts – Cancer," http://www.who.int/news-room/fact-sheets/detail/cancer (last access on 15/02/2019).
[4] J. Ferlay, I. Soerjomataram, R. Dikshit, S. Eser, C. Mathers, M. Rebelo, D. M. Parkin, D. Forman, F. Bray, *Int. J. Cancer* **2015**, *136*, E359-386.
[5] D. Forman, J. Ferlay, *The Global and Regional Burden of Cancer*, in *World Cancer Report 2014* (Eds.: B. W. Stewart, C. P. Wild), International Agency for Research on Cancer, Lyon, **2014**, pp. 16–53.
[6] M. Plummer, C. de Martel, J. Vignat, J. Ferlay, F. Bray, S. Franceschi, *Lancet Glob. Health* **2016**, *4*, e609-616.
[7] G. Danaei, S. Vander Hoorn, A. D. Lopez, C. J. L. Murray, M. Ezzati, The Comparative Risk Assessment collaborating group (Cancers), *Lancet* **2005**, *366*, 1784–1793.
[8] R. A. DePinho, *Nature* **2000**, *408*, 248–254.
[9] "Cancer Treatment," https://www.cancer.gov/about-cancer/treatment (last access on 15/02/2019).
[10] R. Demicheli, M. W. Retsky, W. J. M. Hrushesky, M. Baum, I. D. Gukas, *Ann. Oncol.* **2008**, *19*, 1821–1828.
[11] L. Wyld, R. A. Audisio, G. J. Poston, *Nat. Rev. Clin. Oncol.* **2015**, *12*, 115–124.
[12] R. Baskar, K. A. Lee, R. Yeo, K.-W. Yeoh, *Int. J. Med. Sci.* **2012**, *9*, 193–199.
[13] P. P. Connell, S. Hellman, *Cancer Res* **2009**, *69*, 383–392.
[14] S. Gianfaldoni, R. Gianfaldoni, U. Wollina, J. Lotti, G. Tchernev, T. Lotti, *Open Access Maced. J. Med. Sci.* **2017**, *5*, 521.
[15] B. A. Jereczek-Fossa, H. R. Marsiglia, R. Orecchia, *Crit. Rev. Oncol. Hematol.* **2002**, *41*, 317–325.
[16] V. T. DeVita, E. Chu, *Cancer Res.* **2008**, *68*, 8643–8653.
[17] K. O. Alfarouk, C.-M. Stock, S. Taylor, M. Walsh, A. K. Muddathir, D. Verduzco, A. H. H. Bashir, O. Y. Mohammed, G. O. Elhassan, S. Harguindey, S. J. Reshkin, M. E. Ibrahim, C. Rauch, *Cancer Cell Int.* **2015**, *15*, 71.
[18] A. H. Partridge, H. J. Burstein, E. P. Winer, *J. Natl. Cancer Inst. Monogr.* **2001**, *30*, 135–142.
[19] S. P. Pricker, *Gold Bull.* **1996**, *29*, 53–60.
[20] F. E. G. Cox, *Clin. Microbiol. Rev.* **2002**, *15*, 595–612.
[21] S. Norn, H. Permin, E. Kruse, P. R. Kruse, *Dan. Medicinhist. Arbog.* **2008**, *36*, 21–40.
[22] H. H. A. Dollwet, J. R. J. Sorenson, *Trace Elem. Med.* **1985**, *2*, 80–87.
[23] K. Williams, *J. R. Soc. Med.* **2009**, *102*, 343–348.
[24] N. C. Lloyd, H. W. Morgan, B. K. Nicholson, R. S. Ronimus, *Angew. Chem. Int. Ed.* **2005**, *44*, 941–944.
[25] S. H. van Rijt, P. J. Sadler, *Drug Discov. Today* **2009**, *14*, 1089–1097.
[26] B. Rosenberg, L. Van camp, J. E. Trosko, V. H. Mansour, *Nature* **1969**, *222*, 385–386.
[27] B. Rosenberg, L. Van Camp, T. Krigas, *Nature* **1965**, *205*, 698–699.
[28] M. M. Peyrone, *Ann. Chim. Phys.* **1844**, *3*, 193.
[29] L. Kelland, *Nat. Rev. Cancer* **2007**, *7*, 573–584.
[30] T. C. Johnstone, K. Suntharalingam, S. J. Lippard, *Chem. Rev.* **2016**, *116*, 3436–3486.
[31] I. A. Riddell, *Cisplatin and Oxaliplatin: Our Current Understanding of Their Actions*, in *Metal Ions in Life Sciences*, vol. 18 (Eds.: A. Sigel, H. Sigel, E. Freisinger, R. K. O. Sigel), De Gruyter, Berlin/Boston, **2018**, pp. 1–42.
[32] S. J. Berners-Price, T. G. Appleton, in *Platinum-Based Drugs in Cancer Therapy* (Eds.: L.R. Kelland, N.P. Farrell), Humana Press, Totowa, **2000**, pp. 3–35.
[33] E. R. Jamieson, S. J. Lippard, *Chem. Rev.* **1999**, *99*, 2467–2498.
[34] A. Eastman, *The Mechanism of Action of Cisplatin: From Adducts to Apoptosis*, in *Cisplatin: Chemistry and Biochemistry of a Leading Anticancer Drug* (Ed.: B. Lippert), Wiley-Blackwell, Hoboken, **2006**, pp. 111–134.
[35] R. P. Miller, R. K. Tadagavadi, G. Ramesh, W. B. Reeves, *Toxins* **2010**, *2*, 2490–2518.

[36] M. Adams, I. J. Kerby, I. Rocker, A. Evans, K. Johansen, C. R. Franks, *Acta Oncologica* **1989**, *28*, 57–60.
[37] J. M. Ward, K. A. Fauvie, *Toxicol. Appl. Pharmacol.* **1976**, *38*, 535–547.
[38] Z. H. Siddik, *Oncogene* **2003**, *22*, 7265–7279.
[39] L. R. Kelland, P. Mistry, G. Abel, S. Y. Loh, C. F. O'Neill, B. A. Murrer, K. R. Harrap, *Cancer Res.* **1992**, *52*, 3857–3864.
[40] N. J. Wheate, S. Walker, G. E. Craig, R. Oun, *Dalton Trans.* **2010**, *39*, 8113–8127.
[41] I. Kostova, *Recent Pat. Anti-Canc.* **2006**, *1*, 1–22.
[42] L. Astolfi, S. Ghiselli, V. Guaran, M. Chicca, E. Simoni, E. Olivetto, G. Lelli, A. Martini, *Oncol. Rep.* **2013**, *29*, 1285–1292.
[43] L. P. Rybak, D. Mukherjea, S. Jajoo, V. Ramkumar, *Tohoku J. Exp. Med.* **2009**, *219*, 177–186.
[44] N. Pabla, Z. Dong, *Kidney Int.* **2008**, *73*, 994–1007.
[45] R. J. Cersosimo, *Cancer Treat. Rev.* **1989**, *16*, 195–211.
[46] D.-W. Shen, L. M. Pouliot, M. D. Hall, M. M. Gottesman, *Pharmacol. Rev.* **2012**, *64*, 706–721.
[47] L. Galluzzi, L. Senovilla, I. Vitale, J. Michels, I. Martins, O. Kepp, M. Castedo, G. Kroemer, *Oncogene* **2012**, *31*, 1869–1883.
[48] G. Ciarimboli, T. Ludwig, D. Lang, H. Pavenstädt, H. Koepsell, H.-J. Piechota, J. Haier, U. Jaehde, J. Zisowsky, E. Schlatter, *Am. J. Pathol.* **2005**, *167*, 1477–1484.
[49] S. Ishida, J. Lee, D. J. Thiele, I. Herskowitz, *Proc. Natl. Acad. Sci. USA*, **2002**, *99*, 14298–14302.
[50] P. D. Sadowitz, B. A. Hubbard, J. C. Dabrowiak, J. Goodisman, K. A. Tacka, M. K. Aktas, M. J. Cunningham, R. L. Dubowy, A.-K. Souid, *Drug. Metab. Dispos.* **2002**, *30*, 183–190.
[51] J. C. Dabrowiak, *Drug Metab. Dispos.* **2002**, *30*, 1378–1384.
[52] S. J. Berners-Price, P. W. Kuchel, *J. Inorg. Biochem.* **1990**, *38*, 305–326.
[53] K. Bracht, Boubakari, R. Grünert, P. J. Bednarski, *Anticancer Drugs* **2006**, *17*, 41–51.
[54] Boubakari, K. Bracht, C. Neumann, R. Grünert, P. J. Bednarski, *Archiv. Pharm. (Weinheim)* **2004**, *337*, 668–671.
[55] Y. Kasherman, S. Sturup, D. Gibson, *J. Med. Chem.* **2009**, *52*, 4319–4328.
[56] J. Reedijk, *Chem. Rev.* **1999**, *99*, 2499–2510.
[57] X. Wang And, Z. Guo, *Anticancer Agents Med. Chem.* **2007**, *7*, 19–34.
[58] M. Sooriyaarachchi, G. N. George, I. J. Pickering, A. Narendran, J. Gailer, *Metallomics* **2016**, *8*, 1170–1176.
[59] L. Ronconi, C. Nardon, G. Boscutti, D. Fregona, *Perspective Gold(III)-Dithiocarbamato Anticancer Therapeutics: Learning from the Past, Moving to the Future*, in *Advances in Anticancer Agents in Medicinal Chemistry* (Ed.: M. Prudhomme), Bentham Science Publishers, Bussum, **2013**, pp. 130–172.
[60] D. L. Bodenner, P. C. Dedon, P. C. Keng, R. F. Borch, *Cancer Res.* **1986**, *46*, 2745–2750.
[61] M. Treskes, U. Holwerda, L. G. J. Nijtmans, H. M. Pinedo, W. J. F. van der Vijgh, *Cancer Chemother. Pharmacol.* **1992**, *29*, 467–470.
[62] M. M. Jones, M. A. Basinger, *J. Appl.Toxicol.* **1989**, *9*, 229–233.
[63] N. Segovia, G. Crovetto, P. Lardelli, M. Espigares, *J. Appl. Toxicol.* **2002**, *22*, 353–357.
[64] M. Treskes, W. J. F. van der Vijgh, *Cancer Chemother. Pharmacol.* **1993**, *33*, 93–106.
[65] L. Ronconi, D. Fregona, *Dalton Trans.* **2009**, 10670.
[66] E. M. Nagy, L. Ronconi, C. Nardon, D. Fregona, *Mini Rev. Med. Chem.* **2012**, *12*, 1216–1229.
[67] E. M. Nagy, S. Sitran, M. Montopoli, M. Favaro, L. Marchiò, L. Caparrotta, D. Fregona, *J. Inorg. Biochem.* **2012**, *117*, 131–139.
[68] E. M. Nagy, A. Pettenuzzo, G. Boscutti, L. Marchiò, L. Dalla Via, D. Fregona, *Chem. Eur. J.* **2012**, *18*, 14464–14472.
[69] L. Giovagnini, S. Sitran, M. Montopoli, L. Caparrotta, M. Corsini, C. Rosani, P. Zanello, Q. P. Dou, D. Fregona, *Inorg. Chem.* **2008**, *47*, 6336–6343.
[70] L. Giovagnini, C. Marzano, F. Bettio, D. Fregona, *J. Inorg. Biochem.* **2005**, *99*, 2139–2150.
[71] V. Alverdi, L. Giovagnini, C. Marzano, R. Seraglia, F. Bettio, S. Sitran, R. Graziani, D. Fregona, *J. Inorg. Biochem.* **2004**, *98*, 1117–1128.
[72] D. Fregona, L. Giovagnini, L. Ronconi, C. Marzano, A. Trevisan, S. Sitran, B. Biondi, F. Bordin, *J. Inorg. Biochem.* **2003**, *93*, 181–189.
[73] A. Trevisan, C. Marzano, P. Cristofori, M. Borella Venturini, L. Giovagnini, D. Fregona, *Arch. Toxicol.* **2002**, *76*, 262–268.
[74] G. Faraglia, D. Fregona, S. Sitran, L. Giovagnini, C. Marzano, F. Baccichetti, U. Casellato, R. Graziani, *J. Inorg. Biochem.* **2001**, *83*, 31–40.
[75] https://clinicaltrials.gov/ct2/results?cond=&term=picoplatin&cntry=&state=&city=&dist= (last accessed on: 13/09/2018).
[76] F. I. Raynaud, F. E. Boxall, P. M. Goddard, M. Valenti, M. Jones, B. A. Murrer, M. Abrams, L. R. Kelland, *Clin. Cancer Res.* **1997**, *3*, 2063–2074.

[77] H. Osswald, N. Frank, *J. Cancer Res. Clin. Oncol.* **1990**, *116*, 448–452.
[78] C. Marzano, D. Fregona, F. Baccichetti, A. Trevisan, L. Giovagnini, F. Bordin, *Chem.-Biol. Interact.* **2002**, *140*, 215–229.
[79] C. Marzano, F. Bettìo, F. Baccichetti, A. Trevisan, L. Giovagnini, D. Fregona, *Chem.-Biol. Interact.* **2004**, *148*, 37–48.
[80] P. Cristofori, E. Zanetti, D. Fregona, A. Piaia, A. Trevisan, *Toxicol. Pathol.* **2007**, *35*, 270–275.
[81] C. Marzano, A. Trevisan, L. Giovagnini, D. Fregona, *Toxicol. in Vitro* **2002**, *16*, 413–419.
[82] I. Ott, *Coord. Chem. Rev.* **2009**, *253*, 1670–1681.
[83] L. Messori, G. Marcon, *Met. Ions Biol. Syst.* **2004**, *41*, 279–304.
[84] J. M. Madeira, D. L. Gibson, W. F. Kean, A. Klegeris, *Inflammopharmacol.* **2012**, *20*, 297–306.
[85] I. Landini, A. Lapucci, A. Pratesi, L. Massai, C. Napoli, G. Perrone, P. Pinzani, L. Messori, E. Mini, S. Nobili, *Oncotarget* **2017**, *8*, 96062–96078.
[86] C. Marzano, V. Gandin, A. Folda, G. Scutari, A. Bindoli, M. P. Rigobello, *Free Radic. Biol. Med.* **2007**, *42*, 872–881.
[87] A. Nakaya, M. Sagawa, A. Muto, H. Uchida, Y. Ikeda, M. Kizaki, *Leuk. Res.* **2011**, *35*, 243–249.
[88] T. Marzo, D. Cirri, C. Gabbiani, T. Gamberi, F. Magherini, A. Pratesi, A. Guerri, T. Biver, F. Binacchi, M. Stefanini, A. Arcangeli, L. Messori, *ACS Med. Chem. Lett.* **2017**, *8*, 997–1001.
[89] S.-J. Park, I.-S. Kim, *Br. J. Pharmacol.* **2005**, *146*, 506–513.
[90] C. K. Mirabelli, R. K. Johnson, C. M. Sung, L. Faucette, K. Muirhead, S. T. Crooke, *Cancer Res.* **1985**, *45*, 32–39.
[91] T. M. Simon, D. H. Kunishima, G. J. Vibert, A. Lorber, *Cancer Res.* **1981**, *41*, 94–97.
[92] S. Nobili, E. Mini, I. Landini, C. Gabbiani, A. Casini, L. Messori, *Med. Res. Rev.* **2010**, *30*, 550–580.
[93] https://clinicaltrials.gov/ct2/results?cond=&term=auranofin&cntry=&state=&city=&dist= (last access on 05/06/2018).
[94] C. Roder, M. J. Thomson, *Drugs R. D.* **2015**, *15*, 13–20.
[95] L. Ronconi, L. Giovagnini, C. Marzano, F. Bettìo, R. Graziani, G. Pilloni, D. Fregona, *Inorg. Chem.* **2005**, *44*, 1867–1881.
[96] C. Nardon, F. Chiara, L. Brustolin, A. Gambalunga, F. Ciscato, A. Rasola, A. Trevisan, D. Fregona, *ChemistryOpen* **2015**, *4*, 183–191.
[97] G. Boscutti, L. Feltrin, D. Lorenzon, S. Sitran, D. Aldinucci, L. Ronconi, D. Fregona, *Inorg. Chim. Acta* **2012**, *393*, 304–317.
[98] L. Ronconi, C. Marzano, P. Zanello, M. Corsini, G. Miolo, C. Maccà, A. Trevisan, D. Fregona, *J. Med. Chem.* **2006**, *49*, 1648–1657.
[99] D. Saggioro, M. P. Rigobello, L. Paloschi, A. Folda, S. A. Moggach, S. Parsons, L. Ronconi, D. Fregona, A. Bindoli, *Chem. Biol.* **2007**, *14*, 1128–1139.
[100] A. Bindoli, M. P. Rigobello, G. Scutari, C. Gabbiani, A. Casini, L. Messori, *Coord. Chem. Rev.* **2009**, *253*, 1692–1707.
[101] V. Milacic, D. Fregona, Q. P. Dou, *Histol. Histopathol.* **2008**, *23*, 101–108.
[102] V. Milacic, Q. P. Dou, *Coord. Chem. Rev.* **2009**, *253*, 1649–1660.
[103] D. Nandi, P. Tahiliani, A. Kumar, D. Chandu, *J. Biosci.* **2006**, *31*, 137–155.
[104] V. Milacic, D. Chen, L. Ronconi, K. R. Landis-Piwowar, D. Fregona, Q. P. Dou, *Cancer Res.* **2006**, *66*, 10478–10486.
[105] C. Marzano, L. Ronconi, F. Chiara, M. C. Giron, I. Faustinelli, P. Cristofori, A. Trevisan, D. Fregona, *Int. J. Cancer* **2011**, *129*, 487–496.
[106] T. Terada, K. Sawada, M. Irie, H. Saito, Y. Hashimoto, K. Inui, *Pflügers Arch. - Eur. J. Physiol.* **2000**, *440*, 679–684.
[107] M. Brandsch, I. Knütter, E. Bosse-Doenecke, *J. Pharm. Pharmacol.* **2008**, *60*, 543–585.
[108] M. Negom Kouodom, L. Ronconi, M. Celegato, C. Nardon, L. Marchiò, Q. P. Dou, D. Aldinucci, F. Formaggio, D. Fregona, *J. Med. Chem.* **2012**, *55*, 2212–2226.
[109] M. Negom Kouodom, G. Boscutti, M. Celegato, M. Crisma, S. Sitran, D. Aldinucci, F. Formaggio, L. Ronconi, D. Fregona, *J. Inorg. Biochem.* **2012**, *117*, 248–260.
[110] M. Celegato, D. Fregona, M. Mongiat, L. Ronconi, C. Borghese, V. Canzonieri, N. Casagrande, C. Nardon, A. Colombatti, D. Aldinucci, *Future Med. Chem.* **2014**, *6*, 1249–1263.
[111] J. M. Berg, J. L. Tymoczko, L. Stryer, *Biochemistry. 5th ed.* W. H. Freeman and Company, New York, **2002**.
[112] A. Pettenuzzo, R. Pigot, L. Ronconi, *Metallodrugs* **2016**, *1*, 36-61.
[113] M. G. Vander Heiden, L. C. Cantley, C. B. Thompson, *Science* **2009**, *324*, 1029–1033.
[114] O. Warburg, F. Wind, E. Negelein, *J. Gen. Physiol.* **1927**, *8*, 519–530.
[115] T. Pfeiffer, S. Schuster, S. Bonhoeffer, *Science* **2001**, *292*, 504–507.
[116] O. Warburg, *Science* **1956**, *123*, 309–314.
[117] W. H. Koppenol, P. L. Bounds, C. V. Dang, *Nat. Rev. Cancer* **2011**, *11*, 325–337.

[118] O. H. Warburg, *Clin. Orthop. Relat. Res.* **2010**, *468*, 2833–2839.
[119] N. C. Denko, *Nat. Rev. Cancer* **2008**, *8*, 705–713.
[120] G. L. Semenza, *Drug Discov. Today* **2007**, *12*, 853–859.
[121] S. Kizaka-Kondoh, S. Tanaka, H. Harada, M. Hiraoka, *Adv. Drug Deliv. Rev.* **2009**, *61*, 623–632.
[122] A. Giaccia, B. G. Siim, R. S. Johnson, *Nat. Rev. Drug Discov.* **2003**, *2*, 803–811.
[123] C. Granchi, F. Minutolo, *ChemMedChem* **2012**, *7*, 1318–1350.
[124] P. E. Porporato, S. Dhup, R. K. Dadhich, T. Copetti, P. Sonveaux, *Front. Pharmacol.* **2011**, *2*, 49.
[125] F.-Q. Zhao, A. F. Keating, *Curr. Genomics* **2007**, *8*, 113–128.
[126] M. L. Macheda, S. Rogers, J. D. Best, *J. Cell. Physiol.* **2005**, *202*, 654–662.
[127] A. Krzeslak, K. Wojcik-Krowiranda, E. Forma, P. Jozwiak, H. Romanowicz, A. Bienkiewicz, M. Brys, *Pathol. Oncol. Res.* **2012**, *18*, 721–728.
[128] R. A. Gatenby, R. J. Gillies, *Nat. Rev. Cancer* **2004**, *4*, 891–899.
[129] F. R. R. Ayala, R. M. Rocha, K. C. Carvalho, A. L. Carvalho, I.W. Da Cunha, S. V. Lourenço, F. A. Soares, *Molecules* **2010**, *15*, 2374–2387.
[130] R. A. Medina, G. I. Owen, *Biol. Res.* **2002**, *35*, 9–26.
[131] S. S. Gambhir, *Nat. Rev. Cancer* **2002**, *2*, 683–693.
[132] T. Zhan, M. Digel, E.-M. Küch, W. Stremmel, J. Füllekrug, *J. Cell. Biochem.* **2011**, *112*, 849–859.
[133] M. Kobori, H. Shinmoto, T. Tsushida, K. Shinohara, *Cancer Lett.* **1997**, *119*, 207–212.
[134] R. P. Singh, S. Dhanalakshmi, A. K. Tyagi, D. C. F. Chan, C. Agarwal, R. Agarwal, *Cancer Res.* **2002**, *62*, 3063–3069.
[135] T. Halmos, M. Santarromana, K. Antonakis, D. Scherman, *Eur. J. Pharmacol.* **1996**, *318*, 477–484.
[136] T. E. Wood, S. Dalili, C. D. Simpson, R. Hurren, X. Mao, F. S. Saiz, M. Gronda, Y. Eberhard, M. D. Minden, P. J. Bilan, A. Klip, R. A. Batey, A. D. Schimmer, *Mol. Cancer Ther.* **2008**, *7*, 3546–3555.
[137] D. A. Chan, P. D. Sutphin, P. Nguyen, S. Turcotte, E. W. Lai, A. Banh, G. E. Reynolds, J.-T. Chi, J. Wu, D. E. Solow-Cordero, M. Bonnet, J. U. Flanagan, D. M. Bouley, E. E. Graves, W. A. Denny, M. P. Hay, A. J. Giaccia, *Sci. Transl. Med.* **2011**, *3*, 94ra70.
[138] M. Kitagawa, M. Misawa, S. Ogawa, E. Tashiro, M. Imoto, *Biosci. Biotechnol. Biochem.* **2011**, *75*, 367–369.
[139] B. Hellwig, H. G. Joost, *Mol. Pharmacol.* **1991**, *40*, 383–389.
[140] Y. Zhao, E. B. Butler, M. Tan, *Cell Death Dis.* **2013**, *4*, e532.
[141] L. Sun, X. Zeng, C. Yan, X. Sun, X. Gong, Y. Rao, N. Yan, *Nature* **2012**, *490*, 361–366.
[142] D. Deng, C. Xu, P. Sun, J. Wu, C. Yan, M. Hu, N. Yan, *Nature* **2014**, *510*, 121–125.
[143] D. Deng, P. Sun, C. Yan, M. Ke, X. Jiang, L. Xiong, W. Ren, K. Hirata, M. Yamamoto, S. Fan, N. Yan, *Nature* **2015**, *526*, 391–396.
[144] N. Nomura, G. Verdon, H. J. Kang, T. Shimamura, Y. Nomura, Y. Sonoda, S. A. Hussien, A. A. Qureshi, M. Coincon, Y. Sato, H. Abe, Y. Nakada-Nakura, T. Hino, T. Arakawa, O. Kusano-Arai, H. Iwanari, T. Murata, T. Kobayashi, T. Hamakubo, M. Kasahara, S. Iwata, D. Drew, *Nature* **2015**, *526*, 397–401.
[145] G. Cantuaria, A. Magalhaes, R. Angioli, L. Mendez, R. Mirhashemi, J. Wang, P. Wang, M. Penalver, H. Averette, P. Braunschweiger, *Cancer* **2000**, *88*, 381–388.
[146] E. Briasoulis, I. Judson, N. Pavlidis, P. Beale, J. Wanders, Y. Groot, G. Veerman, M. Schuessler, G. Niebch, K. Siamopoulos, E. Tzamakou, D. Rammou, L. Wolf, R. Walker, A. Hanauske, *J. Clin. Oncol.* **2000**, *18*, 3535–3544.
[147] Q. Gao, M. Gallop, J.-N. Xiang, **2006**, US20060205677A1.
[148] M. Patra, T. C. Johnstone, K. Suntharalingam, S. J. Lippard, *Angew. Chem. Int. Ed.* **2016**, *55*, 2550–2554.
[149] M. Patra, S. G. Awuah, S. J. Lippard, *J. Am. Chem. Soc.* **2016**, *138*, 12541–12551.
[150] P. Liu, Y. Lu, X. Gao, R. Liu, D. Zhang-Negrerie, Y. Shi, Y. Wang, S. Wang, Q. Gao, *Chem. Commun.* **2013**, *49*, 2421.
[151] H. Li, X. Gao, R. Liu, Y. Wang, M. Zhang, Z. Fu, Y. Mi, Y. Wang, Z. Yao, Q. Gao, *Eur. J. Med. Chem.* **2015**, *101*, 400–408.
[152] T. Li, X. Gao, L. Yang, Y. Shi, Q. Gao, *ChemMedChem* **2016**, *11*, 1069–1077.
[153] J. Han, X. Gao, R. Liu, J. Yang, M. Zhang, Y. Mi, Y. Shi, Q. Gao, *Chem. Biol. Drug Des.* **2016**, *87*, 867–877.
[154] Q. Mi, Y. Ma, X. Gao, R. Liu, P. Liu, Y. Mi, X. Fu, Q. Gao, *J. Biomol. Struct. Dyn.* **2016**, *34*, 2339–2350.
[155] M. Wu, H. Li, R. Liu, X. Gao, M. Zhang, P. Liu, Z. Fu, J. Yang, D. Zhang-Negrerie, Q. Gao, *Eur. J. Med. Chem.* **2016**, *110*, 32–42.
[156] X. Gao, S. Liu, Y. Shi, Z. Huang, Y. Mi, Q. Mi, J. Yang, Q. Gao, *Eur. J. Med. Chem.* **2017**, *125*, 372–384.

[157] R. Liu, Z. Fu, M. Zhao, X. Gao, H. Li, Q. Mi, P. Liu, J. Yang, Z. Yao, Q. Gao, *Oncotarget* **2017**, *8*, 39476–39496.
[158] J. Ma, Q. Wang, Z. Huang, X. Yang, Q. Nie, W. Hao, P. G. Wang, X. Wang, *J. Med. Chem.* **2017**, *60*, 5736–5748.
[159] Q. Wang, Z. Huang, J. Ma, X. Lu, L. Zhang, X. Wang, P. G. Wang, *Dalton Trans.* **2016**, *45*, 10366–10374.
[160] J. Ma, Q. Wang, X. Yang, W. Hao, Z. Huang, J. Zhang, X. Wang, P. G. Wang, *Dalton Trans.* **2016**, *45*, 11830–11838.
[161] W. C. Eckelman, G. Meinken, P. Richards, *J. Nucl. Med.* **1972**, *13*, 577–581.
[162] M. L. Bowen, C. Orvig, *Chem. Commun.* **2008**, *0*, 5077–5091.
[163] R. Alberto, K. Ortner, N. Wheatley, R. Schibli, A. P. Schubiger, *J. Am. Chem. Soc.* **2001**, *123*, 3135–3136.
[164] R. Alberto, J. K. Pak, D. van Staveren, S. Mundwiler, P. Benny, *Biopolymers* **2004**, *76*, 324–333.
[165] A. Badar, J. Williams, R. T. de Rosales, R. Tavaré, F. Kampmeier, P. J. Blower, G. E. Mullen, *EJNMMI Res.* **2014**, *4*, 14.
[166] M. P. Coogan, R. P. Doyle, J. F. Valliant, J. W. Babich, J. Zubieta, *J. Labelled Compd. Radiopharm.* **2014**, *57*, 255–261.
[167] R. Schibli, C. Dumas, J. Petrig, L. Spadola, L. Scapozza, E. Garcia-Garayoa, P. A. Schubiger, *Bioconjugate Chem.* **2005**, *16*, 105–112.
[168] H.-W. Liu, K. Y. Zhang, W. H.-T. Law, K. K.-W. Lo, *Organometallics* **2010**, *29*, 3474–3476.
[169] W. H.-T. Law, L. C.-C. Lee, M.-W. Louie, H.-W. Liu, T. W.-H. Ang, K. K.-W. Lo, *Inorg. Chem.* **2013**, *52*, 13029–13041.
[170] M.-W. Louie, H.-W. Liu, M. H.-C. Lam, Y.-W. Lam, K. K.-W. Lo, *Chem. Eur. J.* **2011**, *17*, 8304–8308.
[171] C. F. Burant, J. Takeda, E. Brot-Laroche, G. I. Bell, N. O. Davidson, *J. Biol. Chem.* **1992**, *267*, 14523–14526.
[172] K. K.-W. Lo, W. H.-T. Law, J. C.-Y. Chan, H.-W. Liu, K. Y. Zhang, *Metallomics* **2013**, *5*, 808.
[173] K. Y. Zhang, K. K.-S. Tso, M.-W. Louie, H.-W. Liu, K. K.-W. Lo, *Organometallics* **2013**, *32*, 5098–5102.
[174] L. N. Lameijer, S. L. Hopkins, T. G. Brevé, S. H. C. Askes, S. Bonnet, *Chem. Eur. J.* **2016**, *22*, 18484–18491.
[175] H. Sasaki, M. Shitara, K. Yokota, Y. Hikosaka, S. Moriyama, M. Yano, Y. Fujii, *Mol. Med. Rep.* **2012**, *5*, 599–602.
[176] K. C. Carvalho, I. W. Cunha, R. M. Rocha, F. R. Ayala, M. M. Cajaíba, M. D. Begnami, R. S. Vilela, G. R. Paiva, R. G. Andrade, F. A. Soares, *Clinics (Sao Paulo)* **2011**, *66*, 965–972.
[177] Y. R. Hussein, S. Bandyopadhyay, A. Semaan, Q. Ahmed, B. Albashiti, T. Jazaerly, Z. Nahleh, R. Ali-Fehmi, *Transl. Oncol.* **2011**, *4*, 321–327.
[178] J. E. G. Barnett, G. D. Holman, K. A. Munday, *Biochem. J.* **1973**, *131*, 211–221.
[179] M. Mueckler, C. Makepeace, *Biochemistry* **2009**, *48*, 5934–5942.
[180] M. Patt, D. Sorger, M. Scheunemann, G. Stöcklin, *Appl. Radiat. Isot.* **2002**, *57*, 705–712.
[181] E. C. Calvaresi, P. J. Hergenrother, *Chem. Sci.* **2013**, *4*, 2319–2333.
[182] Y.-S. Lin, R. Tungpradit, S. Sinchaikul, F.-M. An, D.-Z. Liu, S. Phutrakul, S.-T. Chen, *J. Med. Chem.* **2008**, *51*, 7428–7441.
[183] K. Yamada, M. Nakata, N. Horimoto, M. Saito, H. Matsuoka, N. Inagaki, *J. Biol. Chem.* **2000**, *275*, 22278–22283.
[184] K. Yoshioka, H. Takahashi, T. Homma, M. Saito, K. B. Oh, Y. Nemoto, H. Matsuoka, *Biochim. Biophys. Acta* **1996**, *1289*, 5–9.
[185] P. G. LeFevre, *Pharmacol. Rev.* **1961**, *13*, 39–70.
[186] D. Melisi, A. Curcio, E. Luongo, E. Morelli, M. G. Rimoli, *Curr. Top. Med. Chem.* **2011**, *11*, 2288-2298.
[187] M. Mueckler, B. Thorens, *Mol. Aspects Med.* **2013**, *34*, 121–138.
[188] M. Wenzel, A. de Almeida, E. Bigaeva, P. Kavanagh, M. Picquet, P. Le Gendre, E. Bodio, A. Casini, *Inorg. Chem.* **2016**, *55*, 2544–2557.
[189] R. D. Goff, J. S. Thorson, *J. Med. Chem.* **2010**, *53*, 8129–8139.

Chapter 2

Synthesis of the carbohydrate and the zinc(II)-dithiocarbamato precursors

Chapter 2. Synthesis of the carbohydrate and the zinc(II)-dithiocarbamato precursors

For full experimental procedures and characterizations see Chapter 8.

2.1 Rationale

As previously pointed out, the complexity of carbohydrate chemistry may severely hamper glycoconjugation to drugs, in particular when metal-based scaffolds are involved. Therefore, more efficient synthetic approaches to glyco-functionalization are required. As shown in **Figure 2.1**, the suggested strategy relies on the pre-generation of a zinc(II)-dithiocarbamato glycoconjugate precursor followed by the transfer of the whole dithiocarbamato ligand to the desired metal centre through a ligand exchange reaction (also called transmetallation).

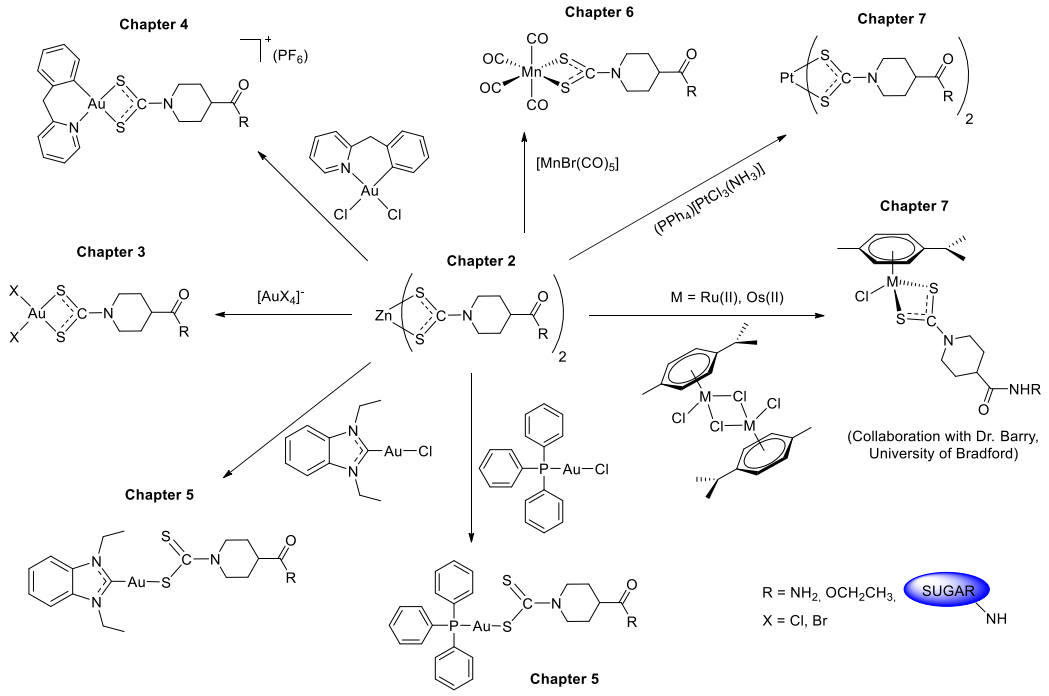

Figure 2.1. Schematic overview of the metal-based conjugates generated in this PhD project by means of transmetallation reaction from zinc(II) intermediates.

Specifically, a facile and reproducible protocol has been developed, in which an amino acidic linker (*i.e.* isonipecotic acid) is functionalized with the dithiocarbamato moiety (–NCSS) at the amino terminus and coordinated to a zinc(II) centre in a one-pot reaction. Subsequently, the carboxylate tail is first activated and then coupled to an amino sugar *via* an amide link. The rationale of this strategy is based on the following considerations.

- Zinc(II) is a "borderline" Lewis acid [1] and, although it forms stable covalent adducts with the "soft" dithiocarbamato ligands,[2] it is well-known to serve as a source of such ligands for the transfer of a "softer" metal (possibly much more reliable and

controllable than the commonly employed ionic sodium, potassium or ammonium dithiocarbamato salts).[3] Therefore, zinc(II) dithiocarbamates may undergo transmetallation reactions with many "soft" transition metals.[4–6]

- The use of an amino acidic linker between the dithiocarbamato function and the conjugated sugar has a two-fold purpose. From a practical synthetic point of view it allows the straightforward conversion of the amino terminus into an –NCSS group without worrying about the possible side-reactions involving the carbohydrate scaffold, should the latter be present.[7] Moreover, the carboxylic function can be easily activated with *N*,*N*,*N*′,*N*′-tetramethyl-*O*-(*N*-succinimidyl)uronium tetrafluoroborate (TSTU) and subsequently coupled to an amino sugar to attain glycoconjugation through the formation of an amide bond.[8]
- From a biological perspective, if the final goal is to target the GLUTs overexpressed in tumours to achieve selectivity, the anomeric position of the glucose-like unit should be sufficiently accessible to be recognized (and, thus, to allow internalization inside the tumour cell) by such transporters.[9] Therefore, the inclusion of a rigid linker (like the isonipecotic moiety used in this work) would reduce the steric hindrance around the anomeric site of the sugar, thus allowing, at least in principle, its recognition by GLUTs.

2.2 Synthesis of the carbohydrate precursors

Based on the previous considerations, four different glucose-like scaffolds bearing an amino group (**Figure 2.2**) have been chosen. All the isolated intermediates were characterized by monodimensional ^{1}H and $^{13}C\{^{1}H\}$ NMR, bidimensional [^{1}H-^{1}H] COSY and [^{1}H-^{13}C] HMQC NMR (where needed), and FT-IR spectroscopy.

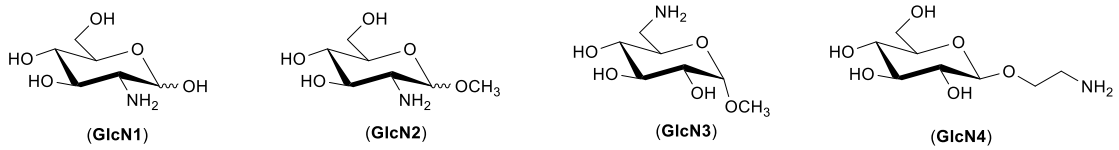

Figure 2.2. Chemical structures of the amino sugar precursors coupled to metal-based dithiocarbamates.

- 2-Amino-2-deoxy-(α,β)-D-glucose ((α,β)-D-glucosamine, **GlcN1**) hydrochloride, bearing the amino function in the C2 position of the glucose, is commercially available and is sold as a mixture of α and β anomers (the former largely predominating, see Chapter 8 for full characterization). Glucosamine-appended ligands have been already used in some cases to obtain metal-glycoconjugates.[10,11]

- 1-*O*-methyl-2-amino-2-deoxy-(α,β)-D-glucopyranoside (**GlcN2**) acetic acid was prepared as ammonium acetate according to a literature procedure.[12,13] An α:β anomers ratio of approximately 5:1 was obtained. Methylation of the anomeric hydroxyl group (C1 position) aimed at avoiding side-reactions involving the anomeric carbon in the subsequent steps, as well as at simplifying the NMR characterization of the final products (see Chapter 8 for full synthetic procedure and characterization).
- 1-*O*-methyl-6-amino-6-deoxy-α-D-glucopyranoside (**GlcN3**) was prepared according to a literature procedure[14–16] with the aim of investigating the feasibility of our synthetic method for amino sugars bearing the amino function in positions other than the C2 site of the glucose (i.e. C6 position, see Chapter 8 for full synthetic procedure and characterization).
- 2-Aminoethyl-β-D-glucopyranoside (**GlcN4**) was prepared according to a modified literature procedure[17] in order to design a derivative bearing a spacer arm attached to the C1 position of the glucose ring *via* an ether linkage, as shown in **Figure 2.3**.

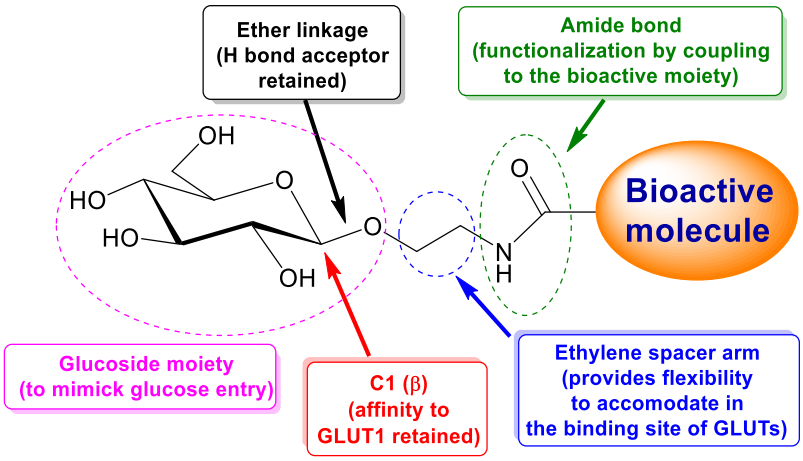

Figure 2.3. Schematic overview on the rational design of C1-substitued glycoconjugates.

In this specific case, the avowed goals are: i) to obtain a derivative conjugated at the C1 position which is expected to retain high affinity to GLUT1;[18,19] ii) to add a short spacer arm, such as an ethylene moiety (–CH_2CH_2–), which should provide flexibility for fitting into the cavity of the active site of the transporter; iii) and to include an ether linkage, which can retain affinity to the transporter by maintaining an H bond acceptor crucial for substrate recognition[9] and, subsequently, may be cleaved *in cellulo* by β-glucosidase enzymes, devoted to hydrolyze β-glycosidic bonds of glucosides or other oligosaccharides. Consequently, the conjugate would

act as a prodrug, first delivered as a whole through its sugar cargo and then the bioactive aglycone released after enzymatic cleavage.[20,21]

Although the **GlcN4** amino sugar was already reported in the literature, its multistep synthesis has been modified and optimized as discussed below.

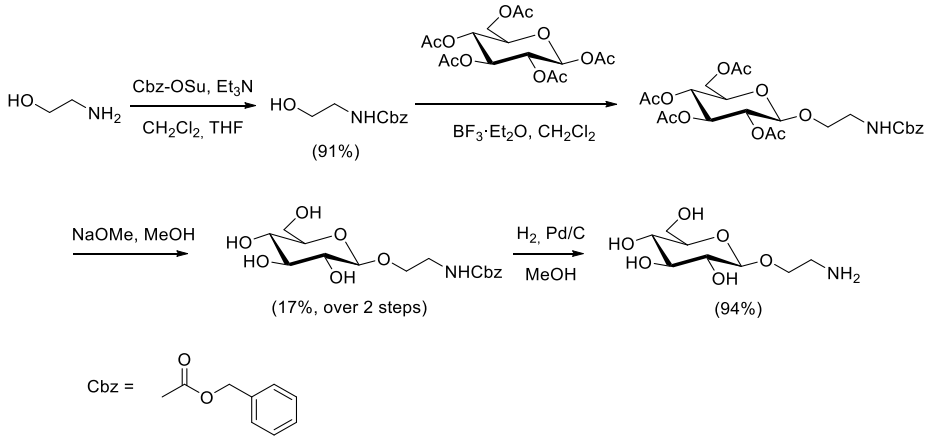

Figure 2.4. General synthetic route to the synthesis of 2-aminoethyl β-D-glucopyranoside (**GlcN4**).

With reference to **Figure 2.4**, the sugar was functionalized with an ethanolamine arm in the C-1 anomeric position by means of a glycosylation reaction of β-D-glucose pentaacetate (the glycosyl donor) with Cbz-ethanolamine (the glycosyl acceptor) in the presence of boron trifluoride diethyletherate ($BF_3 \cdot Et_2O$). The amino group of ethanolamine must be protected in order to avoid side-reactions giving glycosylamines.[22,23] Cbz-ethanolamine (carbobenzyloxy- or Z-) was obtained through a modified reaction protocol for the protection of the amino moiety using *N*-(benzyloxycarbonyloxy)succinimide (Z-OSu or Cbz-OSu) as a source of Cbz-protecting groups.[24,25] This intermediate was preferred instead of using the well-established protocol with 2-azidoethanol because organic azides with low molecular weight are potentially explosive when manipulated dry.[26] The Cbz-protecting group can be easily removed in nearly quantitative yields by means of catalytic hydrogenation at the end of the reaction. Furthermore, the Cbz-protecting group is stable under acidic and alkaline conditions, both used during the glycosylation and deacetylation steps, respectively.

The glycosylation step is critical due to the relatively low yields (a number of side-products may be generated), a quite high side-product profile, and the need of working strictly under anhydrous conditions when using Lewis acids. The chosen Lewis acid for this type of reaction is boron trifluoride diethyletherate, required to activate the glycosyl donor. After selective removal of the acetyl group in the anomeric position by BF_3, the reaction may proceed with generation of a flattened glycosyl cation that can be stabilized by the formation of an oxocarbenium intermediate (**Figure 2.5**). In presence of an acyl

neighbouring group, an acyloxonium intermediate can be formed as a result of the participation from the carbonyl group in position C2. This stabilization is also called anchimeric assistance. Subsequently, the attack by any nucleophilic glycosyl acceptor (ROH) may generate the corresponding α,β-glycosides (usually present as a mixture), or a 1,2-orthoester if the acceptor attacks the carbonyl carbon atom of the acyloxonium intermediate.[27] Therefore, the use of dry solvents and an inert atmosphere during the reaction prevents the nucleophilic attack of water molecules, thus giving the specie 2,3,4,6-tetraacetylglucose (as mixture of α,β-anomers) with consequent diminished yields.

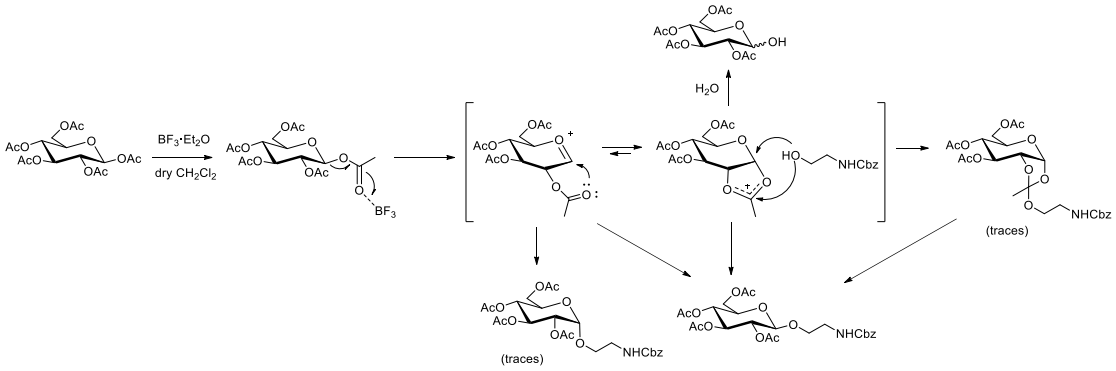

Figure 2.5. Reaction mechanism of the glycosylation reaction of pentaacetylglucose with Cbz-aminoethanol in the presence of $BF_3 \cdot Et_2O$.

The isolated crude of reaction is a mixture consisting of 2-(benzyloxycarbonyl)aminoethyl 2,3,4,6-tetra-*O*-acetyl-β-D-glucopyranoside, 2,3,4,6-α,β-D-tetraacetylglucose, and only traces of the 1,2-orthoester and 2-(benzyloxycarbonyl)aminoethyl 2,3,4,6-tetra-*O*-acetyl-α-D-glucopyranoside. The prevalent formation of the desired β anomer over the α is indicative of the regioselective assistance of the acetyl group, while the formation of unwanted 2,3,4,6-tetraacetylglucose can be due to the presence of moisture during the reaction.

Purification of the compound by column chromatography proved challenging since the product and the side-product 2,3,4,6-tetraacetylglucose run with similar retention factors. For the sake of easiness, the crude was kept as a mixture of these compounds for the next step, the Zemplen deacetylation.[28] After deacetylation in methanol with a catalytic amount of sodium methylate, the corresponding deacetylated products, Z-aminoethyl glucose and glucose, run with much different retention factors, which makes the subsequent purification step easier to carry out (**Figure 2.6**).

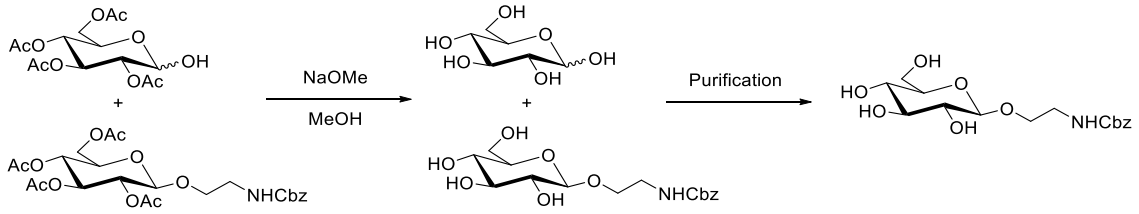

Figure 2.6. Reaction scheme of the Zemplen deactylation step and subsequent purification.

Finally, catalytic hydrogenation with Pd/C in methanol removes the Z- protecting group, affording the free amine 2-aminoethyl β-D-glucopyranoside (**GlcN4**). The overall reaction yield over the multisynthetic steps is quite low (ca. 16%, based on β-D-glucose pentaacetate, see Chapter 8 for full synthetic procedure and characterizations).

2.3. Dithiocarbamate ligands and zinc(II)-dithiocarbamato precursors

2.3.1 Synthesis of the dithiocarbamate ligands

Dithiocarbamates of primary and secondary amines are generally synthesized by reaction with carbon disulfide (CS_2) under basic conditions (e.g. NaOH, KOH, Et_3N) at low temperature, yielding the corresponding dithiocarbamato salts.[29,30] Dithiocarbamates generated from primary amines are often unstable and tend to decompose to give the corresponding isothiocyanates.[31] The secondary amine counterparts are generally more stable and a number of simple dithiocarbamates have been prepared and isolated as sodium or ammonium salts.[32] Nevertheless, isolation and storage of free dithiocarbamates is often challenging since, at room temperature, they may decompose back to the starting amine and CS_2, especially under acidic conditions.[33] For this reason, dithiocarbamates are best prepared *in situ*: once generated in solution they are reacted with the metal precursor in the appropriate stoichiometric ratio to obtain the corresponding metal-dithiocarbamato derivative.[34]

In principle, direct functionalization of an amino sugar could be achieved. To the best of our knowledge, only one of such example is reported in the literature. Zhang and coworkers synthesized and isolated 2-deoxy-2-dithiocarbamato-D-glucose as sodium salt by reacting D-glucosamine hydrochloride with CS_2 and NaOH, and used it to obtain the corresponding ^{99m}Tc-nitrido bis-dithiocarbamato complex.[35] Unfortunately, when following the same experimental procedure, the analogous gold(III) complex could not be obtained. Notwithstanding various attempts, the experimental conditions employed always led to the reduction of gold(III) to gold(I) and the simultaneous degradation of the carbohydrate scaffold resulting from the intramolecular attack of the –NCSS group located in the C2 position of the glucose to the anomeric site (**Figure 2.7**).[36]

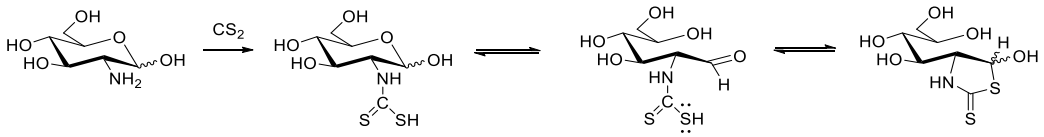

Figure 2.7. Rearrengement of glucosamine-dithiocarbamate in the open form and subsequent formation of the thioazolidinethione cyclization side-product.

Taking into account the aforementioned issues, an alternative pathway to obtain dithiocarbamato-based glycoconjugates proved necessary. Accordingly, the strategy involving the pre-generation of zinc(II)-dithiocarbamato complexes and the subsequent transfer of the dithiocarbamato ligand to other metal centres was devised.[37]

The feasibility of such synthetic approach was first evaluated by generating non-glycosylated dithiocarbamato complexes coordinated to various metal ions *via* transmetallation from the corresponding zinc(II) intermediates. Specifically, the focus was on ethyl isonipecotate (Inp-OEt) and isonipecotamide (Inp-NH_2) dithiocarbamates as model ligands since their amino group is a symmetric secondary amine and, as such, can lead to very stable, symmetric compounds.[2] In addition, isonipecotamide would serve as an aglycone for further structure-activity relationship studies (*i.e.* model non-glycosylated compounds).

The isonipecotamide-dithiocarbamato ligand was obtained as sodium salt (Na(dtc-InpNH_2)·MeOH, **Scheme 2.1**, right) through a conventional protocol,[38] in which isonipecotamide is reacted with an equimolar amount of sodium hydroxide (NaOH) and carbon disulfide (CS_2) at 0°C (**Scheme 2.1**, left) in methanol.

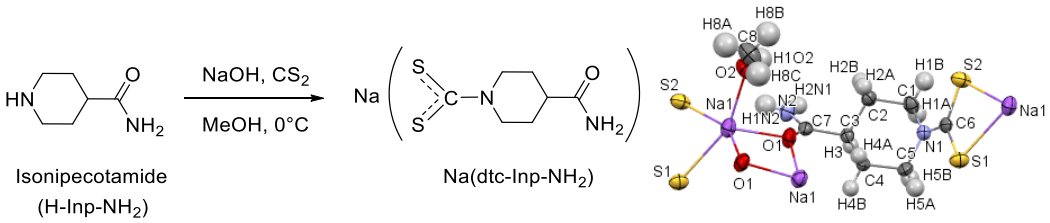

Scheme 2.1. Synthetic route to the isonipecotamide-dithiocarbamato ligand (left), and its X-ray crystal structure with atom numbering scheme of the methanol solvate (50% displacement ellipsoids, CCDC 1835869, right).

However, when moving toward ester scaffolds, such as ethyl isonipecotate, the use of alkalis as a base (NaOH, KOH, *etc.*) is not appropriate owing to the formation of transesterification side-products. Therefore, one equiv. of starting amine can serve as a reagent while another equiv. as a base, leading to the corresponding dithiocarbamato ligand as an ammonium salt without any use of sodium hydroxide. Ethyl isonipecotate-dithiocarbamate, (H_2-Inp-OEt)(dtc-Inp-OEt), was obtained in this way (**Scheme 2.2**).[39]

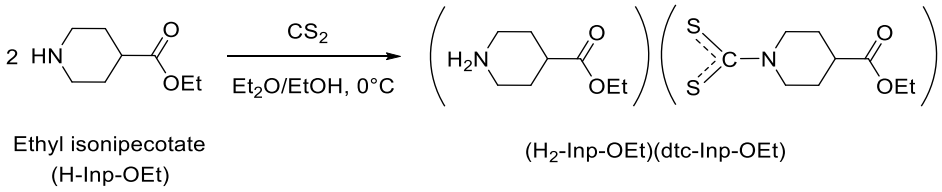

Scheme 2.2. Synthetic route to the ethyl isonipecotate dithiocarbamate ligand.

The ligand with sarcosine (*N*-methyl glycine) ethyl ester was also obtained in a similar way (**Scheme 2.3**), albeit the final product could not be easily isolated as an ammonium salt. Thus, the sarcosinedithiocarbamato ligand was precipitated by addition of a tetraphenylphosphonium chloride aqueous solution and subsequent exchange of the positive counterion. Good quality crystals (yellow plates) for XRD crystallography, shown in **Scheme 2.3** were obtained by evaporation of an aqueous solution of the ligand. The sarcosine ethyl ester dithiocarbamato ligand, (PPh_4)(dtc-Sar-OEt) (Sar: sarcosine, *N*-methyl glycine), was mainly used to obtain the corresponding of gold(I)-carbene complexes (see Chapter 5).

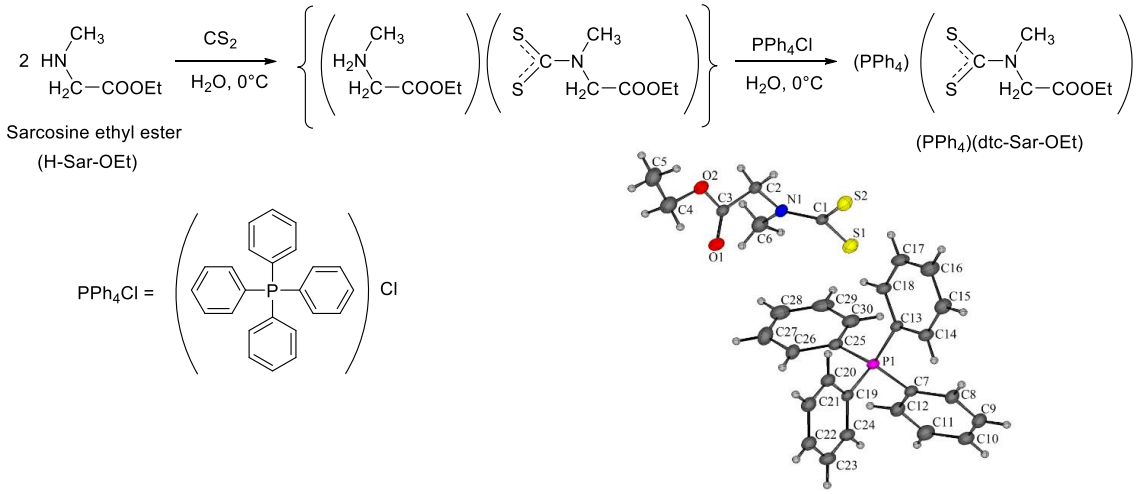

Scheme 2.3. Synthetic route to the tetraphenylphosphonium ethyl sarcosine dithiocarbamato ligand (up), and its X-ray crystal structure with atom numbering scheme (50% displacement ellipsoids, down).

2.3.2 Synthesis of the zinc(II)-dithiocarbamato precursors

Both [Zn(dtc-Inp-OEt)$_2$] (**Zn1**) and [Zn(dtc-Inp-NH$_2$)$_2$] (**Zn2**) were obtained in a one-pot reaction. **Zn2** was also obtained by reacting the free ligand Na(dtc-Inp-NH$_2$)·MeOH with zinc acetate dihydrate ([Zn(OAc)$_2$·2H$_2$O]) in a 2:1 ligand-to-metal ratio (**Scheme 2.4**).

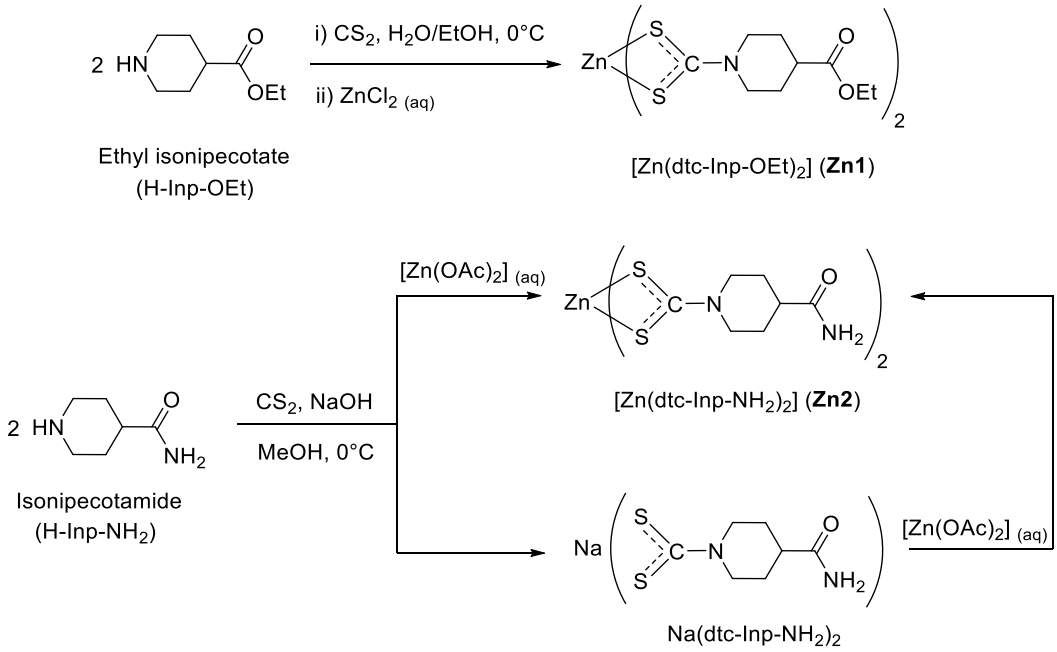

Scheme 2.4. Synthetic routes to the synthesis of [Zn(dtc-Inp-OEt)$_2$] (**Zn1**) and [Zn(dtc-Inp-NH_2)$_2$] (**Zn2**).

IR spectroscopy proved useful to identify the synthesized compounds. By comparison with the spectra recorded for the starting ethyl isonipecotate and isonipecotamide reagents, the appearance of a strong band at 1494 (**Zn1**)/1492 (**Zn2**) cm^{-1} in the zinc(II) derivatives (the so-called "thioureide" band, ν(N–CSS)) is consistent with a chelating dithiocarbamato ligand coordinated to a zinc(II) centre.[40,41] Additionally, the detection of a single band at ca. 1000 cm^{-1} in all complexes (attributed to the ν_a(SCS)) clearly supports a symmetrical bidentate coordination of the –NCSS moiety to the metal centers, in agreement with the Bonati-Ugo criterion.[42] In the far-IR spectra of a number of metal-dithiocarbamato complexes, bands recorded in the range 420-320 cm^{-1} are regarded as highly diagnostic since they are assigned to the metal-sulfur stretching vibrations. **Zn1** and **Zn2** show an intense absorption at ca. 395 cm^{-1} originating from the $\nu_a(ZnS_4)$,[43] whereas the corresponding symmetric stretching is absent as it is not IR-active in the tetrahedral bis-dithiocarbamato zinc derivatives.[44]

Mono- and multinuclear NMR spectroscopy provided further insights into the identification of the dithiocarbamato complexes. For example, compared with the starting ethyl isonipecotate reagent, a general downfield shift of the proton signals is observed for the zinc(II) intermediate **Zn1**. This is consistent with the decreased electron density experienced by the hydrogen atoms of the isonipecotate scaffold upon introducing the dithiocarbamato moiety and the subsequent coordination to the metal centres.[45] As expected, the larger shift involves the piperidine hydrogens, the $C^{2',6'}H$ equatorial protons undergoing a 1.9 ppm downfield shift. On moving away from the dithiocarbamato

moiety, the magnitude of the chemical shift change decreases until being negligible for the farther ester group.[46]

The most diagnostic peak recorded in the $^{13}C\{^{1}H\}$ NMR spectra is attributed to the dithiocarbamic carbon atom and is generally found in the range 180-220 ppm.[47] It is usually assumed that the ^{13}C chemical shifts of the −NCSS moiety are strongly dependent on both the type of metal-dithiocarbamate bonding and the oxidation state of the metal centre. As to the dithiocarbamato complexes of transition metals owning a d^{10} electron configuration (such as zinc(II)), the $\delta(N^{13}CSS)$ peaks are recorded in the range 202-206 ppm.[48]

Crystals suitable for X-ray diffraction crystallography were obtained for **Zn1** (**Figure 2.8**). Although crystal structures of monomeric *bis*-dithiocarbamato-zinc(II) complexes are known, which have highly strained structures with two four-membered rings,[49] a common arrangement for this class of compounds is dinuclear centrosymmetric,[37] and this was observed also for **Zn1**. Dimeric structures, in which one four-membered zinc(II)-dithiocarbamato ring is retained whereas the other has opened to form an eight-membered ring, were first reported for the *bis*-diethyldithiocarbamato zinc(II) complex, and have since been reported for several other analogous derivatives.[50] Relief of distortion is the most likely reason for the adoption of the dimeric structure, and the angle at the zinc(II) center in the four-membered ring is 75.79(4)°.

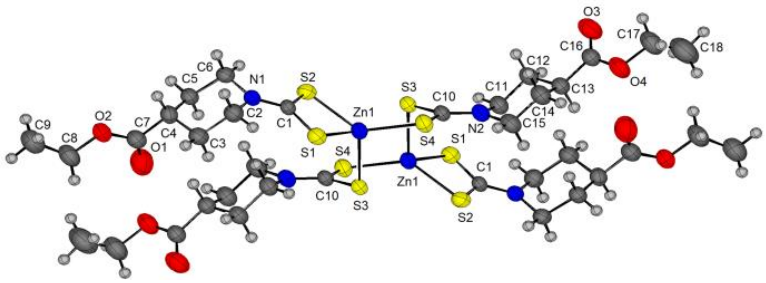

Figure 2.8. X-ray crystal structure with atom numbering scheme for **Zn1** (CCDC 1835870) (50% displacement ellipsoids).

The same synthetic strategy was applied to obtain the corresponding glycoconjugate counterparts. With reference to **Scheme 2.5**, the zinc(II)-dithiocarbamato derivative of isonipecotic acid, $Na_2[Zn(dtc\text{-}Inp\text{-}O)_2]\cdot 2H_2O$ (**Zn0a**) was first prepared by optimizing a literature procedure.[51] In order to conjugate the amino sugars to the isonipecotic linker, the carboxylic function of **Zn0a** was subsequently activated by converting it into the corresponding succinimidyl ester, $[Zn(dtc\text{-}Inp\text{-}OSu)_2]$ (**Zn0b**).

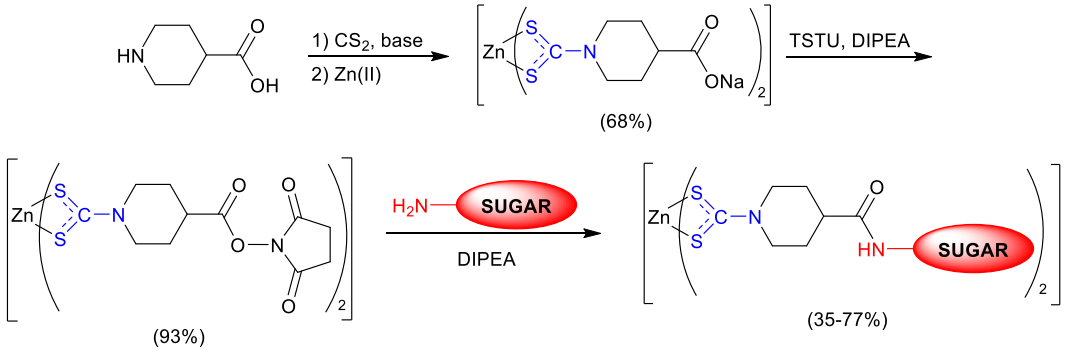

Scheme 2.5. General synthetic route to zinc(II)-dithiocarbamato glycoconjugates.

Although this is a well-known process, common synthetic routes involve the use of acidic media in which dithiocarbamates tend to decompose.[33] Therefore, the method reported by Suades and coworkers which makes use of the peptide coupling reagent *N*,*N*,*N*′,*N*′-tetramethyl-*O*-(*N*-succinimidyl)uronium tetrafluoroborate (TSTU) in presence of *N*,*N*-diisopropylethylamine (DIPEA) was exploited.[37] This procedure proved very efficient and straightforward also because **Zn0b** could be easily isolated from the DMF reaction medium by precipitation after addition of a 1:1 water/ethanol mixture. Both **Zn0a** and **Zn0b** were obtained in high yield (68% and 93%, respectively) and purity, and their spectroscopic characterization was fully consistent with literature data.[37]

An excess of each amino sugar (2.4-2.5 eq.) was reacted with the activated zinc(II) precursor **Zn0b** in anhydrous DMF under basic conditions (DIPEA), leading to the coupling of the amino function of the glucose-like unit to the carboxylic group of the isonipecotic moiety. This resulted in the formation of an amide bond and the generation of the corresponding complexes [Zn(dtc-Inp-GlcN1)$_2$] (**Zn3**), [Zn(SSC-Inp-GlcN2)$_2$] (**Zn4**), [Zn(dtc-Inp-GlcN3)$_2$] (**Zn5**) and [Zn(dtc-Inp-GlcN4)$_2$] (**Zn6**) with moderate to good yields (35-77%) (**Scheme 2.6**).[46]

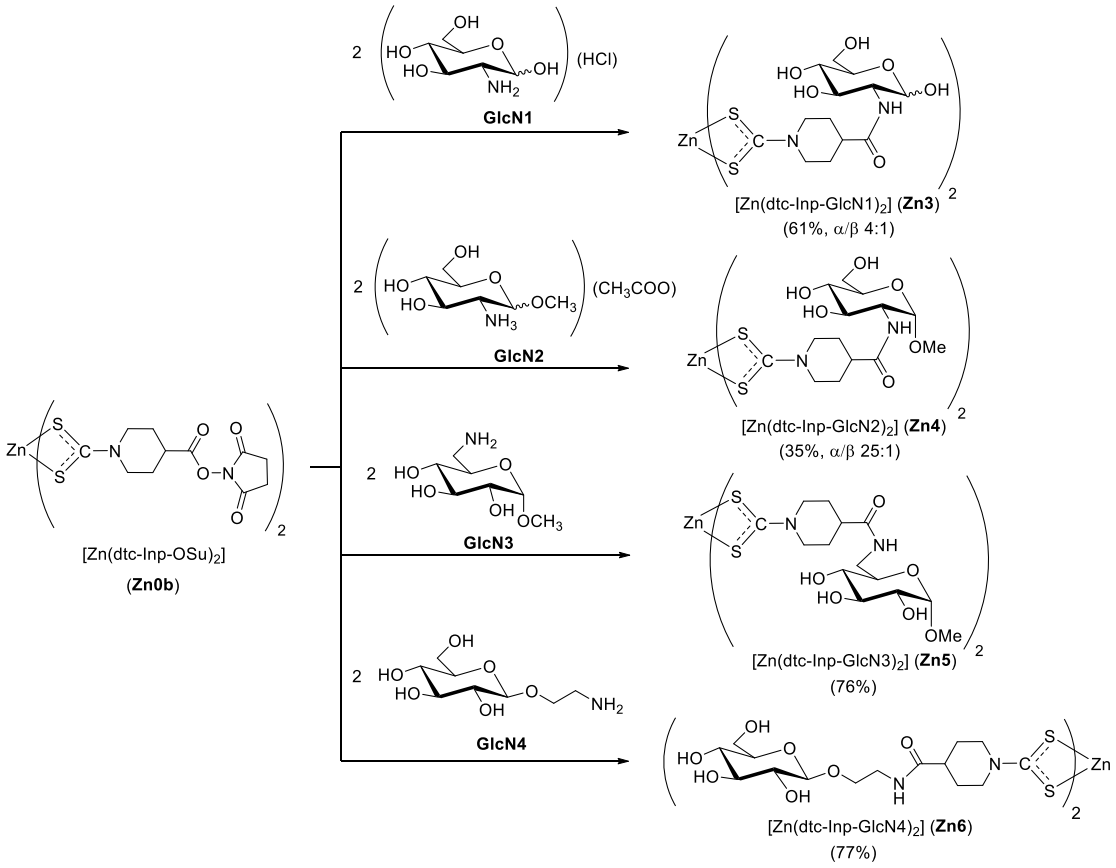

Scheme 2.6. Synthesis of the zinc(II)-dithiocarbamato glycoconjugates

The glycoconjugation with other sugars was also attempted through the same method, but with no success (**Scheme 2.7**). Among these, the conjugation with 1-amino-β-D-glucose, provided a zinc(II)-glycoconjugate, although the purification proved challenging and therefore the product could not be isolated. The conjugation with 1,3,4,6-β-D-tetraacetylglucosamine, due to the poor reactivity of the substrate, proceeded with very low yields of a non-isolatable mixture of products.

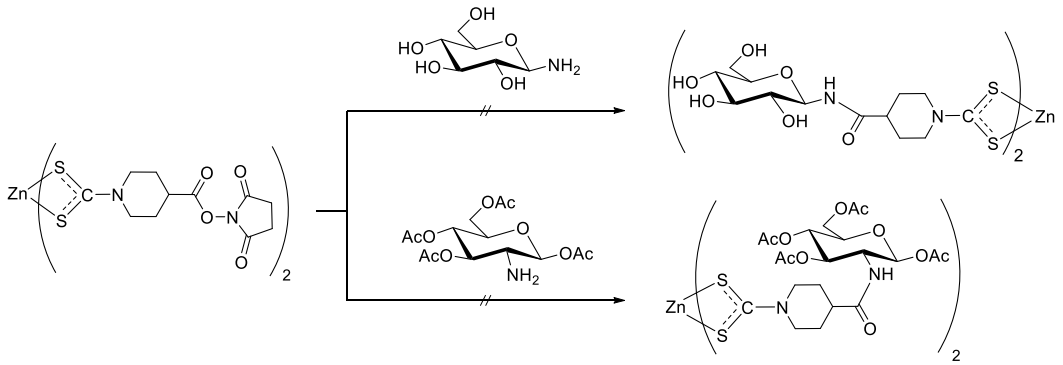

Scheme 2.7. Unsuccessful glycoconjugation reactions.

By comparing the spectroscopic features of the starting reagents with those of the zinc(II)-dithiocarbamato glycoconjugates, the most affected signals were those related to the atoms in close proximity to the newly formed amide bond. In the IR spectra of **Zn3-Zn6**

the absorption bands originating from both the succinimidyl fragment of **Zn0b** (ν_{ip}(C=O succinimidyl), ν_{oop}(C=O succinimidyl) and ν(C=O ester) at 1817, 1780 and 1737 cm^{-1})[37] and from the amino/ammonium group of the sugar substrates **GlcN1-GlcN4** ($\nu_a(NH_3^+)$, $\nu_s(NH_3^+)$, $\delta_a(NH_3^+)$, $\delta_s(NH_3^+)$, $\nu(NH_2)$ and $\delta(NH_2)$ at ~3090, 2840, 1620, 1580, 3260 and 1600 cm^{-1}, respectively)[52] disappeared. Instead, new intense bands at ~1640 (ν(C=O, amide I)) and ~1550 (δ_{ip}(CNH, amide II)) cm^{-1} were detected,[53] consistent with the replacement of the succinimidyl ester located in the same position by an amide group. On the contrary, ν(N–CSS), ν_a(SCS), ν_s(SCS) and $\nu_a(ZnS_4)$ remained substantially unchanged (at ~1490, 1000, 570 and 370 cm^{-1}, respectively) compared with **Zn0b** (**Table 2.1**).

Complex	ν(C=O)	δ_{ip}(CNH) (amide II)	ν(N–CSS)	$\nu_{a/s}$(SCS)	$\nu_a(ZnS_4)$
Zn0a	1555/1409[a]	-	1487	1002/566	397
Zn0b	1737[b]	-	1496	990/562	397
Zn1	1733	-	1494	1007/568	398
Zn2	1667[c]	1649	1492	1007/531	391
Zn3	1638[c]	1547	1487	959/570	374
Zn4	1645[c]	1557	1494	950/576	382
Zn5	1637[c]	1543	1494	1010/564	366
Zn6	1647[c]	1556	1494	1004/563	386

[a] $\nu_{a/s}(COO^-)$.
[b] ν(C=O) of ester group; ν(C=O) succinimidyl moieties detected at 1817 (in plane) and 1784 (out of plane) cm^{-1}.
[c] ν(C=O) (amide I).

Table 2.1. Selected FT-IR absorptions (CsI disk, wavenumber in cm^{-1}) of the metal-ligand scaffold of the zinc(II)-dithiocarbamato series.

Analogously, the ^1H and $^{13}C\{^1H\}$ NMR signals corresponding to the zinc(II)-dithiocarbamato isonipecotic fragment and the glucose moiety recorded for **Zn3-Zn6** were observed at chemical shifts similar to those found for the starting reagents. Anyway, some exceptions were observed, such as the peaks associated with the $C^{4'}H$ group of the piperidine ring (**Figure 2.9**), or the moieties closer to the newly formed amide bond, like the C^2H group (for **Zn3** and **Zn4**) and the C^6H_2 group (for **Zn5**, **Figure 2.10**) of the glucose unit, or the CH_2 group bound to the nitrogen of the aminoethylene linker (for **Zn6**).

Figure 2.9. Numbering scheme of the piperidine (or isonipecotic, Inp) fragment (left) and of the glucose ring (right).

For what concerns the $^{13}C\{^{1}H\}$ NMR characterization, it is worth mentioning the presence of the diagnostic peak at about 202 ppm of the dithiocarbamic carbon in all the obtained derivatives (**Table 2.2**).

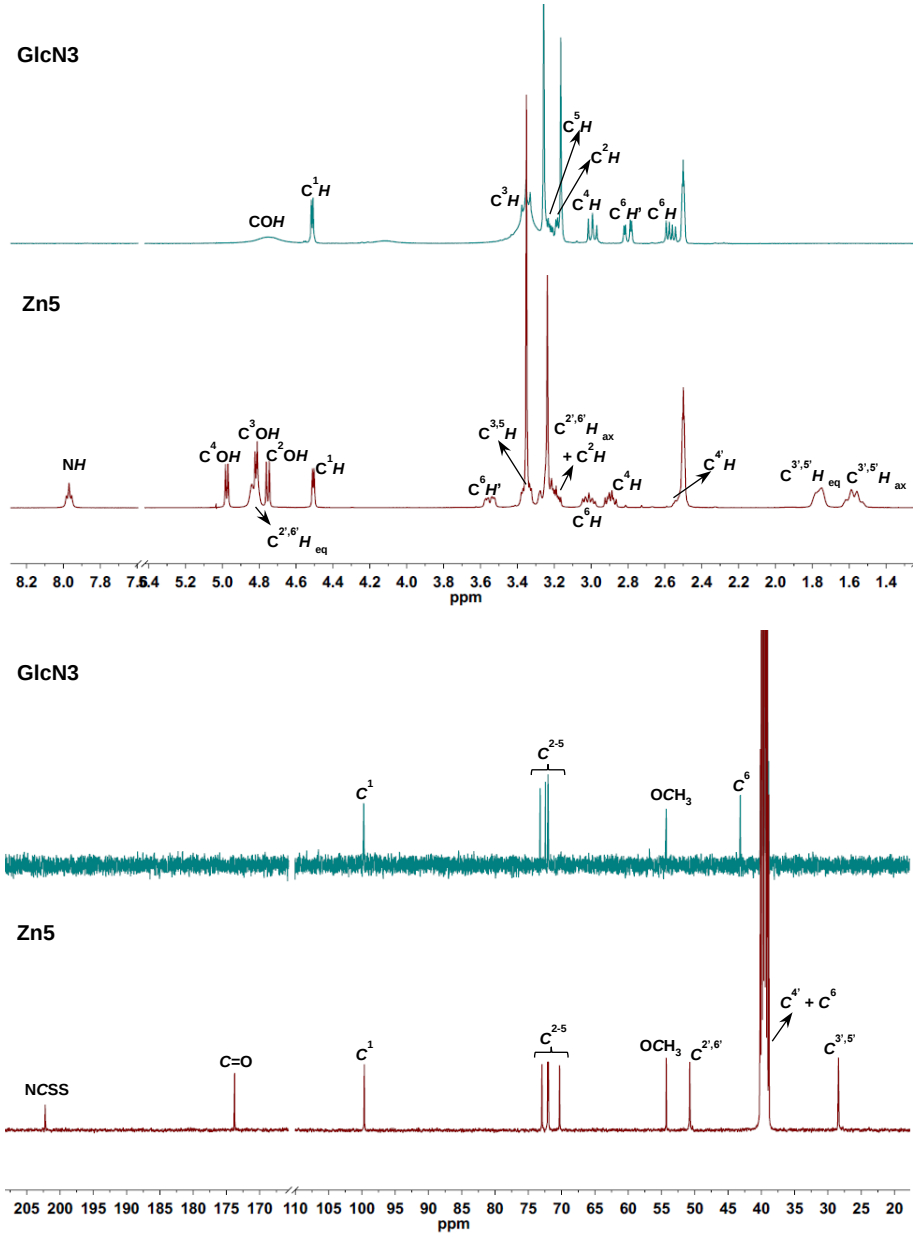

Figure 2.10. Comparison of the ^{1}H (upper) and ^{13}C (lower) NMR spectra in DMSO-d_6 of 1-*O*-methyl-6-amino-6-deoxy-α-D-glucopyranoside (**GlcN3**) and [Zn(dtc-Inp-GlcN3)$_2$] (**Zn5**). The peaks were assigned by means of DEPT, [^{1}H-^{1}H] COSY, [^{1}H-^{13}C] HSQC and HMBC NMR.

In terms of the reactivity of the different anomers, the α-to-β ratio is generally retained when using sugars substituted at the anomeric C1 position. Only the derivative with the (α,β)-D-glucosamine (**GlcN1**) pendant, **Zn3**, can undergo anomerization in solution, resulting always in a 4:1 mixture of α,β anomers. Exceptionally, the percentage of the α anomer dramatically increased by moving from *O*-methyl-2-amino-2-deoxy-D-glucopyranoside (**GlcN2**, α:β ≈ 5:1) to the corresponding zinc(II)-dithiocarbamato glycoconjugate (**Zn4**, α:β ≈ 25:1). This was assessed by measuring the $^{3}J(C^{1}H, C^{2}H)$

coupling constants in the ^{1}H NMR spectra which were in the 1-4 Hz and 6-8 Hz for the α and β anomers, respectively.[54] A variation in the anomeric ratio can be explained by a different solubility in the reaction medium of the two anomers during the work-up procedure, which helps removing most of the β anomer. Finally, 1-*O*-methyl-6-amino-6-deoxy-α-D-glucopyranoside (**GlcN3**) and 2-aminoethyl β-D-glucopyranoside (**GlcN4**) were obtained only in their α and β anomeric form respectively and, as expected, no anomerization processes occurred during the subsequent reactions.

Complex	^{1}H NMR (ppm)			^{13}C NMR (ppm)			
	N*H*	C$^{2',6'}$*H* $_{eq}$	C^{1}*H*	N*C*SS	*C*=O	*C*1	*C*$^{2',6'}$
Zn0a[a]	-	4.93	-	201.66	183.14	-	51.81
Zn0b	-	4.72	-	203.30	170.17/169.90[b]	-	49.87
Zn1	-	4.72	-	202.62	173.59	-	50.37
Zn2	7.36/6.87[c]	4.82	-	202.29	175.60	-	50.72
Zn3	7.70 (β)/ 7.66 (α)	4.82	4.92 (α)/ 4.44 (β)	202.33	173.74	95.43 (β)/ 90.49 (α)	50.71
Zn4	7.80	4.82	4.54	202.23	173.91	97.88	50.80
Zn5	7.97	4.83	4.51	202.22	173.78	99.64	50.74
Zn6	7.89	4.83	4.13	202.65	173.69	103.17	50.54

[a] in D_2O.
[b] 170.17 ppm *C*=O succinimidyl, 169.90 ppm *C*=O ester.
[c] two broad singlets (7.36 ppm N*H* $_{cis}$, 6.87 ppm N*H* $_{trans}$).

Table 2.2. Selected ^{1}H and ^{13}C{^{1}H} NMR resonances (400 MHz, DMSO-d_6) of complexes **Zn0a**-**Zn6**.

As far as the UV-Vis characterization is concerned, this was carried out in solutions of the complexes in dimethyl sulfoxide or, in the case of $Na_2[Zn(dtc\text{-}Inp\text{-}O)_2]$ (**Zn0a**), in water (**Table 2.3**). All spectra show a similar pattern, with a slight exception for **Zn0a**, in which two intense absorption bands (plus a shoulder at around 300 nm) are present at *ca*. 260-280 nm. These absorptions are commonly assigned to π*←π intraligand transitions located on the –NCS and –CSS moieties of the dithiocarbamato ligand.[55,56] Furthermore, no d–d or LMCT (ligand to metal charge transfer) transitions are observed owing to the fully-filled d orbitals of the Zn(II) centre (which possesses $3d^{10}$ electron configuration).[57]

Complex	λ, nm (ε, M^{-1} cm^{-1})		
Zn0a[a]	259 (27000)	275 (22500)	-[b]
Zn0b	266 (28800)	278 (23100)	~298 (sh, ~10900)
Zn1	267 (28000)	276 (24500)	~297 (sh, ~9600)
Zn2	268 (28600)	276 (25000)	~296 (sh, ~9500)
Zn3	267 (26300)	276 (22600)	~298 (sh, ~9000)
Zn4	268 (27700)	278 (22800)	~295 (sh, ~9500)
Zn5	268 (29100)	279 (sh, ~23300)	~295 (sh, ~9900)
Zn6	268 (20200)	276 (sh, ~18200)	~297 (sh, ~11100)

[a] in H_2O.
[b] not detected, overlapped with neighbouring peaks.
sh = shoulder

Table 2.3. UV-Vis absorptions of the synthesized zinc(II)-dithiocarbamato complexes in DMSO.

2.4 References

[1] R. G. Pearson, *J. Am. Chem. Soc.* **1963**, *85*, 3533–3539.
[2] G. Hogarth, in *Progress in Inorganic Chemistry* (Ed.: K.D. Karlin), John Wiley & Sons, Inc., Hoboken, **2005**, pp. 71–561.
[3] M. Sokolov, H. Imoto, T. Saito, *Inorg. Chem. Commun.* **1999**, *2*, 422–423.
[4] O. D. Fox, J. Cookson, E. J. S. Wilkinson, M. G. B. Drew, E. J. MacLean, S. J. Teat, P. D. Beer, *J. Am. Chem. Soc.* **2006**, *128*, 6990–7002.
[5] I. A. Lutsenko, A. V. Ivanov, M. A. Kiskin, G. V. Ogil'ko, *Russ. J. Inorg. Chem.* **2015**, *60*, 92–99.
[6] W. W. H. Wong, J. Cookson, E. A. L. Evans, E. J. L. McInnes, J. Wolowska, J. P. Maher, P. Bishop, P. D. Beer, *Chem. Commun.* **2005**, *0*, 2214–2216.
[7] W.-D. Rudorf, *J. Sulfur Chem.* **2007**, *28*, 295–339.
[8] E. Valeur, M. Bradley, *Chem. Soc. Rev.* **2009**, *38*, 606–631.
[9] E. C. Calvaresi, P. J. Hergenrother, *Chem. Sci.* **2013**, *4*, 2319.
[10] T. Storr, C. L. Fisher, Y. Mikata, S. Yano, M. J. Adam, C. Orvig, *Dalton Trans.* **2005**, *0*, 654–655.
[11] D. J. Yang, C.-G. Kim, N. R. Schechter, A. Azhdarinia, D.-F. Yu, C.-S. Oh, J. L. Bryant, J.-J. Won, E. E. Kim, D. A. Podoloff, *Radiology*, **2003**, *226*, 465–473.
[12] F. Gao, X. Yan, T. Shakya, O. M. Baettig, S. Ait-Mohand-Brunet, A. M. Berghuis, G. D. Wright, K. Auclair, *J. Med. Chem.* **2006**, *49*, 5273–5281.
[13] X. Hu, W. Zhang, I. Carmichael, A. S. Serianni, *J. Am. Chem. Soc.* **2010**, *132*, 4641–4652.
[14] L. Wiebe, J. Diakur, **2007**, US20070021380A1.
[15] P. Wang, G. J. Shen, Y. F. Wang, Y. Ichikawa, C. H. Wong, *J. Org. Chem.* **1993**, *58*, 3985–3990.
[16] T. Muhizi, S. Grelier, V. Coma, *J. Agric. Food Chem.* **2009**, *57*, 8770–8775.
[17] R. Šardzík, G. T. Noble, M. J. Weissenborn, A. Martin, S. J. Webb, S. L. Flitsch, *Beilstein J. Org. Chem.* **2010**, *6*, 699–703.
[18] M. Patra, T. C. Johnstone, K. Suntharalingam, S. J. Lippard, *Angew. Chem. Int. Ed.* **2016**, *55*, 2550–2554.
[19] P. Liu, Y. Lu, X. Gao, R. Liu, D. Zhang-Negrerie, Y. Shi, Y. Wang, S. Wang, Q. Gao, *Chem. Commun.* **2013**, *49*, 2421–2423.
[20] V. Oliveri, M. Viale, G. Caron, C. Aiello, R. Gangemi, G. Vecchio, *Dalton Trans.* **2013**, *42*, 2023–2034.
[21] H. Cheng, X. Cao, M. Xian, L. Fang, T. B. Cai, J. J. Ji, J. B. Tunac, D. Sun, P. G. Wang, *J. Med. Chem.* **2005**, *48*, 645–652.
[22] T. Muhizi, V. Coma, S. Grelier, *Carbohydr. Res.* **2008**, *343*, 2369–2375.
[23] R. A. Khan, S. Yadav, Z. Hussain, F. Arjmand, S. Tabassum, *Dalton Trans.* **2014**, *43*, 2534–2548.
[24] T. Hara, S. R. Durell, M. C. Myers, D. H. Appella, *J. Am. Chem. Soc.* **2006**, *128*, 1995–2004.
[25] L. Espelt, T. Parella, J. Bujons, C. Solans, J. Joglar, A. Delgado, P. Clapés, *Chem. Eur. J.* **2003**, *9*, 4887–4899.

[26] M. Popr, S. Hybelbauerová, J. Jindřich, *Beilstein J. Org. Chem.* **2014**, *10*, 1390–1396.
[27] S. C. Ranade, A. V. Demchenko, *J. Carbohydr. Chem.* **2013**, *32*, 1–43.
[28] B. Ren, M. Wang, J. Liu, J. Ge, X. Zhang, H. Dong, *Green Chem.* **2015**, *17*, 1390–1394.
[29] N. Azizi, M. Khajeh, M. Hasani, S. Dezfooli, *Tetrahedron Lett.* **2013**, *54*, 5407–5410.
[30] D. C. Onwudiwe, T. Arfin, C. A. Strydom, *Electrochim. Acta* **2014**, *127*, 283–289.
[31] G. Li, H. Tajima, T. Ohtani, *J. Org. Chem.* **1997**, *62*, 4539–4540.
[32] J. D. E. T. Wilton-Ely, D. Solanki, G. Hogarth, *Eur. J. Inorg. Chem.* **2005**, *2005*, 4027–4030.
[33] P. A. Antunes, S. T. Breviglieri, G. O. Chierice, É. T. G. Cavalheiro, *J. Braz. Chem. Soc.* **2001**, *12*, 473–480.
[34] G. Hogarth, *Mini-Rev. Med. Chem.* **2012**, *12*, 1202–1215.
[35] J. Zhang, J. Ren, X. Lin, X. Wang, *Bioorg. Med. Chem. Lett.* **2009**, *19*, 2752–2754.
[36] J. C. Jochims, *Chem. Ber.* **1975**, *108*, 2320–2328.
[37] J. Lecina, A. Carrer, A. Álvarez-Larena, U. Mazzi, L. Melendez-Alafort, J. Suades, *Organometallics*, **2012**, *31*, 5884–5893.
[38] L. D. Nyamen, V. S. R. R. Pullabhotla, A. A. Nejo, P. T. Ndifon, J. H. Warner, N. Revaprasadu, *Dalton Trans.* **2012**, *41*, 8297–8302.
[39] N. Salvarese, N. Morellato, A. Venzo, F. Refosco, A. Dolmella, C. Bolzati, *Inorg. Chem.* **2013**, *52*, 6365–6377.
[40] G. Aravamudan, D. H. Brown, D. Venkappayya, *J. Chem. Soc. A*, **1971**, *0*, 2744–2747.
[41] B. Arul Prakasam, K. Ramalingam, G. Bocelli, A. Cantoni, *Polyhedron*, **2007**, *26*, 4489–4493.
[42] F. Bonati, R. Ugo, *J. Organomet. Chem.* **1967**, *10*, 257–268.
[43] R. Kellner, G. St. Nikolov, *J. Inorg. Nucl. Chem.* **1981**, *43*, 1183–1188.
[44] K. Nakamoto, *Infrared and Raman Spectra of Inorganic and Coordination Compounds: Part A: Theory and Applications in Inorganic Chemistry, Sixth Edition*, John Wiley & Sons, Inc., Hoboken, **2008**.
[45] J. J. Criado, I. Fernandez, B. Macias, J. M. Salas, M. Medarde, *Inorg. Chim. Acta*, **1990**, *174*, 67–75.
[46] A. Pettenuzzo, D. Montagner, P. McArdle, L. Ronconi, *Dalton Trans.* **2018**, *47*, 10721–10736.
[47] H. L. M. Van Gaal, J. W. Diesveld, F. W. Pijpers, J. G. M. Van der Linden, *Inorg. Chem.* **1979**, *18*, 3251–3260.
[48] F. W. Pijpers, A. H. Dix, J. G. M. Van Der Linden, *Inorg. Chim. Acta*, **1974**, *11*, 41–45.
[49] M. Bonamico, G. Dessy, V. Fares, L. Scaramuzza, *J. Chem. Soc. Dalton Trans.* **1972**, *0*, 2515–2517.
[50] E. M. Nagy, S. Sitran, M. Montopoli, M. Favaro, L. Marchiò, L. Caparrotta, D. Fregona, *J. Inorg. Biochem.* **2012**, *117*, 131–139.
[51] M. M. Jones, P. K. Singh, S. G. Jones, C. R. Mukundan, J. A. Banton, G. R. Gale, L. M. Atkins, A. B. Smith, *Chem. Res. Toxicol.* **1991**, *4*, 27–34.
[52] E. Wiercigroch, E. Szafraniec, K. Czamara, M. Z. Pacia, K. Majzner, K. Kochan, A. Kaczor, M. Baranska, K. Malek, *Spectrochim. Acta A*, **2017**, *185*, 317–335.
[53] M. Picquart, Z. Abedinzadeh, L. Grajcar, M. H. Baron, *Chem. Phys.* **1998**, *228*, 279–291.
[54] A. Blaskó, C. A. Bunton, S. Bunel, C. Ibarra, E. Moraga, *Carbohydr. Res.* **1997**, *298*, 163–172.
[55] G. E. Manoussakis, C. A. Bolos, *Inorg. Chim. Acta*, **1985**, *108*, 215–220.
[56] Z. B. Leka, V. M. Leovac, S. Lukić, T. J. Sabo, S. R. Trifunović, K. M. Szécsényi, *J. Therm. Anal. Calorim.* **2006**, *83*, 687–691.
[57] R. D. Webster, G. A. Heath, A. M. Bond, *J. Chem. Soc. Dalton Trans.* **2001**, *0*, 3189–3195.

Chapter 3

Gold(III)-dithiocarbamato glycoconjugates

Chapter 3. Gold(III)-dithiocarbamato glycoconjugates

For full experimental procedures and characterizations see Chapter 8.

3.1 Synthesis

As anticipated in Chapter 2, reaction of D-glucosamine hydrochloride with CS_2 under different basic conditions did not afford 2-deoxy-2-dithiocarbamato-D-glucose, leading instead to the reduction of gold(III) to gold(I) and to intramolecular cyclization side-products.

Considering the aforementioned issues, the feasibility of the new synthetic approach was first evaluated by generating non-glycosylated gold(III)-dithiocarbamato complexes *via* transmetallation from the corresponding zinc(II) intermediates. Specifically, the focus was on ethyl isonipecotate (Inp-OEt) and isonipecotamide (Inp-NH_2) dithiocarbamates as model ligands that, once coordinated to zinc(II), would subsequently undergo transmetallation reactions with many "soft" transition metals, including gold(III).[1–3] Several attempts aimed at optimizing the reaction protocol were carried out, *e.g.* by varying solvents and reaction times (**Table 3.1**).

Solvent	***Ratio* Zn/$[AuX_4]^-$**	**Time (h)**	**Temperature (°C)**
Methanol	1:2	3	r.t.
Methanol	1:2	16	r.t.
Water	1:2	2	r.t.
Acetone	1:2	48	r.t.
Methanol/acetone (1:1)	1:2	4	r.t.
Methanol/acetone (1:5)	1:2	8	0
DMF	1:2	1.5-3	r.t.

Table 3.1. Optimization of the synthesis of the gold(III)-dithiocarbamato complexes *via* transmetallation.

Eventually, the zinc(II)-gold(III) transmetallation readily took place by reaction in DMF at room temperature with a zinc precursor/gold salt 1:2 ratio, yielding the gold(III) counterparts [$AuBr_2$(dtc-Inp-OEt)] (**Au1**) and [$AuBr_2$(dtc-Inp-NH_2)] (**Au2**) in high yields (>70-80%) and no need of further purification (**Scheme 3.1**). The obtainment of a crystal structure of **Au1** supported the unambiguous identification of the reaction product with the expected geometry and coordination fashion (see XRD crystallography section).[4]

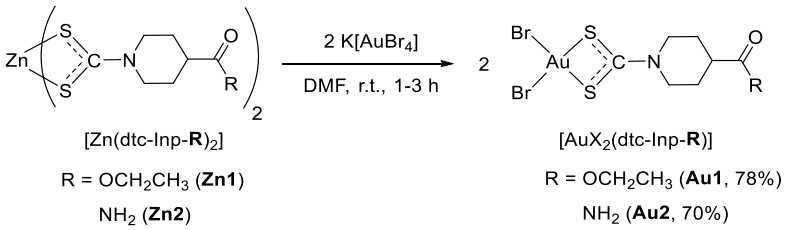

Scheme 3.1. Synthesis of the gold(III)-dithiocarbamato aglycones *via* transmetallation.

Following the successful generation of the model non-glycosylated gold(III)-dithiocarbamato complexes, the same synthetic strategy was applied to obtain the corresponding glycoconjugate counterparts. The zinc(II)-gold(III) transmetallation was achieved by reacting the zinc(II) precursors **Zn3**–**Zn5** with $K[AuBr_4]\cdot 2H_2O$ in DMF, affording the final corresponding gold(III)-dithiocarbamato glycoconjugates [$AuBr_2$(dtc-Inp-GlcN1)] (**Au3**), [$AuBr_2$(dtc-Inp-GlcN2)] (**Au4**) and [$AuBr_2$(dtc-Inp-GlcN3)] (**Au5**) (**Scheme 3.2**) in high yields (>75%) and no need of further purification. The synthesized gold(III) complexes were characterized by the usual analytical and spectroscopic techniques.

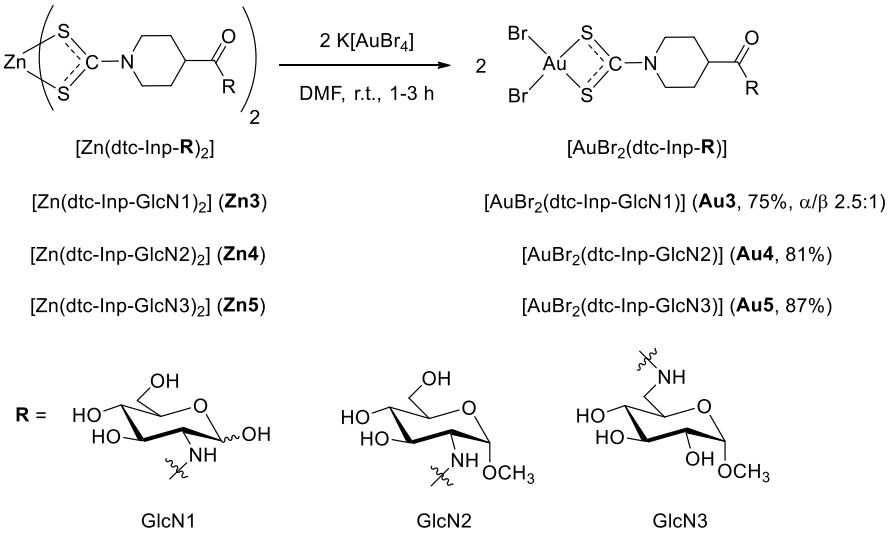

Scheme 3.2. Synthesis of the dibromo-gold(III)-dithiocarbamato glycoconjugates *via* transmetallation.

Analogous gold(III)-dithiocarbamato complexes have been previously obtained through one-pot template reactions in which an excess of carbon disulfide was added to a mixture of an equimolar amount of amine and a base (typically NaOH or KOH) to generate *in situ* the dithiocarbamato ligand, which was then added to a solution of the gold(III) salt.[5–7] However, such procedure often resulted in the generation of a mixture of two gold(III)-dithiocarbamato derivatives, whose relative abundance varies depending on the synthetic conditions. This mixture was proved to consist of the expected gold(III) derivative and a dimeric form in which two bridging dithiocarbamato ligands are bound to both gold(III)

centers whose coordination sphere is completed by two *trans*-bromide moieties (**Figure 3.1**).[8]

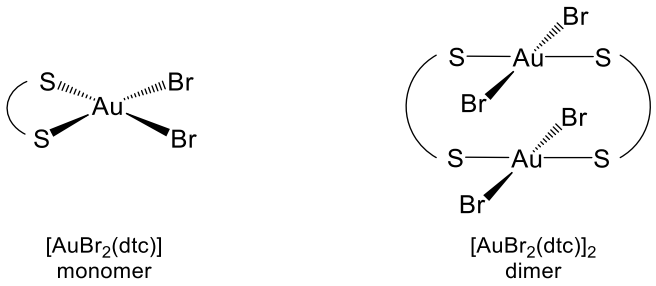

Figure 3.1. Chemical drawing of the two isomeric forms of dibromo gold(III)-dithiocarbamato derivatives.

Remarkably, the zinc(II)-gold(III) transmetallation strategy led to the generation of the expected monomeric form only.

An alternative route was also investigated to synthesize such gold(III)-glycoconjugates, which makes use of the gold(III)-dithiocarbamato derivative bearing a succinimidyl activated ester moiety, [$AuBr_2$(dtc-Inp-OSu)] (**Au6**) (**Scheme 3.3**). The derivative **Au6** was obtained in very good yield (88%) by means of the optimized protocol of transmetallation from **Zn0b** with 2 equivalents of K[$AuBr_4$] in DMF. Then, conjugation of **Au6** with glucosamine hydrochloride was attempted in DMF or DMSO in presence of DIPEA (2.5 eq.).

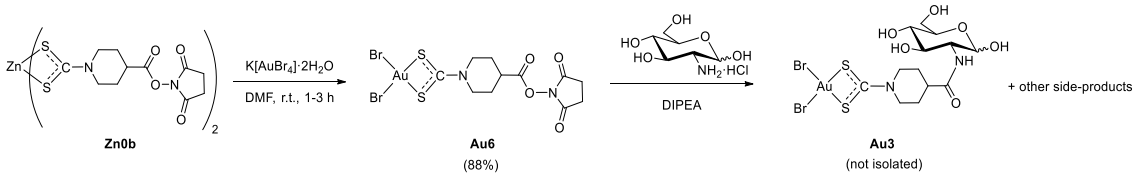

Scheme 3.3. Alternative synthetic route to [$AuBr_2$(dtc-Inp-GlcN1)].

The reaction, monitored by ^{1}H NMR in DMSO-d_6, led to the formation of the desired product **Au3**, with the concomitant formation of *N*-hydroxysuccinimide. Unfortunately, other side-products (not identified) formed in the reaction medium, likely due to the instability of the gold(III)-dithiocarbamato scaffold in the presence of tertiary amines. As a consequence, this synthetic route was not investigated any further.
However, although this route proved less feasible, complex **Au6** would be exploited to achieve the covalent attachment of the gold(III)-dithiocarbamato scaffold to platinum(IV) derivatives and mesoporous silica nanoparticles (see Chapter 7).

In the attempt to generate also the gold(III)-dichloride analogues, the zinc(II) precursors **Zn3-5** were reacted with sodium tetrachloroaurate(III) dihydrate (Na[$AuCl_4$]·$2H_2O$) in

DMF (**Scheme 3.4**). The reaction was also monitored by ^{1}H NMR in DMSO-d_6 and, although the reagents readily reacted to yield the desired product (t<5 min), the reaction afforded in most cases a mixture of two species that proved not quantitatively isolatable. Only the glycoconjugates [$AuCl_2$(dtc-Inp-GlcN1)] (**Au7**) and [$AuCl_2$(dtc-Inp-GlcN3)] (**Au8**) were obtained pure, the first as a mixture of α and β anomers, the latter only as the α anomer.

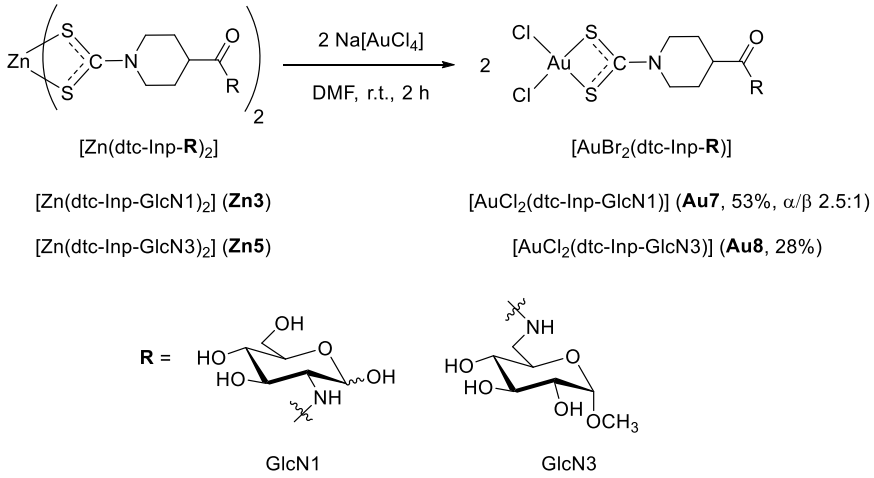

Scheme 3.4. Synthesis of the dichloro-gold(III)-dithiocarbamato glycoconjugates via transmetallation.

All the synthesized compounds are very soluble in DMSO and DMF; **Au1** and **Au8** are also soluble in methanol, while only **Au1** is soluble in acetone and ethanol. Interestingly, the glycoconjugates exhibit also a discrete water solubility (up to 0.1 mM), although they undergo hydrolysis (see section 3.6).

3.2 XRD crystallography

Crystals of **Au1** suitable for X-ray diffraction crystallography were obtained by slow evaporation of an acetone solution of the compound (**Figure 3.2**). There is a significant distortion from square-planar geometry due to the small bite angle of the dithiocarbamato ligand, corresponding to 75.35° versus 90° of a pure square-planar geometry. However, there is a small deviation of 0.008 Å from the least-squares plane defined by the gold(III) center and the ligating atoms S1 and S2. The bond distances are in the range previously reported and are close to those found in other dibromo-dithiocarbamato-gold(III) complexes.[6,9] Interestingly, compared with the Zn–S distances within the four-membered rings of **Zn1**, which differ by a near constant 0.1 Å, in the gold(III) counterpart, **Au1**, the Au–S distances have differences which are ten times smaller. Further details of the structures are provided in the Appendix section.

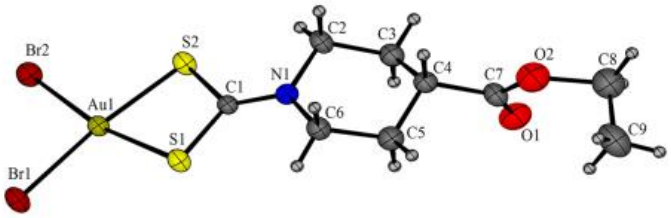

Figure 3.2. X-ray crystal structure with atom numbering scheme for **Au1** (CCDC 1835871) (30% displacement ellipsoids).

3.3 IR spectroscopy

IR spectroscopy proved useful to identify the synthesized compounds and shed light on the coordination fashion around the metal centre. By comparison with the spectra recorded for the starting ethyl isonipecotate and isonipecotamide reagents, the appearance of a strong band at 1494 (**Zn1**)/1492 (**Zn2**) cm^{-1} in the zinc(II) derivatives (the so-called "thioureide" band, ν(N–CSS)) is consistent with a chelating dithiocarbamato ligand coordinated to a zinc(II) center.[10,11] When taking into account the gold(III) counterparts (**Table 3.2**), the strong band ν(N–CSS) is recorded at higher frequencies at around 1570-1550 cm^{-1} due to the increased electron-withdrawing effect upon moving from zinc(II) to the more positively charged gold(III) centre, suggesting a greater contribution of the "thioureide" resonance form (**Scheme 3.5**).[5]

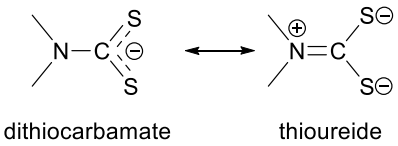

Scheme 3.5. Resonance forms of the dithiocarbamato ligands.

Complex	ν(N–CSS)	$\nu_{a/s}$(SCS)	$\nu_{a/s}$(SAuS)	$\nu_{a/s}$(XAuX)[a]
Au1	1571	1002/536	413/398	249/228
Au2	1565	1019/534	411/397	232/227
Au3	1561	1008/575	412/392	244/227
Au4	1561	1007/577	410/393	246/220
Au5	1555	1011/570	398[b]	254/227
Au6	1575	989/573	405/372	245/232
Au7	1554	1028/575	406[b]	357[a]
Au8	1552	1012/543	394/376	342/314

[a] X: Br for **Au1-6**, X: Cl for **Au7-8**.

[b]overlapped

Table 3.2. Selected FT-IR absorptions (CsI disk, wavenumber in cm^{-1}) of the metal-ligand scaffold in the dibromo- and dichloro-gold(III)-dithiocarbamato series.

Additionally, the detection of a single band at *ca*. 1010-1000 cm^{-1} in all complexes (attributed to the ν_a(SCS)) clearly supports a symmetrical bidentate coordination of the –NCSS moiety to the metal centers, in agreement with the Bonati-Ugo criterion.[12] In the far-IR spectra of a number of metal-dithiocarbamato complexes, bands recorded in the range 420-320 cm^{-1} are regarded as highly diagnostic since they are assigned to the metal-sulfur stretching vibrations. Both $\nu_{a/s}$(SAuS) are recorded for the complexes (at *ca*. 410/390 cm^{-1}, respectively), in agreement with those reported in the literature for similar gold(III)-dithiocarbamates.[13] Finally, other informative bands are observed at lower frequencies at around 350/320 and 240/220 cm^{-1}, attributed to the $\nu_{a/s}$(ClAuCl) and $\nu_{a/s}$(BrAuBr), respectively, for terminal *cis*-halides.[14]

3.4 NMR spectroscopy

Mono- and multinuclear NMR spectroscopy provided further insights into the identification of the metal-dithiocarbamato derivatives. For example, compared with the starting ethyl isonipecotate reagent, a general downfield shift of the proton signals is observed for the zinc(II) intermediate **Zn1** and the corresponding transmetallation product **Au1** (**Figure 3.3**). This is consistent with the decreased electron density experienced by the hydrogen atoms of the isonipecotate scaffold upon introducing the dithiocarbamato moiety and the subsequent coordination to the metal centres, the gold(III) ion exerting greater deshielding effect than zinc(II) due to the higher oxidation state.[15]

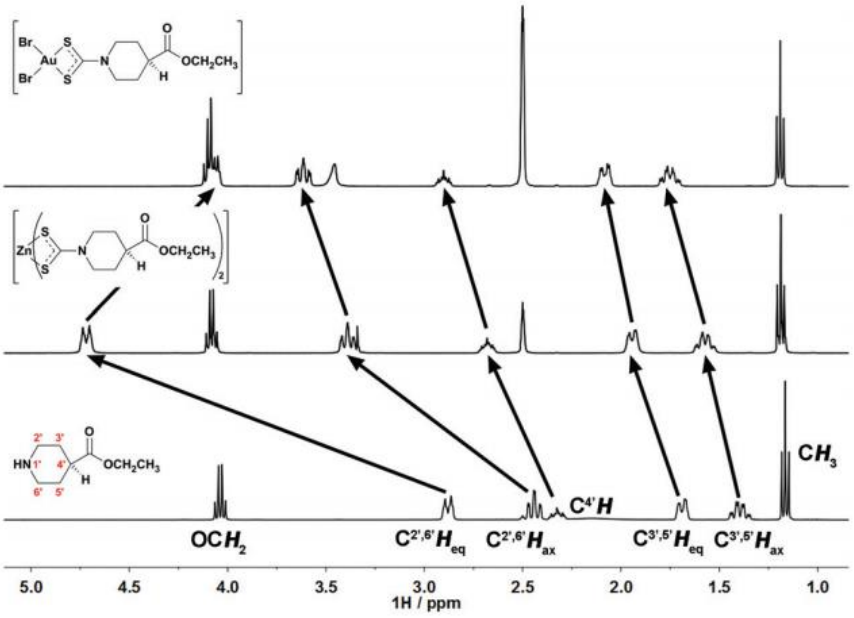

Figure 3.3. Comparison of the ^{1}H NMR spectra in DMSO-d_6 of ethyl isonipecotate, [Zn(dtc-Inp-OEt)$_2$] (**Zn1**) and [AuBr$_2$(dtc-Inp-OEt)] (**Au1**).

As expected, the larger shift involves the piperidine hydrogens, the only partial exception to this trend being the $C^{2',6'}H$ equatorial protons which undergo a 0.7 ppm upfield shift in **Au1** with respect to **Zn1**. On moving away from the dithiocarbamato moiety, the magnitude of the chemical shift change decreases until being negligible for the farther ester group. The most diagnostic peak recorded in the $^{13}C\{^1H\}$ NMR spectra is attributed to the dithiocarbamic carbon atom and is generally found in the range 180–220 ppm (**Table 3.3**).[16] It is generally assumed that the ^{13}C chemical shifts of the –NCSS moiety are strongly dependent on both the type of metal-dithiocarbamate bonding and the oxidation state of the metal center. For derivatives of high oxidation state transition metals (such as gold(III)), the dithiocarbamic carbon signals appear upfield.[17,18] There is a strong empirical correlation between $\delta(N^{13}CSS)$ values and the N–CSS stretching vibrations in the infrared spectra: higher ν(N–CSS) values indicate an increased carbon–nitrogen double bond character, which well correlates with lower $\delta(N^{13}CSS)$ values because of a greater electron density on the –NCSS moiety, and the other way round.[16] All these considerations are fully consistent with the experimental ν(N–CSS) frequencies and the $N^{13}CSS$ carbon signals recorded for the object dithiocarbamato complexes (202.6 (**Zn1**), 202.3 (**Zn2**), 187.9 (**Au1**) and 186.9 (**Au2**) ppm).

In line with the model non-glycosylated complexes, when moving from the zinc(II) to the gold(III) glycoconjugates, major changes in the NMR spectra were detected for the signals associated with the isonipecotic dithiocarbamato fragments. A comparative example is given in **Figure 3.4** for **Au5**.

Complex	^1H NMR (ppm)			^{13}C NMR (ppm)			
	N*H*	$C^{2',6'}H_{eq}$	C^1H	N*C*SS	*C*=O	*C*1	$C^{2',6'}$
Au1	-	4.06	-	187.86	173.16	-	48.64
Au2	7.40/6.97[a]	4.11	-	186.90	174.50	-	48.42
Au3	7.75 (β)/ 7.73 (α)	4.12	4.91 (α)/ 4.45 (β)	186.92	172.76 (α)/ 172.74 (β)	95.33 (β)/ 90.51 (α)	48.44 (α)/ 48.34 (β)
Au4	7.86	4.12	4.52	186.93	172.89	97.83	48.44
Au5	7.99	4.13	4.51	187.00	172.74	99.65	48.41
Au6	-	4.12	-	188.07	170.13/169.11[b]	-	47.65
Au7	7.78 (α)/ 7.75 (β)	4.21-4.13	4.92 (α)/ 4.45 (β)	192.52	172.91	95.38 (β)/ 90.49 (α)	49.05 (β)/ 48.77 (α)/
Au8	8.05	4.20	4.51	192.61	172.91	99.66	48.73

[a] two broad singlets (7.40 ppm NH_{cis}, 6.97 ppm NH_{trans}).
[b] 170.13 ppm *C*=O succinimidyl, 169.11 ppm *C*=O ester.

Table 3.3. Selected ^1H and $^{13}C\{^1H\}$ NMR resonances (400 MHz, DMSO-d_6) of complexes **Au1**-**Au8**.

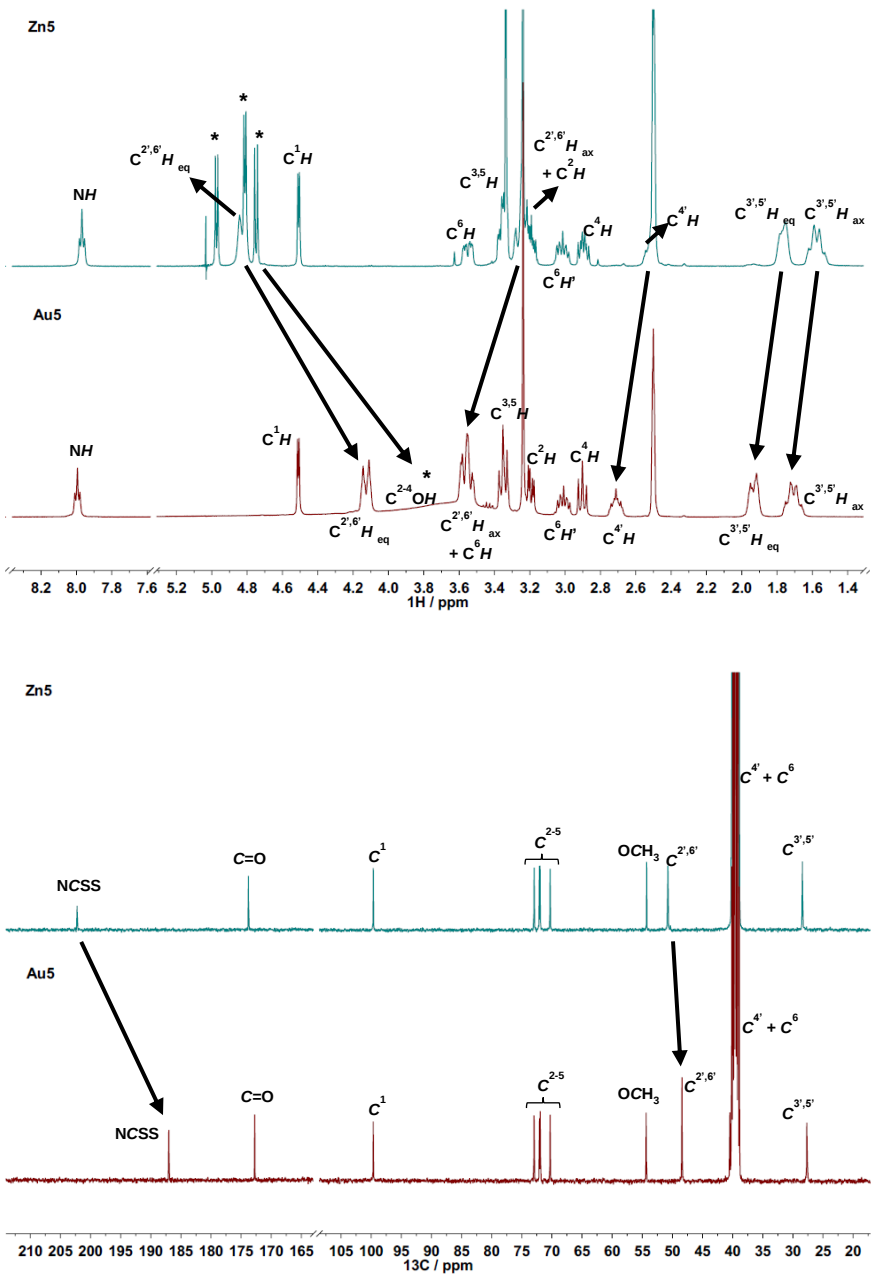

Figure 3.4. Comparison of the ^{1}H (upper) and ^{13}C (lower) NMR spectra in DMSO-d_6 of [Zn(dtc-Inp-GlcN3)$_2$] (**Zn5**) and [AuBr$_2$(dtc-Inp-GlcN3)] (**Au5**). The peaks were assigned by means of DEPT, [^{1}H-^{1}H] COSY, [^{1}H-^{13}C] HSQC and HMBC NMR.

Remarkably, as a general trend, the ^{1}H signals recorded for the glucose hydroxyl groups are properly resolved for various metal derivatives obtained in this project, including zinc(II), platinum(II), and gold(I), whereas for both the starting amino-sugars and the corresponding gold(III) derivatives peaks tend to collapse into a single very broad band. In terms of the reactivity of the different anomers, the α to β ratio was substantially retained when using (α,β)-D-glucosamine (**GlcN1**, α:β ≈ 4:1). On the contrary, when using *O*-methyl-2-amino-2-deoxy-(α,β)-D-glucopyranoside (**GlcN2**) the percent of the β anomer dramatically decreased (**GlcN2**, α:β ≈ 5:1) in the corresponding zinc(II)-dithiocarbamato glycoconjugate (**Zn4**, α:β ≈ 25:1, see Chapter 2), to be completely absent

in the gold(III) analogue (**Au4**). Finally, 1-*O*-methyl-6-amino-6-deoxy-D-glucopyranoside (**GlcN3**) was obtained in its α anomeric form only and, as expected, no α to β anomerization occurred.

3.5 UV-Vis spectroscopy

Absorption spectra were recorded in solutions of the compounds in dimethyl sulfoxide (DMSO). The major absorptions of the compounds are summarized in **Table 3.4**.

Complex	λ, nm (ε, M^{-1} cm^{-1})				
Au1	-[a]	273 (26000)	283 (27700)	-[a]	372 (3900)
Au2	268 (14200)	272 (14500)	281 (15100)	-[a]	360 (2600)
Au3	-[a]	-[a]	277 (19700)	~320 (sh, ~8100)	~365 (sh, ~2600)
Au4	-[a]	-[a]	280 (20500)	314 (12400)	~354 (sh, ~3500)
Au5	-[a]	-[a]	278 (15600)	313 (8700)	~355 (sh, ~2700)
Au6	-[a]	-[a]	279 (16000)	~315 (sh, ~8400)	-[a]
Au7	-[a]	-[a]	277 (18800)	319 (13800)	-[a]
Au8	-[a]	-[a]	278 (18400)	320 (14700)	-[a]

[a] not detected, overlapped with neighbouring peaks.
sh = shoulder

Table 3.4. UV-Vis absorptions of the synthesized gold(III)-dithiocarbamato complexes performed in DMSO in the range 250-800 nm.

The absorption bands in the range 260-280 and 310-320 show large molar extinction coefficients (ε 1-2·10^4 M^{-1} cm^{-1}). These absorptions correspond to π*←π intraligand transitions mainly located in the –NCS and –CSS moieties.[5,14,19] The transitions related to the –NCSS moiety usually depend on the nature of the alkyl moiety bound to the nitrogen atom[20] and, partly, on the nature of the halogen atom.[14] As expected, no significant structural changes take place in close proximity of the metal-ligand scaffold for all the gold(III)-dithiocarbamato complexes here reported, resulting in minimum deviations in the absorption maxima for these transitions.

As to the weakest band at ~350 nm, this can be assigned to d–d metal orbitals transitions. Position and intensity are indicative of a square-planar environment of the metal. In gold(III) square-planar metal complexes, the set of d metal orbitals splits up in accordance with the following order of increasing energy: $d_{z^2} > d_{xz,yz} > d_{xy} > d_{x^2-y^2}$, in which orbitals with x and y components are destabilized as they point towards the ligands, while orbitals with z components remain unaffected and, as such, more stable.[21–23] In particular, this band may be attributed to $^1A_{2g}\leftarrow{}^1A_{1g}$ and $^1E_g\leftarrow{}^1A_{1g}$ transitions, that are spin-allowed but

symmetry-forbidden and involving $d_{x^2-y^2} \leftarrow d_{xy}$ and $d_{x^2-y^2} \leftarrow d_{xz,yz}$ orbitals transitions, respectively.[21,24] However, the assignment of this band is still subject of debate since other authors attributed it to an intramolecular MLCT transition from the d orbitals of the metal to the σ* orbitals.[25,26]

3.6 Solution studies

Stability studies in solution were carried out on some selected compounds of the series prior to the *in vitro* biological evaluation. The stability in DMSO, DMF and phosphate buffer saline (PBS) was evaluated by means of ^{1}H NMR spectroscopy or UV-Vis spectroscopy. DMF and DMSO are commonly used to prepare the stock solutions of the compounds before the cytotoxicity assays. As observed by ^{1}H NMR spectroscopy, the complexes are relatively stable in DMSO-d_6 and DMF-d_7. However, in the UV-Vis spectra a dramatic change can be observed a few minutes after dissolution. As already evidenced by Fregona and coworkers,[27] such behaviour may be due to the presence of traces of water in the solvent. In order to further clarify this aspect, the absorption spectra of compounds **Au2** and **Au3** were recorded at 37°C in PBS. As shown in **Figure 3.5**, once dissolved in the physiological medium two different behaviours may be observed for **Au2** and **Au3**. In both the compounds, two new bands appear.

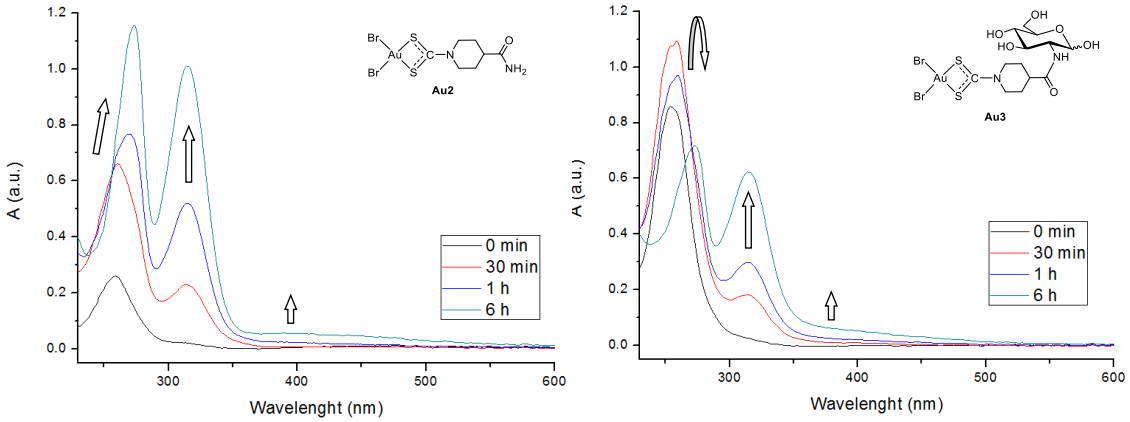

Figure 3.5. UV-Vis spectra over time (50 μM in PBS, 37°C) of **Au2** (left) and **Au3** (right).

The large increase of intensity occurring during the first minutes may be explained by the rapid hydrolysis of the complex in water to form a more hydrosoluble mono-aquo species (**Scheme 3.6**). Subsequently, a second water molecule coordinates to the gold(III) centre, displacing a second bromide with a slower process. The formation of the mono- and diaquo cationic species is accompanied by the loss of one or two protons to form, respectively, the mono- or dihydroxo gold(III) species (a yellow precipitate may be observed in some cases). In fact, the dominant species in solution at physiological pH

generally contain coordinated hydroxo groups, the gold(III) center being strongly acidic and drastically lowering the pK_a of the coordinated water molecules.[28,29] This overall process induces the increase of the absorbance at 280 and 320 nm abscribed to the intraligand $\pi^* \leftarrow \pi$ transition located in the NCS and SCS moieties, respectively. On the contrary, compared to **Au3**, whose intraligand bands decrease after 1-2 hours, in **Au2** the bands keep increasing over 24 hours. In addition, a new low intensity band appears at around 380 nm in the UV-Vis spectrum of **Au2**, assignable to a metal-to-ligand charge-transfer transition due to the presence of gold(III)-bound hydroxo groups.[30]

Finally, after more than 24 hours, the formation of a dimeric gold(I) species with two bridged dithiocarbamato ligands, obtained upon reduction of the gold(III)-hydroxo species, can be observed (brown-violet residue). A similar mechanism was experimentally verified by Ronconi and coworkers through electrochemical studies.[31]

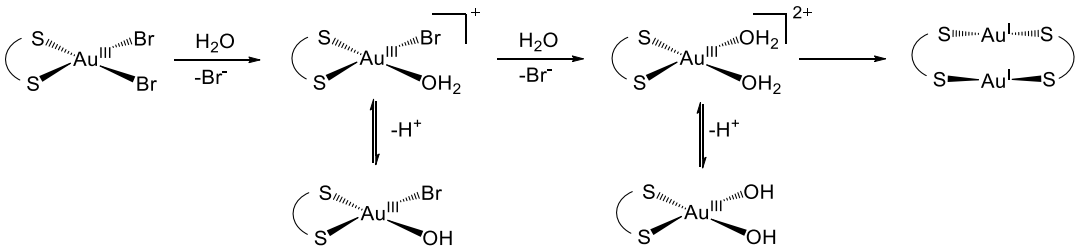

Scheme 3.6. Proposed mechanism of hydrolisis of the gold(III)-dithiocarbamato compounds.

3.7 Computational studies

The recent publications of the crystal structure of GLUT1 in the inward conformation and of XylE, a GLUT1 homologue, in the outward conformation, provided researchers a valuable set of tools for the investigation and design of glycoconjugates with GLUT1-interacting properties.[32,33] The sodium-independent membrane protein GLUT1 behaves like a double-gate transporter that regulates the intracellular flux of glucose (**Figure 3.6**). Once glucose binds to the active site of the protein in the outward conformation, on the outside of the cell membrane, a conformational change makes the protein adopt an inward conformation, thus releasing the sugar into the intracellular milieu after crossing the protein inner channel. Therefore, it is crucial to assess whether the designed conjugates can interact with the transporter, both in the outward (for binding and entrance), and in the inward (for subsequent release) conformation.

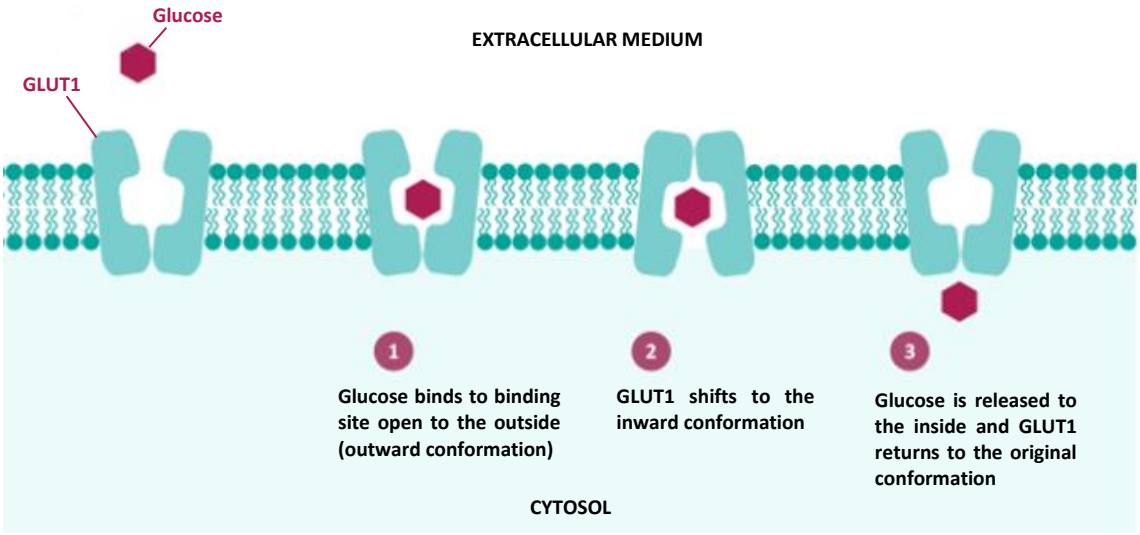

Figure 3.6. Mechanism of transport of glucose inside the cell mediated by GLUT1 (adapted from http://usmle.biochemistryformedics.com/wp-content/uploads/GLUT-1-DETAILS.jpg).

In this regard, *ab initio* docking studies were performed on two compounds, namely **Au3** and **Au5**, by Dr. Alessio Terenzi at the University of Vienna. Gold(III) glycoconjugates attached to the C2 (**Au3**) or to the C6 (**Au5**) position were selected on purpose. **Au3**, being conjugated in the C2-position by an amide bond, is structurally analogous to other GLUT-interacting compounds, such as 2-NBDG and 2-deoxy-glucose-SNAP.[34] Instead **Au5**, conjugated to position C6 of the glucose ring, should not prevent receptor binding since this position is not involved in hydrogen-bonding interactions with the amino acidic residues of the transporter in the outward conformation.[35–37]

In addition, the α-methyl substituent in the anomeric position should not be an issue either, since C1 substituted α anomers possess increased recognition by the facilitative glucose transporters in cancer cells. In fact, despite the relative prevalence of the β-anomer in aqueous solution, it has been recently reported a crystal structure of D-glucose bound to human GLUT3, which shares 66% sequence homology with human GLUT1. In the binding site of GLUT3, the occupancy of the α-anomer was dominant (69%) over that of the β-anomer.[38] For this reason, the C6 glycoconjugate **Au5** would be recognized while retaining substrate specificity, and it was therefore chosen for the docking study. Finally, the structure of GLUT1 (bound to *n*-nonyl-β-D-glucose) in the inward-facing conformation has been chosen for the computational studies.

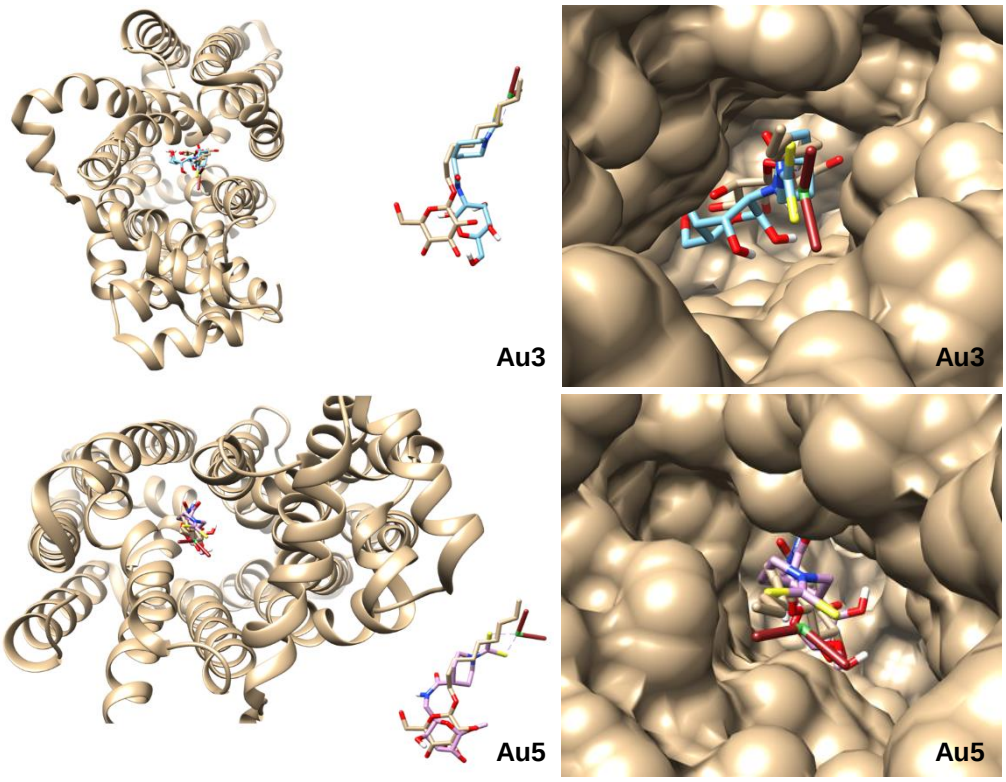

Figure 3.7. Docking of compounds **Au3** (top) and **Au5** (bottom) and superimposed with *n*-nonyl-β-D-glucose, shown as sticks, in the channel of GLUT1 (on the right the channel is shown as space filling). The insets on the left show the superimposition with *n*-nonyl-β-D-glucose (pictures obtained by Dr. Alessio Terenzi).

In the superimposition in **Figure 3.7**, the synthesized compounds and *n*-nonyl-β-D-glucose match well, in particular **Au5**. The compounds **Au3** and **Au5** fit well also into the binding pocket of GLUT1 in the inward-facing conformation. This reveals that, at least in principle, no steric constraints would occur between the glycoconjugates and GLUT1.

3.8 Biological studies

3.8.1 Cytotoxicity studies

In vitro cytotoxicity assays were carried out on human breast (MCF7 and MDA-MB-231), colorectal (HT-29) and osteosarcoma (U2OS) cancer cell lines. In order to compare the selectivity towards tumorigenic cell lines, the antiproliferative activity was also evaluated on the human kidney (RC-124) non-cancerous cell line. All studies, except those on U2OS cancer cells which were performed in Prof. Corrado Santocanale laboratory at NUI Galway, were carried out in Prof. Ingo Ott laboratory at the University of Braunschweigh (Germany). As shown in **Table 3.5**, the glycoconjugated gold(III) complexes did not exhibit relevant cytotoxic activity (IC_{50} > 50 μM). Whenever possible, when precipitation of the compounds in the medium did not represent a significant issue,

the cytotoxicity was tested at higher concentration (up to 250 μM) but, again, none of the tested gold(III) complexes showed any activity.

Complex	IC_{50} (μM)[a]				
	MCF7	MDA-MB-231	HT-29	U2OS	RC-124
Au2	5.1 ± 1.0	8.9 ± 1.1	20.1 ± 0.1	2.3 ± 0.2	9.9 ± 0.8
Au3	> 50	> 50	> 50	> 50	> 50
Au4	> 50	> 50	> 50	> 50	48.2 ± 13.2
Au5	> 50	> 50	> 50	> 50	18.8 ± 1.7
Au7	> 50	> 50	> 50	> 50	> 50
Au8	> 50	41.7 ± 11.9	> 50	23.6 ± 1.4	> 50
Cisplatin[b]	1.6 ± 0.1[c]	1.5 ± 0.1[c]	4.1 ± 0.3[c]	3.2 ± 0.4	-[d]

[a] after 72 h (HT-29 and U2OS) or 96 h (MCF7, MDA-MB-231 and RC-124).
[b] predissolved in saline (0.9% NaCl w/v).
[c] from [39].
[d] not tested.

Table 3.5. IC_{50} values (in μM) of the gold(III)-dithiocarbamato compounds on cancer cell lines.

Only the dichloro-gold(III) derivative conjugated in the C6 position (**Au8**) showed modest cytotoxic activity on breast MDA-MB-231 and bone U2OS cancer cells, with IC_{50} values of 42 μM and 24 μM, respectively. On the contrary, the aglycone **Au2** displayed cytotoxic activity on the tested cancer cell lines. In addition, some complexes displayed modest cytotoxic activity on the non-cancerous cell line. These data suggest that glycoconjugation to this scaffold does not improve the *in vitro* anticancer activity nor the selectivity towards cancer cells.

On account of the poor cytotoxicity data, no further cytotoxicity tests in the presence of GLUT inhibitors were carried out. However, uptake studies could be carried out on selected compounds in order to investigate if any gold compound can be internalized in the cytosol.

3.8.2 Cell uptake studies

Uptake studies in MCF7 cells were carried out in Prof. Ingo Ott laboratory on two selected derivatives, the aglycone [$AuBr_2$(dtc-Inp-NH_2)] (**Au2**, cytotoxic) and the glycoconjugate [$AuBr_2$(dtc-Inp-GlcN2)] (**Au4**, non cytotoxic). The amount of intracellular gold was measured by atomic absorption spectroscopy (AAS) in four different sets of measurements: with or without cytochalasin B, a potent GLUT1-inhibitor, and in normal or glucose-free medium. The uptake was tested also under glucose depletion because the glucose content in the cell medium is approximately 25000-fold higher than the tested compounds (25 mM glucose vs 10 μM compound), which may result in a competitive substrate recognition. As reported in **Figure 3.8**, **Au2** and **Au4** showed surprisingly comparable cell uptake, as the intracellular content of gold is approximately unchanged

and in the range 1.5-3.0 nmol Au/mg protein. This was also observed in the presence of a GLUT-inhibitor (in which the gold uptake should, in principle, decrease if the transporter was inhibited), or in the presence of D-glucose (in which uptake should decrease in the presence of competitive binding).

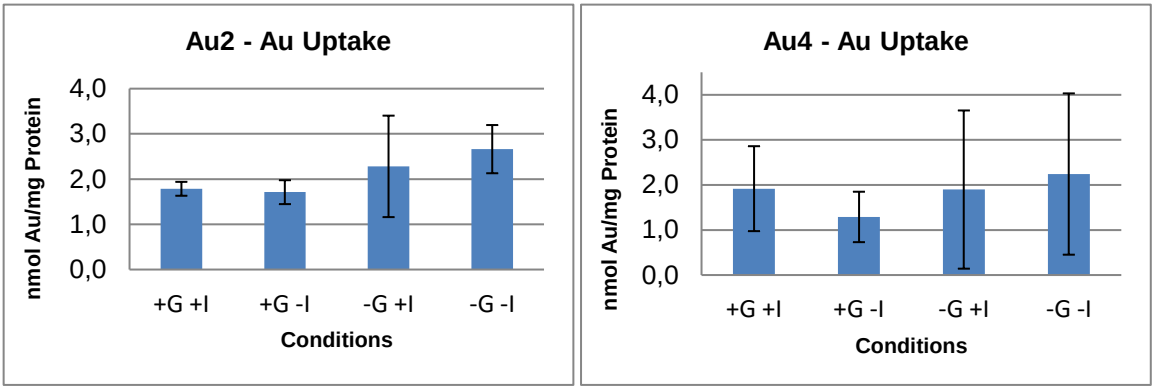

+G: medium with/without D-glucose (4.5 g L^{-1}).
+/-I: with/without cytochalasin B (50 μM).

Figure 3.8. Gold uptake in MCF7 cancer cells (after 6 h co-incubation) of **Au2** and **Au4** (10 μM) determined by atomic absorption.

Remarkably, these results point out the complexity of the *in vitro* behaviour of the gold(III)-dithiocarbamato glycoconjugates here reported. Although they seem to be internalized inside the cells, they showed no cytotoxic activity, compared to the non-glycoconjugate model counterparts. In addition, the studies in the presence or absence of cytochalasin B and glucose seem to exclude that the mechanism of uptake is mediated by the GLUT1, likely involving a passive diffusion mechanism instead.

3.9 Conclusions

A series of new glycoconjugated gold(III)-dithiocarbamato complexes of the type $[AuX_2(dtc\text{-}Inp\text{-}sugar)]$ have been obtained by exploiting an innovative approach which exploits transmetallation reactions from zinc(II)-dithiocarbamato precursors. The dibromo and dichloro derivatives were obtained in good yields and *via* straightforward workups, if $[AuBr_4]^-$ or $[AuCl_4]^-$ are reacted with the zinc(II) precursors.

In addition, two non-glycoconjugated model complexes $[AuBr_2(dtc\text{-}Inp\text{-}OEt)]$ (**Au1**) and $[AuBr_2(dtc\text{-}Inp\text{-}NH_2)]$ (**Au2**) were synthesized with the same method. The XRD crystal structure of the complex **Au1** was also obtained, confirming the expected coordination mode to the gold(III) centre. All compounds have been characterized by means of ^1H and ^{13}C NMR, FT-IR, UV-Vis spectroscopy and elemental analysis. In particular, UV-Vis

spectroscopy in PBS revealed that they undergo rapid hydrolysis, in agreement with data reported for analogous complexes.

Unfortunately, such gold(III)-dithiocarbamato glycoconjugates were non-cytotoxic, proving that the glycoconjugation of the dithiocarbamato scaffold did not increase the anticancer activity compared with the non-glycoconjugated complex which, in turn, showed IC_{50} values in the low-micromolar range. However, cell uptake studies showed interestingly that the compounds can be internalized but *via* a process that is probably non-GLUT-mediated.

3.10 References

[1] W. W. H. Wong, J. Cookson, E. A. L. Evans, E. J. L. McInnes, J. Wolowska, J. P. Maher, P. Bishop, P. D. Beer, *Chem. Commun.* **2005**, *0*, 2214–2216.

[2] O. D. Fox, J. Cookson, E. J. S. Wilkinson, M. G. B. Drew, E. J. MacLean, S. J. Teat, P. D. Beer, *J. Am. Chem. Soc.* **2006**, *128*, 6990–7002.

[3] I. A. Lutsenko, A. V. Ivanov, M. A. Kiskin, G. V. Ogil'ko, *Russ. J. Inorg. Chem.* **2015**, *60*, 92–99.

[4] A. Pettenuzzo, D. Montagner, P. McArdle, L. Ronconi, *Dalton Trans.* **2018**, *47*, 10721–10736.

[5] L. Ronconi, L. Giovagnini, C. Marzano, F. Bettìo, R. Graziani, G. Pilloni, D. Fregona, *Inorg. Chem.* **2005**, *44*, 1867–1881.

[6] M. Negom Kouodom, L. Ronconi, M. Celegato, C. Nardon, L. Marchiò, Q. P. Dou, D. Aldinucci, F. Formaggio, D. Fregona, *J. Med. Chem.* **2012**, *55*, 2212–2226.

[7] M. Negom Kouodom, G. Boscutti, M. Celegato, M. Crisma, S. Sitran, D. Aldinucci, F. Formaggio, L. Ronconi, D. Fregona, *J. Inorg. Biochem.* **2012**, *117*, 248–260.

[8] G. Boscutti, L. Marchiò, L. Ronconi, D. Fregona, *Chem. Eur. J.* **2013**, *19*, 13428–13436.

[9] P. T. Beurskens, H. J. A. Blaauw, J. A. Cras, J. J. Steggerda, *Inorg. Chem.* **1968**, *7*, 805–810.

[10] G. Aravamudan, D. H. Brown, D. Venkappayya, *J. Chem. Soc. A.* **1971**, *0*, 2744–2747.

[11] B. Arul Prakasam, K. Ramalingam, G. Bocelli, A. Cantoni, *Polyhedron*, **2007**, *26*, 4489–4493.

[12] F. Bonati, R. Ugo, *J. Organomet. Chem.* **1967**, *10*, 257–268.

[13] G. Boscutti, L. Feltrin, D. Lorenzon, S. Sitran, D. Aldinucci, L. Ronconi, D. Fregona, *Inorg. Chim. Acta*, **2012**, *393*, 304–317.

[14] F. Forghieri, C. Preti, L. Tassi, G. Tosi, *Polyhedron*, **1988**, *7*, 1231–1237.

[15] J. J. Criado, I. Fernandez, B. Macias, J. M. Salas, M. Medarde, *Inorg. Chim. Acta*, **1990**, *174*, 67–75.

[16] H. L. M. Van Gaal, J. W. Diesveld, F. W. Pijpers, J. G. M. Van der Linden, *Inorg. Chem.* **1979**, *18*, 3251–3260.

[17] L. Ronconi, C. Maccato, D. Barreca, R. Saini, M. Zancato, D. Fregona, *Polyhedron*, **2005**, *24*, 521–531.

[18] J. Willemse, J. A. Cras, J. J. Steggerda, C. P. Keyzers, Dithiocarbamates of transition group elements in "unusual" oxidation states, in *Electrons in Oxygen- and Sulphur-Containing Ligands* (Ed.: J. D. Dunits, P. Hemmerich, R. H. Holm, J. A. Ibers, C. K. Jørgensen, J. B. Neilands, D. Reinen, R. J. P. Williams), Springer, Berlin, **1976**, pp. 83–126.

[19] J. J. Criado, J. A. Lopez-Arias, B. Macias, L. R. Fernandez-Lago, J. M. Salas, *Inorg. Chim. Acta*, **1992**, *193*, 229–235.

[20] G. A. Katsoulos, C. A. Tsipis, *Inorg. Chim. Acta*, **1984**, *84*, 89–94.

[21] H. Ito, J. Fujita, K. Saito, *Bull. Chem. Soc. Jpn.* **1967**, *40*, 2584–2591.

[22] A. K. Gangopadhayay, A. Chakravorty, *J. Chem. Phys.* **1961**, *35*, 2206–2209.

[23] J. Chatt, G. A. Gamlen, L. E. Orgel, *J. Chem. Soc.* **1958**, *0*, 486–496.

[24] R. J. H. Clark, P. C. Turtle, *J. Chem. Soc. Dalton Trans.* **1977**, *0*, 2142–2148.

[25] C. C. Hadjikostas, G. A. Katsoulos, S. K. Shakhatreh, *Inorg. Chim. Acta*, **1987**, *133*, 129–132.

[26] G. C. Franchini, A. Giusti, C. Preti, L. Tassi, P. Zannini, *Polyhedron* **1985**, *4*, 1553–1558.

[27] G. Boscutti, C. Nardon, L. Marchiò, M. Crisma, B. Biondi, D. Dalzoppo, L. Dalla Via, F. Formaggio, A. Casini, D. Fregona, *ChemMedChem* **2018**, *13*, 1131–1145.

[28] G. Marcon, S. Carotti, M. Coronnello, L. Messori, E. Mini, P. Orioli, T. Mazzei, M. A. Cinellu, G. Minghetti, *J. Med. Chem.* **2002**, *45*, 1672–1677.

[29] L. Messori, F. Abbate, G. Marcon, P. Orioli, M. Fontani, E. Mini, T. Mazzei, S. Carotti, T. O'Connell, P. Zanello, *J. Med. Chem.* **2000**, *43*, 3541–3548.
[30] P. Calamai, A. Guerri, L. Messori, P. Orioli, G. P. Speroni, *Inorg. Chim. Acta* **1999**, *285*, 309–312.
[31] L. Ronconi, C. Marzano, P. Zanello, M. Corsini, G. Miolo, C. Maccà, A. Trevisan, D. Fregona, *J. Med. Chem.* **2006**, *49*, 1648–1657.
[32] L. Sun, X. Zeng, C. Yan, X. Sun, X. Gong, Y. Rao, N. Yan, *Nature*, **2012**, *490*, 361–366.
[33] D. Deng, C. Xu, P. Sun, J. Wu, C. Yan, M. Hu, N. Yan, *Nature*, **2014**, *510*, 121–125.
[34] G. Cantuaria, A. Magalhaes, R. Angioli, L. Mendez, R. Mirhashemi, J. Wang, P. Wang, M. Penalver, H. Averette, P. Braunschweiger, *Cancer*, **2000**, *88*, 381–388.
[35] L. Speizer, R. Haugland, H. Kutchai, *Biochim. Biophys. Acta BBA - Biomembr.* **1985**, *815*, 75–84.
[36] P. Kumar, G. Shustov, H. Liang, V. Khlebnikov, W. Zheng, X.-H. Yang, C. Cheeseman, L. I. Wiebe, *J. Med. Chem.* **2012**, *55*, 6033–6046.
[37] M. Gynther, J. Ropponen, K. Laine, J. Leppänen, P. Haapakoski, L. Peura, T. Järvinen, J. Rautio, *J. Med. Chem.* **2009**, *52*, 3348–3353.
[38] D. Deng, P. Sun, C. Yan, M. Ke, X. Jiang, L. Xiong, W. Ren, K. Hirata, M. Yamamoto, S. Fan, N. Yan, *Nature*, **2015**, *526*, 391–396.
[39] M. Proetto, W. Liu, A. Hagenbach, U. Abram, R. Gust, *Eur. J. Med. Chem.* **2012**, *53*, 168–175.

Chapter 4

Gold(III)-dithiocarbamato organometallic glycoconjugates

Chapter 4. Gold(III)-dithiocarbamato organometallic glycoconjugates

For full experimental procedures and characterizations see Chapter 8.

4.1 Anticancer gold(III) organometallic compounds

As previously discussed, a number of gold(III) compounds displaying anticancer activity have been reported. However, the +3 oxidation state is generally unstable/reactive under physiological conditions, and reduction to gold(I) or gold(0) may readily occur in the presence of biological intracellular reductants (e.g. thiols).[1] As depicted in **Scheme 4.1**, four-coordinated gold(III) species can be reduced to two-coordinated gold(I) species or to gold(0), accompanied by the release of the ligands.

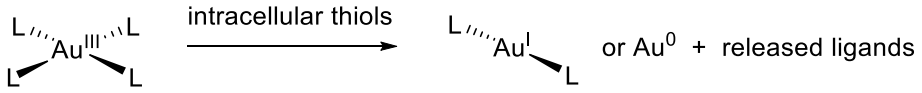

Scheme 4.1. Intracellular reduction of four-coordinated gold(III)-species by sulfur-containing molecules.

In contrast, cyclometalated gold(III) complexes coordinated to deprotonated carbon donor ligands exhibit higher stability even in the presence of cellular reducing agents. Gold(III) complexes stabilized with C-deprotonated bidentate C^N, tridentate C^N^C and C^N^N ligands have been extensively studied and showed promising anticancer activities (**Figure 4.1**).[2]

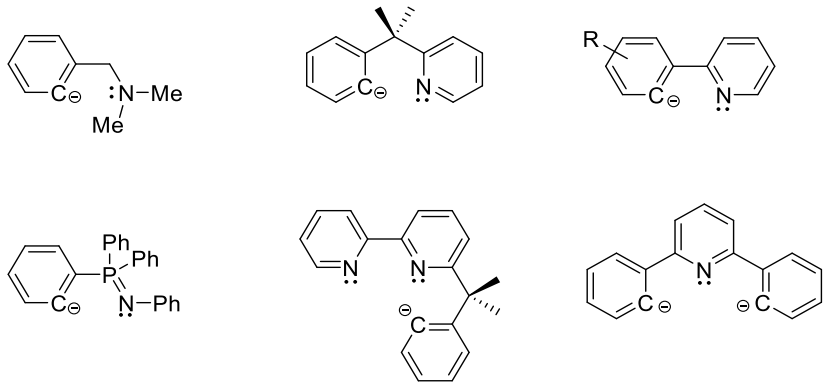

Figure 4.1. Reported ligands used for the design of anticancer gold(III) organometallic derivatives.

Some C^N-tethered gold(III) derivatives with 2-phenylpyridine bearing dithiocarbamato ligands have been reported independently by Parish and Che.[3,4] Among all, an ionic cyclometalated complex coordinated to a diethyldithiocarbamato ligand (**Figure 4.2**) exhibited selective *in vitro* cytotoxicity towards MCF-7 breast cancer cells, associated with high cellular uptake of gold, and induced cell-cycle arrest, apoptosis and antiangiogenic properties that could be related to deubiquitinase (DUB) inhibitory activity.[4,5]

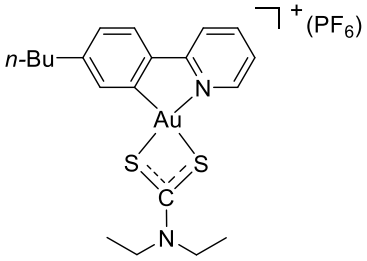

Figure 4.2. Chemical structure of the bioactive organometallic gold(III) dithiocarbamato complex studied by Che and coworkers.

Accordingly, this type of scaffolds can, in principle, combine the promising antitumour profile of the metal-dithiocarbamato moiety with increased physiological stability, an essential prerequisite for a potential pharmaceutical development.

4.2 Aims and objectives

Owing to the overall lack of stability of the gold(III) complexes described in Chapter 3, the aim of this project was to design and synthesize novel cyclometalated C^N gold(III)-dithiocarbamato glyco- and non-glycoconjugated of the type [Au(2-benzylpyridine)(dtc)]$^{+}$ (dtc: various dithiocarbamato ligands, **Figure 4.3**).

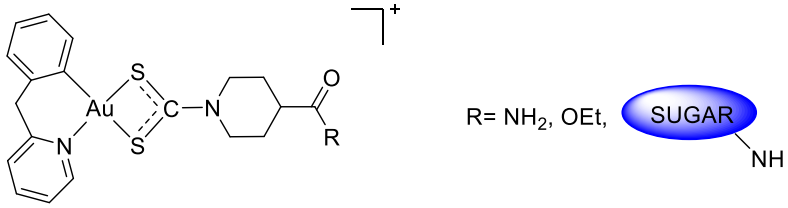

Figure 4.3. General chemical structure of the organometallic gold(III) dithiocarbamato conjugates synthesized.

As already observed for similar analogues, the Au–C bond would stabilize the metal centre towards hydrolysis and/or reduction. Moreover, the ionic nature of the complex would improve water solubility and hydrophilicity. In theory, this could make the derivative more likely to be internalized into the intracellular environment *via* facilitated diffusion mechanisms, such as the uniporter active transport promoted by the GLUTs.

In this regard, prior to the biological tests, the stability of these derivatives under physiological-like conditions and the *n*-octanol/water distribution coefficient (Log*D*) were evaluated.

In addition, only for the derivative conjugated in position C1-β of the glucose ring, an assay in presence of the enzyme β-glucosidase was carried out. This assay aimed at evaluating the potential of the derivative as a prodrug by activation of an enzyme overexpressed in tumour cells.

The final aim is the evaluation of the biological activity of the series of compounds towards: i) a panel human tumour cell lines in order to assess the cytotoxicity; ii) the same human tumour cell lines in the presence of a GLUT inhibitor in order to assess any possible involvement of the glucose transporters in the internalization mechanism.

4.3 Synthesis

The synthesis of the target complexes was accomplished by ligand exchange reaction between the gold(III) complex [Au(Bnpy)Cl_2], (Bnpy: 2-benzylpyridine) and the corresponding zinc dithiocarbamato precursors as discussed in Chapter 3 (**Scheme 4.2**).

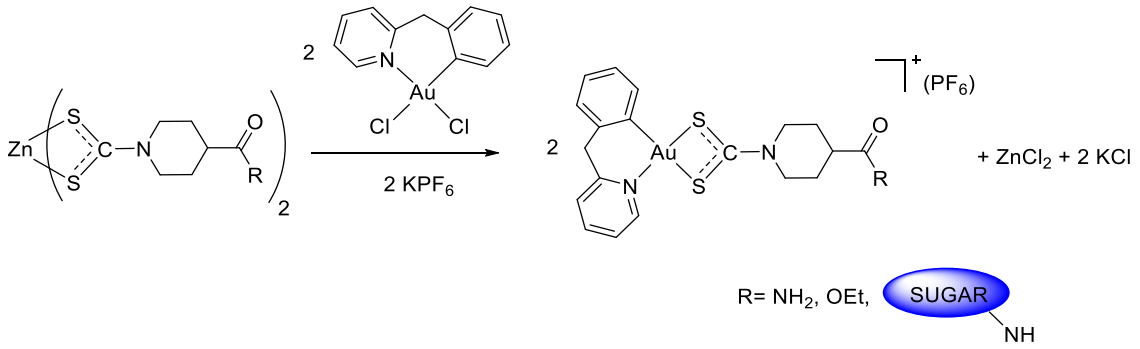

Scheme 4.2. General reaction scheme for the synthesis of the organometallic gold(III)-dithiocarbamato derivatives.

The precursor [Au(Bnpy)Cl_2] (**Au9**) was synthesized according to a literature procedure by reacting sodium tetrachloroaurate (Na[$AuCl_4$]) with 2-benzylpyridine in water under reflux.[6] Despite of what is reported in the literature,[7] in our case conventional heating afforded slightly better yields of the product compared to microwave heating. However, addition 2-benzylpyridine to the gold(III) salt at room temperature readily affords a yellow precipitate due to coordination of the nitrogen to the metal centre (**Scheme 4.3**). Prolonged heating and reaction time favour insertion of the metal into the C–H bond of the aromatic ring in *ortho* position, and the concomitant formation of HCl as by-product, generating the white precipitate of [Au(Bnpy)Cl_2].

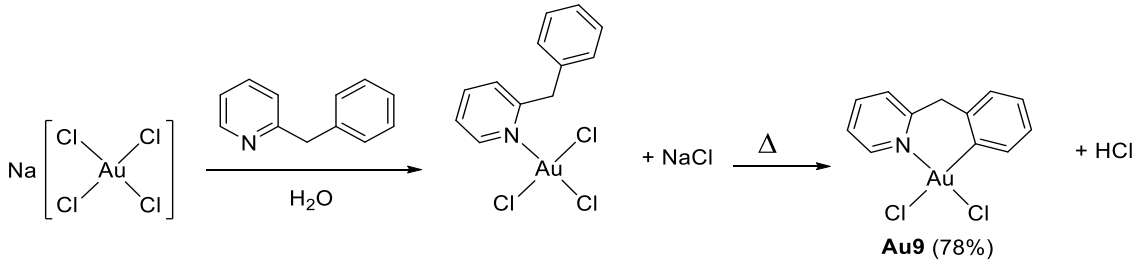

Scheme 4.3. Synthesis of [Au(Bnpy)Cl_2] (**Au9**).

In order to assess the feasibility of the transmetallation approach, some derivatives with ethyl isonipecotate (Inp-OEt) and isonipecotamide (Inp-NH_2) moieties were obtained either with the free dithiocarbamato ligands already isolated, or with the corresponding zinc dithiocarbamato analogues (as discussed in Chapter 3, **Scheme 4.4**). The characterization of the compounds obtained by means of the two protocols confirmed the obtainment of identical products.

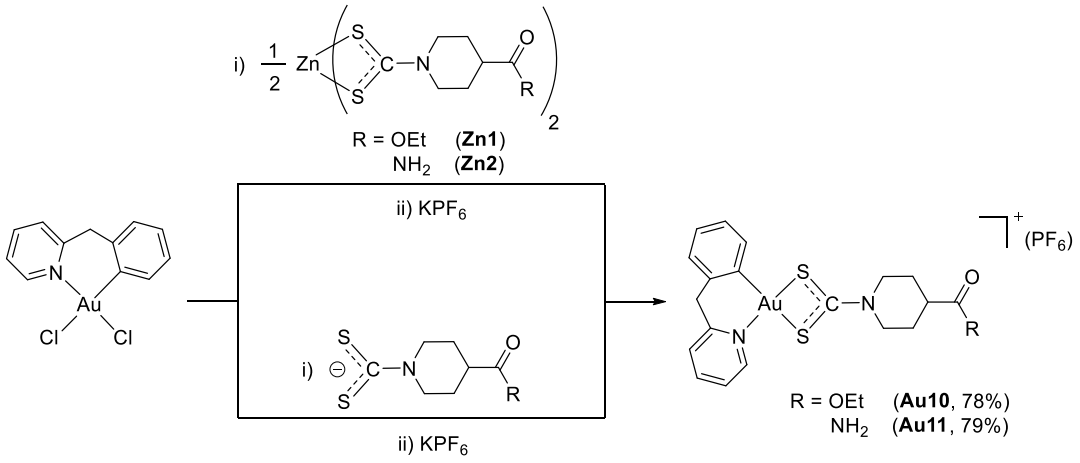

Scheme 4.4. Synthesis of [Au(Bnpy)(dtc-Inp-OEt)]PF_6 (**Au10**) and [Au(Bnpy)(dtc-Inp-NH_2)]PF_6 (**Au11**).

Different reaction conditions/solvents have been tested, but all afforded the desired compounds in very good yields (79-89%) and high purity. The structures of the desired derivatives **Au10** and **Au11** were also confirmed by XRD crystallography. The complexes are very soluble in DMSO, DMF, acetonitrile, methanol, ethanol and dichloromethane.

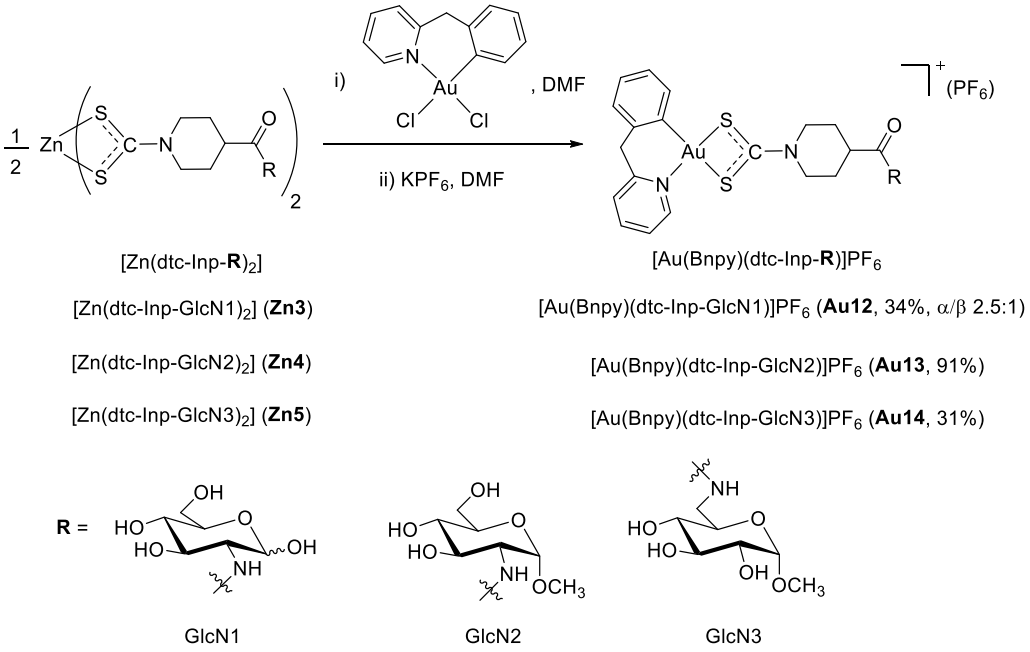

Scheme 4.5. Synthesis of the organometallic gold(III)-dithiocarbamato glycoconjugates.

As to the glycoconjugated complexes **Au12-14**, these were synthesized *via* a one-pot reaction by addition of a solution of the zinc(II)-dithiocarbamato complexes **Zn3-5** (0.5 eq.) to a solution of [Au(Bnpy)Cl_2] (1 eq.) in DMF at room temperature. Subsequently, a solution of potassium hexafluorophosphate (KPF_6) was added in excess to exchange the negative counterion (**Scheme 4.5**).

On the other hand, the derivative with the appended glucose in C1-β position [Au(Bnpy)(dtc-Inp-GlcN4)]PF_6, **Au15**, could not be obtained with the same method used for the other glycoconjugates. Therefore, it was synthesized *via* a two-step procedure, in which the zinc(II)-dithiocarbamato precursor **Zn6** is first added to **Au9** in DMF. Then, after isolation of the corresponding gold(III)-dithiocarbamato derivative, the negative counterion tethrachlorozincate ($ZnCl_4^-$) is exchanged with KPF_6 in methanol (**Scheme 4.6**).

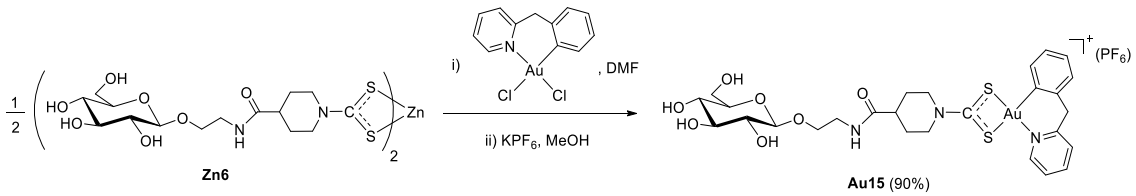

Scheme 4.6. Synthesis of [Au(Bnpy)(dtc-Inp-GlcN4)]PF_6 (**Au15**).

All complexes are soluble in DMSO, DMF and, in some cases, methanol (**Au15**), acetonitrile, acetone and chlorinated solvents. Remarkably, the complex with the appended glucose in C1 position, [Au(Bnpy)(dtc-Inp-GlcN4)]PF_6 (**Au15**), is highly soluble in water (> 10 mg/mL). Moreover, all are air- and photo-stable in solid.

4.4 XRD crystallography

Crystals of **Au10** and **Au11** suitable for X-ray diffraction crystallography were obtained by slow evaporation of dichloromethane/methanol solutions of the compounds (**Figure 4.4**). Crystals of **Au11** as an acetonitrile solvate can be obtained also by slow evaporation of an acetonitrile solution. Both **Au10** and **Au11** crystallize in a $P2_1/c$ monoclinical space group.

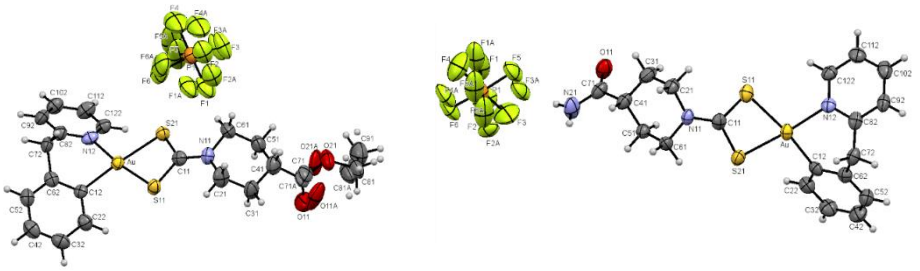

Figure 4.4. ORTEP views of [Au(Bnpy)(dtc-Inp-OEt)]PF_6 (**Au10**, left) and [Au(Bnpy)(dtc-Inp-NH_2)]PF_6 (**Au11**, right) . Some structural disorder can be observed around the ester and exafluorophosphate moieties.

There is a significant distortion from square-planar geometry due to the small bite angle of the dithiocarbamato ligand, corresponding to 75.70° and 75.78° for **Au10** and **Au11** respectively, versus 90° of a pure square-planar geometry. In contrast, the gold atom displays a slight distortion around the carbon and nitrogen atoms of the 2-benzylpyridine ligand of 89.70° and 88.48° for **Au10** and **Au11**, respectively. Moreover, the six-membered metallacycle is in a boat-like conformation, which is in line with previous observations made by Bertrand and Fuchita for 2-benzylpyridine gold(III) metallacycles.[6] The boat conformation around the metallacycle forces the two aromatic rings to adopt a distorted spatial arrangement with an angle between the Au–N12–C122 and Au–C12–C22 bonds of around 120-124°, which corresponds to a nearly 56-60° distortion from the plane (**Table 4.1**).

The bond distances between the Au–C and Au–N bonds are similar to what observed by Bertrand and others, around 2.06 and 2.07 Å for Au–C and Au–N respectively, but anyway significantly shorter of 0.2-0.3 Å when compared to the two Au–S bond lengths.[3,6] Furthermore, the Au–S11 bond (trans to the N atom) is longer than the Au–S21 one (trans to the C atom) (2.38 vs 2.29 Å) in compound **Au10**, while these are substantially of the same length in **Au11**.

	Au10	**Au11**
Bond angles (°)		
S–Au–S	75.70	75.78
C–Au–N	89.7	88.48
N–Au–S	96.9	99.74
C–Au–S	97.7	95.95
S–C–S	112.4	111.8
Bond lengths (Å)		
Au–C	2.056	2.059
Au–N	2.071	2.069
Au–S11	2.3824	2.335
Au–S21	2.2869	2.339

Table 4.1. Selected bond angle and lengths for the compounds [Au(Bnpy)(dtc-Inp-OEt)]PF_6 (**Au10**) and [Au(Bnpy)(dtc-Inp-NH_2)]PF_6 (**Au11**).

Further details of the structures are provided in the Appendix section.

4.5 IR spectroscopy

Infrared spectra in cesium iodide disks (CsI) were collected for compounds **Au10-15**, either in the mid- (4000-600 cm^{-1}) and far-infrared (600-200 cm^{-1}) spectral windows (**Figure 4.5**). The most relevant IR bands are listed in **Table 4.2**. As already described in the previous chapters, the strong diagnostic stretching vibration of the N–CSS moiety ("thioureide band") is usually detected at 1550 cm^{-1}, significantly differing from the values recorded for the zinc precursors at ca. 1490 cm^{-1}. This vibration usually overlaps with the in-plane bending (δ_{ip}) vibration of the CNH moiety of secondary amides (also called amide II) in the glycoconjugated compounds **Au12-15**.[8]

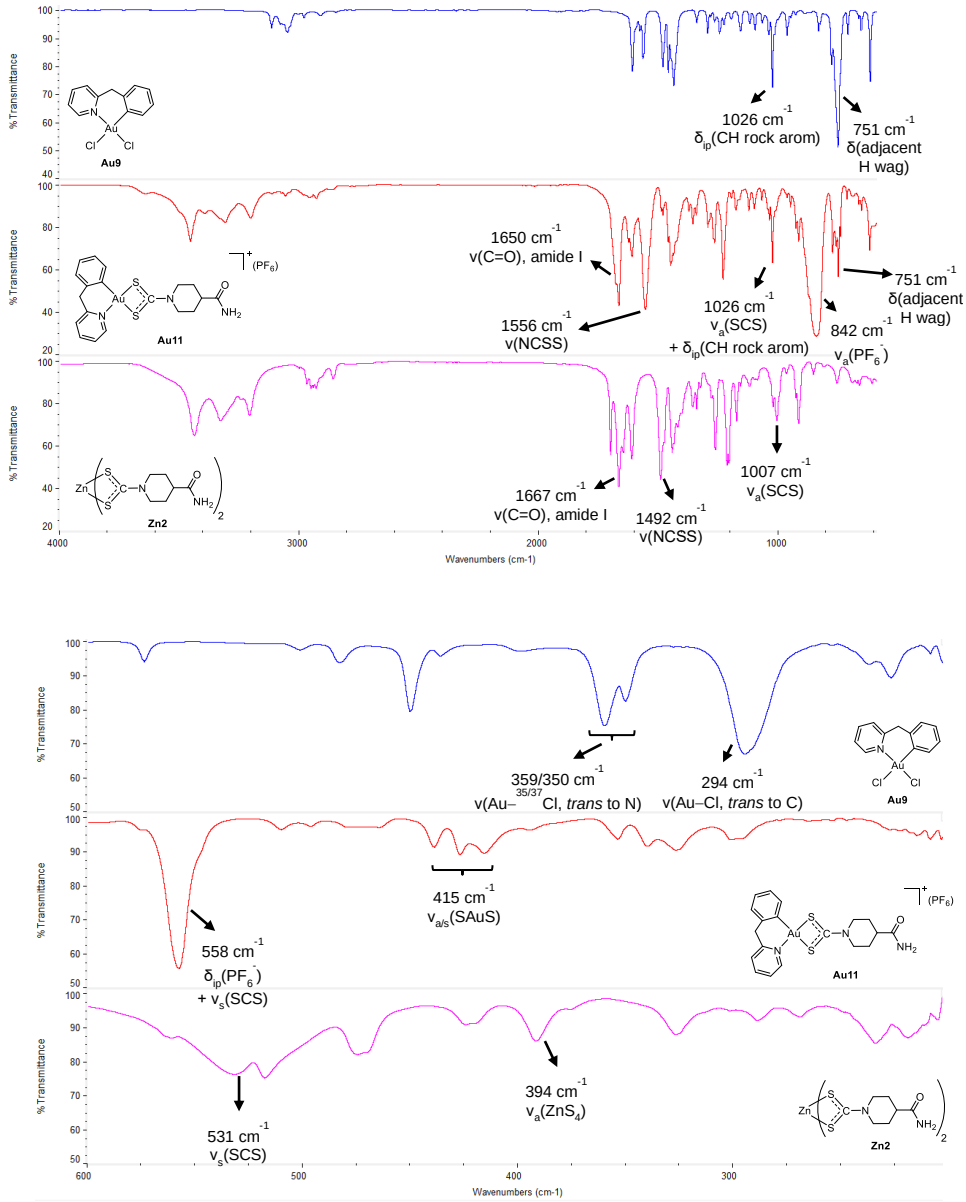

Figure 4.5. Stacked infrared spectra (CsI disk) of compounds **Au9**,**10** and **Zn2** in the mid- (4000-600 cm^{-1}, lower) and far- (600-200 cm^{-1}, upper) infrared region.

A single absorption at about 1020 cm^{-1} was recorded, attributable to the antisymmetric stretching of the SCS moiety. This confirms, as already observed for the compounds of the $[AuX_2(dtc)]$ series, that the dithiocarbamato ligand is coordinated to the gold(III) centre in a symmetrical bidentate fashion, according to the Bonati-Ugo criterion.[9] This vibration cannot always be undoubtedly assigned due to the overlap with the much stronger and broader stretching of the C–O bonds of the sugar skeleton.

By comparison with the spectrum of the starting reagent, $[Au(Bnpy)Cl_2]$ (**Au9**), the disappearance of the bands corresponding to the stretching of the Au–Cl bonds at *ca*. 350 cm^{-1} (Au–Cl *trans* to the N atom) and 300 cm^{-1} (Au–Cl *trans* to the C atom), respectively, is observed.[6] This evidences the loss of the chlorides in favour of other donor atoms. In addition, some typical vibrations due to the 2-benzylpyridinato ring are detected, in both the precursor **Au9** and in the corresponding derivatives, in the mid-IR region at ca. 1610-1450 cm^{-1} (C–C stretching of the aromatic rings), 1020 cm^{-1} (C–H rocking), and 750 cm^{-1} (adjacent H wagging).[8]

Finally, two very intense bands are recorded at around 840 and 550 cm^{-1}, confirming the presence of the exafluorophosphate counterion. These bands correspond, respectively, to an antisymmetric stretching and an in-plane bending (scissoring) vibration of the octahedral hexafluorophosphate (PF_6^-).[10]

Complex	$\tilde{\nu}_{max}$, cm^{-1}		
	ν(N–CSS)	$\nu_{a/s}$(SCS)	$\nu_{a/s}$(SAuS)[c]
Au10	1551	1026/578	409
Au11	1556	1026/558[b]	415
Au12	1554[a]	1028/575	405
Au13	1551[a]	1024/575	403
Au14	1554[a]	1025/558[b]	412
Au15	1544[a]	1027/559[b]	412

[a] overlapped with in-plane bending (δ_{ip}) CNH (amide II) vibration.
[b] overlapped with in-plane bending (δ_{ip}, scissoring) PF_6^- vibration.
[c] symmetric and antisymmetric modes overlapped.

Table 4.2. Selected FT-IR data (CsI disk, wavenumber in cm^{-1}) of compounds **Au10-15**.

4.6 NMR spectroscopy

Monodimensional ^1H, $^{13}C\{^1H\}$ and $^{13}C\{^1H\}$ DEPT NMR and bidimensional [^1H-^1H] COSY and [^1H-^{13}C] HMQC NMR spectra were recorded for all complexes in DMSO-d_6 at room temperature.

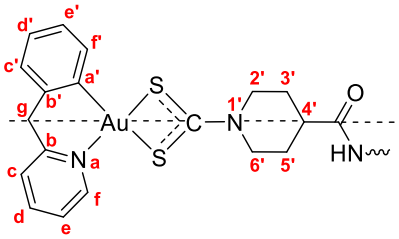

Figure 4.6. Numbering scheme for the gold(III) organometallic complexes.

As already found for the compounds of the "dihalogenido series" described in Chapter 3, a general upfield shift of the proton signals of the isonipecotate scaffold is observed for the corresponding transmetallation products **Au10-15** (**Figure 4.6** and **4.7**), the $C^{2',6'}H$ equatorial protons being the only exception. This is consistent with the greater deshielding effect of the gold(III) ion than zinc(II) due to the higher oxidation state.[11]

In all ^{1}H NMR spectra recorded, the signals assigned to the methylene protons of the isonipecotic linker are split due to the loss of symmetry upon coordination of 2-benzylpyridine. The effect is more evident in the signals of the equatorial and axial $C^{2',6'}H$ protons (0.1 ppm) rather than the $C^{3',5'}$ protons (negligible). However, the axial proton in position $C^{4'}$ is not involved in this effect since it lies along the plane of simmetry.

[^{1}H-^{1}H] COSY NMR proved useful to assign the resonances of the aromatic protons of the 2-benzylpyridine ligand and of the amide moiety (N*H*) in the region 9.0-7.0 ppm. Anyway, the pattern is substantially maintained with slight differences compared to the starting gold(III) precursor **Au9**. As already mentioned, also the peaks corresponding to the carbohydrate pendants are substantially unchanged when shifting from zinc(II) to gold(III).

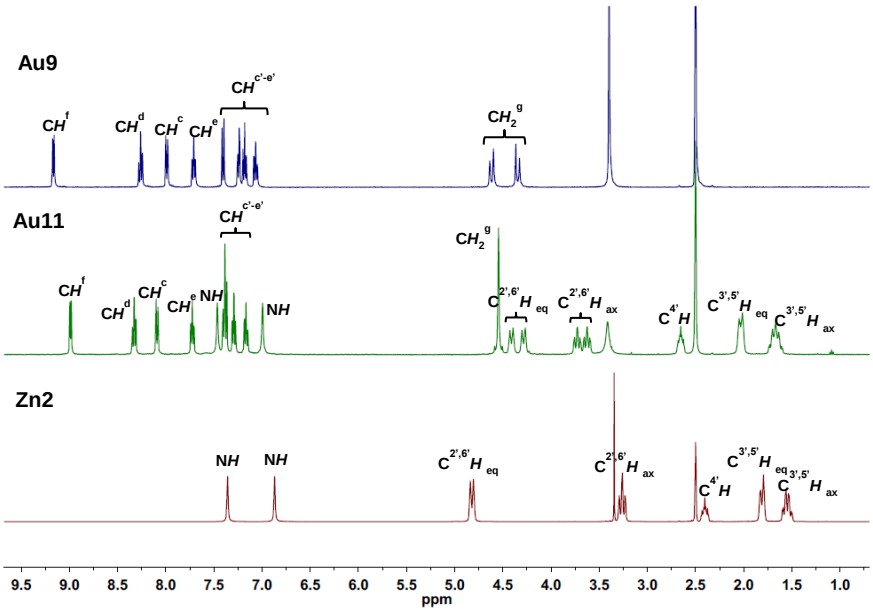

Figure 4.7. Stacked ^{1}H NMR spectra (400 MHz, DMSO-d_6) of **Au9** (top), **Au11** (middle), **Zn2** (bottom).

As far as the anomer *ratio* of the glycoconjugates is concerned, complex **Au12** was obtained as an α,β mixture of anomers owing to the presence of the (α,β)-D-glucosamine pendant (**GlcN1**). Compared to the starting zinc(II)-precursor **Zn3**, the α:β *ratio* slightly differed (α:β ≈ 2:1 for **Au12** vs 4:1 for **Zn3**). On the contrary, the α to β ratio was substantially retained in compounds **Au14-15** (only α anomer for **Au14** and only β anomer for **Au15**, **Figure 4.8**). Finally, in line with what described for **Au4**, when using *O*-methyl-2-amino-2-deoxy-(α,β)-D-glucopyranoside (**GlcN2**) the percent of the β anomer dramatically decreased (**GlcN2**, α:β ≈ 5:1) in the corresponding zinc(II)-dithiocarbamato glycoconjugate (**Zn4**, α:β ≈ 25:1, see Chapter 2), to be completely absent in the gold(III) analogue (**Au13**).

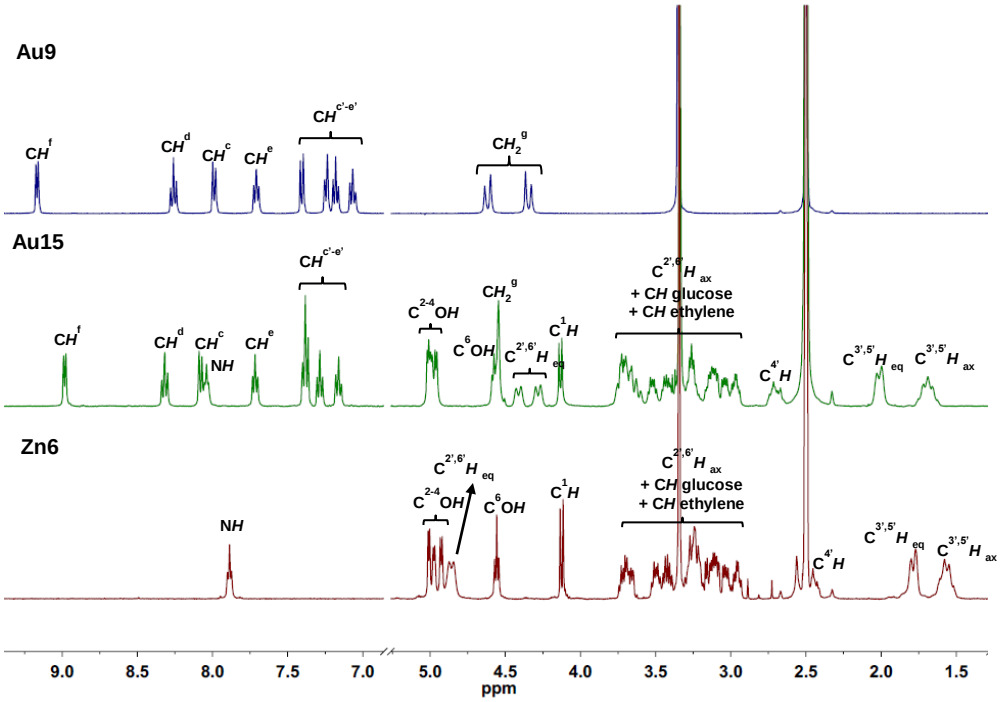

Figure 4.8. Stacked ^{1}H NMR spectra (400 MHz, DMSO-d_6) of **Au9** (top), **Au15** (middle), **Zn6** (bottom).

In the $^{13}C\{^{1}H\}$ NMR spectra, the diagnostic peak arising from the –NCSS carbon was recorded at 192 ppm (**Figure 4.9** and **4.10**). As to the compounds of the "dihalogenido series" described in Chapter 3, the dithiocarbamic signal is shifted upfield compared to the signal of the corresponding zinc(II) derivative (202 ppm). The δ(N^{13}CSS) values, together with an higher ν(N–CSS) values in the infrared spectra, indicate an increased C–N double bond character that is, anyway, in a lower extent compared with the compounds of the type [AuX_2(dithiocarbamate)].

In agreement with what observed in the ^{1}H NMR spectra, the CH_2 signals in the isonipecotic linker are split due to the loss of symmetry upon coordination of 2-

benzylpyridine. This effect is higher for the nuclei closer to the metal centre, with the splitting following the order $C^{2',6'} > C^{3',5'}$.

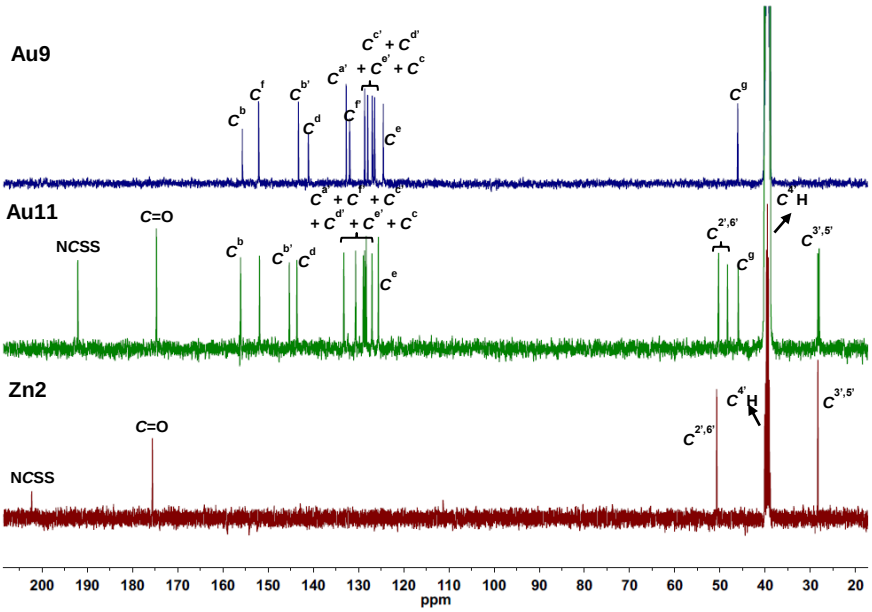

Figure 4.9. Stacked ^{13}C NMR spectra (100 MHz, DMSO-d_6) of **Au9** (top), **Au11** (middle), **Zn2** (bottom).

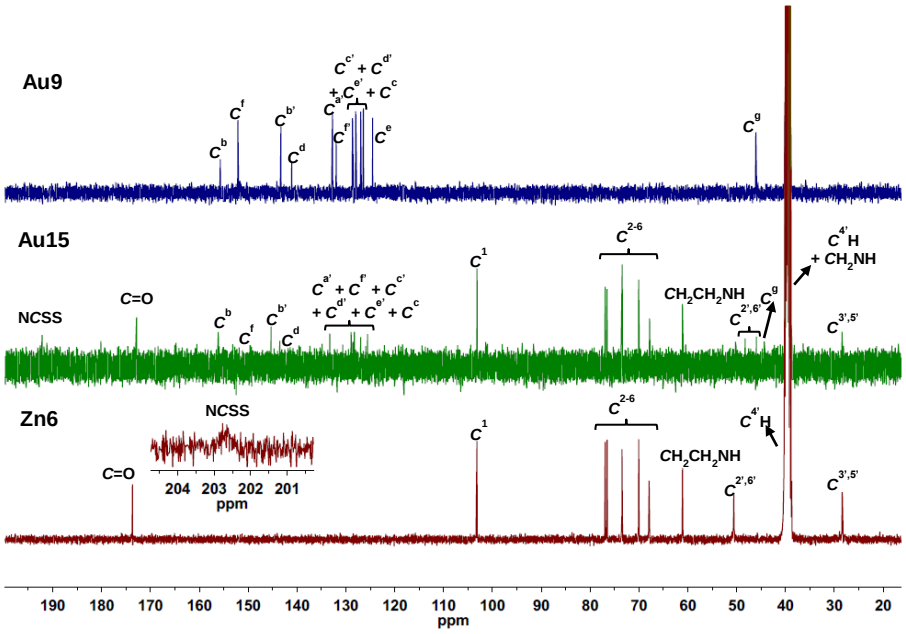

Figure 4.10. Stacked ^{13}C NMR spectra (100 MHz, DMSO-d_6) of **Au9** (top), **Au15** (middle), **Zn6** (bottom).

4.7 ESI-MS analysis

Mass spectrometry coupled with electrospray ionization (ESI-MS) provided further insights to assess the identity of the synthesized molecules. However, mass spectrometry analysis on neutral gold(III)-dithiocarbamato derivatives can give scarce information due

to their general sensitivity to the ionization conditions, leading to: i) lack to detect of the molecular ion peak; ii) formation of $[Au^{III}(dithiocarbamate)_2]^+$ ions in the positive mode, and iii) formation of $[Au^{III}X_4]^-$ and $[Au^{I}X_2]^-$ ions in the negative mode.[12,13]

Anyway, it was envisaged that the ionic nature of the organometallic gold(III) derivatives of the type [Au(Bnpy)(dithiocarbamate)]$^+$ could provide more valuable information. For this reason, ESI-MS analysis was carried out on this series of compounds (**Figure 4.11**). As expected, a peak with 100% intensity is observed in every compound, corresponding to the cation [Au(Bnpy)(dithiocarbamate)]$^+$.

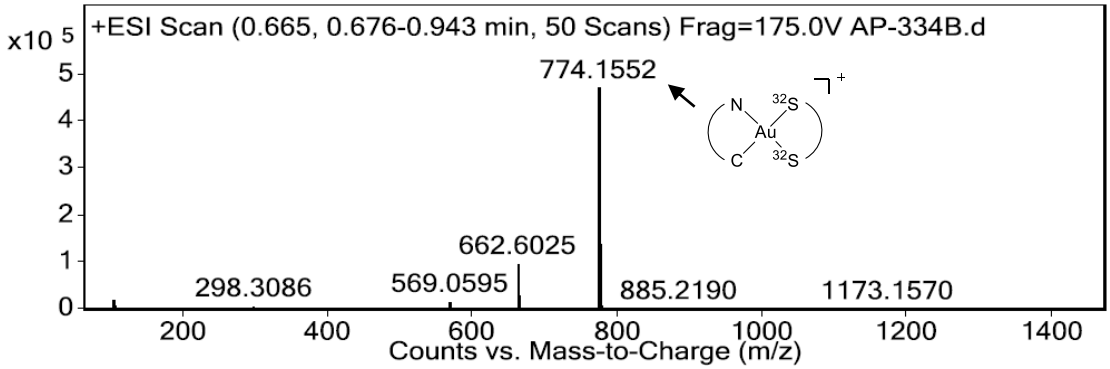

Figure 4.11. ESI/MS spectrum of complex [Au(Bnpy)(dtc-Inp-GlcN4)]PF_6 (**Au15**).

Sulfur has a big impact in the fragmentation pattern of the cation peak since it can be seen with gradually m/z +1 decreasing peaks. Sulfur, in fact, can be found in nature distributed into four stable isotopes, ^{32}S, ^{33}S, ^{34}S and ^{36}S, with 95.02, 0.75, 4.21 and 0.014% relative abundance, respectively. In the case of dithiocarbamato-containing complexes, the presence of two sulfur atoms further splits the fragmentation pattern. For example, in the case of [Au(Bnpy)(dtc-Inp-GlcN4)]PF_6 (**Au15**), the most abundant peak of the cation containing two ^{32}S atoms can be detected at 774.1552 m/z (100% relative abundance), with a decreasing pattern according to **Scheme 4.7**. Experimental data are well in agreement with theoretical ones.

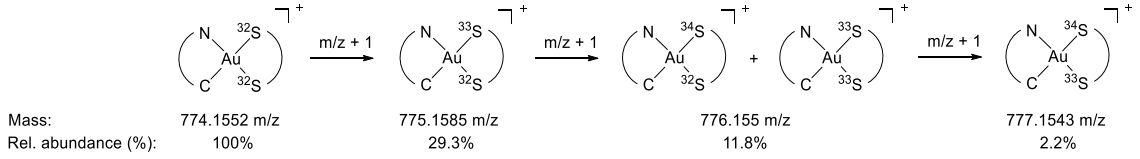

Scheme 4.7. Isotopic distribution and relative %abundance of complex [Au(Bnpy)(dtc-Inp-GlcN4)]PF_6 (**Au15**).

4.8 UV-Vis spectroscopy

Optical absorption spectra were recorded for compounds **Au10**-**Au15** in dimethyl sulfoxide at room temperature and the major absorption data are listed in **Table 4.3**. Similar absorption patterns were observed in all the compounds.

Complex	λ, nm (ε, M^{-1} cm^{-1})		
Au10	268 (30000)	~293 (sh, ~15700)	-
Au11	268 (32200) / 271 (31800)	~292 (sh, ~17000)	~342 (br, ~3200)
Au12	268 (44500) / 271 (45100)	~294 (sh, ~24300)	~340 (br, ~3500)
Au13	268 (30000)	~292 (sh, ~15800)	~340 (br, ~1700)
Au14	268 (31600) / 271 (31000)	~293 (sh, ~16500)	~333 (br, ~3400),
Au15	262 (23200) / 268 (26300)	~294 (sh, ~13200)	~350 (br, ~2100)

Table 4.3. Optical absorption data for compounds **Au10**-**15**.

Two types of spin-allowed bands are detected in the UV-region. The most intense band (ε 2.5-4.5·10^4 $M^{-1}cm^{-1}$) at high energies, localized at 260-270 nm, is sometimes split in two further bands. This absorption corresponds to the sum of two transitions, whose contributions can be abscribed to intraligand p*←p transitions involving orbitals predominantly localized on 2-benzylpyridinate (ε 1·10^4 M^{-1} cm^{-1}) and π*←π intraligand transitions mainly located in the –NCS and –CSS moieties (ε 1-2·10^4 M^{-1} cm^{-1}).[14,15] A second intense band (shoulder) at around 290-300 nm, which is not observed in the spectrum of free 2-benzylpyridine, is assigned to the π*←d metal-to-ligand charge transfer.[16] Finally, a very broad band of low intensity (ε ~ 1500-3500 M^{-1} cm^{-1}) is recorded at around 340 nm, which can be attributed to d←d transitions

4.9 Solution studies

Prior to the *in vitro* biological investigation, the compounds were screened for their stability in DMSO and in phosphate buffer saline solution (PBS, pH 7.4). All compounds did not show great stability in DMSO after a couple of days. The formation of a yellowish solution and, in some cases, the precipitation of a grey solid is observed, even when solutions are stored at 4°C. For this reason, the preparation of fresh mother solutions was always required.

In addition, the stability of the compounds in PBS (pH 7.4) was studied by means of UV-Vis spectroscopy, whose spectra are shown in **Figure 4.12**. Contrary to what observed for the gold(III)-dithiocarbamato compounds of the dihalogenido series, for the organometallic derivatives no significant changes take place in the UV-Vis spectra after

72 h. A similar behaviour was already observed by Che and coworkers with analogous 2-phenylpyridine derivatives.[4] This seems to suggest that the Au–C bond greatly increases the stability of the compounds towards hydrolysis.

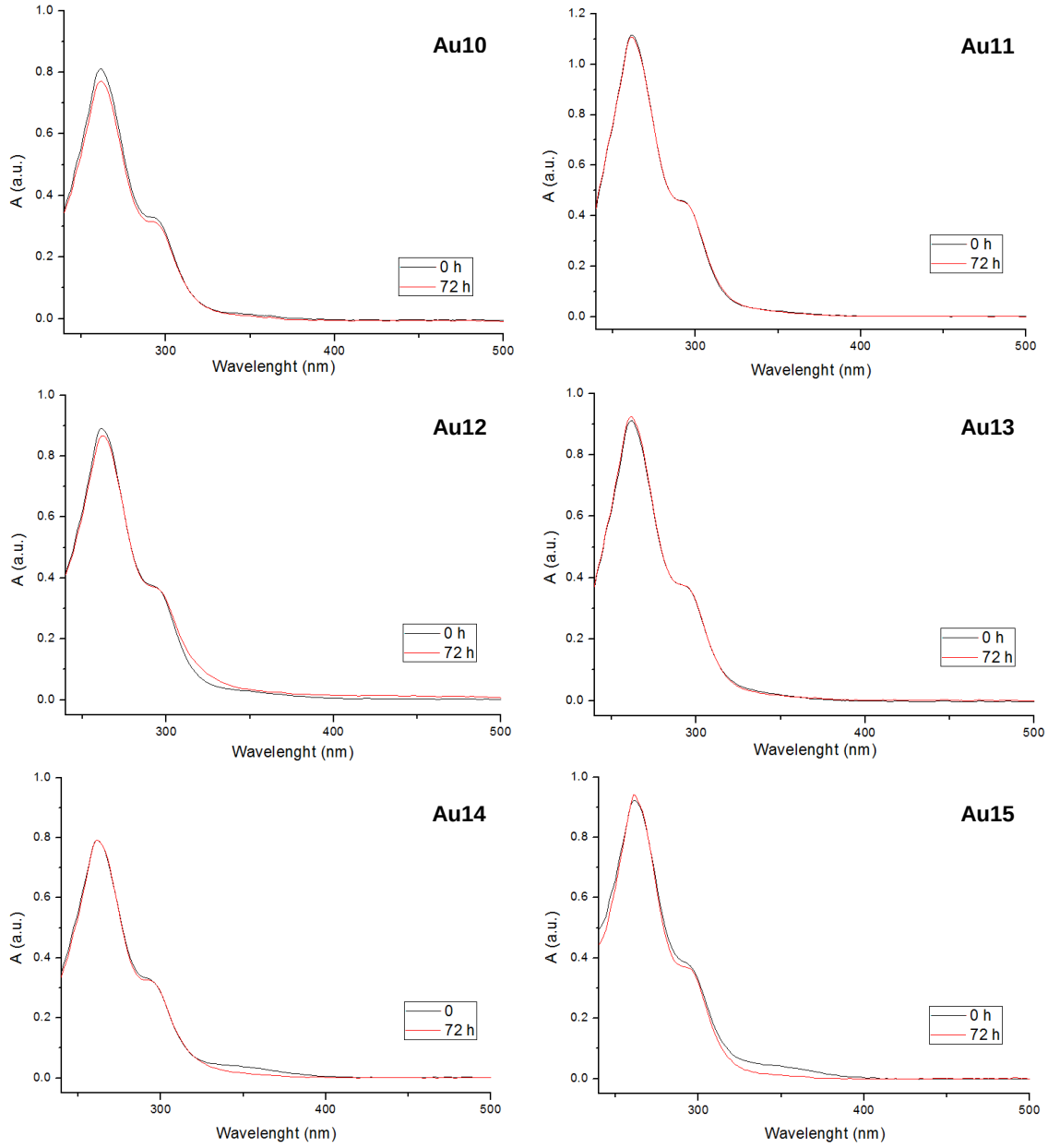

Figure 4.12. UV-Vis spectra of compounds **Au10-15** in PBS (37°C, 25 μM) at different time lapses.

4.10 Lipophilicity studies

The determination of the lipophilicity is an important asset to evaluate the drugability of a substance. Lipophilicity indicates the affinity of a substance for a lipid environment or, in other words, the ability of a substance to permeate through the lipidic membrane *via* passive diffusion pathways.[17] The lipophilicity is usually expressed by the partition (or

distribution) coefficient between two non-miscible phases, taken as a model of the lipid bilayer of a cell membrane and the extra/intracellular medium.[18]

The *n*-octanol-water partition coefficient, *P*, or its logarithmic-scale analogue, Log*P*, that refers to the ratio of compound concentration between *n*-octanol and water, is by far the most common way to express lipophilicity. However, the distribution coefficient, Log*D*, usually refers when a two-phase system is equilibrated at a pH where it is partially ionized. In addition, when Log*D* is determined at pH 7.4 (Log$D_{7.4}$), it is more representative of the distribution in a physiological medium:

$$\mathrm{Log}D = \log \frac{\mathrm{C_{oct}}}{\mathrm{C_w}}$$

where C_{oct} and C_w are, respectively, the concentrations of a substance in an *n*-octanol and aqueous solution after mutual partitioning.

Log*D* is one of the properties identified by Lipinski in the "Rule of 5" for drug-like molecules and, therefore, one of the key physiochemical features to be considered in drug discovery, being related to the bioavailability of a substance.[19,20] Moreover, lipophilicity is a crucial parameter for orally administered drugs, as a Log*D* ranging from 0 to 3 can be considered optimal for oral bioavailability.[21]

There are many different approaches to experimentally determine the distribution coefficient but, among all, the shake-flask method is the most common.[22] In this method, an aqueous solution of the analyte is mixed with a non-miscible organic solvent (in this case, *n*-octanol) and shaken mechanically.[23]

When using the shake-flask method, it is essential from a practical point of view that the samples to be tested are stable in the solvent system because of the lengthy experimental procedure. The high stability of this series of compounds in the physiological-like buffer makes them suitable for the estimation of the lipophilicity by this method.

Therefore, solutions of the compounds were mutually shaken with the non-miscible solvent, separated by centrifugation, and the concentration in each sample was calculated by absorbance measurements at 261 nm. Due to some precipitation issues, a predissolution in a minimum amount of DMSO (that do not interfere with the final estimation of lipophilicity) was required. Due to a general higher hydrophobicity of the model complex [Au(Bnpy)(dtc-Inp-OEt)]PF_6, (**Au10**) the Log*D* value was obtained by measuring the absorbance of a solution in PBS-saturated *n*-octanol before and after partitioning (see Chapter 8 for details). For the other compounds, Log*D* was obtained the other way round, that is by measuring the absorbance of a solution in *n*-octanol-saturated PBS. The calculated values are summarized in **Table 4.4**.

Complex	Log$D_{7.4}$
[Au(Bnpy)(dtc-Inp-OEt)]PF_6 (**Au10**)	0.95 ± 0.01
[Au(Bnpy)(dtc-Inp-NH_2)]PF_6 (**Au11**)	0.26 ± 0.08
[Au(Bnpy)(dtc-Inp-GlcN1)]PF_6 (**Au12**)	-0.68 ± 0.18
[Au(Bnpy)(dtc-Inp-GlcN2)]PF_6 (**Au13**)	-0.76 ± 0.07
[Au(Bnpy)(dtc-Inp-GlcN3)]PF_6 (**Au14**)	-0.54 ± 0.01
[Au(Bnpy)(dtc-Inp-GlcN4)]PF_6 (**Au15**)	-0.65 ± 0.17

Table 4.4. Log$D_{7.4}$ values of the organometallic gold(III) complexes.

The partition coefficient *n*-octanol/water at pH 7.4 for the model complexes is 0.95 and 0.25 for **Au10** and **Au11**, respectively, showing that they tend to distribute more in the octanolic rather than in the aqueous phase (approximately 10 and 2-fold more in octanol than water for **Au10** and **Au11**, respectively).

On the contrary, Log*D* is between -0.76 and -0.54 for the glycoconjugates, which highlights their tendency to distribute more in the aqueous phase. As expected, the conjugation of a highly hydrophilic carbohydrate to a metal-based derivative, quite lipophilic in nature due to the presence of the cyclometalated aromatic ring, generally increases the overall hydrophilicity of the final derivatives. Remarkably, increased hydrophilicity would also reduce tendency to enter the cellular membrane *via* passive diffusion, as active transport pathways, such as glucose transporters, would be favoured.

4.11 β-glucosidase activity assay

β-glucosidase are enzymes devoted to hydrolize β-glycosidic bonds to release non-reducing terminal glucosyl residues from glycosides and oligosaccharides.[24] These enzymes are ubiquitous in all domains of living organisms, in which they play a variety of functions. These include conversion of biomass, breakdown of glycolipids and exogenous glucosides in mammals, catabolism of oligosaccharides involved in cell-cell recognition and signal transduction through membrane.[25,26] In particular, β-glucosidases are expressed in tumour cells, and this can be exploited by activating suitably glycosylated prodrugs.[27,28] In order to assess the potential prodrug character of glycoconjugates, the cleavage of the β-glycosidic bond by β-glucosidase can be monitored. Various enzymatic assays have been employed, monitored through a number techniques, such as NMR spectroscopy, UV-Vis, and TLC.[29–31] Due to the high solubility and stability of compound **Au15** in aqueous solutions, the effect of β-glucosidase could be tracked by NMR spectroscopy, following a modified procedure reported in the literature (**Scheme 4.8**).[29] **Au15** was incubated at 37°C with the enzyme

in buffer acetate (pH 5) in D_2O, and the ^1H NMR spectra were recorded over time (**Figure 4.13**).

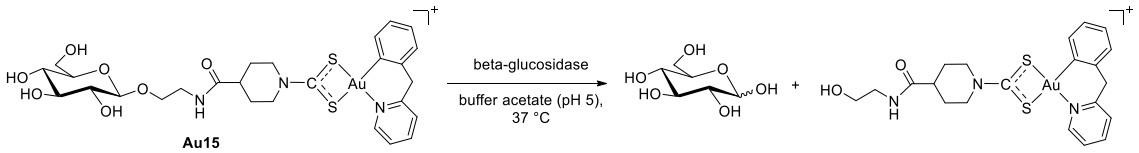

Scheme 4.8. Expected hydrolysis of the glycoconjugate **Au15** catalyzed by β-glucosidase.

As depicted in **Figure 4.13**, two doublets at 5.24 and 4.65 ppm ($^3J_{HH}$ = 3.7 and 7.9 Hz, respectively) with increasing intensities appear over time, which can be attributed to the C1–H protons belonging to the α and β glucose anomers (•). The same behaviour can be observed in a positive control experiment performed by co-incubating cellobiose and the enzyme (**Figure 4.14**). At the same time, the signals corresponding to the complex **Au15** gradually decrease in intensity. This can be clearly seen in the decrease of the C2–H peak at 3.31 ppm of **Au15**, with the concomitant appereance at 3.26 ppm of the C2–H signal of glucose (β anomer). In addition, signals belonging to a minor impurity (*), which was not identified, appear in the spectra (possibly, a degradation product of the complex).

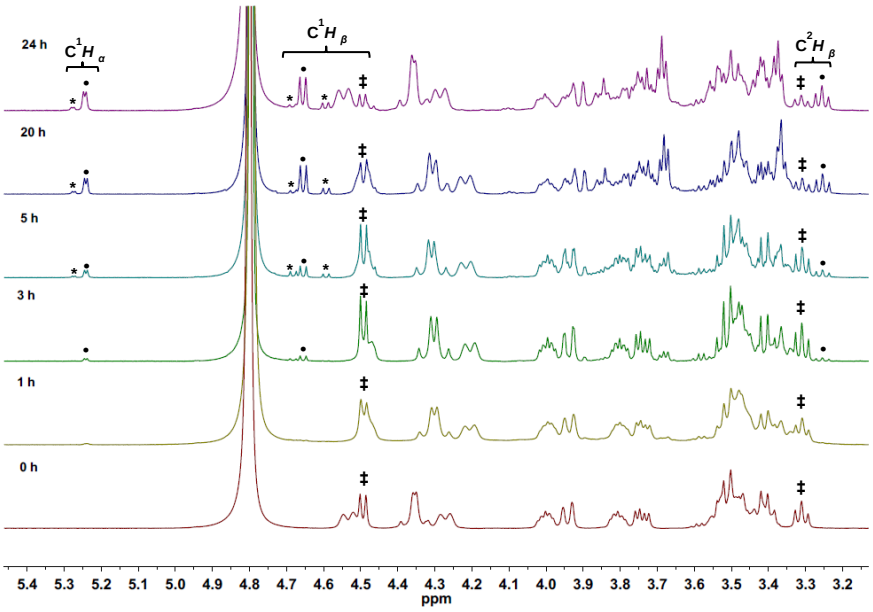

Figure 4.13. Stacked ^1H NMR spectra (500 MHz, buffer acetate in D_2O) recorded over time of compound **Au15** (‡) co-incubated with β-glucosidase (37°C). The formation of α,β-D-glucose (•) and an impurity (*) can be observed.

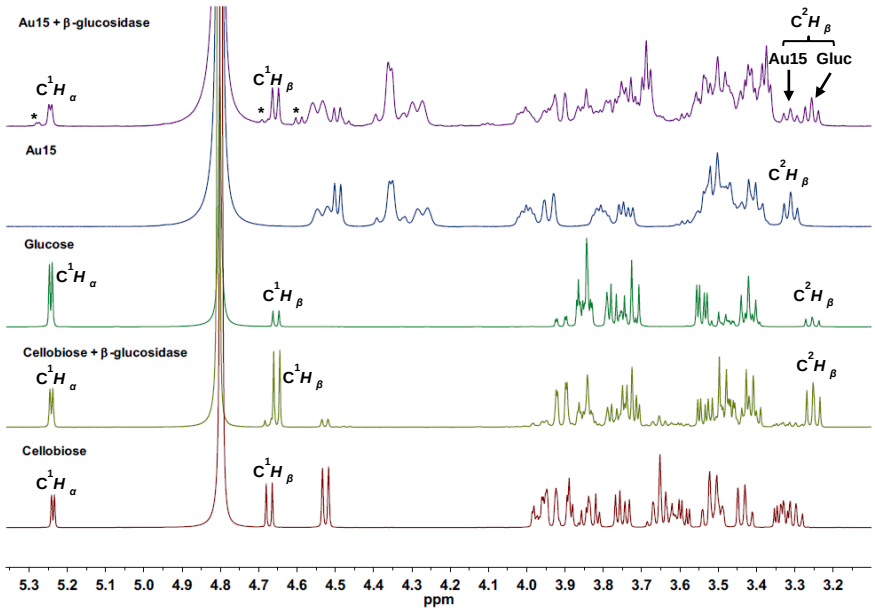

Figure 4.14. Stacked ^{1}H NMR spectra (500 MHz, buffer acetate in D_2O) of Au15 before and after co-incubation with β-glucosidase (24 h at 37°C). The spectra of glucose and cellobiose before and after co-incubation with β-glucosidase are also reported for comparison. The formation of an impurity (*) can be observed.

Finally, the hydrolysis of the **Au15** and subsequent formation of glucose was confirmed also by means of $^{13}C\{^{1}H\}$ NMR. Again, the formation of α,β-D-glucose was observed (two signals at 97.38 and 93.55 ppm assigned to the β and α anomers, respectively), with the concomitant decrease of the signals associated to the pristine compound **Au15** (one signal at 103.15 ppm, β anomer only, **Figure 4.15**).

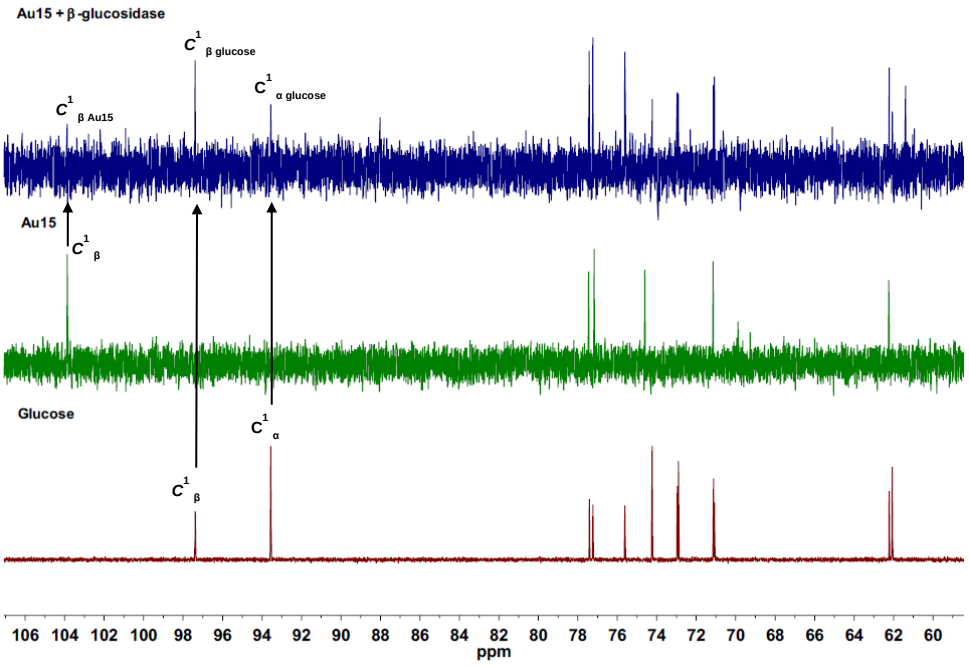

Figure 4.15. Stacked $^{13}C\{^{1}H\}$ NMR spectra (500 MHz, buffer acetate in D_2O) of glucose, **Au15** and **Au15** after co-incubation with β-glucosidase.

In conclusion, these experiments confirmed that the compound linked to the glucose moiety via a C1-β glycosidic bond, **Au15**, can be cleaved by β-glucosidase enzymes thus proving that it can behave as a prodrug into the cells.

4.12 Biological studies

In vitro cytotoxicity studies were carried out on the obtained organometallic compounds in the laboratories of Prof. Corrado Santocanale (National University of Ireland, Galway) on human osteosarcoma (U2OS) and of Prof. Lisa Dalla Via (University of Padova, Italy) on human cervix adenocarcinoma (HeLa), ovarian carcinoma (A2780), and cisplatin-resistant ovarian carcinoma (A2780cis) cell lines. The cytotoxicity values listed in **Table 4.5** are expressed as IC_{50}, that is, the concentration of compound that caused 50% inhibition of cell proliferation compared to untreated control cells.

Complex	IC_{50} (μM, 48 h)				RF
	U2OS	HeLa	A2780	A2780cis	
[Au(Bnpy)(dtc-Inp-OEt)]PF_6 (**Au10**)	6.2	15.9	0.2	0.5	2.1
[Au(Bnpy)(dtc-Inp-NH_2)]PF_6 (**Au11**)	16.3	> 20	1.1	6.2	5.8
[Au(Bnpy)(dtc-Inp-GlcN1)]PF_6 (**Au12**)	29.0	> 20	1.4	13.9	9.9
[Au(Bnpy)(dtc-Inp-GlcN2)]PF_6 (**Au13**)	32.9	> 20	2.7	14.3	5.3
[Au(Bnpy)(dtc-Inp-GlcN3)]PF_6 (**Au14**)	26.7	> 20	2.6	17.1	6.5
[Au(Bnpy)(dtc-Inp-GlcN4)]PF_6 (**Au15**)	n.d.	> 20	1.9	15.6	8.0
Cisplatin	3.7 ± 1.1	1.6	0.8	7.2	9.0

n.d. not determined

Table 4.5. Preliminary IC_{50} data of compounds **Au10-15** (expressed in μM, 48 h) on U2OS, HeLa, A2780, and cisplatin-resistant A2780 cells, and resistance factor (RF, calculated as IC_{50} A2780cis/IC_{50} A2780).

The compounds were deemed poorly or not active (IC_{50} > 20 μM) on U2OS (**Figure 4.16a**) and HeLa cells, respectively. On the contrary, they showed significant cytotoxic activity on the ovarian cancer cells A2780. Furthermore, the cytotoxicity was higher against the wild-type cells (A2780) than the cisplatin-resistant ones (A2780cis), with a resistance factor, that is, the ratio between the IC_{50} of the cisplatin resistant type and the IC_{50} of the wild type, comparable or lower to cisplatin.

This difference in biological activity is not surprising. In fact, it has been observed that the major acknowledged mechanism of transport of platinum-based drugs through the cell membrane in cisplatin-resistant cancer cells is *via* passive diffusion.[32] Conversely, the other active transporters usually overexpressed in non-resistant cancer cells, like the

copper transporter 1 (CTR1) responsible for the cell uptake and accumulation of platinum-based drugs, are underexpressed.[33] The reduced cytotoxicity in the resistant cells would be consistent with an internalization mechanism more likely mediated *via* active transporters rather than passive diffusion.

Moreover, it has been reported that in cisplatin-resistant cells the uptake of different nutrients, including glucose, is significantly reduced.[34,35] A reduced glucose uptake, along with an altered glycolytic metabolism is usually associated with increased cisplatin resistance.[36,37] Thus, the reduced uptake of glucose may simply decrease the internalization rate of the gold(III)-glycoconjugates.

Therefore, the difference in cytotoxic potency between wild type and cisplatin-resistant variant of A2780 cancer cells may be an indication of a cell internalization pathway different from a passive diffusion mechanism. Since active transport *via* either OCTs or GLUTs cannot be ruled out for this type of cells, further studies in the presence of inhibitors of the two transporters will be required in order to investigate the actual mechanism of uptake.

Regarding the human osteosarcoma U2OS cells, *in vitro* biological activity studies in the presence of a GLUT inhibitor were carried out in order to elucidate a possible mechanism of uptake. U2OS cells were treated with the glycoconjugates **Au12-14**, or the model complex **Au10**, and coincubated with the exofacial GLUT1 inhibitor EDG (4,6-*O*-ethylidene-α-D-glucose). If the cell uptake of the glycoconjugates was mediated by GLUT1, an increase in cell viability would be observed in the presence of EDG, since less cytotoxic compound would be internalized. The graph in **Figure 4.16b** shows that the differences in cell viability between cells treated with or without the GLUT-inhibitor are negligible, with the only exception of **Au14** with a slight increase (ca. 8%). These results suggest that, at least in U2OS cells, the cell uptake may not be GLUT1-mediated. For complex **Au14**, this may not be excluded, although other major mechanisms may be involved in the cell uptake of the derivatives.

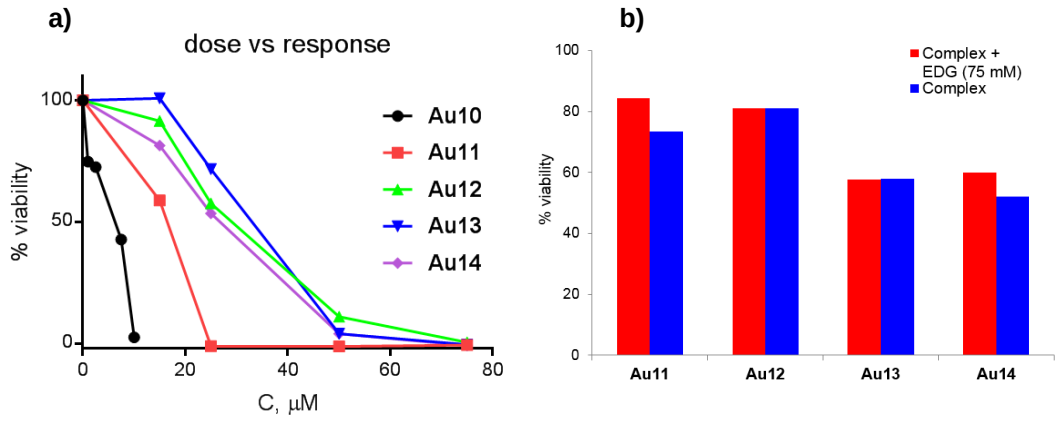

Figure 4.16. a) Dose vs response curve of compounds **Au10-14** against U2OS cells after 48 h. **b)** Effect of GLUT1 inhibitor EDG (75 mM) on U2OS cell viability (15 μM **Au11**, 50 μM **Au12-14**, 24 h).

4.13 Conclusions

The aforementioned gold(III) organometallic compounds **Au10-15** were obtained via ligand exchange reaction from preformed zinc(II)-dithiocarbamato derivatives. The compounds were characterized by a combination of NMR and IR spectroscopy, microanalysis, mass spectrometry and, in some cases, by single-crystal X-ray crystallography.

Remarkably, all the complexes displayed high stability in PBS solution. Furthermore, the complex with the glucose pendant in position C1, **Au15**, possessed high water-solubility. Lipophilicity (Log$D_{7.4}$) studies revealed that the distribution coefficient varied significantly of about one unit after glycoconjugation, thus suggesting that the lipophilicity may be tuned in order to increase interaction with active transporters.

Preliminary cytotoxicity assays indicated that the complexes display cytotoxic activity on ovarian cancer cells A2780, although they do not display a significant antiproliferative activity against U2OS and HeLa cells. In addition, they possessed a reduced cytotoxic activity on the cisplatin-resistant variant of ovarian cancer cells, A2780cis, with resistance factors in line or slightly lower when compared to cisplatin. These discrepancies in biological activity may be an indication of a possible facilitative mechanism of uptake. However, *in vitro* biological activity studies in the presence of GLUT1-inhibitors in U2OS cells seem to exclude (completely or, in the case of **Au14**, partially) a possible involvement of GLUT1 in the cell internalization.

This will constitute the basis for future in-depth investigations on the possible involvement of active transport (by cell viability studies with/without specific inhibitors) and on the amount of compound internalized in A2780 and A2780cis cells (by cell uptake studies).

4.14 References

[1] T. Zou, C. T. Lum, C.-N. Lok, J.-J. Zhang, C.-M. Che, *Chem. Soc. Rev.* **2015**, *44*, 8786–8801.
[2] B. Bertrand, A. Casini, *Dalton Trans.* **2014**, *43*, 4209–4219.
[3] R. V. Parish, J. P. Wright, R. G. Pritchard, *J. Organomet. Chem.* **2000**, *596*, 165–176.
[4] J.-J. Zhang, K.-M. Ng, C.-N. Lok, R. W.-Y. Sun, C.-M. Che, *Chem. Commun.* **2013**, *49*, 5153–5155.
[5] B. Bertrand, M. R. M. Williams, M. Bochmann, *Chem. Eur. J.* **2018**, *24*, 11840–11851.
[6] B. Bertrand, S. Spreckelmeyer, E. Bodio, F. Cocco, M. Picquet, P. Richard, P. Le Gendre, C. Orvig, M. A. Cinellu, A. Casini, *Dalton Trans.* **2015**, *44*, 11911–11918.
[7] A. P. Shaw, M. Tilset, R. H. Heyn, S. Jakobsen, *J. Coord. Chem.* **2011**, *64*, 38–47.
[8] D. Lin-Vien, N. Colthup, W. Fateley, J. Grasselli, *The Handbook of Infrared and Raman Characteristic Frequencies of Organic Molecules, 1st Edition*, Academic Press, Cambridge, MA, **1991**.
[9] F. Bonati, R. Ugo, *J. Organomet. Chem.* **1967**, *10*, 257–268.
[10] K. Nakamoto, *Infrared and Raman Spectra of Inorganic and Coordination Compounds: Part A: Theory and Applications in Inorganic Chemistry, Sixth Edition*, John Wiley and Sons, Inc., Hoboken, **2008**.
[11] J. J. Criado, I. Fernandez, B. Macias, J. M. Salas, M. Medarde, *Inorg. Chim. Acta* **1990**, *174*, 67–75.
[12] M. Altaf, A. A. Isab, J. Vančo, Z. Dvořák, Z. Trávníček, H. Stoeckli-Evans, *RSC Adv.* **2015**, *5*, 81599–81607.
[13] M. Altaf, M. Monim-ul-Mehboob, A.-N. Kawde, G. Corona, R. Larcher, M. Ogasawara, N. Casagrande, M. Celegato, C. Borghese, Z. H. Siddik, D. Aldinucci, A. A. Isab, *Oncotarget*, **2017**, *8*, 490–505.
[14] M. A. Mansour, R. J. Lachicotte, H. J. Gysling, R. Eisenberg, *Inorg. Chem.* **1998**, *37*, 4625–4632.
[15] L. Ronconi, L. Giovagnini, C. Marzano, F. Bettìo, R. Graziani, G. Pilloni, D. Fregona, *Inorg. Chem.* **2005**, *44*, 1867–1881.
[16] M. A. Ivanov, M. V. Puzyk, *Russ. J. Gen. Chem.* **2001**, *71*, 1660–1661.
[17] A. Leo, C. Hansch, D. Elkins, *Chem. Rev.* **1971**, *71*, 525–616.
[18] X. Liu, B. Testa, A. Fahr, *Pharm. Res.* **2011**, *28*, 962–977.
[19] C. A. Lipinski, F. Lombardo, B. W. Dominy, P. J. Feeney, *Adv. Drug Deliv. Rev.* **2001**, *46*, 3–26.
[20] C. Hansch, *Acc. Chem. Res.* **1969**, *2*, 232–239.
[21] J. B. Taylor, D. J. Triggle, *Comprehensive Medicinal Chemistry II*, Elsevier, Amsterdam, **2007**.
[22] A. Andrés, M. Rosés, C. Ràfols, E. Bosch, S. Espinosa, V. Segarra, J. M. Huerta, *Eur. J. Pharm. Sci.* **2015**, *76*, 181–191.
[23] *OECD Guidelines for the Testing of Chemicals, Test No. 107: Partition Coefficient (n-Octanol/Water): Shake Flask Method*, Organization for Economic Cooperation and Development, Paris, **1995**.
[24] J. R. Ketudat Cairns, A. Esen, *Cell. Mol. Life Sci.* **2010**, *67*, 3389–3405.
[25] M. Aureli, A. P. Masilamani, G. Illuzzi, N. Loberto, F. Scandroglio, A. Prinetti, V. Chigorno, S. Sonnino, *FEBS Lett.* **2009**, *583*, 2469–2473.
[26] R. R. Singhania, A. K. Patel, R. K. Sukumaran, C. Larroche, A. Pandey, *Bioresour. Technol.* **2013**, *127*, 500–507.
[27] V. Oliveri, M. Viale, G. Caron, C. Aiello, R. Gangemi, G. Vecchio, *Dalton Trans.* **2013**, *42*, 2023–2034.
[28] H. Cheng, X. Cao, M. Xian, L. Fang, T. B. Cai, J. J. Ji, J. B. Tunac, D. Sun, P. G. Wang, *J. Med. Chem.* **2005**, *48*, 645–652.
[29] G. R. Periyannan, B. A. Lawrence, A. E. Egan, *J. Chem. Educ.* **2015**, *92*, 1244–1249.
[30] E. S. Lymar, B. Li, V. Renganathan, *Appl. Environ. Microbiol.* **1995**, *61*, 2976–2980.
[31] G. N. Presley, M. J. Payea, L. R. Hurst, A. E. Egan, B. S. Martin, G. R. Periyannan, *Microbiology*, **2014**, *160*, 635–645.
[32] S. Y. Sharp, P. M. Rogers, L. R. Kelland, *Clin. Cancer Res.* **1995**, *1*, 981–989.
[33] S. B. Howell, R. Safaei, C. A. Larson, M. J. Sailor, *Mol. Pharmacol.* **2010**, *77*, 887–894.
[34] X.-J. Liang, D.-W. Shen, S. Garfield, M. M. Gottesman, *Cancer Res.* **2003**, *63*, 5909–5916.
[35] D.-W. Shen, A. Su, X.-J. Liang, A. Pai-Panandiker, M. M. Gottesman, *Br. J. Cancer*, **2004**, *91*, 270–276.
[36] D.-W. Shen, L. M. Pouliot, M. D. Hall, M. M. Gottesman, *Pharmacol. Rev.* **2012**, *64*, 706–721.
[37] X.-J. Liang, T. Finkel, D.-W. Shen, J.-J. Yin, A. Aszalos, M. M. Gottesman, *Mol. Cancer Res.* **2008**, *6*, 1499–1506.

Chapter 5

Gold(I)-dithiocarbamato glycoconjugates

Chapter 5. Gold(I)-dithiocarbamato glycoconjugates

For full experimental procedures and characterizations see Chapter 8.

5.1. Anticancer gold(I) compounds

As already mentioned in Chapter 1, the groundbreaking discovery of the anticancer properties of cisplatin and its congeners triggered research into novel alternative metallodrugs. Among these, gold-based compounds showed promise, especially because of their different mode of action at a mitochondrial level. A milestone in the field was the introduction in the market of the antiarthritic drug auranofin (**Figure 1.8e**). Its peculiar pharmacological profile seems to support a correlation between antiarthritic activity and anti-inflammatory properties. Despite being still under debate, the ability to relieve pain and halt disease progression seems to originate from various biological targets, including the enzymes cyclooxygenase (COX) and thioredoxin reductase (TrxR), that are also involved to a great extent in the proliferation of malignancies.[1–3] For this reason, the discovery by Mirabelli and coworkers that auranofin displayed also antiproliferative activity on a number of tumour cell lines should not surprise.[4] As a natural consequence, structural analogues sharing the same key features of auranofin were investigated, such as the +1 oxidation state of the gold metal centre. Gold(I) has a d^{10} closed-shell electron configuration that may induce three different possible coordination geometries, that is tricoordinated trigonal, tetracoordinated tetrahedral, or dicoordinated linear planar.[5,6] Spatial arrangement of the ligands around the metal centre depends on the type of the ligand.

Various anticancer gold(I)-complexes were reported, such as derivatives of carbenes, phosphines, alkynes, *N*-containing ligands and thiolates.[1,7]

Owing to the well-known therapeutic benefits of the benchmark drug auranofin, there is a steady interest in the discovery of novel Au(I) complexes possessing the key structural feature S–Au–P. Apart from the antiarthritic properties, similar derivatives showed anticancer, antimalarial, anti-HIV and antibacterial properties.[8] For this reason, phosphines have been the most common ligand for designing gold(I)-compounds. In particular, several linear phosphino-gold(I) analogues coordinated to dithiocarbamato ligands have been synthesized and studied, showing promising anticancer activity. Keter and coworkers reported a series of mono- and bridged dinuclear gold(I) complexes with dithiocarbamato ligands derived from pyrazoles and indazoles (**Figure 5.1**),[9] with the dinuclear series being more active against HeLa cells.

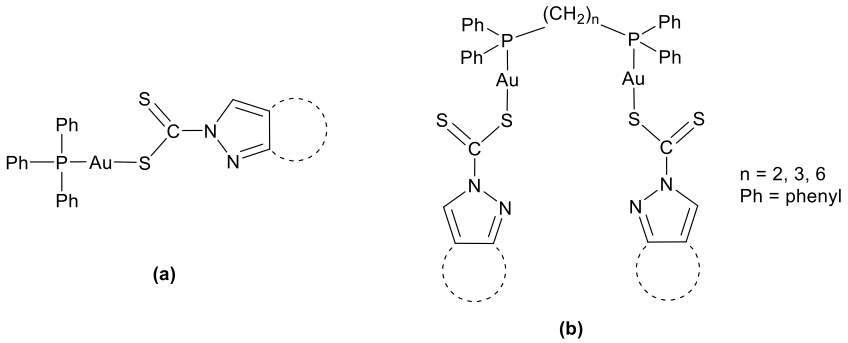

Figure 5.1. Chemical drawings of gold(I)-phopshino complexes with dithiocarbamato ligands with anticancer activity reported by Keter and coworkers.[9]

Compounds with trimethyl-, triethyl-, and tri-*tert*-butyl-phosphine and various dithiocarbamato ligands showed good to moderate anticancer activity against HeLa, A549, HepG2 and MCF7 cells (**Figure 5.2a**).[10,11] In addition, compounds like those depicted in **Figure 5.2b** proved more cytotoxic than doxorubicin and cisplatin against the doxorubicin-resistant variant breast adenocarcinoma MCF7R. The triphenylphosphino derivative was shown to induce cell apoptosis and to inhibit the activity of topoisomerase I.[12]

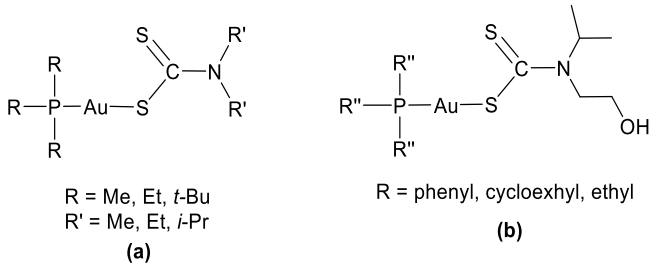

Figure 5.2. Chemical structures of reported gold(I)-phosphino complexes with dithiocarbamato ligands with anticancer activity.

Interestingly, some phosphane-gold(I) dithiocarbamato derivatives showed also antibacterial properties against a broad spectrum of gram positive and gram negative bacteria.[13]

Among the ligands explored for designing novel gold(I) metallodrugs, *N*-heterocyclic carbenes (NHC) are emerging nowadays as a versatile class of coordinating scaffolds[7] leading to compounds having a variety of applications, ranging from catalysis and medicinal chemistry to photoluminescent agents and materials.[14]

A carbene is defined as a neutral compound containing a divalent carbon atom with only six electrons in its valence shell (a pair of unshared, non-bonding electrons) which can adopt a linear or bent geometry, depending on its hybridization.[15,16] Carbenes can be classified in two categories that is, singlet or triplet (**Figure 5.3**). In singlet carbenes, the

two paired non-bonding electrons possess antiparallel spins, a total spin of zero and the carbon atom is sp^2-hybridized, whereas in triplet carbenes the two unpaired non-bonding electrons possess parallel spins, a total spin of one and the carbon atom can hybridize to either *sp* or sp^2.

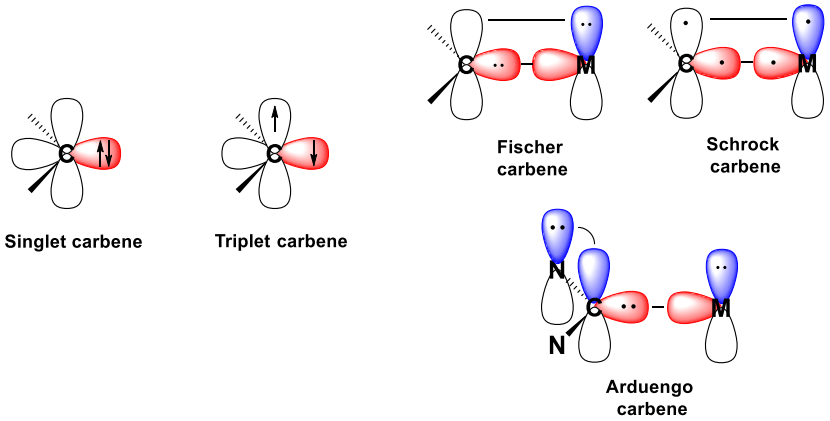

Figure 5.3. Classification of carbenes by spin (left) and by metal coordination (right).

Carbenes were commonly believed to be highly reactive and short-lived molecules,[17,18] although the presence of π-electrons donated by neighbouring heteroatoms such as nitrogen atoms can greatly improve their stability. In fact, the presence of two nitrogens incorporated in an aromatic ring in α position with respect to the carbene carbon enforces the overall stability by a mesomeric stabilization effect (+M/+M).[19] Despite *N*-heterocyclic carbene (NHC) ligands having been known since the 1960s, this research topic has remained relatively underdeveloped until Arduengo's discovery of stable and isolatable free carbene ligands.[16,20,21]

Coordination of carbenes to a metal can enhance their overall stability providing carbene ligands with donor properties similar to phosphines. Therefore, upon coordination carbenoids can be furtherly subdivided into different categories depending on their intrinsic reactivity.[22,23]

- Fischer-type carbenes are electrophilic carbenoids of low oxidation state metals with 18 electrons. Fischer carbenes are electron deficient at the carbon atom and consequently are easily attacked by nucleophiles.
- Schrock-type carbenes are nucleophilic carbenoids of high oxidation state metals with less than 18 electrons. Schrock carbenes are electron rich at the carbon atom and are thus prone to attack by electrophiles.
- Carbenes derived from *N*-heterocyclic molecules (NHC), such as the Arduengo-type, possess relative long half-life, stability and low reactivity. As previously mentioned, the presence of two nitrogen atoms and an aromatic imidazole ring

helps stabilizing the carbene. While Fischer- and Schrock-type carbene complexes are considered to have a metal-carbon double bond and substantial π-backbonding from the metal, *N*-heterocyclic carbenes are considered to have a metal-carbon single bond and minimal π-backbonding. The majority of research efforts have been focusing so far on metal complexes with this type of ligands (from now only referred to simply as "carbene").

Metal-NHC complexes are widely used in organometallic catalysis,[24–26] although they have rapidly gained popularity in the last decade as an emerging class of compounds with intriguing therapeutic potential. In fact, NHC ligands match the essential prerequisites for effective drug design since they are readily accessible in a few steps and their main physico-chemical properties and reactivity can be easily fine-tuned by ligand tailoring of the carbene and/or the ancillary ligand(s).[14,27–29] A huge amount of literature has been published on a number of carbene complexes with transition metals including gold(I/III), silver(I), platinum(II), palladium(II), copper(I/II), nickel (II), ruthenium (II) and rhodium(I) amongst others, with anticancer and antimicrobial properties.[7,30] As to the development of NHC-metal complexes with potential chemotherapeutic properties, gold(I) derivatives are predominant. Several complexes, such as those depicted in **Figure 5.4**, display antiproliferative activity towards tumour cell lines in the micromolar or sub-micromolar range.

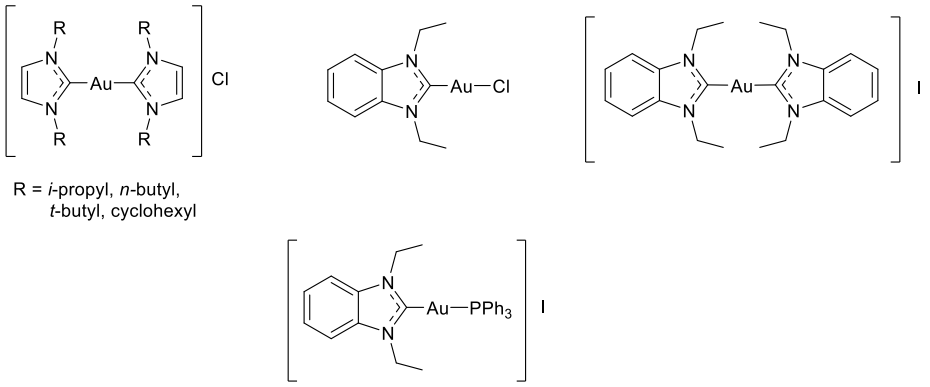

Figure 5.4. Chemical structures of selected gold(I)-carbene derivatives with anticancer properties.

NHC-gold glycoconjugate analogues of the benchmark drug auranofin have been reported, in which the phosphine is replaced by various carbene ligands.[31] NHC-carbene derivatives of tetraacetyl-1-thio-β-D-glucose-gold(I) (**Figure 5.5a**) exhibited cell growth inhibition in the micromolar range against human HT29 colon adenocarcinoma, MCF7 and MDA-MB-231 breast adenocarcinoma cells *in vitro*, generally overperforming the clinically-established drugs cisplatin and 5-fluorouracil.[32] Hackenberg *et al*. reported on the anticancer activity of NHC-carbene analogues of auranofin in which the alkyl

substituents on the carbene were systematically modified (**Figure 5.5b**).[33] Cytotoxicity results were encouraging especially on human MCF7 breast adenocarcinoma and Caki-1 skin carcinoma cells, in particular in comparison to analogues where either the carbene or the thioglucose ligands are replaced by chlorides. On the contrary, variation of the alkyl chains did not substantially affect the anticancer activity.

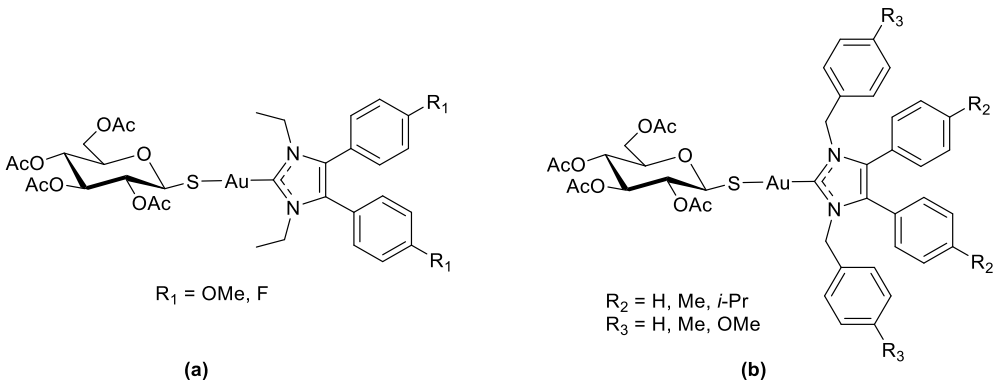

Figure 5.5. Chemical structures of gold(I)-carbene glycoconjugates with anticancer activity.

The versatility of these compounds allows wide functionalization of the Au(I)-carbene scaffold, including dithiocarbamato ligands. However, very little is known about the anticancer activity of mixed carbene gold(I)-dithiocarbamato complexes. In fact, to the best of our knowledge only two related papers and one patent are reported in the literature.[34–36]

Sun and coworkers synthesized a series of mono- and di-nuclear gold(I) carbene complexes bearing a pyrrolidinedithiocarbamato ligand (PDT, **Figure 5.6**).[34] The compounds showed potent inhibitory activity in cisplatin-resistant ovarian cancer cells A2780cis. Interestingly, the best-performing binuclear ionic derivative (**Figure 5.6b**) was incorporated into a zinc(II)-based metal organic framework (MOF), which served as a carrier for the delivery and the subsequent release of the drug. The zinc-MOF was biologically compatible, capable of moderately efficient loading and subsequent release of the complex over time under physiologically relevant conditions with IC_{50} on cisplatin-resistant A2780cis cells of *ca*. 8 μM.[34]

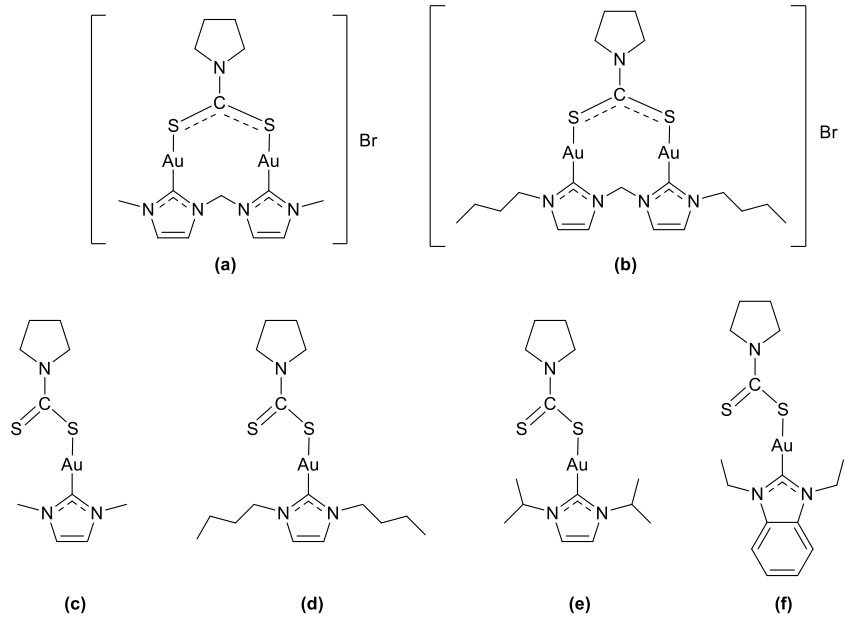

Figure 5.6. Chemical drawings of gold(I)-carbene complexes with pyrrolidinedithiocarbamate with anticancer activity published by Sun and coworkers.[34]

Altaf and coworkers reported on a series of gold(I)-carbene derivatives of dimethyl-, diethyl- and dibenzyldithiocarbamates (**Figure 5.7**), although their antiproliferative activity on A549, HeLa, and HCT15 cells was very modest.[35,36]

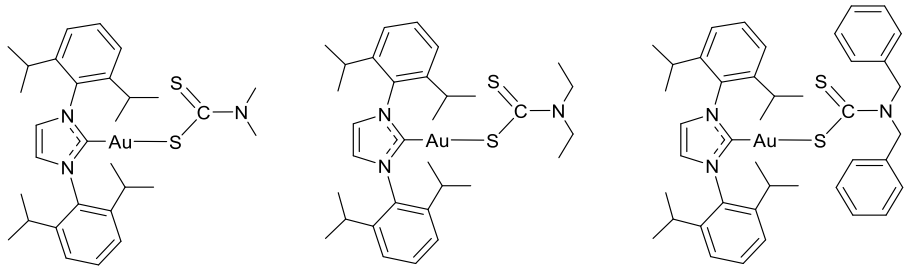

Figure 5.7. Chemical drawings of gold(I)-carbene complexes with dithiocarbamato ligands with anticancer activity reported by Altaf and co-workers.[35,36]

5.2. Aim and objectives

Owing to the aforementioned promising anticancer properties reported for gold(I)-dithiocarbamato complexes bearing either carbene or phosphino ligands, the following approach was implemented.

- Synthesis and characterization of a series of carbene-gold(I)-dithiocarbamato derivatives (both non-glycosylated and glyco-functionalized).
- Evaluation of the solution behaviour of selected carbene derivatives.
- *In vitro* cytotoxicity studies towards a panel of human tumour cell lines.
- Synthesis and characterization of heteroleptic gold(I) complexes containing both a dithiocarbamato and a triphenylphosphine moieties. The purpose was to obtain

the corresponding glycoconjugated derivatives (as well as the non-glycoconjugated counterpart) *via* a ligand exchange reaction. The choice of triphenylphosphine ligand is dictated by the need to have phenyl substituents on the organophosphano ligand in order to increase activity of the gold(I) derivatives, as suggested by Mirabelli *et al*.[37]

5.3 Gold(I)-carbene derivatives

5.3.1 Synthesis

As a starting point, the synthesis of the mixed dithiocarbamato gold(I)-carbene analogues was attempted by addition of a solution of the dithiocarbamato ligand at different ratios to the metal precursor chlorido-(1,3-diethylbenzimidazol-2-ylidene)gold(I) ([Au(BImEt$_2$)Cl]), synthesized in Prof. Ott lab using an established procedure.[38,39]

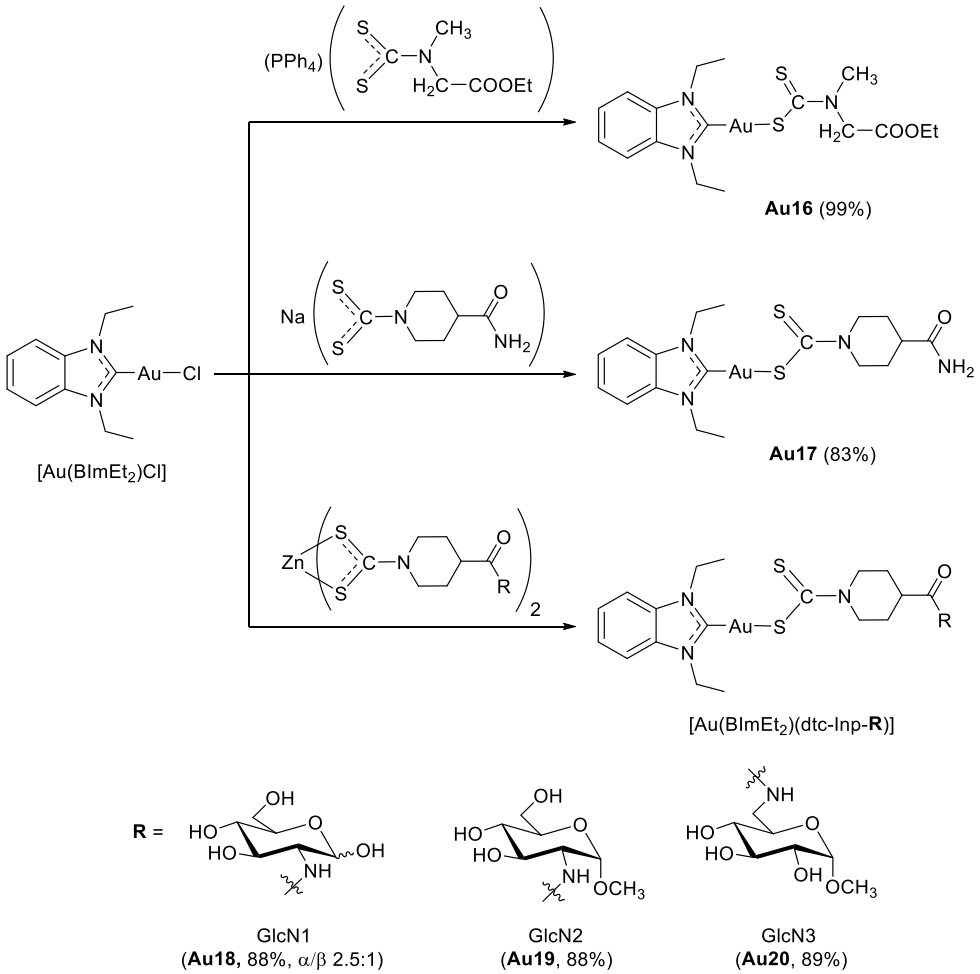

Scheme 5.1. Synthetic route to the synthesis of gold(I)-carbene complexes with dithiocarbamato ligands.

When 1 eq. of the ligand (PPh$_4$)(dtc-Sar-OEt) is reacted with 1 eq. of [Au(BImEt$_2$)Cl] in a water/acetone mixture, a fluffy ivory solid can be isolated in nearly quantitative yields (99%) (**Scheme 5.1**). XRD crystallography, ^{1}H and ^{13}C NMR spectroscopy confirmed the

identity of the neutral mononuclear complex of the type [Au(BImEt$_2$)(dtc-Sar-OEt)] (**Au16**). Similarly, the same synthetic procedure was applied to obtain the complex [Au(BImEt$_2$)(dtc-Inp-NH$_2$)] (**Au17**) as a light yellow powder. Both complexes [Au(BImEt$_2$)(dtc-Sar-OEt)] and [Au(BImEt$_2$)(dtc-Inp-NH$_2$)] are stable in the solid state. They are also soluble in DMSO, DMF, slightly soluble in chlorinated solvents, very slightly soluble in alcohols and stable in DMF and DMSO solution (see section Solution studies for details).

The gold(I)-carbene glycoconjugates were obtained *via* ligand exchange in DMF by reacting 1 eq. of the corresponding zinc(II)-dithiocarbamato glycoconjugate with 2 eq. of chlorido-(1,3-diethylbenzimidazol-2-ylidene)gold(I) ([Au(BImEt$_2$)Cl]) (**Scheme 5.1**). The reaction kinetics was preliminarily monitored by means of ^{1}H NMR spectroscopy in DMF-d$_7$ (**Figure 5.6**). Soon after mixing of the reactants (t < 5 min), some peaks attributable to the zinc(II)-precursor and to [Au(BImEt$_2$)Cl] disappeared in the NMR spectrum of the mixture, with the simultaneous appearance of new peaks. In particular, the peak of the equatorial protons of the NCH$_2$ moiety of the isonipecotic ring shifted downfield from 4.95 to 5.25 ppm, and the peaks of the *N*-ethyl substituents of the carbene moiety, which shifted from 4.62 to 4.68 ppm (CH$_2$, quartet) and from 1.52 to 1.46 (CH$_3$, triplet). On the other hand, the peaks attributable to the protons of the carbohydrate moiety and the aromatic benzimidazole ring were only slightly affected. No further advantage was observed upon prolonging the reaction time, and decomposition side-products were generated after 1 h (see section Solution studies for details). These observations clearly proved that the zinc(II)-dithiocarbamato precursor undergoes transmetallation to the gold(I)-carbene complex quite immediately, with total conversion to the expected gold(I)-carbene-dithiocarbamato derivative, and the formation of zinc chloride as a by-product.

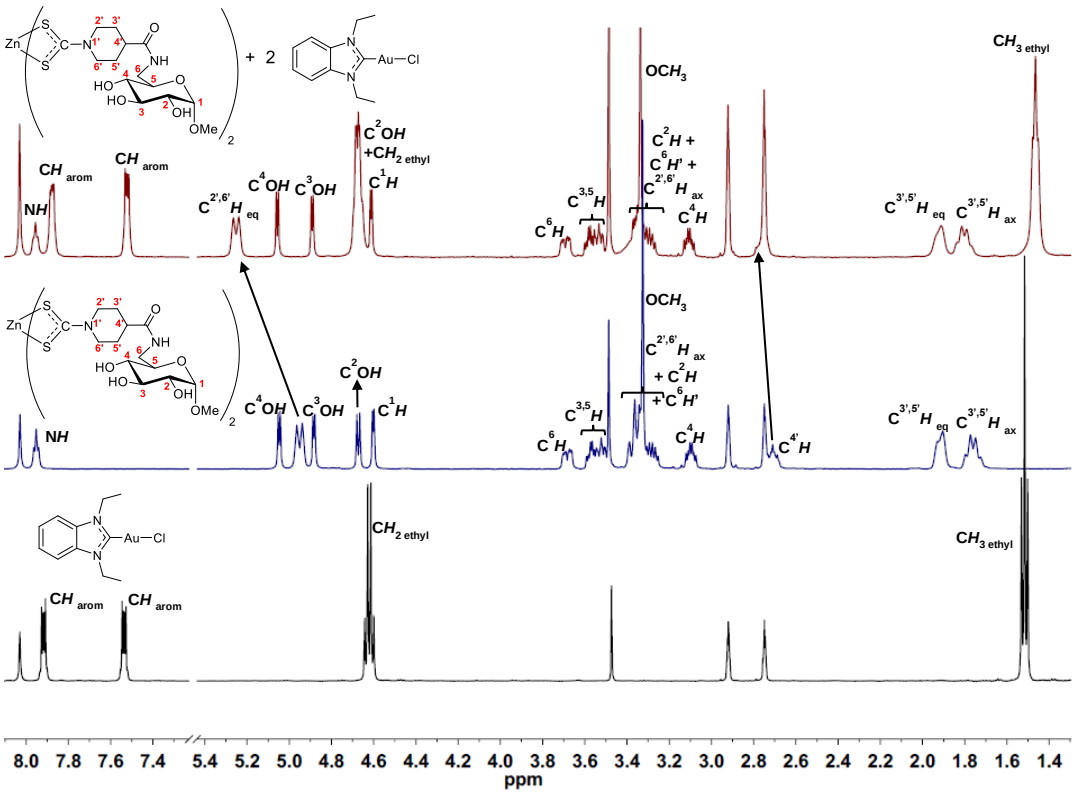

Figure 5.6. Stacked ^{1}H NMR spectra (400 MHz, DMF-d_7) of [Au(BImEt$_2$)Cl] (bottom), **Zn5** (middle) and reaction mixture after reacting for 5 min (top).

5.3.2 Characterization

Colourless needle-shaped crystals of the complexes [Au(BImEt$_2$)(dtc-Sar-OEt)] (**Au16**) and [Au(BImEt$_2$)(dtc-Inp-NH$_2$)] (**Au17**) suitable for single crystal XRD were obtained by slow evaporation of DMF solutions of the compounds. The X-ray crystal structures of the complexes shown in **Figure 5.7** reveals that in the monoclinic asymmetric unit the gold(I) atom is coordinated to one C donor atom of the carbene moiety and one S donor atom of the dithiocarbamato ligand adopting a linear distorted fashion.

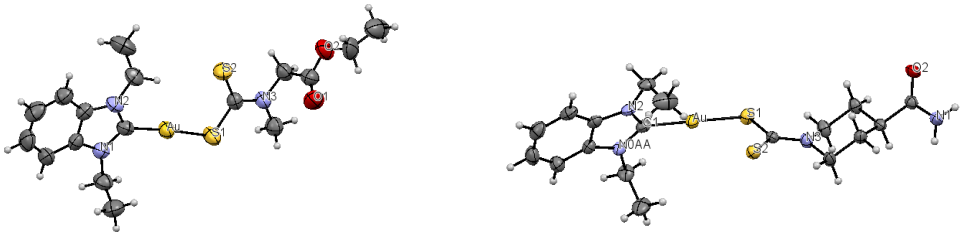

Figure 5.7. ORTEP views of the single crystal XRD structures of [Au(BImEt$_2$)(dtc-Sar-OEt)] (**Au16**, left) and [Au(BImEt$_2$)(dtc-Inp-NH$_2$)] (**Au17**, right) (thermal ellipsoid drawn at 30% probability level).

The Au–C and Au–S bond lengths are 1.985 and 2.288 Å respectively for [Au(BImEt$_2$)(dtc-Sar-OEt)], and 1.997 and 2.307 Å, respectively, for [Au(BImEt$_2$)(dtc-Inp-NH$_2$)] (**Table 5.1**). Compared to the Au–P bond lengths of the phosphino analogues,

the Au–C bond length varies significantly, likely due to a stronger interaction between metal centre and NHC carbene ligand. The C–Au–S bond angles are 174.9° for [Au(BImEt$_2$)(dtc-Sar-OEt)] and 176.2° for [Au(BImEt$_2$)(dtc-Inp-NH$_2$)], which deviate from an ideal bond angle of 180° for a linear geometry, as it has been also reported by Altaf et *al*.[35] Attempts to grow crystals of the glycoconjugates proved unsuccessful so far, leading exclusively to the formation of a *bis*-carbene specie [Au(BImEt$_2$)$_2$]$^+$, which forms in solution as a by-product over time.

	Au16	**Au17**
Bond angles (°)		
C–Au–S	174.9	176.2
S–C–S	122.8	120.2
N–C–N	105.5	106.6
Bond lengths (Å)		
Au–C	1.985	1.997
Au–S1	2.288	2.307
C–S1	1.745	1.743
C–S2	1.677	1.698
C–N3	1.338	1.340

Table 5.1. Selected bond angle and lengths for the compounds [Au(BImEt$_2$)(dtc-Sar-OEt)] (**Au16**) and [Au(BImEt$_2$)(dtc-Inp-NH$_2$)] (**Au17**).

For all the gold(I) derivatives, the characteristic strong IR band attributed to the stretching of the N–CSS moiety of the so-called "thioureide band" falls in the range at *ca*. 1470-1490 cm^{-1}, which slightly differs from the value 1487-1494 cm^{-1} of the zinc(II) precursors (**Table 5.2**). The different formal charge of the metal centre (from Zn(II) to Au(I)) and coordination mode (from two *bis*-chelate to one monodentate dithiocarbamato ligands) invariably affects also the force constant of the N–CSS bond. This is also evident by comparing gold(I)- and gold(III)-dithiocarbamato analogues. In fact, the detection of the ν(N–CSS) vibration at lower energy with respect to the gold(III) counterparts (∼1485 cm^{-1}, −70 cm^{-1}) is consistent with a reduced electron-withdrawing effect upon moving from the gold(III) to the less positively charged gold(I) centre.[40,41]

The proposed molecular structure was confirmed by the presence in the mid-IR spectra of two bands at *ca.* 1000 and 914 cm^{-1} assignable to the stretching vibrations of the S=C–S moiety. This is in agreement with the Bonati-Ugo criterion according to which a split band in the 1050-900 cm^{-1} spectral region with a splitting larger than 20 cm^{-1} indicates monodentate bonding of the dithiocarbamato ligand.[40,42] With some glycoconjugate

derivatives, these bands often overlap with the broad and very strong absorptions arising from the C–O bonds of the sugar skeleton.

In the far-IR spectrum (600-200 cm^{-1}), the disappearance of the relatively strong ν(Au–$^{35/37}$Cl) bands, recorded at 340/333 cm^{-1} for the [Au(BImEt$_2$)Cl] precursor, confirms the removal of the chlorido ligand. Whereas, the concomitant recording of a new band in the 380-420 cm^{-1} range assignable to the stretching of the Au–S bond is consistent with the monodentate coordination of the dithiocarbamato scaffold.

The main infrared absorptions attributable to the carbohydrate pendant and to the amide link are similar to those previously discussed in Chapters 2-4 for the zinc(II)- and gold(III) glycoconjugate analogues.

Complex	ν(C=O)	δ_{ip}(CNH) (amide II)	ν(N–CSS)	ν(S=C–S)	ν(Au–C)	ν(Au–S)
Au16	1739	-	1483	1001/982	569	346
Au17	1684	1623	1463	1004/915	559	327
Au18	1657	1543	1483	998/914	506	385
Au19	1658	1542	1491	1000/914	568	384
Au20	1656	1545	1484	1007/914	513	384

Table 5.2. Selected FT-IR data (CsI disk, wavenumber in cm^{-1}) of compounds **Au16-20**.

Compared with the gold(III) counterparts, the ^{1}H and ^{13}C{^{1}H} NMR peaks of the glucosedithiocarbamato scaffold are recorded at similar chemical shifts with the exception of the atoms closer to the gold(I) core, which are more sensitive to the different metal center and coordination mode of the –NCSS group (**Figure 5.8**). In particular, a significant downfield shift is observed for the equatorial C$^{2',6'}$H (^{1}H: ~4.9-5.1 ppm, +0.7-0.9 ppm, ^{13}C: ~51 ppm, +2 ppm) and the NCSS (^{13}C: ~203-205 ppm, +16-18 ppm) moieties, in agreement with a reduced electron-withdrawing effect upon moving from the gold(III) to the less positively charged gold(I) center (**Table 5.3**).[40,41]

In addition, in the case of the carbene analogues, characteristic peaks can be recorded for the ethylbenzimidazole moiety. Particularly, a signal at ~185 ppm in the ^{13}C NMR spectrum can be attributed to the "carbene carbon" bound to the two neighbouring nitrogen atoms, which shifts downfield by about 10 ppm when compared with the spectrum of [Au(BImEt$_2$)Cl] (^{13}C: ~176 ppm). This observation agrees with a decreased electron-donating effect by π-backdonation when the chlorido ligand is replaced by a dithiocarbamate. Conversely, another set of signals attributable to the carbene moiety

appears with the glycoconjugates after 1-3 h, with a characteristic signal at ~189 ppm due to the carbene carbon of a *bis*-carbene adduct (see section Solution studies for further details).

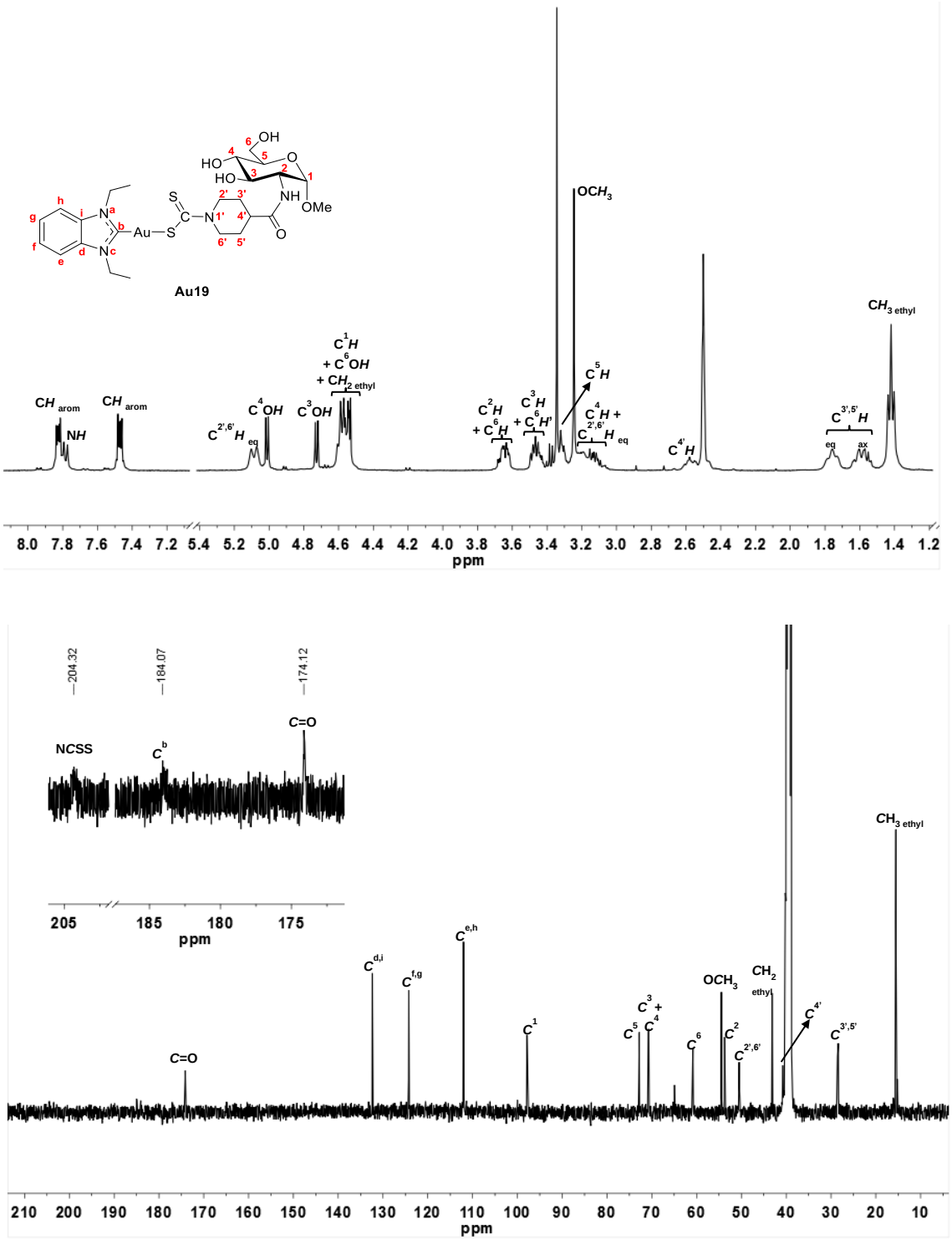

Figure 5.8. ^{1}H (top) and $^{13}C\{^{1}H\}$ (bottom) NMR spectra in DMSO-d_6 of complex **Au19**.

Complex	^{1}H NMR (ppm)			^{13}C NMR (ppm)				
	N*H*	C$^{2',6'}$*H* $_{eq}$	C^{1}*H*	N*C*SS	*C*^{b}	*C*=O	*C*1	*C*$^{2',6'}$
Au16a	-	-	-	210.56	185.60	168.42	-	-
Au17	7.35/6.86^{b}	5.08	-	204.49	184.17	175.81	-	50.42
Au18	7.69 (β)/ 7.65 (α)	5.09	4.91 (α)/ 4.43 (β)	204.47	184.18	173.94	95.44 (β)/ 90.49 (α)	50.54
Au19	7.83-7.77^{c}	5.09	4.61-4.53^{d}	204.32	184.07	174.12	97.87	50.50
Au20	7.97	5.09	4.51	204.98	184.62	174.55	100.17	50.51

[a] in $CDCl_3$.
[b] two broad singlets (7.35 ppm N*H* $_{cis}$, 6.86 ppm N*H* $_{trans}$).
[c] overlapped with C*H* $_{arom}$.
[d] overlapped with C^{6}O*H* and C*H*$_2$ $_{ethyl}$.

Table 5.3. Selected ^{1}H and ^{13}C{^{1}H} NMR resonances (400 MHz) of complexes **Au21-Au25**.

The UV-visible spectra of the object compounds were recorded in DMF (20 μM) at room temperature (**Table 5.4**). An intense band is observed at around 286 nm, together with a shoulder at around 280-283 nm, with molar extinction coefficients (ε) in the range of 35000-50000 and 25000-40000 M^{-1} cm^{-1}, respectively. These bands are usually attributed to intramolecular intraligand transitions π*←π of the –SCS moiety and –NCS moieties, respectively.[10,41,43] The shoulder band (ε ~12000-18000 M^{-1} cm^{-1}) over 300 nm is recorded only for gold(I) complexes and is commonly abscribed to an intramolecular ligand-to-metal charge-transfer transition (LMCT) Au(p)←S(p).[41,44]

Complex	λ_{max} in nm (ε, M^{-1} cm^{-1})		
Au16	280 (sh, ~25000)	286 (33500)	305 (12200)
Au17	283 (sh, ~32800)	287 (39900)	303 (sh, ~12000)
Au18	283 (sh, ~40600)	287 (50100)	302 (sh, ~17600)
Au19	282 (sh, ~30600)	287 (38500)	303 (sh, ~13000)
Au20	282 (sh, ~27800)	287 (34800)	301 (sh, ~11900)

Table 5.4. Optical absorption data of compounds **Au16-20** (20 μM in DMF).

5.3.3 Solution studies

The synthesized complexes are all very soluble in DMSO and DMF. Interestingly, the glycoconjugates shows solubility also in water. Preliminary stability studies were carried out by means of ^{1}H NMR and UV-Vis spectroscopy. The model compounds **Au16,17** proved to be very stable in DMF, even after prolonged periods (1 month). No major

changes were observed in the ^{1}H NMR spectrum 30 days after dissolution of the complex **Au16** in DMF-d_7 (**Figure 5.9**).

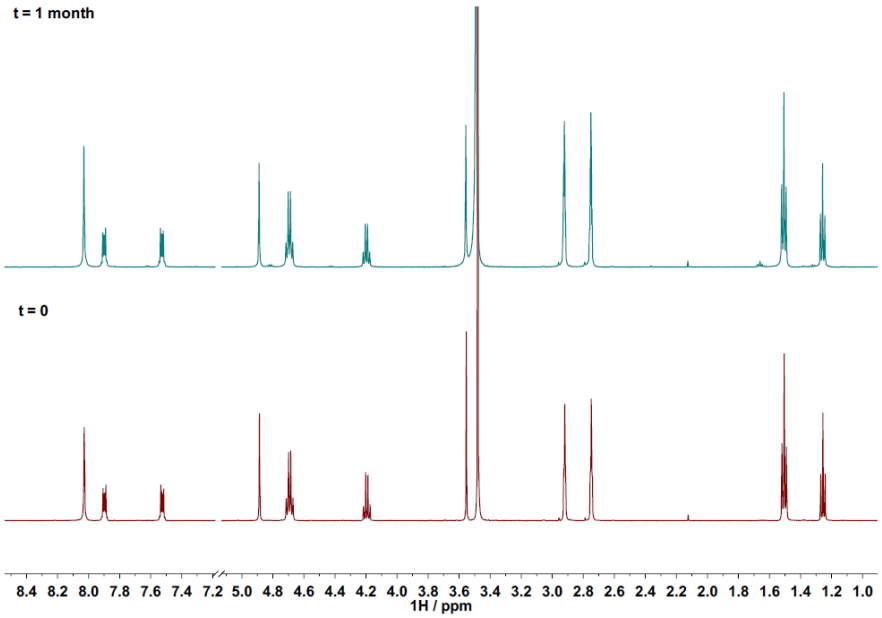

Figure 5.9. Stacked ^{1}H-NMR spectra (500 MHz) of **Au16** in DMF-d_7 recorded over time.

On the contrary, the glycoconjugate complexes showed lower stability in DMF and DMSO. It has been observed *via* ^{1}H NMR that the peaks corresponding to a side-product form at 1.56 (triplet, CH_3 ethyl moiety), 4.67 (quartet, CH_2 ethyl moiety), 7.55 and 7.93 ppm (multiplet, aromatic protons), accompanied by the precipitation in DMSO of a brown-orange insoluble residue (**Figure 5.10**).

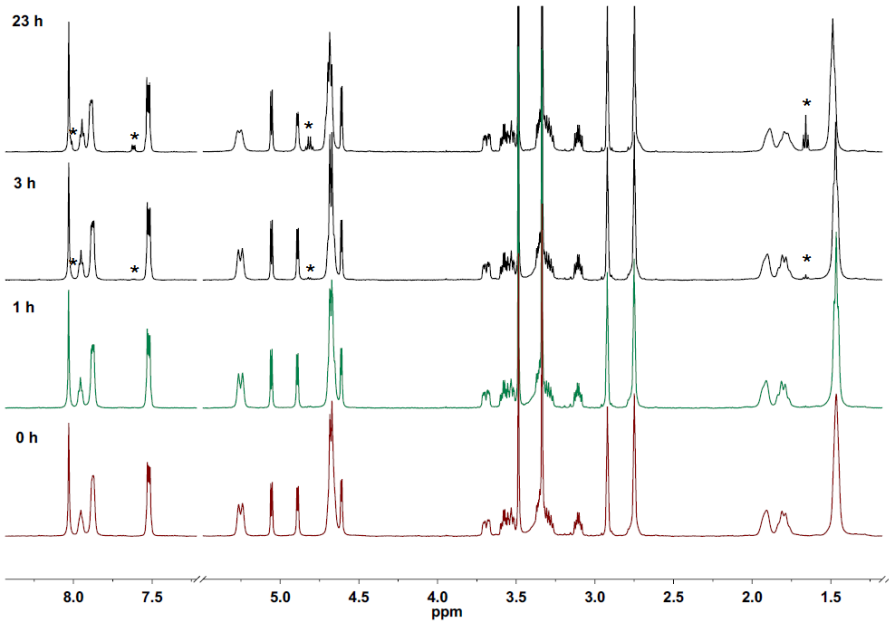

Figure 5.10. Stacked ^{1}H-NMR spectra (500 MHz) of **Au20** in DMF-d_7 recorded over time, and formation of the *bis*-carbene side-product (*****).

Such set of chemical shifts are consistent with the formation of the *bis*-carbene species $[Au(BImEt_2)_2]^+$. Crystals of the *bis*-carbene were obtained also by slow evaporation of the complexes $[Au(BImEt_2)(dtc\text{-}Inp\text{-}GlcN3)]$ in methanol/dichloromethane/DMF solution (**Figure 5.11**).

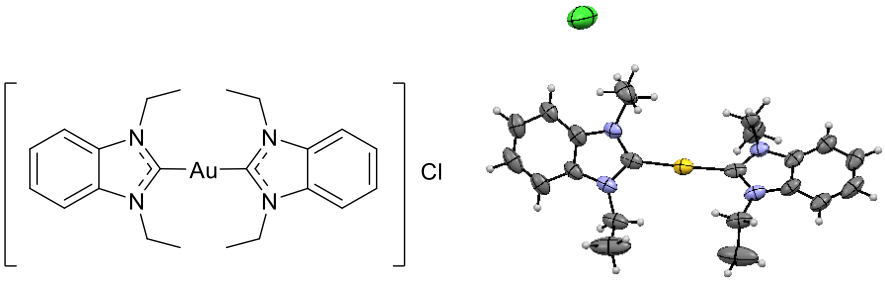

Figure 5.11. Chemical structure (left) and ORTEP view of the single crystal XRD structure of the *bis*-carbene side-product (right).

Moreover, in the $^{13}C\{^1H\}$ NMR spectrum the diagnostic peak at around 189 ppm can be attributed to the two N_2C carbons of the benzimidazole ring, compared to the peak at 185 ppm due to only one N_2C carbon of the coordinated carbene.

Kinetic stability studies in physiological buffer pH 7.4 (PBS) were carried out on the complexes **Au16** and **Au18** at 37°C. As it can be observed in **Figure 5.12**, the UV-Vis spectra of the complex **Au16** change dramatically soon after dissolution in PBS. An initial increase of the absorbance maximum within 1 h incubation is observed, followed then by a decrease of the absorbance over the next 18 h. This suggests that a multistep ligand exchange reaction may occur in the physiological buffer, possibly leading to the formation of the *bis*-carbene adduct.

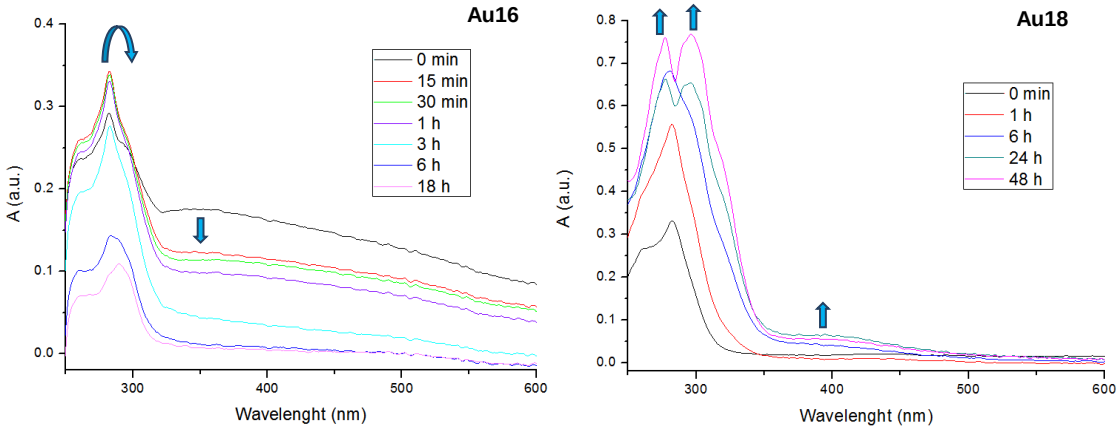

Figure 5.12. UV-Vis spectra of complex **Au16** (left) and **Au18** (right), 50 µM in PBS pH 7.4 at 37°C at different time frames.

5.3.4 Biological studies

In vitro cytotoxicity studies were carried out in Prof. Ott laboratories at the Technische Universität Braunschweig on a panel of human tumour cell lines (**Table 5.5**).

Complex	IC_{50} (μM)			
	HT-29	MCF7	MDA-MB-231	RC-124
Au16	1.0 ± 0.1	0.5 ± 0.1	0.8 ± 0.1	0.6 ± 0.1
Na(dtc-Sar-OEt)	2.2 ± 0.4	1.0 ± 0.2	1.7 ± 0.1	1.5 ± 0.7
Au17	6.4 ± 1.3	4.9 ± 0.6	4.7 ± 0.3	-[a]
Au18	22.7 ± 1.0	12.3 ± 1.4	11.5 ± 0.6	-[a]
Au19	11.3 ± 0.4	10.3 ± 0.3	10.5 ± 0.4	-[a]
Au20	11.8 ± 1.1	10.6 ± 0.6	9.6 ± 1.5	-[a]

[a] Not determined.

Table 5.5. Cytotoxicity data (IC_{50} in μM) for compounds **Au16-Au20**.

Cell viability evaluation performed on different cell lines showed a moderate activity of the glyco-functionalized derivatives, the O^1-methyl substituted derivatives **Au19-20** displaying a slightly higher activity than the derivative with the free hydroxyl moiety at the anomeric site (**Au18**, around 10 μM). In addition, the non-glycoconjugated derivatives possessed a remarkably higher activity. IC_{50} values of the model complexes are, in fact, in the low micromolar range, with the lower values (<1 μM) for the ethyl sarcosine dithiocarbamato analogue, **Au16**. The high cytotoxicity on the non-tumorigenic human kidney cell line RC-124 for this derivative showed also a nearly absent selectivity towards tumour cell lines. As a comparison, also the free ligand Na(dtc-Sar-OEt), obtained *via* exchange of the tetraphenylphosphonium counterion (PPh_4)(dtc-Sar-OEt) with sodium tetraphenylborate ($NaBPh_4$), was tested. Interestingly, it is demonstrated that the cytotoxicity of the carbene-dithiocarbamato gold(I) complex does not depend on a possible release of the ligand in solution, since the gold(I) derivative is more cytotoxic than the free ligand itself.

In order to quantify the amount of intracellular gold, uptake studies were carried out on MCF7 cells for some selected compounds, **Au17** and **Au19**, with and without cytochalasin B (a GLUT-inhibitor), as well as in normal and glucose-free medium. Surprisingly, no gold was detected in any AAS measurements after 6 h coincubation. This seems to suggest that such complexes are not internalized into the cells, supporting the hypothesis that they might induce cell death by acting at the cell membrane extracellular level. Therefore, no evident benefits have been achieved by glycoconjugation in terms of tumour selectivity.

5.4 Gold(I)-phosphino derivatives

5.4.1 Synthesis

The gold(I)-phosphino compounds were obtained in a similar manner to that of the carbene ones. The non-glycoconjugated derivatives [Au(dtc-Inp-OEt)(PPh_3)] (**Au21**) and [Au(dtc-Inp-NH_2)(PPh_3)] (**Au22**) were synthesized in high yields (86-91%) *via* conventional addition of a solution of the ligand to commercially available chloro(triphenylphopshine)gold(I) ([AuCl(PPh_3)]) (**Scheme 5.2**).

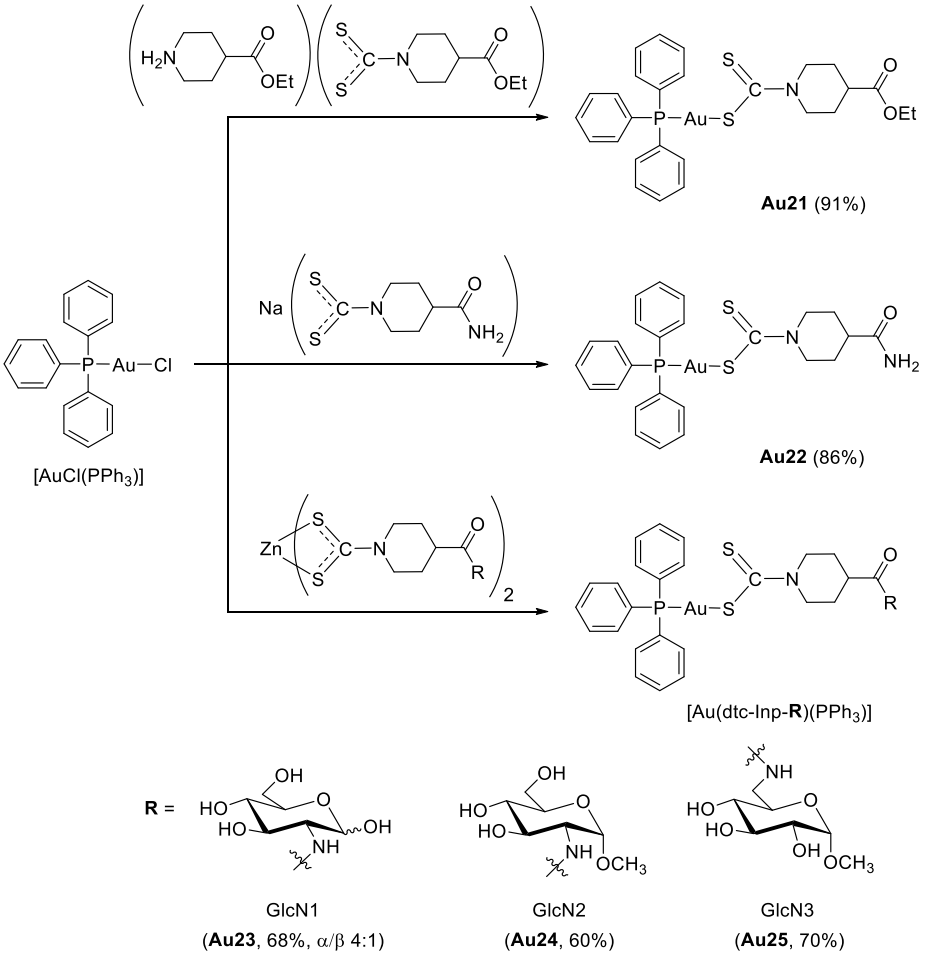

Scheme 5.2. General synthetic scheme for the synthesis of gold(I)-phosphino complexes with dithiocarbamato ligands.

As concerns the synthesis of the corresponding glycoconjugates, the transmetallation approach was again applied, by reacting 1 eq. of the zinc(II)-dithiocarbamato precursors with 2 eq. of chloro(triphenylphosphine)gold(I) in DMF. Precipitation by addition of diethyl ether, and subsequent washing with diethyl ether and dichloromethane to remove the by-product zinc chloride and residual unreacted reagents afforded the desired products in moderate to good yield (60-70%) as pale yellow-beige solids. In contrast with the reaction protocol of the carbene series, the phosphino-gold(I) compounds are more stable in the reaction solvent, which allows the reaction mixture to be kept under stirring for

longer times, without formation of side-products. All the synthesized compounds of the type [Au(dithiocarbamate)(PPh_3)] are stable in the solid state. In addition, all the synthesized complexes of the "phosphino series" are very soluble and stable in DMSO and DMF and, in certain cases, in methanol (**Au21,22** and **Au24,25**) or chlorinated solvents (**Au21,22**).

5.4.2 Characterization

Yellow plate-shaped crystals of the complex [Au(dtc-Inp-NH_2)(PPh_3)] (**Au22**) suitable for single crystal XRD were obtained by slow evaporation of a solution in dichloromethane/methanol. The X-ray crystal structure of the complex shown in **Figure 5.13** reveals that two molecules are present in a monoclinic asymmetric unit cell, with the primary amide moieties undergoing hydrogen bonding. In both molecules the gold(I) atom is coordinated to one P donor atom of triphenylphosphine and one S donor atom of the dithiocarbamato ligand adopting a slightly distorted linear geometry, with some minor conformational differences.

Figure 5.13. ORTEP view of the single crystal XRD structure of [Au(dtc-Inp-NH_2)(PPh_3)] (**Au22**).

The Au–P and Au–S bond distances are 2.2503 and 2.3263 Å for Au1, and 2.2535 and 2.3345 Å for Au2, respectively. Compared to the gold(I)-carbene analogues, the length of the Au–P bond of *ca*. 2.25 Å is remarkably higher than the Au–C of 1.98-2.00 Å, thus suggesting that the latter is stronger. The S–Au–P bond angle is 171.70° for Au1 and 174.38° for Au2, which deviates from an ideal bond angle of 180° for a linear geometry. This deviation can be explained by the presence of a different environment around the gold(I) centre, but also to the short contacts S11–H23B and S13–H21B (hydrogens of the NH_2 moiety trans to the O atom). In this context, Altaf *et al.* observed a correlation between angle distortion and Au–S interaction: a longer Au–S interaction reflects in an increase of the deviation from a linear angle of 180°.[11] However, such correlation is not observed in this case.

Any attempt to grow crystals of the compound [Au(dtc-Inp-OEt)(PPh_3)] or the glycoconjugated derivatives proved unsuccessful so far.

As far as the IR characterization of the object gold(I)-phosphino dithiocarbamato complexes is concerned, the identification of the main absorption band arising from the coordinated monodentate dithiocarbamato moiety resembles (substantially) that previously discussed for the carbene-gold(I) analogues (**Table 5.6**). Regarding the metal-sulfur and metal-phosphorus stretching bands, expected in the far-IR detection range, these cannot be unambiguously assigned because the triphenylphosphine scaffold itself exhibits a number of bands in the low frequency region.[45] In particular, the stretching of the newly formed Au–S bond in some cases overlaps with the stronger vibration of the triphenylphosphine called *t*-vib. By comparison with the infrared spectrum of the [AuCl(PPh_3)] precursor, some typical vibrations of the triphenylphosphine ligand can be identified anyway, according to the Whiffen's classification of the vibrations for monosubstituted benzenes.[46] Thus, the stretching of the P–Ph_3 moiety at around 1100 cm^{-1} (also called *q*-vib), 710/694 cm^{-1} (*r*-vib), the bending of the P–Ph_3 moiety at 539/510/500 (*y*-vib), and 430 cm^{-1} (*t*-vib) can be assigned.

Complex	ν(C=O)	δ_{ip}(CNH) (amide II)	ν(N–CSS)	ν(P–Ph_3) (*q*-vib)	ν(S=C–S)	ν(Au–S)
Au21	1729	-	1480	1101	999/917	393
Au22	1676	1614	1477	1101	998/914	420
Au23	1650	1544	1481	1101	998/913	369
Au24	1651	1544	1490	1100	1001/914	380
Au25	1654	1544	1483	1101	1000/914	397

Table 5.6. Selected FT-IR data (CsI disk, wavenumber in cm^{-1}) of compounds **Au21-25**.

As concerns the ^{1}H and ^{13}C NMR characterization, the same discussion done with the gold(I) carbene complexes applies for the derivatives of the "phosphine series", the only obvious difference being related to the replacement of the phosphine ancillary ligand (**Figure 5.14** and **Table 5.7**). In addition, the resonance due to the NCSS carbon in the ^{13}C NMR spectrum of the gold(I) phosphine derivatives are slightly shifted downfield (*ca*. 2 ppm) compared to the gold(I) carbene counterparts (207 vs 205 ppm). This behaviour may be explained by an increased electron-donating behaviour of the metal by

π-backdonation compared to the carbene derivatives, in which the π-backdonation of the metal is negligible.

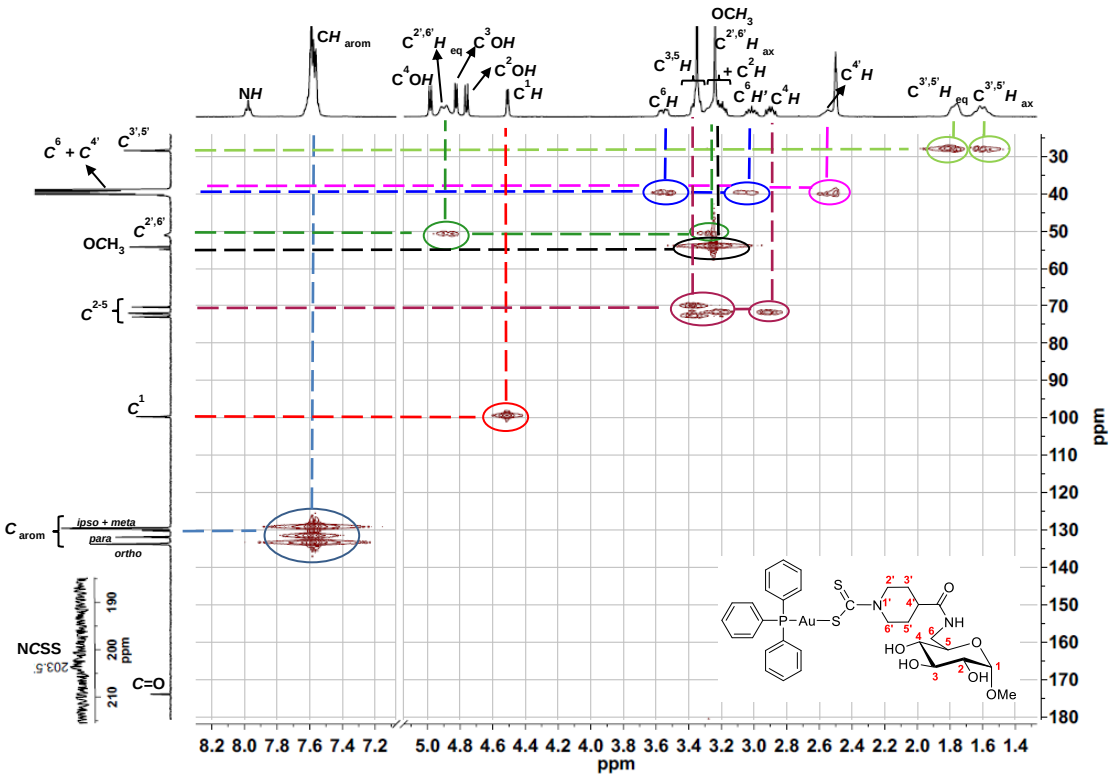

Figure 5.14. [^{1}H-^{13}C] HSQC NMR spectrum in DMSO-d_6 of complex **Au25**.

Complex	Solvent	^{1}H NMR (ppm)		
		N*H*	C$^{2',6'}$*H* $_{eq}$	C^{1}*H*
Au21[a]	$CDCl_3$	-	4.97	-
Au22[a]	$CDCl_3$	5.55/5.44[a]	5.18	-
Au23	DMSO-d_6	7.70 (β)/ 7.66 (α)	4.93-4.89	4.93 (α)/ 4.44 (β)
Au24	DMSO-d_6	7.81	4.85	4.53
Au25	DMSO-d_6	7.98	4.89	4.51

	^{13}C NMR (ppm)				^{31}P NMR (ppm)
	N*C*SS	*C*=O	*C*1	*C*$^{2',6'}$	*P*Ph$_3$
Au21[a]	206.98	174.34	-	50.96	36.59
Au22[a]	207.15	176.28	-	51.04	36.57
Au23	204.39	173.87	95.44 (β)/ 90.50 (α)	50.73	36.46
Au24	202.18	173.88	97.86	50.81	36.46
Au25	203.57	173.85	99.64	51.16	36.47

[a] two broad singlets (5.55 ppm N*H* $_{cis}$, 5.44 ppm N*H* $_{trans}$).

Table 5.7. Selected ^{1}H and ^{13}C{^{1}H} NMR resonances (400 MHz) of complexes **Au21-Au25**.

In the case of metal complexes coordinated to phosphorous-containing ligands, ^{31}P NMR spectroscopy is a powerful analytical tool. Phosphorous-31 is a high sensitivity NMR-active nucleus with 100% natural abundance, nuclear spin ½, and usually yields sharp lines in the corresponding NMR spectrum over a wide range of chemical shifts (from -180 to 250 ppm).[47] As to the mononuclear complexes of the type [Au(dtc)(PPh_3)] (dtc: dithiocarbamato ligand) here reported, a single signal arising from the phosphorous atom of the triphenylphosphine ligand is detected at ~36 ppm (**Table 5.7**). This value is consistent with the chemical shift of coordinated triphenylphosphines and other similar adducts gold(I)-triphenylphosphine.[9,48–50]

The UV-visible spectra of the compounds with phosphine ligands were recorded in dichloromethane or in DMSO at 25 μM at room temperature (**Table 5.8**). By comparison with the spectrum of chloro(triphenylphosphine)gold(I), a band at 270 nm with molar extinction coefficients (ε) of *ca*. 20000-29000 M^{-1} cm^{-1} is observed, with a weaker shoulder at 293 nm (ε ~7000-9000 M^{-1} cm^{-1}), which can be assumed to be intramolecular intraligand transitions π*←π of the –NCS and –CSS moieties, respectively.[10,41,43] These bands overlap also three much weaker π*←π transitions that are attributed to the aromatic rings of the triphenylphosphine ligand with ε 1600-2400 M^{-1} cm^{-1} (also called B band).[51–53] The band (weak shoulder, ε ~5000 M^{-1} cm^{-1}) over 300 nm is recorded only for gold(I) complexes and is commonly abscribed to an intramolecular ligand-to-metal charge-transfer transition (LMCT) Au(p)←S(p).[41,44]

In the spectra of the compounds [Au(dtc-Inp-OEt)(PPh_3)] (**Au21**) and [Au(dtc-Inp-NH_2)(PPh_3)] (**Au22**) recorded in dichloromethane, a structured pattern of bands involving π*←n transitions (R band) is also observed at 230-246 nm with ε *ca*. 22000-29000 M^{-1} cm^{-1}.[51]

Complex	λ_{max} in nm (ε, M^{-1} cm^{-1})			
Au21[a]	231/236/240/243/246 (~26000)	268 (28400)	296 (sh, ~9000)	316 (sh, ~6400)
Au22[a]	230/237/242/245 (24000)	268 (24700)	295 (sh, ~7700)	316 (sh, ~5200)
Au23[b]	-	272 (19700)	296 (sh, ~8400)	316 (sh, ~4900)
Au24[b]	-	270 (29700)	293 (sh, ~12300)	313 (sh, ~9300)
Au25[b]	-	272 (19400)	293 (sh, ~9300)	313 (sh, ~5000)

[a] in CH_2Cl_2
[b] in DMSO

Table 5.8. Optical absorption data of compounds **Au21-25** (25 μM in DMSO).

For what concerns the phosphine series, instead, all the compounds are rather soluble and stable in DMSO and DMF for a couple of days.

5.5 Conclusions

Two series of gold(I) derivatives containing dithiocarbamato ligands conjugated to carbohydrates have been synthesized, one with *N*-heterocyclic carbene ligands and the other with phosphine ligands. Model non-glycoconjugated complexes were obtained *via* a classical synthetic approach, while the corresponding glycoconjugates were obtained through a ligand exchange synthesis, starting from zinc(II) precursors. All complexes were fully characterized by means of elemental analysis, multinuclear NMR, IR, and UV-Vis spectroscopy. Single crystal XRD structures were also obtained for the carbene-bound model complexes [Au(BImEt$_2$)(dtc-Sar-OEt)] and [Au(BImEt$_2$)(dtc-Inp-NH$_2$)], and for the phosphine model compound [Au(PPh$_3$)(dtc-Inp-NH$_2$)], revealing a linear fashion of the coordinated ligands around the gold(I) centre. Antiproliferative assays carried out on the metal-carbene series showed that the glycoconjugated compounds are moderately active towards various cancer cell lines, although the non-glycoconjugated model analogues displayed higher cytotoxicity. Finally, cell uptake studies revealed that the carbene-dithiocarbamato complexes are not internalized into the breast cancer cells MCF7, thus suggesting that other cell-death mechanisms may occur, likely involving an extracellular mode of action.

For this reason, further experiments are in progress. First, more antiproliferative studies will be carried out in the presence of a GLUT-inhibitor in order to understand any possible role in the cytotoxicity and/or lack of detectable intracellular gold. Secondly, some cell cycle arrest experiments will be carried out. Finally, the cytotoxic activity of the phosphine derivatives is currently ongoing.

5.6 References

[1] I. Ott, *Coord. Chem. Rev.* **2009**, *253*, 1670–1681.
[2] B. Liu, L. Qu, S. Yan, *Cancer Cell Int.* **2015**, *15*, 106.
[3] J. Lu, E.-H. Chew, A. Holmgren, *Proc. Natl. Acad. Sci. USA* **2007**, *104*, 12288–12293.
[4] C. K. Mirabelli, R. K. Johnson, C. M. Sung, L. Faucette, K. Muirhead, S. T. Crooke, *Cancer Res.* **1985**, *45*, 32–39.
[5] C. F. Shaw, *Chem. Rev.* **1999**, *99*, 2589–2600.
[6] S. Nobili, E. Mini, I. Landini, C. Gabbiani, A. Casini, L. Messori, *Med. Res. Rev.* **2010**, *30*, 550–580.
[7] W. Liu, R. Gust, *Chem. Soc. Rev.* **2012**, *42*, 755–773.
[8] C. Roder, M. J. Thomson, *Drugs RD* **2015**, *15*, 13–20.
[9] F. K. Keter, I. A. Guzei, M. Nell, W. E. van Zyl, J. Darkwa, *Inorg. Chem.* **2014**, *53*, 2058–2067.
[10] S. S. Al-Jaroudi, M. Altaf, A. A. Seliman, S. Yadav, F. Arjmand, A. Alhoshani, H. M. Korashy, S. Ahmad, A. A. Isab, *Inorg. Chim. Acta* **2017**, *464*, 37–48.

[11] M. Altaf, M. Monim-ul-Mehboob, A. A. Seliman, M. Sohail, M. I. M. Wazeer, A. A. Isab, L. Li, V. Dhuna, G. Bhatia, K. Dhuna, *Eur. J. Med. Chem.* **2015**, *95*, 464–472.

[12] N. S. Jamaludin, Z.-J. Goh, Y. K. Cheah, K.-P. Ang, J. H. Sim, C. H. Khoo, Z. A. Fairuz, S. N. B. A. Halim, S. W. Ng, H.-L. Seng, E. R. T. Tiekink, *Eur. J. Med. Chem.* **2013**, *67*, 127–141.

[13] B.-J. Chen, N. S. Jamaludin, C.-H. Khoo, T.-H. See, J.-H. Sim, Y.-K. Cheah, S. N. A. Halim, H.-L. Seng, E. R. T. Tiekink, *J. Inorg. Biochem.* **2016**, *163*, 68–80.

[14] L. Mercs, M. Albrecht, *Chem. Soc. Rev.* **2010**, *39*, 1903–1912.

[15] P. de Frémont, N. Marion, S. P. Nolan, *Coord. Chem. Rev.* **2009**, *253*, 862–892.

[16] F. E. Hahn, M. C. Jahnke, *Angew. Chem. Int. Ed. Engl.* **2008**, *47*, 3122–3172.

[17] T. Dröge, F. Glorius, *Angew. Chem. Int. Ed.* **2010**, *49*, 6940–6952.

[18] D. Bourissou, O. Guerret, F. P. Gabbaï, G. Bertrand, *Chem. Rev.* **2000**, *100*, 39–92.

[19] H. V. Huynh, *The Organometallic Chemistry of N-Heterocyclic Carbenes*, John Wiley & Sons, Inc., Hoboken, **2017**.

[20] O. Schuster, L. Yang, H. G. Raubenheimer, M. Albrecht, *Chem. Rev.* **2009**, *109*, 3445–3478.

[21] A. J. Arduengo, R. L. Harlow, M. Kline, *J. Am. Chem. Soc.* **1991**, *113*, 361–363.

[22] C. D. Montgomery, *J. Chem. Educ.* **2015**, *92*, 1653–1660.

[23] J. Santamaría, E. Aguilar, *Org. Chem. Front.* **2016**, *3*, 1561–1588.

[24] S. Díez-González, N. Marion, S. P. Nolan, *Chem. Rev.* **2009**, *109*, 3612–3676.

[25] S. Budagumpi, R. A. Haque, A. W. Salman, *Coord. Chem. Rev.* **2012**, *256*, 1787–1830.

[26] S. P. Nolan, *Acc. Chem. Res.* **2011**, *44*, 91–100.

[27] K. M. Hindi, M. J. Panzner, C. A. Tessier, C. L. Cannon, W. J. Youngs, *Chem. Rev.* **2009**, *109*, 3859–3884.

[28] M.-L. Teyssot, A.-S. Jarrousse, M. Manin, A. Chevry, S. Roche, F. Norre, C. Beaudoin, L. Morel, D. Boyer, R. Mahiou, A. Gautier, *Dalton Trans.* **2009**, *0*, 6894–6902.

[29] A. Gautier, F. Cisnetti, *Metallomics* **2012**, *4*, 23–32.

[30] L. Oehninger, R. Rubbiani, I. Ott, *Dalton Trans.* **2013**, *42*, 3269–3284.

[31] M. V. Baker, P. J. Barnard, S. J. Berners-Price, S. K. Brayshaw, J. L. Hickey, B. W. Skelton, A. H. White, *J. Organomet. Chem.* **2005**, *690*, 5625–5635.

[32] A. Pettenuzzo, R. Pigot, L. Ronconi, *Metallodrugs* **2015**, *1*, 36-61.

[33] F. Hackenberg, H. Müller-Bunz, R. Smith, W. Streciwilk, X. Zhu, M. Tacke, *Organometallics* **2013**, *32*, 5551–5560.

[34] R. W.-Y. Sun, M. Zhang, D. Li, Z.-F. Zhang, H. Cai, M. Li, Y.-J. Xian, S. W. Ng, A. S.-T. Wong, *Chem. Eur. J.* **2015**, *21*, 18534–18538.

[35] M. Altaf, M. Monim-ul-Mehboob, A. A. A. Seliman, A. A. Isab, V. Dhuna, G. Bhatia, K. Dhuna, *J. Organomet. Chem.* **2014**, *765*, 68–79.

[36] M. Altaf, A. A. Isab, **2016**, US20160326187A1.

[37] C. K. Mirabelli, D. T. Hill, L. F. Faucette, F. L. McCabe, G. R. Girard, D. B. Bryan, B. M. Sutton, J. O. L. Barus, S. T. Crooke, R. K. Johnson, *J. Med. Chem.* **1987**, *30*, 2181–2190.

[38] R. Rubbiani, I. Kitanovic, H. Alborzinia, S. Can, A. Kitanovic, L. A. Onambele, M. Stefanopoulou, Y. Geldmacher, W. S. Sheldrick, G. Wolber, A. Prokop, S. Wölfl, I. Ott, *J. Med. Chem.* **2010**, *53*, 8608–8618.

[39] H. M. J. Wang, C. Y. L. Chen, I. J. B. Lin, *Organometallics* **1999**, *18*, 1216–1223.

[40] A. Pettenuzzo, D. Montagner, P. McArdle, L. Ronconi, *Dalton Trans.* **2018**, *47*, 10721–10736.

[41] L. Ronconi, L. Giovagnini, C. Marzano, F. Bettìo, R. Graziani, G. Pilloni, D. Fregona, *Inorg. Chem.* **2005**, *44*, 1867–1881.

[42] R. Kellner, G. St. Nikolov, N. Trendafilova, *Inorg. Chim. Acta* **1984**, *84*, 233–239.

[43] F. Forghieri, C. Preti, L. Tassi, G. Tosi, *Polyhedron* **1988**, *7*, 1231–1237.

[44] Y. Jiang, S. Alvarez, R. Hoffmann, *Inorg. Chem.* **1985**, *24*, 749–757.

[45] R. Faggiani, H. E. Howard-Lock, C. J. L. Lock, M. A. Turner, *Can. J. Chem.* **1987**, *65*, 1568–1575.

[46] D. H. Whiffen, *J. Chem. Soc.* **1956**, *0*, 1350–1356.

[47] O. Kühl, *Phosphorus-31 NMR Spectroscopy: A Concise Introduction for the Synthetic Organic and Organometallic Chemist*, Springer-Verlag, Berlin Heidelberg, **2008**.

[48] S. Onaka, Y. Katsukawa, M. Shiotsuka, O. Kanegawa, M. Yamashita, *Inorg. Chim. Acta* **2001**, *312*, 100–110.

[49] M. Bardají, A. Laguna, P. G. Jones, A. K. Fischer, *Inorg. Chem.* **2000**, *39*, 3560–3566.

[50] E. J. Fernández, J. M. López-de-Luzuriaga, M. Monge, E. Olmos, M. C. Gimeno, A. Laguna, P. G. Jones, *Inorg. Chem.* **1998**, *37*, 5532–5536.

[51] D. H. Brown, G. McKinlay, W. E. Smith, *J. Chem. Soc. Dalton Trans.* **1977**, *0*, 1874–1879.

[52] M. A. Omary, M. A. Rawashdeh-Omary, C. C. Chusuei, J. P. Fackler, P. S. Bagus, *J. Chem. Phys.* **2001**, *114*, 10695–10701.

[53] L. J. Larson, E. M. McCauley, B. Weissbart, D. S. Tinti, *J. Phys. Chem.* **1995**, *99*, 7218–7226.

Chapter 6

Manganese(I)-carbonyl dithiocarbamato glycoconjugates as CO-releasing molecules

Chapter 6. Manganese(I)-carbonyl dithiocarbamato glycoconjugates as CO-releasing molecules

For full experimental procedures and characterizations see Chapter 8.

6.1 Metallocarbonyl complexes as CO-releasing molecules (CORMs)

Carbon monoxide (CO) has been regarded as a "silent deadly poison" for hundreds of years since the disclosure of its toxicity by Claude Bernard in 1857. Its chronic health hazard generates from the prolonged exposure to the incomplete combustion of fossil fuels. Carbon monoxide binds very strongly to hemoglobin (Hb) forming carboxyhemoglobin (HbCO). This impairs the oxygen storage capacity of Hb and, as a result, interrupts oxygen transport in the blood with consequent tissue hypoxia.[1]

Despite its well-known toxicity, several findings prompted a new understanding of the physiological role of CO as a gasotransmitter. In fact, endogenous CO is produced in small amounts in the organism and it is important for multiple physiological functions.[2–5] These include anti-inflammation[6] and anti-apoptotic signaling,[7] antiproliferative effects in smooth muscle,[8] vasodilation,[9] inhibition of platelet aggregation,[10] and control of neuroendocrine functions by release of hormones.[11–13]

As a consequence, there is a steadily growing interest in the controlled use of carbon monoxide for clinical applications due to its renowned beneficial therapeutic effects, such as reduction of inflammation, protective effects for cardiovascular diseases, and organ preservation and upon transplantation.[14–20] However, despite a device for the exogenous controlled inhaled delivery of CO, named Covox™, is currently commercialized by Ikaria, safe handling (due to its general toxicity) and site-specific delivery in tissues make the administration of gaseous CO challenging.[15] Therefore, research moved toward the development of biocompatible CO-releasing molecules (CORMs) as an alternative approach. In this context, transition-metal complexes bearing carbonyl ligands have been widely explored as CORMs for the controlled delivery of small doses of CO inside cells.[15–18]

The screening of a number of metal complexes, including ruthenium, rhenium, manganese, molybdenum, iron, cobalt, tungsten and iridium derivatives, has allowed the identification of a wide variety of CORMs. Such derivatives possessed different CO-releasing profiles and biological properties, such as cytotoxicity, lipophilicity and distribution in the body.[21] The most common trigger for CO release is the ligand exchange with solvent molecules.[14,16] The two CO-releasing molecules following this

activation mechanism most often exploited in biological and medicinal studies are the ruthenium(II) complexes CORM-2 and CORM-3 (**Figure 6.1**) patented by Motterlini and coworkers in 2002.[22]

One glycoconjugated Ru(II)-CORM reported by Pamplona and coworkers, named ALF492, was also obtained by conjugating the Ru(II)-tricarbonyl core of CORM-2 with methyl-β-D-thiogalactoside (Gal-S-Me, **Figure 6.1**).[23] Remarkably, the complex was shown to deliver CO *in vivo* without affecting oxygen transport by hemoglobin. In addition, when used in combination with the antimalarial drug artesunate, ALF492 proved effective as an adjuvant treatment for cerebral malaria, conferring protection after the onset of the severe disease. The study paved the way for the potential use of CORMs, such as ALF492, as adjunctive/adjuvant treatment in severe forms of malaria infection.[23]

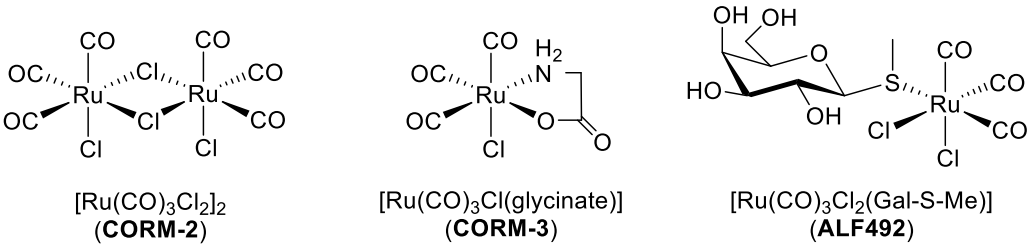

Figure 6.1. Chemical drawings of the ruthenium(II)-based complexes patented by Motterlini and coworkers as CO-releasing molecules.[22]

Photoactivatable manganese-based CORMs have been also widely studied for the controlled release of CO within the body. These compounds are stable in the dark, so as to allow the compound to bioaccumulate in the target tissue.[24] Subsequent photoirradiation triggers the cleavage of the metal-carbonyl bond and the release of a CO molecule (**Scheme 6.1**).[18]

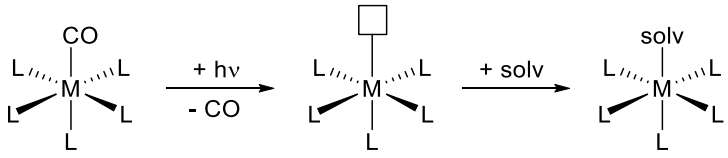

Scheme 6.1. Mechanism of light-triggered CO release and subsequent solvation of metal-CORMs.

In particular, cationic tricarbonyl manganese(I) derivatives bearing tris(1-pyrazolyl)methane ligands reported by Schatzschneider and coworkers showed photoinduced CO-releasing properties (**Figure 6.2**).[25] In addition, the scaffold proved suitable for coupling with biomolecules, such as peptides, *via* click chemistry or Sonogashira coupling.

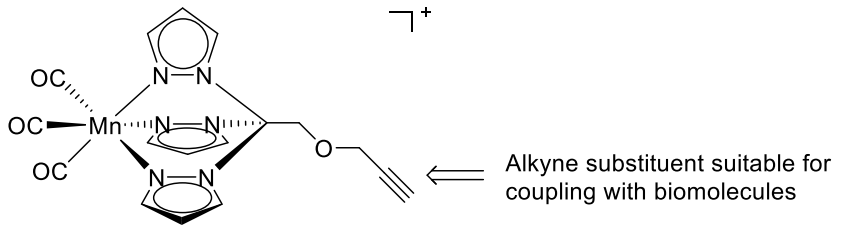

Figure 6.2. Chemical drawings of the manganese(I)-based complex reported by Schatzschneider and coworkers as a CO-releasing platform.

6.2 Manganese(I)-carbonyl dithiocarbamato CORMs

Manganese(I) complexes with dithiocarbamato ligands are well-known since the 1960s, when Cotton reported a number of CO-containing complexes of iron(II), rhodium(I) and manganese(I) with dimethyl- and diethyldithiocarbamato ligands.[26]

Apart from that, the therapeutic potential of this class of compounds in terms of CO-releasing properties was reported only recently by Motterlini and collaborators, resulting in the filing of a patent related to a series of ruthenium- and manganese-CORMs.[27] Among these, also manganese(I)-complexes with dithiocarbamato ligands of the type $[Mn(CO)_4(dtc)]$ (dtc: dithiocarbamato ligand) were reported (**Figure 6.3**). Particularly, the complex with sarcosinedithiocarbamate, named CORM-401, was disclosed in detail in subsequent publications, showing promises as a potential drug candidate.[28]

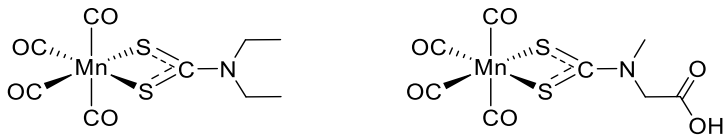

Figure 6.3. Chemical drawings of the manganese(I)-based complexes patented by Motterlini and coworkers as CO-releasing molecules.[22]

The presence of the carboxylic moiety of sarcosine makes the complex ideal for pharmacological developments being soluble in organic solvents when protonated and soluble in water when deprotonated at physiological pH 7.4. The derivative showed reversible release of carbon monoxide in solution, although studies of CO release by trapping with ligands, such as myoglobin, showed that the compound released irreversibly 3.2 moles of CO per mole of CORM with a single rate constant and a half-time of 0.8 min. Biological activity studies with murine RAW264.7 macrophages showed that the CORM-401 produced a decrease of 25% cell viability within 24 h.[28] Further studies highlighted also that CORM-401 was more cytoprotective than other reported metal-CORMs against oxidative stress and cell death, probably due to a higher ability of

the former to release more CO under oxidative conditions. The results pointed out that CORM-401 may be effective in conditions of persistent oxidative stress such as in gastrointestinal disorders.[29] Interestingly, amongst the beneficial therapeutic effects of the complex, it was also observed that the release of CO increased cellular respiration (oxidative phosphorylation), accompanied by inhibition of glycolysis in a non-dependent manner.[30] The same CORM displayed antimicrobial activity by arresting the growth of *E. coli*, *K. pneumoniae*, and other bacterial strains; when co-administered with other antiobiotics, CORM-401 increased their antimicrobial action without interacting.[31]

Zhang and coworkers reported on a series of manganese(I) tetracarbonyl complexes coordinated to dithiocarbamato ligands of proline, hydroxyproline, isonipecotic acid (4-pyperidin carboxylic acid) (**Figure 6.4**).[32]

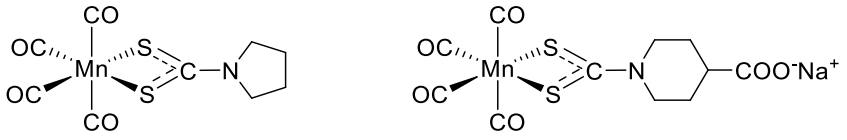

[Mn(CO)$_4$(PDT)] Na[Mn(CO)$_4$(dtc-Inp-O)]

Figure 6.4. Chemical drawings of the manganese(I)-based complexes reported by Zhang and co-workers as CO-releasing molecules.[32]

Among all, the proline-functionalized derivative showed the greatest potential. All the complexes are fast CO-releasers with a pseudo-first order kinetic and half-lives in the range 5÷32 min. Although displaying only modest *in vitro* cytotoxicity towards HeLa and HepG2 cancer cells (IC_{50} 23 and 34 μM, respectively), the complex induced apoptosis in HeLa cells by blocking cell cycle at the G2/M phase. Furthermore, it also showed anti-inflammatory properties.[32]

6.3 Aims and objectives

On account of the aforementioned considerations, the aim of this project was to synthesize a series of manganese(I)-carbonyl derivatives bearing carbohydrate-functionalized dithiocarbamato ligands of the type [Mn(dtc-Inp-glu)(CO)$_4$] (**Figure 6.5**). The structural motif [Mn(dtc-Inp-glu)(CO)$_4$] would allow, at least in principle, to maintain the potential therapeutic performance of the aforementioned Mn-CORMs (fast and efficient release of CO, cytotoxicity against cancer cells, antimicrobial activity, cytoprotection against ischemia reperfusion injury) as well as to attain selective intracellular delivery provided by the presence of the carbohydrate "Trojan Horse". It is believed, in fact, that conjugation with carbohydrates might improve the selective release of carbon monoxide within tumour cells, together with enhancing the overall water-solubility[23] In addition,

a non-glycoconjugated derivative of the type [Mn(dtc-Inp-NH_2)$(CO)_4$] which served as a model complex was also synthesized.

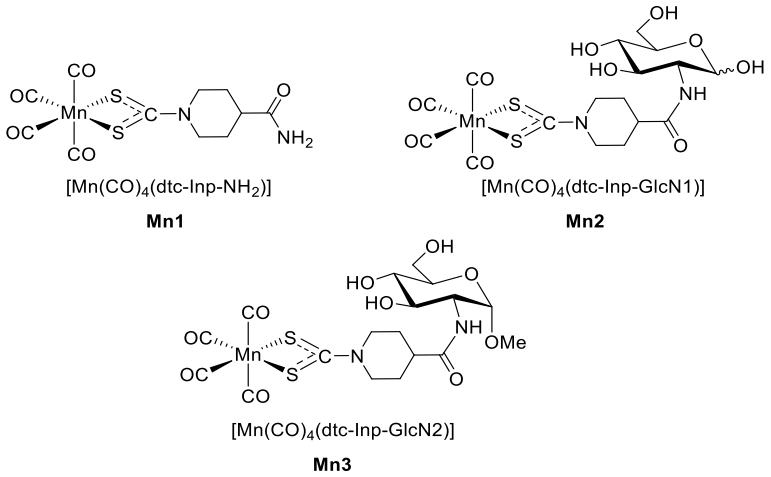

Figure 6.5. Chemical structures of the Mn(I)-tetracarbonyl derivatives containing dithiocarbamato ligands synthesized in this research project.

Finally, the scope of the following research project is to evaluate the CO-releasing properties of the synthesized compounds by means of UV-Vis in presence of myoglobin. This assay is an essential prerequisite to assess the potential of the newly CORMs to deliver CO in biological targets.

6.4 Synthesis

The aforementioned derivatives were synthesized in two different ways. The model complex with the dithiocarbamato ligand derived from isonipecotamide was obtained, according to the procedure reported by Cotton,[26] by reacting a solution containing 1 eq. of ligand Na(dtc-Inp-NH_2) in methanol with 1 eq. of bromopentacarbonylmanganese(I) ([$MnBr(CO)_5$]) in methanol at 40°C in the dark (**Scheme 6.2**). The Mn–Br bond is cleaved and an equatorial CO is liberated, thus generating a neutral octahedral complex containing four CO molecules and a bidentate dithiocarbamato ligand. The complex [$Mn(CO)_4$(dtc-Inp-NH_2)] was isolated in good yields (64%) as a yellow ochre powder. X-ray structures reported for similar analogues support the equatorial coordination of the dithiocarbamato ligand.

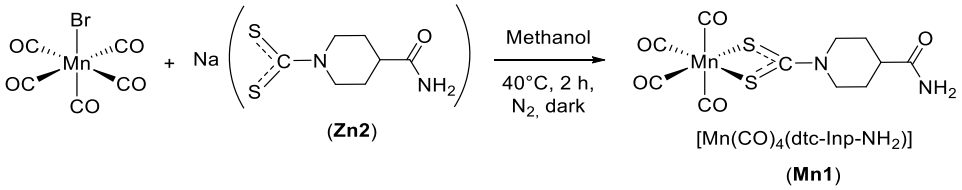

Scheme 6.2. Synthesis of complex [$Mn(CO)_4$(dtc-Inp-NH_2)] (**Mn1**).

The synthesis of the corresponding Mn(I)-dithiocarbamato glycoconjugates was carried out by transmetallation from the corresponding zinc(II)-dithiocarbamato glycoconjugates.

A solution containing 1 eq. of the zinc(II) precursors **Zn3** or **Zn4** in dry DMF was added to a solution of 2 eq. [$MnBr(CO)_5$] in dry DMF/acetone at room temperature in the dark (**Scheme 6.3**). The corresponding compounds were isolated in good yields (70-89%) as yellow ochre-brown powders.

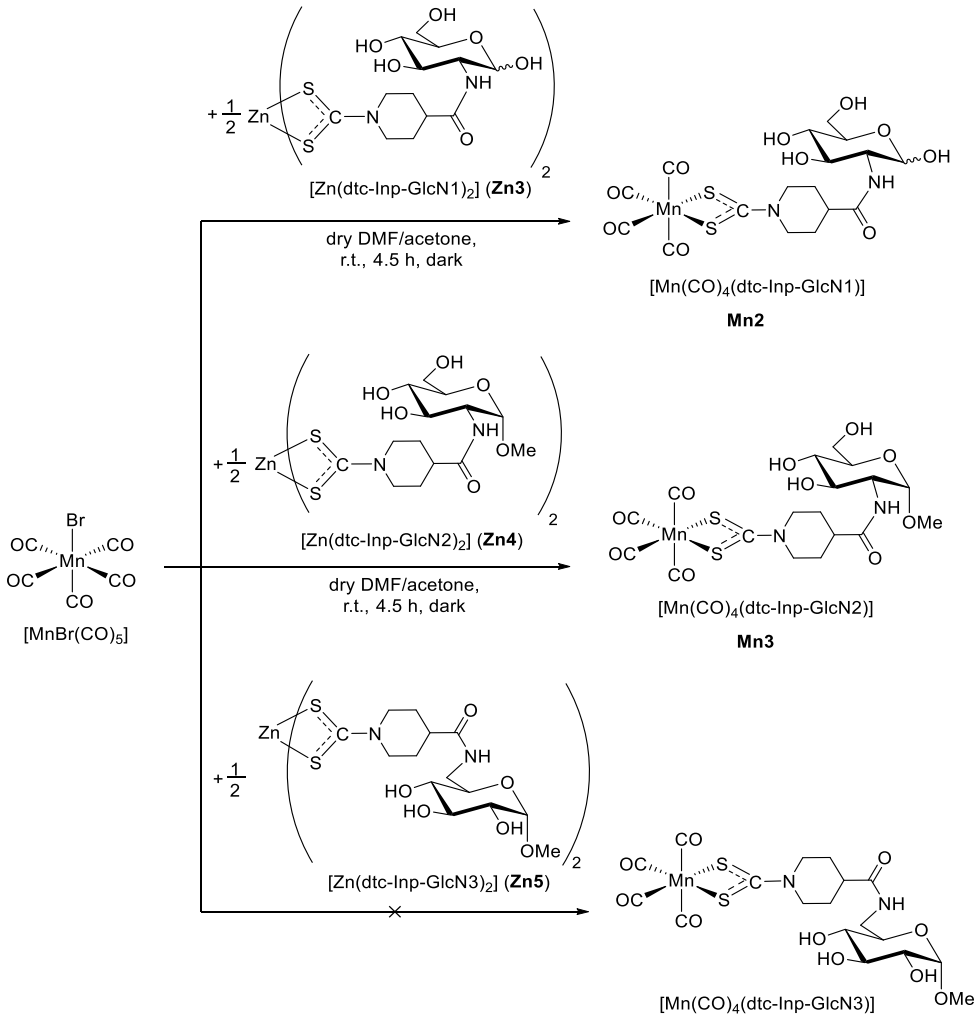

Scheme 6.3. Synthesis of complexes [$Mn(CO)_4$(dtc-Inp-GlcN1)] (**Mn2**) and [$Mn(CO)_4$(dtc-Inp-GlcN2)] (**Mn3**).

Although the reaction seems to proceed well with the zinc(II) precursors **Zn3** and **Zn4**, any attempt to isolate the derivative obtainable by reaction with the C6-glycoconjugate **Zn5** proved unsuccessful so far.

Although the compounds seem to be air-stable in solid, they were stored in the dark and protected from moisture to avoid any possible decomposition. The compounds are soluble in DMSO, DMF and slightly soluble (but not stable) in methanol.

6.5 IR spectroscopy

Infrared spectroscopy provides insights into the coordination mode(s) of the ligands bound to the manganese(I) centre, in particular as far as the carbonyl ligands are concerned. In fact, the IR spectrum of metal complexes containing carbonyl ligands in the region around 2100-1900 cm^{-1} is dominated by strong stretching vibrations of the C≡O bond. The number and pattern of such vibrations are diagnostic to assess the geometry of the metal complex.[33]

All the complexes **Mn1-3** present the same vibrational pattern at ca. 2085/2033/2010/1925 cm^{-1}, which dramatically differs from the pattern of the starting reagent [$MnBr(CO)_5$] (**Figure 6.6**).[34] This difference accounts for a change in the molecular symmetry when [$MnBr(CO)_5$] (C_{4v}) reacts to yield [$Mn(CO)_4$(dtc)], with the equatorial dithiocarbamato ligand (C_{2v}).[33]

As stated by Motterlini *et al.*, the CO infrared stretches are often taken as an indication of the strength of the metal-carbonyl bonding. Higher frequencies reflect in weaker Mn–CO bonding and, as a consequence, in expected easier and faster CO release.[28] Compared with the benchmark reference complex [$Mn(CO)_4$(Sar-dtc-OH)] (CORM-401), the position of the CO IR vibrations differs only slightly (except at 1925 cm^{-1}), thus suggesting a similar coordination fashion.

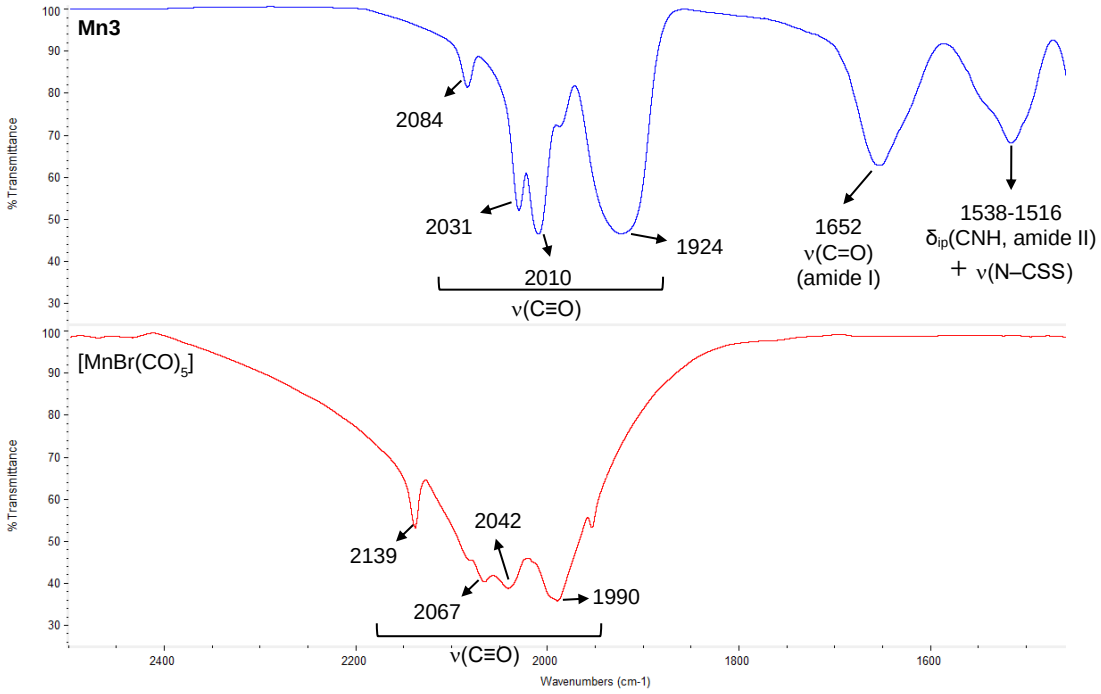

Figure 6.6. Stacked IR spectra (region 2500-1500 cm^{-1}) of compounds **Mn3** and [$MnBr(CO)_5$] (CsI disk, wavenumber in cm^{-1}).

Other diagnostic vibrations attributable to the CO ligand can be found at in the region 680-620 cm^{-1} (bending (δ) Mn–CO) and 440-420 cm^{-1} (stretching (ν) Mn–CO).

For what concerns the vibrations associated with the coordinated dithiocarbamato ligand, typical absorption are observed in a similar manner to what described in the previous chapter for gold(I/III) analogues. The stretching of the chelating N–CSS moiety bound to manganese(I) is detected at *ca*. 1515-1500 cm^{-1}, while the antisymmetric/symmetric stretching of the SCS moiety is recorded at *ca*. 1000/530 cm^{-1}. Another diagnostic signal is recorded at 380-360 cm^{-1}, corresponding to the antisymmetric stretching of the S–Mn–S bonds, with concomitant disappereance of the Mn–Br stretching of the starting reagent (at 222 cm^{-1}).

Other absorptions involve the organic pendant such as stretchings of the amide bond at 1660-1650 cm^{-1} (amide I) and of the C–O bonds of the sugar ring. The main absorptions are summarized in **Table 6.1**.

Complex	$\tilde{\nu}_{max}$, cm^{-1}				
	ν(C≡O)	ν(C=O) (amide I)	ν(N–CSS)	δ(Mn–CO)	ν_a(SMnS)
Mn1	2084/2030/2010/1923[a]	1662	1517	671/628	361
Mn2	2085/2031/2011/1926[a]	1647	1496	670/629	378
Mn3	2084/2031/2010/1924[a]	1654	1516	672/628	379
$[MnBr(CO)_5]$	2139/2067/2042/1990	-	-	629	-

[a] the broad band at ca. 1925 cm^{-1} is a combination of two overlapped vibrations.

Table 6.1. Selected IR frequencies of complexes **Mn1-3** and $[MnBr(CO)_5]$ (CsI disk, wavenumber in cm^{-1}).

6.6 NMR spectroscopy

It is well known that the *J*-multiplet structure of the NMR signals of spin-1/2 nuclei directly bound or in close proximity to a quadrupolar nucleus (*i.e*. nuclear spin I > 1/2) is partially or completely collapsed, and the corresponding NMR spectrum can significantly broaden.[35] This is due to the quadrupolar nuclei possessing electric quadrupole moments which interact with the fluctuating electric field gradients produced at the investigated nucleus by other molecular degrees of freedom. Such interaction leads to rapid spin-lattice relaxation and, consequently, to a broadening of signals.[36] ^{55}Mn is 100% natural abundant, has I = 5/2 and a large quadrupole moment of $33 \cdot 10^{-30}$ m^2.[37] As a consequence, ^{1}H and ^{13}C NMR spectra of manganese(I)-containing compounds **Mn1-3**, generally returned broad peaks, although such quadrupolar effect was somewhat mitigated by choosing appropriate deuterated solvents.

In this regard, the choice of a suitable solvent in which the complexes are reasonably soluble but do not decompose, is not always trivial and may limit the successful applicability of the NMR technique in solution. Owing to the general photosensitivity of these compounds, their solutions were handled in the dark (that is, wrapped in aluminium foil) to limit exposure to light. The complexes were more stable in DMSO than in methanol, darkening and leading to the precipitation of a brown solid within a couple of hours in the latter solvent. Dichloromethane-d_2 (CD_2Cl_2) is often used for the NMR characterization of this class of metal derivatives since it appears to reduce the broadening effect of the manganese-induced quadrupolar relaxation.[37b] Unfortunately, complexes **Mn1-3** were not sufficiently soluble in chlorinated solvents to carry out NMR analysis. Anyway, even if ^{1}H NMR provided scarce information, a pattern of signals consistent with the expected carbonyl-manganese(I)-dithiocarbamato derivatives could be identified (**Figure 6.7**).

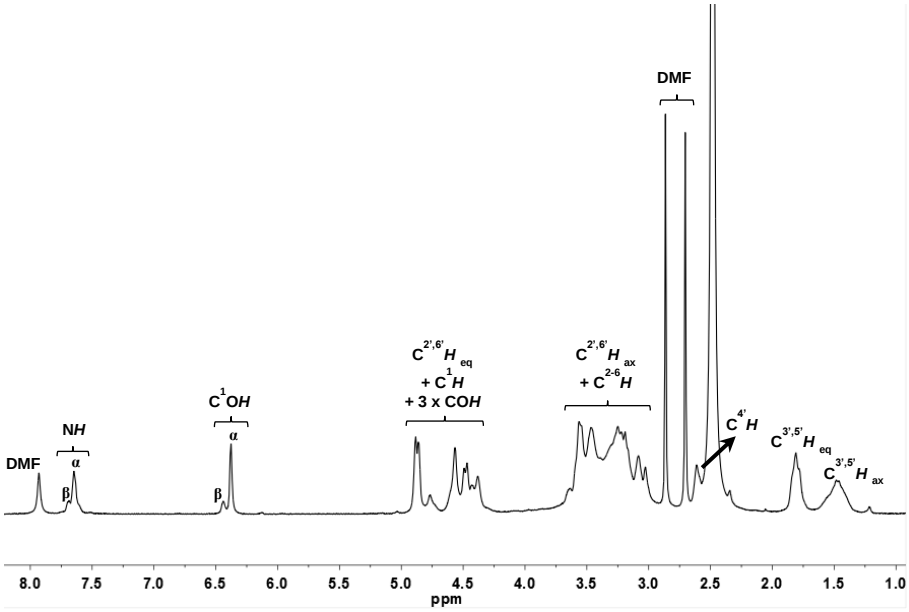

Figure 6.7. ^{1}H NMR spectrum of compound **Mn2** (500 MHz, DMSO-d_6).

Excessivily long acquisition times did not allow the recording of properly resolved $^{13}C\{^1H\}$ NMR spectra in DMSO-d_6. On the contrary, the $^{13}C\{^1H\}$ NMR spectra did not present any of these issues in methanol-d_4 (CD_3OD), although the complexes are stable in solution for less time. ^{13}C peaks proved useful to identify the obtained derivatives. For example, with reference to **Figure 6.8**, the signals in the region 220-200 ppm were assigned to the dithiocarbamic (NCSS, 202 ppm) and to the carbonyl (CO, two axial and two equatorial at *ca*. 217 and 212 ppm) moieties.[22] Other resonances attributable to the dithiocarbamato ligand were observed, with slight deviations from the zinc(II)-dithiocarbamato precursors. As concerns the anomeric distribution of the

glycoconjugates, **Mn2** is present as a mixture of α,β anomers (α/β *ratio* ≈ 4:1), as two distinct patterns of NMR signals are observed in DMSO-d_6, while **Mn3** contains only the α anomer.

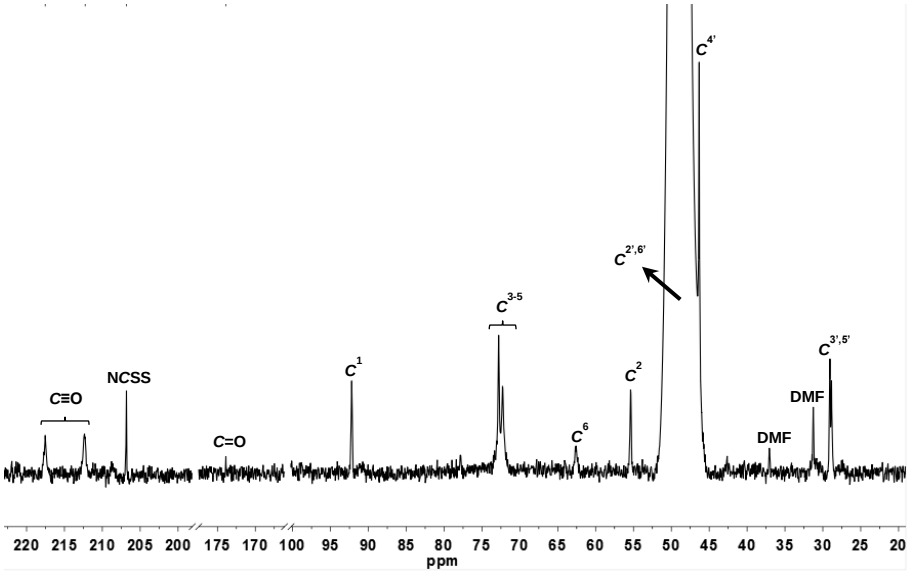

Figure 6.8. $^{13}C\{^1H\}$ NMR spectrum of compound **Mn2** (100 MHz, CD_3OD).

Finally, ^{55}Mn NMR analysis was attempted on a representative compound **Mn1**. However, no signals were detected, even at prolonged acquisition times and at low temperature. This is probably due to the fact that ^{55}Mn NMR gives observable signals only for small molecules, such as $[MnBr(CO)_5]$ (-1139 ppm).[37b]

6.7 UV-Vis spectroscopy

UV-Vis spectra were collected for the compounds in DMSO at 50 μM. The compounds proved stable in the solvent over 48 h (data not shown).

In addition, a stability study in PBS at 37°C was carried out also to assess the stability of the compounds in a physiological-like buffer. As depicted in **Figure 6.9**, the UV-Vis spectra changed significantly over the time. Anyway, minor changes occured during the first 30 min. Since in this stint the CO release was mostly complete (see next section), the lack of stability of the compound is not supposed to interfere with the kinetics of CO release.

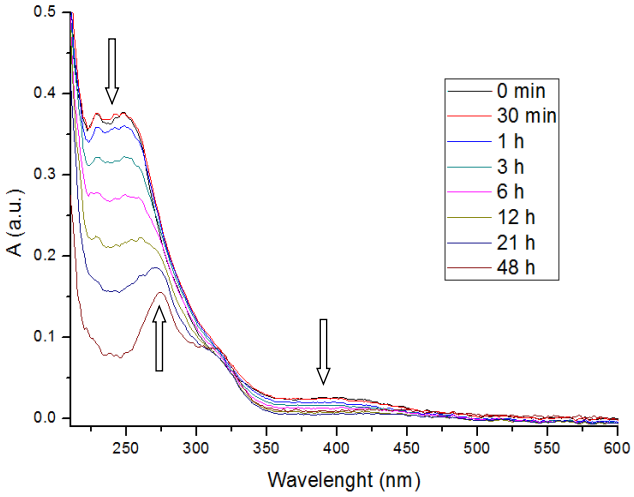

Figure 6.9. UV-Vis spectra recorded at different time lapses (50 μM in PBS, 37°C) of **Mn2**.

6.8 CO-release assay

In order to assess the capability of the synthesized complexes to release CO, an assay in the presence of myoglobin was carried out. The assay, introduced for the first time by Motterlini and coworkers in 2002, is based on the determination of the concentration of carboxy-myoglobin (MbCO) generated when a solution of deoxy-myoglobin (deoxy-Mb, or MbFe(II)) in phosphate buffer (pH = 7.4) is co-incubated with the tested CORM.[19] The concentration of MbCO is determined by measuring the difference in absorbance of the Q band of the heme group after conversion from a solution of myoglobin.

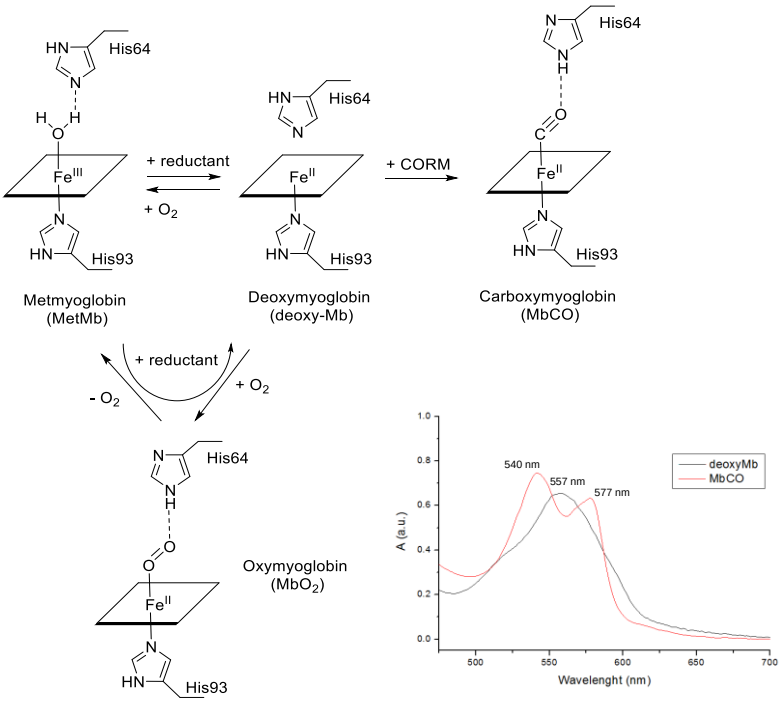

Figure 6.10. Mechanism of reduction of the heme group of myoglobin to deoxy-myoglobin and conversion to carboxymyoglobin (top, right), and Q-band region of the absorption spectrum of deoxy-myoglobin (black) and carboxymyoglobin (red) in PBS (bottom, left).

Changes in the absorption spectra of deoxy-myoglobin to carboxymyoblobin are used to monitor the release of carbon monoxide from metal carbonyl complexes by UV/Vis spectroscopy (**Figure 6.10**). Upon CO liberation and binding to myoglobin, the maximum in the Q band region of deoxy-Mb at 557 nm decreases in intensity while two new bands at 540 and 577 nm appear, arising from MbCO. From the extinction coefficients of deoxy-myoglobin (ε_{560nm} = 13.8 L mmol^{-1} cm^{-1}) and carbonmonoxy-myoglobin (ε_{540nm} = 15.4 L mmol^{-1} cm^{-1}),[38] the starting concentration of MbFe(II) as well as the amount of MbCO formed can be determined. Although the myoglobin assay is the standard method to study the CO release properties of CORMs, it has some major drawbacks.[39]

- Solutions need to be properly degassed with dinitrogen to prevent oxygenation of myoglobin to oxymyoglobin (MbO_2). Another important issue is the need to work always with freshly prepared solutions, since neither deoxy-Mb nor sodium dithionite are stable in PBS over time.
- The compounds should not interfere with the absorption measurements by absorbing in the wavelength range of interest (490-600 nm). Since no significant absorptions of the investigated complexes in PBS were observed in this range, they were supposed not to interfere with the measurements.
- The experiment is dependent on the reductant used. The presence of a reductant, such as sodium dithionite, is required in order to reduce the iron atoms of the heme group of myoglobin from the oxidation state +3 to +2, leading to the formation *in situ* of deoxy-myoglobin. However, it has been proved that without any reductant, the release of carbon monoxide does not take place in CORM-2 and CORM-3, while it is diminished in the case of CORM-401. In addition, various experiments with different reductants (sodium dithionite, NADH, sodium sulfite, *etc*.) revealed that the rate of release is dependent on the type of reductant used.[40]

However, as a first qualitative test, solutions of the compounds in excess (50 μM) were co-incubated at 37°C with deoxy-myoglobin (50 μM), obtained from reduction of a myoglobin solution in PBS with excess sodium dithionite. This preliminary experiment was performed in order to assess the feasibility of the tested experimental conditions and to determine if the synthesized complexes were effective CO-releasers. Therefore, the method introduced by Fairlamb and coworkers, which requires the adjustment at the isosbestic point at 510 nm to intersect the spectra during the conversion from deoxy-Mb to MbCO, was applied.[39]

For all three CORMs here assessed, the fast disappereance of the maximum at 557 nm (Q-band) with the simultaneous formation of two maxima at 540 nm and 577 nm attributable to MbCO were observed (**Figure 6.11**). The conversion reaches completeness within 15 min, since no further spectral changes are observed afterwards. These results confirmed that the synthesized compounds release CO.

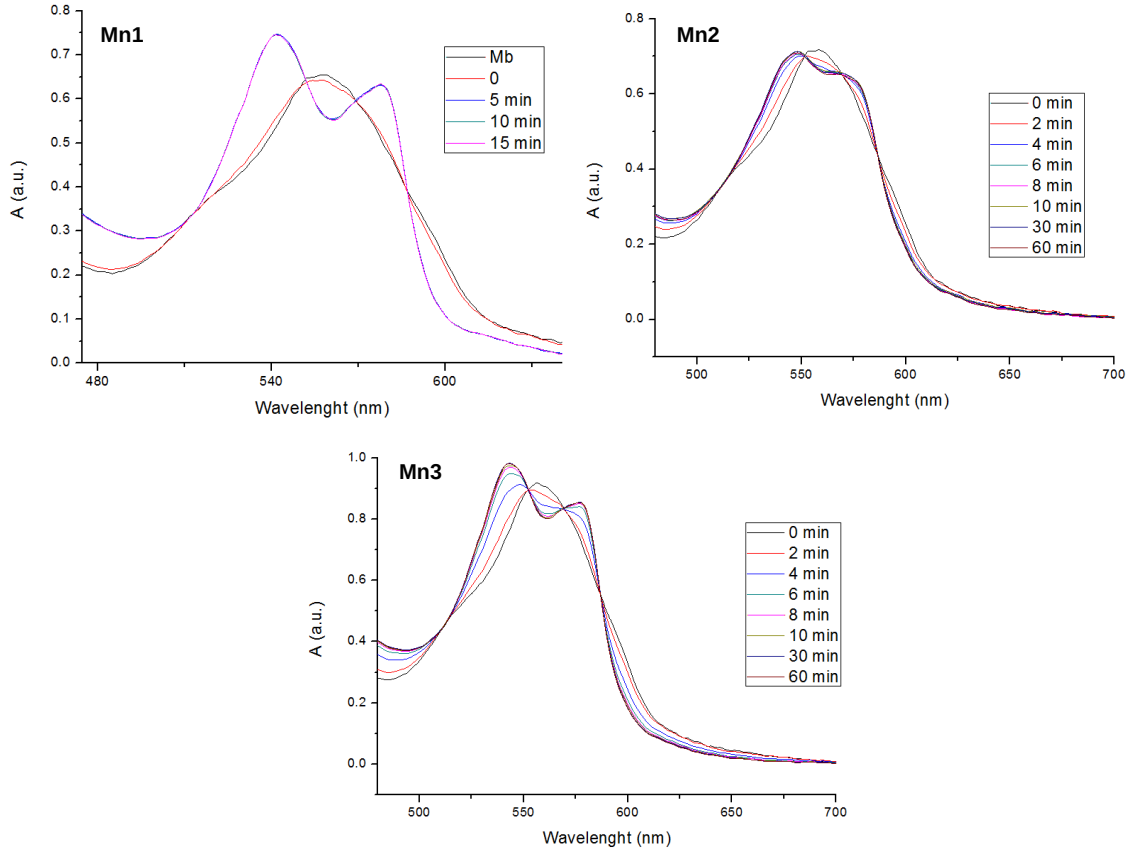

Figure 6.11. Spectral changes in the Q band region of myoglobin in the presence of **Mn1-3.**

Kinetic experiments were also carried out co-incubating CORMs **Mn1-3** at 10 μM with deoxy-Mb at 50 μM in presence of excess sodium dithionite at 37°C. An example is shown in **Figure 6.12** for **Mn3**. The number of released molecules of CO was also calculated by dividing the calculated concentration of MbCO with the initial concentration of CORM.

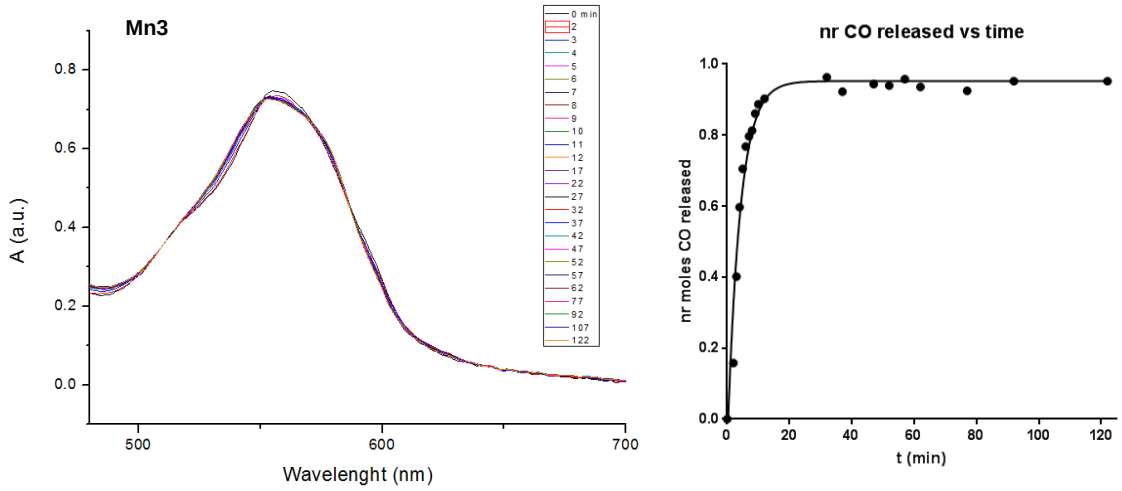

Figure 6.12. Spectral changes in the Q band region of myoglobin at 50 μM in the presence of **Mn3** at 10 μM (left), and plot of number of COs released per CORM calculated from the absorption at 540 nm (right).

The compounds **Mn1-3** showed a relatively fast release of CO, with a half-time of about 1.9-2.6 min (**Table 6.2**). From a practical point of view, such a fast release rate might not be beneficial, since the CORM would require a certain time to reach the target site and thus liberate CO, either intracellularly or in the surroundings of the target cells. In addition, it was observed that **Mn1** and **Mn3** release approximately 1 mol of CO per mol of CORM, whereas **Mn2** liberate only approximately 0.5 mol. This is in contrast with what observed by Motterlini and other research groups independently, who reported that analogous compounds liberate approximately 2-3 COs per CORM.[28]

Complex	$t_{1/2}$ (min)	k (min^{-1})	mol CO released per mol CORM
Mn1	2.62 ± 0.35	0.27 ± 0.03	1.3
Mn2	1.91 ± 0.22	0.37 ± 0.04	0.4
Mn3	2.55 ± 0.27	0.27 ± 0.03	0.9
CORM-401[a]	0.8	-	3.2

[a] value taken from [28]

Table 6.2. Calculated half-times, kinetics constants and mol CO released per mol CORM for complexes **Mn1-3**.

6.9 Conclusions

Carbonyl manganese(I)-dithiocarbamato complexes have shown promising anticancer and other therapeutic properties due to their beneficial capability to release CO selectively in target sites.

On account of these considerations, a series of tetracarbonyl-manganese(I) complexes containing dithiocarbamato ligands have been synthesized in good yields by ligand exchange between the manganese(I) source bromopentacarbonylmanganese(I) and

various zinc(II) dithiocarbamato precursors. The obtained derivatives were either glyco- and non-glycoconjugated (model complex). The compounds were characterized by monodimensional ^{1}H and ^{13}C NMR, FT-IR and UV-Vis spectroscopy.

Stability studies showed that the compounds are not stable in the physiological buffer. However, release of CO in the presence of myoglobin was assessed, revealing that the compounds can effectively liberate carbon monoxide endogenously. The rate of release is fast and comparable to similar analogues already reported, although the number of CO release per number of CORM is lower.

Future experiments will be aimed at assessing the biological activity of these compounds towards a panel of cancer cell lines. As already pointed out by Schatzschenider in a recent review, an unresolved question related to CORM metal derivatives is to establish whether they require a passive or active cell internalization in order to exert their biological activity, or it would be sufficient to liberate the CO close enough to the target site, which will then diffuse into cells through cellular membranes.[41] For this reason further antiproliferative activity assays will be carried out in collaboration with Prof. Schatzschneider (University of Würzburg) and Prof. Foresti (University of Paris-Est) in order to assess whether the conjugation in the so-called CORM coordination sphere with carbohydrates can increase their bioavailability and the intracellular release of CO.

6.10 References

[1] N. B. Hampson, C. A. Piantadosi, S. R. Thom, L. K. Weaver, *Am. J. Respir. Crit. Care Med.* **2012**, *186*, 1095–1101.

[2] T. Sjostrand, *Nature* **1949**, *164*, 580.

[3] R. Tenhunen, H. S. Marver, R. Schmid, *Proc. Natl. Acad. Sci. U. S. A.* **1968**, *61*, 748–755.

[4] S. W. Ryter, J. Alam, A. M. K. Choi, *Physiol. Rev.* **2006**, *86*, 583–650.

[5] S. Oh, S.-C. Choi, *Neural Regen. Res.* **2015**, *10*, 36–38.

[6] S. Li, T. Takahara, X.-K. Li, M. Fujino, T. Sugiyama, K. Tsukada, C. Liu, Y. Kakuta, N. Nonomura, H. Ito, K. Takahashi, M. Nakajima, T. Tanaka, S. Takahara, *Biochem. Biophys. Res. Commun.* **2016**, *470*, 900–906.

[7] Y. Han, W. Yi, J. Qin, Y. Zhao, J. Zhang, X. Chang, *Neurosci. Lett.* **2015**, *585*, 126–131.

[8] H. J. Duckers, M. Boehm, A. L. True, S. F. Yet, H. San, J. L. Park, R. Clinton Webb, M. E. Lee, G. J. Nabel, E. G. Nabel, *Nat. Med.* **2001**, *7*, 693–698.

[9] R. A. Johnson, F. K. Johnson, *Shock (Augusta Ga)* **2008**, *29*, 526–530.

[10] T. Katayama, Y. Ikeda, M. Handa, T. Tamatani, S. Sakamoto, M. Ito, Y. Ishimura, M. Suematsu, *Circ. Res.* **2000**, *86*, 1031–1037.

[11] C. Mancuso, P. Preziosi, A. B. Grossman, P. Navarra, *Neuroimmunomodulation* **1997**, *4*, 225–229.

[12] P. Navarra, C. Dello Russo, C. Mancuso, P. Preziosi, A. Grossman, *Ann. N. Y. Acad. Sci.* **2000**, *917*, 638–646.

[13] S. Errico, R. Shohreh, E. Barone, A. Pusateri, N. Mores, C. Mancuso, *Neurosci. Lett.* **2010**, *471*, 175–178.

[14] B. E. Mann, *Carbon Monoxide: An Essential Signalling Molecule*, in *Med. Organomet. Chem.* (Eds.: G. Jaouen, N. Metzler-Nolte), Springer, Berlin, **2010**, pp. 247–285.

[15] R. Motterlini, L. E. Otterbein, *Nat. Rev. Drug Discov.* **2010**, *9*, 728–743.

[16] C. C. Romão, W. A. Blättler, J. D. Seixas, G. J. L. Bernardes, *Chem. Soc. Rev.* **2012**, *41*, 3571–3583.

[17] R. Alberto, R. Motterlini, *Dalton Trans.* **2007**, *0*, 1651–1660.

[18] U. Schatzschneider, *Inorg. Chim. Acta* **2011**, *374*, 19–23.

[19] R. Motterlini, J. E. Clark, R. Foresti, P. Sarathchandra, B. E. Mann, C. J. Green, *Circ. Res.* **2002**, *90*, E17–24.

[20] J. E. Clark, P. Naughton, S. Shurey, C. J. Green, T. R. Johnson, B. E. Mann, R. Foresti, R. Motterlini, *Circ. Res.* **2003**, *93*, E2-8.

[21] A. C. Kautz, P. C. Kunz, C. Janiak, *Dalton Trans.* **2016**, *45*, 18045–18063.

[22] R. A. Motterlini, B. E. Mann, D. A. Scapens, **2010**, US20100105770A1.

[23] A. C. Pena, N. Penacho, L. Mancio-Silva, R. Neres, J. D. Seixas, A. C. Fernandes, C. C. Romão, M. M. Mota, G. J. L. Bernardes, A. Pamplona, *Antimicrob. Agents Chemother.* **2012**, *56*, 1281–1290.

[24] M. A. Wright, J. A. Wright, *Dalton Trans.* **2016**, *45*, 6801–6811.

[25] H. Pfeiffer, A. Rojas, J. Niesel, U. Schatzschneider, *Dalton Trans.* **2009**, *0*, 4292–4298.

[26] F. A. Cotton, J. A. McCleverty, *Inorg. Chem.* **1964**, *3*, 1398–1402.

[27] R. Motterlini, B. Mann, D. Scapens, **2008**, WO/2008/003953.

[28] S. H. Crook, B. E. Mann, A. J. H. M. Meijer, H. Adams, P. Sawle, D. Scapens, R. Motterlini, *Dalton Trans.* **2011**, *40*, 4230.

[29] D. Babu, G. Leclercq, R. Motterlini, R. A. Lefebvre, *Front. Pharmacol.* **2017**, *8*, 31.

[30] P. Kaczara, R. Motterlini, G. M. Rosen, B. Augustynek, P. Bednarczyk, A. Szewczyk, R. Foresti, S. Chlopicki, *Biochim. Biophys. Acta Bioenerg.* **2015**, *1847*, 1297–1309.

[31] L. K. Wareham, S. McLean, R. Begg, N. Rana, S. Ali, J. J. Kendall, G. Sanguinetti, B. E. Mann, R. K. Poole, *Antioxid. Redox Signal.* **2017**, *28*, 1286–1308.

[32] T. Zhang, M. Li, Y. Gong, N. Xi, Y. Zheng, Q. Zhao, Y. Chen, B. Liu, *J. Biol. Inorg. Chem.* **2016**, *21*, 807–824.

[33] K. Nakamoto, *Infrared and Raman Spectra of Inorganic and Coordination Compounds: Part B: Theory and Applications in Inorganic Chemistry, Sixth Edition*, John Wiley & Sons, Inc., Hoboken, NJ, **2008**, pp. 140-143

[34] D. K. Ottesen, H. B. Gray, L. H. Jones, M. Goldblatt, *Inorg. Chem.* **1973**, *12*, 1051–1061.

[35] D. Rentsch, R. Hany, W. von Philipsborn, *Magn. Reson. Chem.* **1997**, *35*, 832–838.

[36] J. A. Pople, *Mol. Phys.* **1958**, *1*, 168–174.

[37] a) E. Fotopoulou, L. Ronconi, *Application of Heteronuclear NMR Spectroscopy to Bioinorganic and Medicinal Chemistry – 1st Currency Review*, in *Elsevier Reference Module in Chemistry Molecular Sciences and Chemical Engineering* (Ed.: J. Reedijk), Elsevier, Waltham (MA), **2018**, p. 27; b) J. Mason, *Multinuclear NMR*, Plenum Press, New York, **1987**.

[38] E. Antonini, M. Brunori, *Hemoglobin and Myoglobin in Their Reactions with Ligands*, North-Holland Publishing Company, Amsterdam, **1971**.

[39] A. J. Atkin, J. M. Lynam, B. E. Moulton, P. Sawle, R. Motterlini, N. M. Boyle, M. T. Pryce, I. J. S. Fairlamb, *Dalton Trans.* **2011**, *40*, 5755–5761.

[40] S. McLean, B. E. Mann, R. K. Poole, *Anal. Biochem.* **2012**, *427*, 36–40.

[41] U. Schatzschneider, *Br. J. Pharmacol.* **2015**, *172*, 1638–1650.

Chapter 7

Side-projects and concluding remarks

Chapter 7. Side-projects and concluding remarks

During my PhD, I have been also being involved to different extents to some collaborative projects established between my supervisor, Dr. Ronconi, and various collaborators. I contributed either by re-synthesizing compounds already developed within my PhD research project (to be sent to collaborators for specific studies) or by generating new compounds customized on request taking advantage from my synthetic competences and skills. Such side-projects are briefly summarized in this Chapter. For full experimental procedures and characterizations see Chapter 8.

7.1 Platinum(II)-dithiocarbamato glycoconjugates

This is a joint project recently initiated in collaboration with Prof. Lisa Dalla Via (University of Padova, Italy). I contributed by synthesizing and fully characterizing the metal derivatives.

As already described in Chapter 1, platinum(II)-based derivatives bearing dithiocarbamato ligands showed promises as novel anticancer agents both *in vitro*, displaying anticancer activity also against cisplatin-resistant cancer cells, and *in vivo*, with reduction of the tumour volume and no signs of toxicity.[1–5] However, several issues hampered the further development of such promising derivatives, including low water-solubility, poor stability and lengthy synthetic routes. On the basis of these considerations, some platinum(II)-dithiocarbamato compounds with sugar pendants were designed with the aim to obtain novel derivatives with potential anticancer activity and circumvent the aforementioned issues.

Accordingly, glycoconjugation *via* transmetallation was achieved also in presence of a suitable platinum(II) precursor. Reaction of the zinc(II) intermediates **Zn4** and **Zn5** with $(PPh_4)[PtCl_3(NH_3)]$ led to the formation of the complexes $[Pt(dtc\text{-}Inp\text{-}GlcN2)_2]$ (**Pt1**) and $[Pt(dtc\text{-}Inp\text{-}GlcN3)_2]$ (**Pt2**) respectively (**Scheme 7.1**).[6] The original plan was to synthesize the corresponding mono-dithiocarbamato derivatives $[PtCl(dtc\text{-}Inp\text{-}GlcN)(NH_3)]$ but, notwithstanding various attempts and the exploitation of different experimental conditions, the full replacement of both the chloride and the amino ligands with two dithiocarbamato ligands occurred, even when using an excess of the starting platinum(II) reagent.

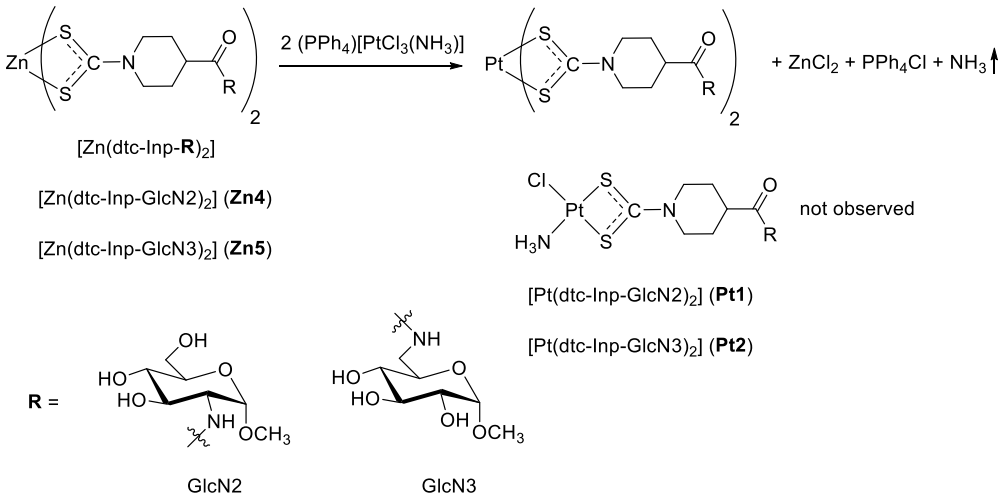

Scheme 7.1. Reaction scheme for the zinc(II)-platinum(II) transmetalation reaction.

Even if no crystals of the platinum(II) glycoconjugates were obtained, analysis and spectroscopic results support the formation of the *bis*-dithiocarbamato adducts. In this regard, the N–CSS stretching vibrations observed at 1523 and 1554 cm^{-1} (compared with the same absorption recorded at 1494 cm^{-1} for the zinc(II) precursors) are in agreement with data reported in the literature for analogous *bis*-dithiocarbamato platinum(II) derivatives.[7,8] Moreover, the absence in the IR spectra of the bands associated with both the NH_3 ligand (at ~3200 ($\nu_{a/s}$), ~1640 (δ_a), ~1290 (δ_s), ~780 (ρ) cm^{-1}) and the chloride ligand (ν(Pt–Cl) at ~330 cm^{-1})[9–11] are consistent with the hypothesis of a complete ligands exchange in favour of the dithiocarbamato ligands.

As far as the NMR characterization is concerned, an illustrative example is given in **Figure 7.1**. The ^{1}H and $^{13}C\{^{1}H\}$ spectra of **Pt2** are very clean and clearly indicate the presence of only one species in solution. Although the majority of the signals resonate at chemical shifts almost identical to those of their counterparts in the zinc(II) precursor **Zn5**, **Pt2** is undoubtedly a different compound, as evidenced by the major upfield shift of the ^{1}H and ^{13}C peaks associated with the $C^{2',6'}H_{eq}$ group. Moreover, the ^{13}C peak at 207 ppm assigned to the dithiocarbamato carbon atom is fully consistent with those reported in the literature for other *bis*-dithiocarbamato platinum(II) derivatives.[7]

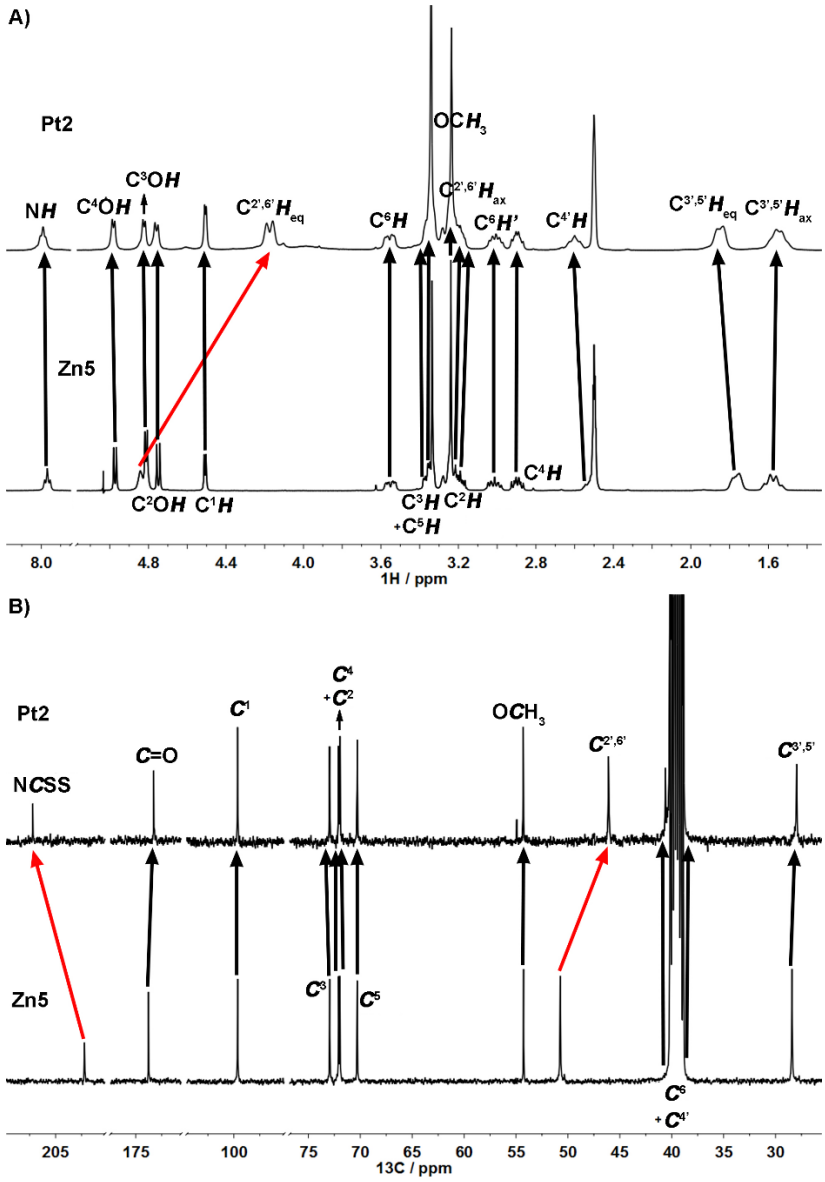

Figure 7.1. Comparison of the ^{1}H (**A**) and $^{13}C\{^{1}H\}$ (**B**) NMR spectra in DMSO-d_6 of [Zn(dtc-Inp-GlcN3)$_2$] (**Zn5**) and [Pt(dtc-Inp-GlcN3)$_2$] (**Pt2**).

Remarkably, no signals attributable to the NH_3 ligand were observed in the ^{1}H NMR spectra. In this regard, both the IR and NMR spectra of the complex obtained by reacting **Zn4** and **Zn5** with the ^{15}N-labelled platinum(II) precursor $(PPh_4)[PtCl_3(^{15}NH_3)]$ turned out to be identical to those of the unlabelled counterparts (data not shown). In particular, no ^{15}N peaks were recorded in the corresponding [^{1}H,^{15}N] HSQC spectra, thus confirming that the NH_3 moiety was replaced.

Notwithstanding the desired mono-dithiocarbamato platinum(II) glycoconjugates were not obtained, the transmetallation reaction proved successful anyway. In perspective, this issue might be overcome by using organophosphine (instead of amino) platinum(II) precursors as recently reported.[12] In this regard, preliminary results obtained by reacting 1 eq. of [Zn(dtc-Inp-NH_2)$_2$] (**Zn2**) or [Zn(dtc-Inp-GlcN3)$_2$] (**Zn5**) with 2 eq. of

[$PtCl_2$(dppe)] (dppe: 1,2-bis(diphenylphosphino)ethane) are consistent with the formation of the $[Pt(dppe)(dtc)]^+$ (dtc: dithiocarbamato ligand) derivative, thus representing a convincing proof-of-concept for the design of platinum(II)-biphosphinoglycoconjugates.

7.2 Ruthenium(II) and osmium(II) organometallic glycoconjugates

This is a joint project commenced in 2017 in collaboration with Dr. Nicholas Barry (University of Bradford, UK). I contributed by resynthesizing the zinc(II)-glycoconjugate intermediates to be transmetallated to ruthenium(II) and osmium(II) organometallic scaffolds.

Organometallic compounds are generally considered toxic and air- or water-unstable although this belief is quite misleading. There is, in fact, a flourishing development of stable and water-soluble organometallic complexes, which fostered a growing interest in the discovery of novel organometallic derivatives for catalytic and medicinal applications.[13] For example, titanocene dichloride has completed phase II clinical trials,[14–16] while ferrocifen, a ferrocenyl derivative of tamoxifen,[17] is expected to enter clinical trials soon.

As far as ruthenium(II)-arene organometallic complexes with biomedical applications are concerned, Sadler and Dyson can be undoubtedly regarded as the pioneers of the field, and their independent research led to the development on the promising anticancer compounds [(η^6-*p*-cymene)Ru(*P*-pta)Cl_2] (RAPTA-C, pta = 1,3,5-triaza-7-phospha-tricyclo-[3.3.1.1]decane),[18] and [(η^6-C_6H_5Ph)Ru(*N*,*N*-en)Cl]PF_6 (en = 1,2-ethylenediamine) (**Figure 7.2**).[19] RAPTA-C and its analogues reported by Dyson, possessed *in vitro* anticancer activity on primary tumours and *in vivo* antimetastatic activity on lung metastases in mice,[20,21] whereas the derivatives reported by Sadler exhibited anticancer activity on primary tumours in a similar way to that of cisplatin.[22]

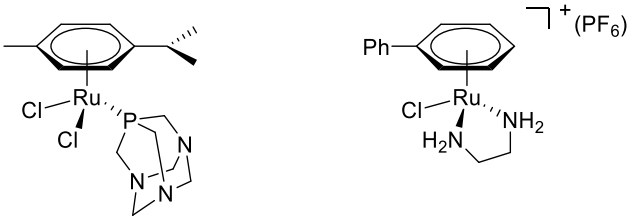

Figure 7.2. Chemical structures of RAPTA-C (left) and [(η^6-C_6H_5Ph)Ru(*N*,*N*-en)Cl]PF_6 (right).

Furthermore, ligand tailoring allows tuning some properties of the compounds, such as hydrophobicity of the arene scaffold, hydrophilicity of the metal centre, stability in the physiological medium, release rate of the leaving ligand, cytotoxic activity, cellular

uptake, *etc*. Monofunctional ruthenium(II) and osmium(II) complexes have been extensively studied in terms of structure-activity relationship, by varying the leaving ligand (X), the chelating ligand (LL), or the arene. However, little is known about derivatives of this type bearing dithiocarbamato ligands. Some *piano stool* ruthenium complexes with dithiocarbamato ligands have shown cytotoxic activity on various cancer cell lines.[23]

Owing to these considerations, several Ru(II)- and Os(II)-organometallic compounds bearing dithiocarbamato ligands were synthesized by the Barry group at the University of Bradford (**Figure 7.3**).

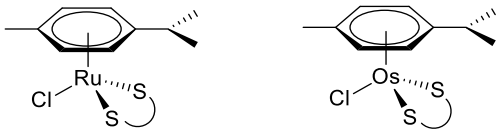

Figure 7.3. General chemical structures of Ru(II)/Os(II) piano stool derivatives with dithiocarabamato ligands.

The derivatives were obtained by means of ligand exchange reaction between the zinc(II)-dithiocarbamato precursors already described in Chapter 2 (provided by us), and the corresponding ruthenium(II)- or osmium(II)-*p*-cymene derivatives, named dichloro(*p*-cymene)ruthenium(II) and dichloro(*p*-cymene)osmium(II) dimers (**Scheme 7.2**). First, the feasibility of the transmetallation was assessed by reacting the ruthenium and osmium starting dimers with the complex [Zn(dtc-Inp-NH_2)$_2$] (**Zn2**), in order also to obtain a non-glycoconjugated model compound. Then, the glycoconjugates bearing the sugar pendants glucosamine (GlcN1), 1-*O*-methyl-α-D-glucosamine (GlcN2), and 1-*O*-methyl-6-amino-6-deoxy-α-D-glucose (GlcN3), were obtained *via* the same approach.

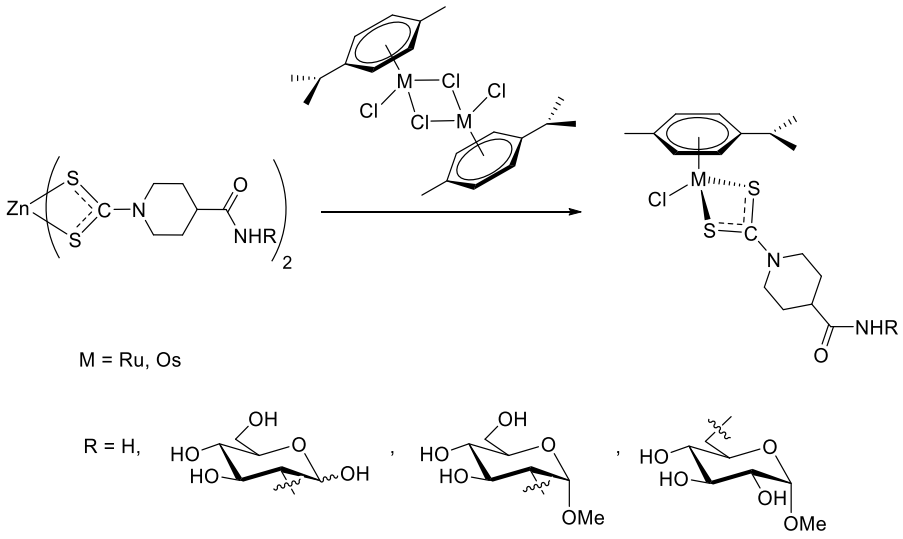

Scheme 7.2. Synthetic route to the *piano stool* Ru(II)/Os(II) with dithiocarbamato ligands via ligand exchange reaction.

Preliminary results have confirmed the successful generation of a complete series of ruthenium(II)- and osmium(II)-dithiocarbamato derivatives (both glycoconjugated and non-glycoconjugated). Full characterization is currently being carried out in the Barry group. After completing the characterization of the compounds and assessing their purity, *in vitro* cytotoxicity studies will be performed.

7.3 Heterometallic platinum(IV)-gold(III) conjugates

This is a joint project commenced in 2015 in collaboration with Prof. Dan Gibson (Hebrew University of Jerusalem, Israel). I contributed by synthesizing the activated gold(III)-dithiocarbamato precursor to be conjugated to the platinum(IV) scaffold and the non-glycoconjugated complex [$AuBr_2$(dtc-Inp-OEt)].

As already mentioned, a valuable and intriguing alternative to the administration of platinum(II) anticancer metallodrugs is represented by platinum(IV) derivatives. Satraplatin (Bis(acetato-*O*)amminedichlorido(cyclohexylamine)platinum(IV), JM-216, **Figure 7.4**) is probably the most remarkable example since this orally active drug has displayed anticancer activity against several platinum sensitive and resistant cancer cell lines, including human lung, ovary, cervix and prostate.[24] Satraplatin is currently under investigation in various Phase I, II and III clinical trials, alone or in combination with other drugs, for the treatment of prostate, brain, metastatic breast, lung and non-small cell lung malignancies.

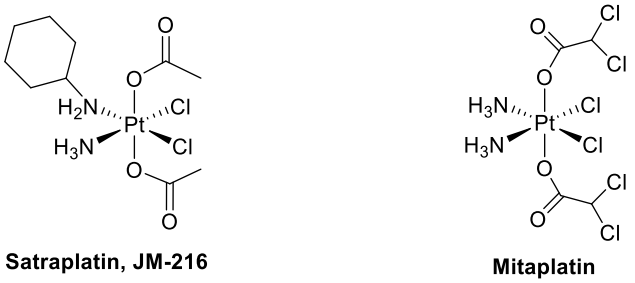

Figure 7.4. Chemical structures of the platinum(IV) derivatives satraplatin (left), and mitaplatin (right).

Octahedral platinum(IV) derivatives behave as prodrugs since, once inside the cell, reduction of the metal centre by intracellular reductants induces the cleavage of the axial ligands, thus releasing the corresponding square-planar platinum(II) counterpart (**Scheme 7.3**). In the case of satraplatin, for example, the axial acetate ligands are released, together with the active platinum(II) species *cis*-amminedichlorido(cyclohexylamine)platinum(II), which prevails among the others.[25]

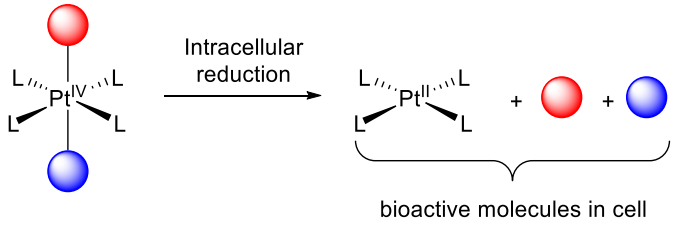

Scheme 7.3. Mechanism of intracellular reduction of platinum(IV) derivatives.

This ligand tailoring strategy allows the design of a wide range of conjugates with potential multiple actions. In fact, modifications may be carried out in the (released) bioactive axial ligands and/or the ancillary ligands of the platinum core.[26]

For this reason, Lippard and coworkers first reported on the activity of the dual action platinum(IV) compound mitaplatin (Bis(dichloroacetato-*O*)amminedichlorido(cyclohexylamine)platinum(IV)), the platinum(IV) derivative of cisplatin with two dichloroacetato (DCA) ligands in axial position (**Figure 7.4**).[27] Mitaplatin combines the ability of cisplatin to bind to DNA with the ability of DCA to interact with cell components at a mitochondrial level.[28]

On account of these considerations, triple-action heterometallic platinum(IV)-gold(III) compounds were designed, synthesized and biologically evaluated in a joint collaboration with the Gibson group.

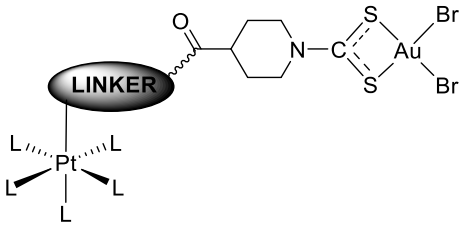

Figure 7.5. General chemical structure of the heterometallic platinum(IV)-gold(III) complexes designed in collaboration with the Gibson group.

These compounds are supposed to act as "cluster bombs" releasing three different bioactive moieties in the cancer cell upon intracellular reduction including: a cisplatin-like metallodrug, 4-phenylbutyrate or octanoate, two well-established histone deacetylase (HDAC) inhibitors:[29,30] and, finally, a bioactive square-planar gold(III)-species attached *via* a linker (**Figures 7.5,6**).

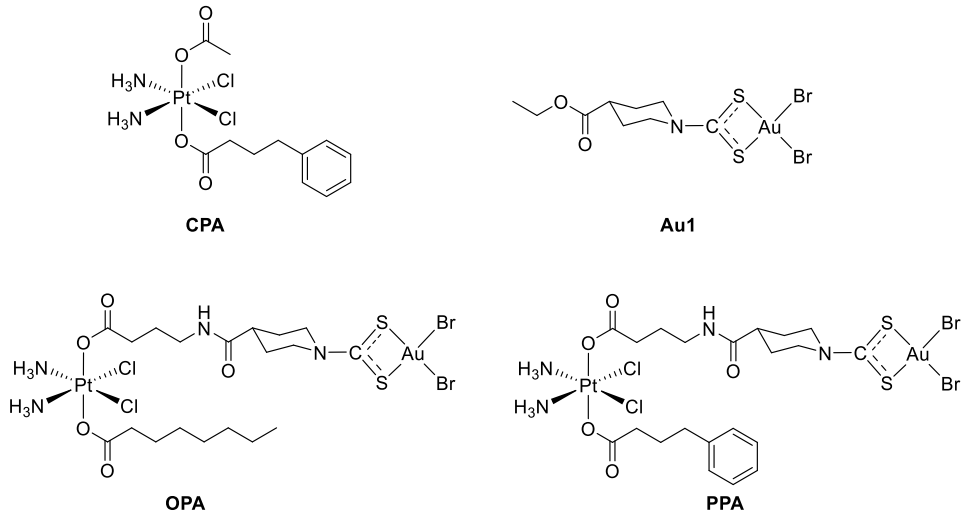

Figure 7.6. Chemical structures of the platinum(IV) and gold(III) complexes **CPA** and [$AuBr_2$(dtc-Inp-OEt)] (**Au1**), and the platinum(IV)-gold(III) mixed complexes synthesized, **OPA** and **PPA**.

The synthesis of the derivatives required the conjugation of the gold(III)-dithiocarbamato precursor bearing a succinimidyl moiety, **Au6**, (whose synthesis was described in Chapter 3) to the corresponding platinum(IV) derivatives bearing an amino group in an axial ligand synthesized in Gibson group (**Scheme 7.4**).

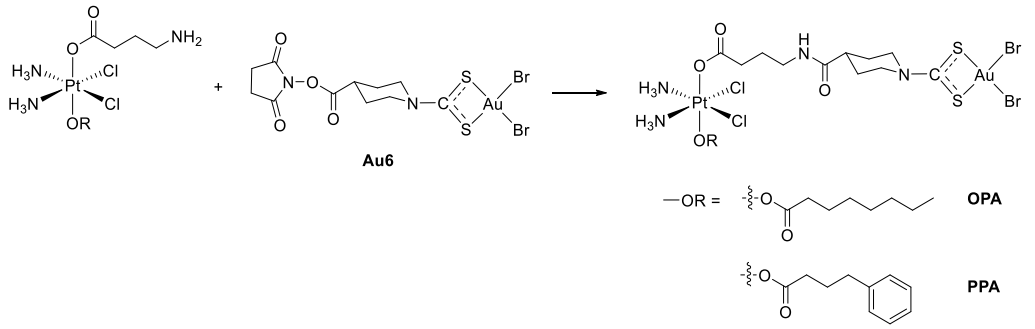

Scheme 7.4. Reaction scheme of the synthesis of heterometallic platinum(IV)-gold(III) complexes.

In vitro antiproliferative studied carried out in collaboration with Prof. Viktor Brabec (Masaryk University, Brno, Czech Republic) on various cancer cell lines highlighted that the binuclear conjugates, although possessing IC_{50} values in the low micromolar range, displayed slightly lower antiproliferative activity when compared to the corresponding mononuclear platinum(IV) and gold(III) model complexes **CPA** and **Au1** (**Table 7.1**).

Complex	IC_{50} (μM, 72 h)					
	A2780	A2780cis	HeLa	MDA-MB-231	CHO-K1	MMC-2
Au1	1.2 ± 0.1	0.6 ± 0.04	-	-	-	-
CPA	2.1 ± 0.1	2.4 ± 0.2	5.6 ± 0.5	1.5 ± 0.2	25.5 ± 3.0	1.3 ± 0.3
OPA	3.3 ± 0.1	4.0 ± 0.4	17.0 ± 0.9	6.9 ± 0.1	56.0 ± 4.0	7.0 ± 0.9
PPA	4.0 ± 0.6	8.4 ± 1.1	29.3 ± 3.2	9.3 ± 0.8	54.0 ± 2.0	5.4 ± 0.9
Cisplatin	3.2 ± 0.1	19.9 ± 1.3	25.0 ± 1.9	29.3 ± 4.5	39.4 ± 4.4	3.9 ± 2.7

Table 7.1. Cytotoxicity data (IC_{50} in μM, 72 h) for compounds **Au1**, **CPA**, **OPA**, **PPA** and cisplatin on A2780 (ovarian cancer), A2780cis (cisplatin resistant-ovarian cancer), HeLa (cervix cancer), MDA-MB-231 (breast cancer), CHO-K1 (hamster ovary) and MMC-2 (osteoblast) cells.

In addition, uptake studies carried out on cisplatin-sensitive and cisplatin-resistant ovarian (A2780 and A2780cis) cancer cell lines revealed that all the platinum(IV) derivatives **CPA**, **OPA** and **PPA** were taken up into the cells at a remarkably higher amount than cisplatin, even if two-fold less than the model gold(III) compound **Au1** (**Table 7.2**). This showed that, in terms of anticancer activity, there is limited advantage in the conjugation of a gold(III)-dithiocarbamato moiety to an axial ligand of a platinum(IV) scaffold.

Complex	nmol complex/10^6 cells	
	A2780	A2780cis
Au1	54.9	90.1
CPA	47.0	50.7
OPA	52.4	54.7
PPA	28.0	32.1
Cisplatin	17.4	4.9

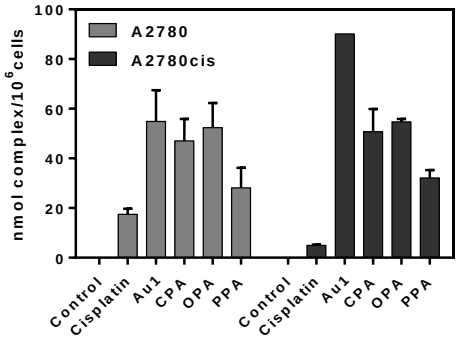

Table 7.2. Intracellular gold and platinum content (in nmol complex/10^6 cells, 24 h) for compounds **Au1**, **CPA**, **OPA**, **PPA** and cisplatin on A2780 (ovarian cancer) and A2780cis (cisplatin resistant-ovarian cancer) cells (left) and column chart (right).

Owing to this preliminary data, further experiments were aimed at the obtainment of novel mixed gold(III)-platinum(IV) derivatives to improve the anticancer potency. For this reason, different ligands have been attached to the platinum(IV) metal centre, such as the ligands 1*S*,2*S*-diaminocyclohexane and 5,6-dimethyl-1,10-phenantroline (**Figure 7.7**).

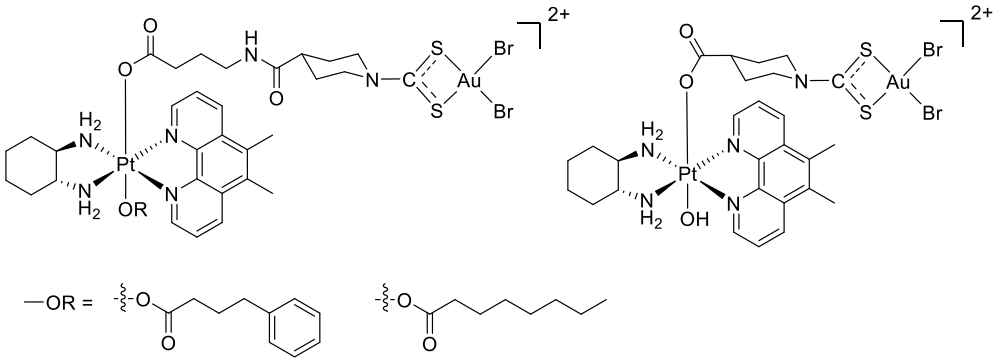

Figure 7.7. Chemical structures of the platinum(IV)-gold(III) derivatives with 5,6-dimethyl-1,10-phenantroline ligands.

These ligands, in fact, were exploited to generate several platinum(IV) compounds, either mono- and binuclear, attached to acetate, dichloroacetate, and phenylbutyrate ligands. Remarkably, the compounds showed far better anticancer activity than cisplatin, in particular towards KRAS mutated cells and colon cancers, whose activity was 200-450 fold higher than cisplatin, and with high selectivity towards cancer cell lines.[31] Owing

to these considerations, the synthesis of the compounds depicted in **Figure 7.7** was attempted in the Gibson group, although the purification of the final adducts proved challenging and is still in progress.

7.4 Encapsulation of gold(III)-dithiocarbamato complexes for drug delivery

These are joint projects commenced in 2017 in collaboration with Prof. Jessica Rouge (University of Connecticut, USA) and Dr. Fabio Cucinotta (Newcastle University, UK). I contributed by re-synthesizing the activated gold(III)-dithiocarbamato complexes to be encapsulated in the various carriers.

A major drawback of the well-established gold(III)- or, in general, the metal-dithiocarbamato complexes, is their relatively low selectivity towards tumour cells. Therefore, their targeted action still remains a challenge, resulting in poor pharmacokinetics and bioavailability.[32] Apart from covalent functionalization of the anticancer drug with biomolecules, one effective approach to tackle this issue is the exploitation of drug delivery systems that would "protect" the cargo along the administration route and direct it to its target site.[33] In the context of metal-dithiocarbamates, research efforts over the last years explored a variety of carriers, including incorporations into cyclodextrins,[34] metal organic frameworks (MOFs),[35] and micelles.[36,37]

This section briefly reports on the results obtained to date concerning the encapsulation of gold(III)-dithiocarbamato complexes into two different nanocarrier systems, namely nucleic acid nanoparticles (NANs) and mesoporous silica nanoparticles (MSNs). The former project has been mainly implemented by Dr. Jessica Rouge, while the latter has been being carried out by Dr. Fabio Cucinotta.

7.4.1 Nucleic acid nanoparticles

Nucleic acid-based therapeutics have increasingly become a hot-topic in recent years thanks to the development of nanoparticle drug carriers. Recent studies have shown that the tight packing of nucleic acids at the surface of nanoparticles can result in the generation of cell-delivery systems more efficient than the nucleic acids alone.[38,39] Such structures, usually referred to as spherical nucleic acids (SNAs), provide desirable delivery properties including increased cellular uptake through endocytosis, a prolonged half-life of nucleic acids, and a uniform size distribution.[40,41]

Recently, the Rouge group has reported on a straightforward assembly strategy of a monodisperse nanoparticle formulation that is suitable for both the attachment of a catalytic oligonucleotide at its surface and the encapsulation of a small molecule drug in the interior.[42–44] These structures, namely nucleic acid nanoparticles (NANs), are constructed with esterified diazido crosslinkers which make the particles fully degradable by endosomal esterase enzymes and, as such, biocompatible.[42]

Following an established procedure, nanocapsules have been obtained in the Rouge group *via* pre-generation of surface crosslinked micelles (SCMs) containing in the internal core two compounds synthesised in this PhD project, [$AuBr_2$(dtc-Inp-OEt)] (**Au1**) or [$AuBr_2$(dtc-Inp-GlcN1)] (**Au3**). The nanoparticles can then be attached with thiolated DNA filaments to form the NANs (**Scheme 7.5**).

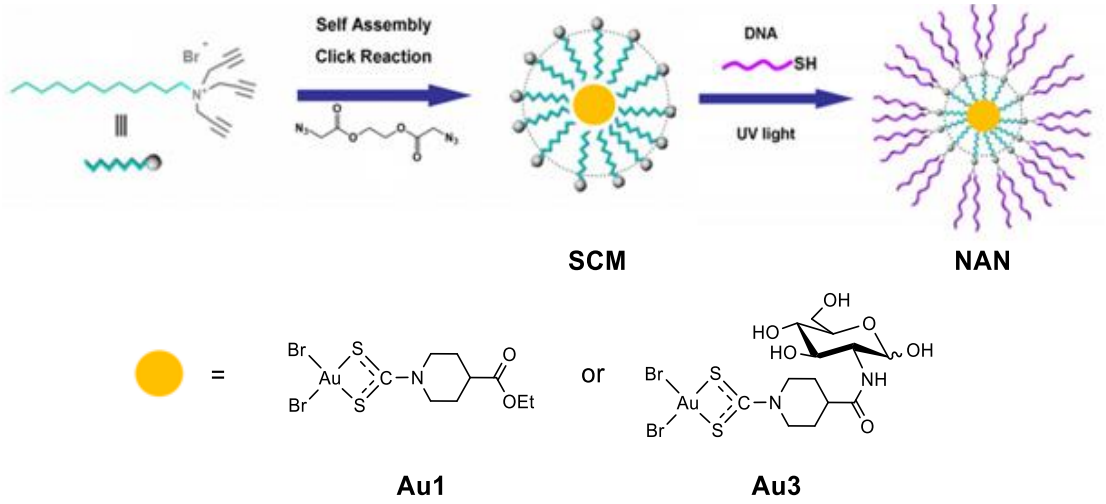

Scheme 7.5. Schematic synthetic approach to the generation and encapsulation of gold(III)-dithiocarbamato complexes into SMCs and NANs.

Dynamic light scattering (DLS) analysis of dry-loaded SCMs and NANs demonstrated that compound [$AuBr_2$(dtc-Inp-OEt)], once encapsulated, possesses a more uniform size distribution, with an average size of 16.5 nm for SCMs and 30.1 nm for NANs, whereas [$AuBr_2$(dtc-Inp-GlcN1)] possessed a less uniform distribution (**Figure 7.8**). These discrepancies between the two compounds may arise from differencies in hydrophobicity. In fact, [$AuBr_2$(dtc-Inp-GlcN1)], owing to the several hydroxyl group in the sugar ring, has a reduced hydrophobicity which may impede the aggregation of the hydrophobic interior and consequently the formation of nanoparticles with homogeneous size. Also tunnelling electron microscopy (TEM) analysis corroborates these observations (**Figure 7.9**).

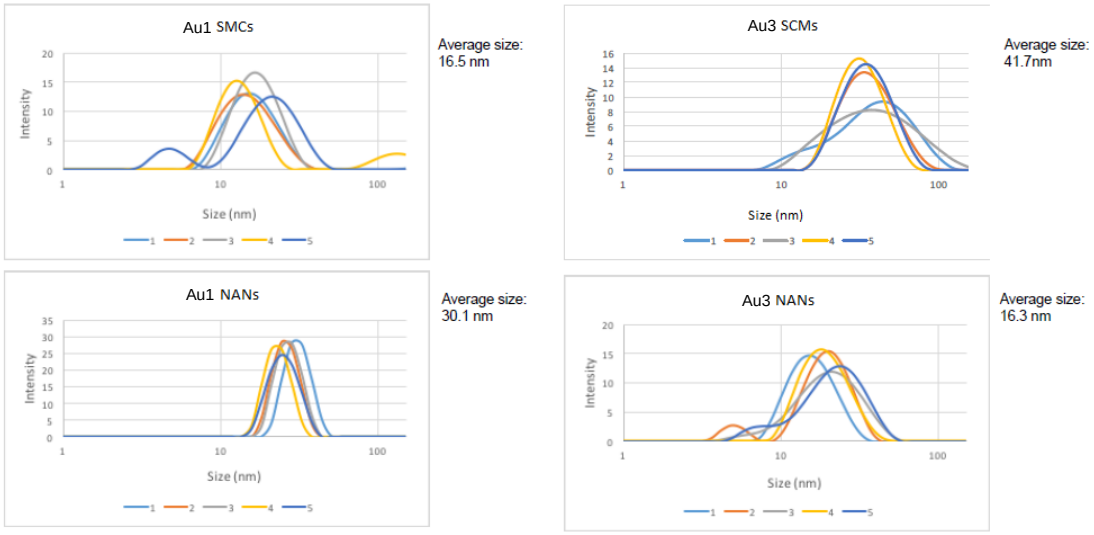

Figure 7.8. DLS analysis of **Au1**- and **Au3**-loaded SCMs and NANs.

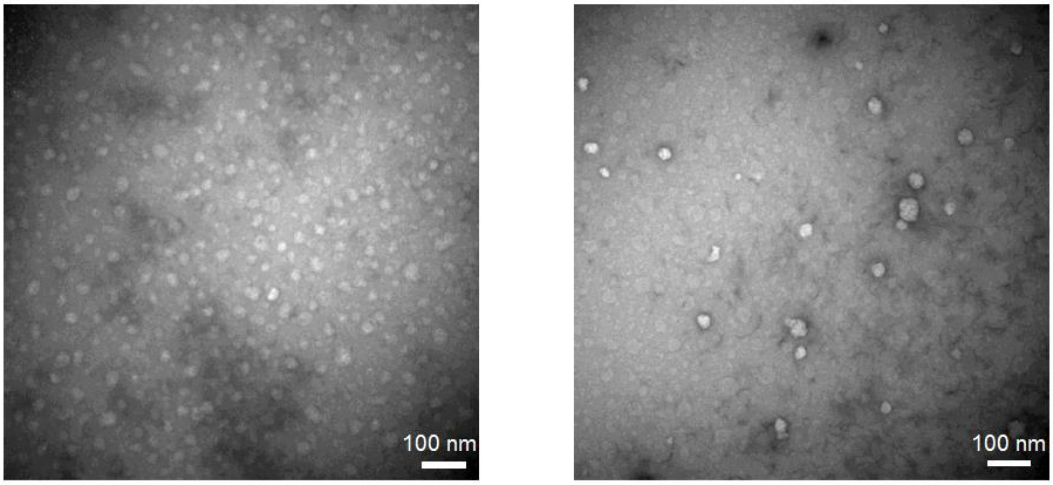

Figure 7.9. TEM analysis of **Au1**-loaded NANs (images obtained by Dr. Jessica Rouge).

Around 0.8 μM of [$AuBr_2$(dtc-Inp-OEt)] were loaded into 10 μM of NANs. ICP-MS studies investigated on the amount of gold taken up in the cells (**Figure 7.10**).

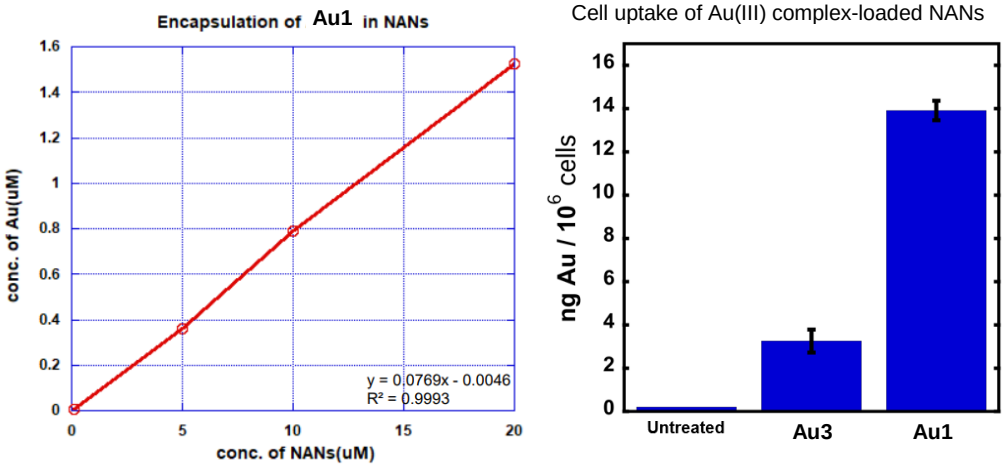

Figure 7.10. ICP-MS analysis of encapsulation of [$AuBr_2$(dtc-Inp-OEt)] (**Au1**) in NANs (left), and cell uptake studies of the gold(III) complexes-loaded NANs in HeLa cells (right).

Finally, the cell viability on the gold complexes functionalized with NANs was evaluated. Although the cytotoxicity of both native complexes is remarkably high on HeLa cells (60% and 80% viability at 1 μM for **Au1** and **Au3**, respectively), the NANs incorporated-gold complexes showed cytotoxicity with an IC_{50} of approximately 10 μM (in terms of NAN concentration). By taking into account the gold/NAN loading *ratio* (0.8 μM Au/10 μM NAN), the cytotoxicity of the complexes incorporated by the NANs is comparable to the free ones (0.8 μM), proving that, once internalized, the degradation of nanoparticles can be enzyme-triggered with subsequent release of the cytotoxic gold-based derivatives.

7.4.2 Mesoporous silica nanoparticles

Recently, mesoporous silica nanoparticles (MSNs) have become an attractive platform for biomedical applications as drug delivery systems of therapeutics and diagnostics.[45] MSNs are solid inorganic porous materials with empty channels arranged in a 2D honeycomb-like structure. These frameworks possess unique features, including high surface area, large pore volume that can host a high amount of drug without destabilization of the silica framework, a uniform pore size, easy-to-tune particle size and morphology.[46,47] In addition, in contrast with the low biocompatibility of other amorphous silica materials, MSNs have shown superior biocompatibility.[48]

On account of these considerations, Cucinotta and coworkers prepared some MSNs functionalized with gold(III)-complexes, either through covalent and non-covalent binding. Covalently functionalized mesoporous silica can be obtained by reaction of silica bearing amino groups, such as the MCM-41 mesoporous silica, with a substrate containing a carboxylic acid (or an active ester derivative), with formation of an amide linkage.[49]

MCM-41 nanoparticles functionalized with amino groups can be synthesized by condensation of tetraethoxysilane (TEOS), an organosilane precursor, and 3-aminopropyltriethoxy silane (APTES), an organosilane source of amino functionalities, with cetyltrimethylammoniumbromide (CTAB), a surfactant that acts as a structure-directing agent (**Figure 7.11**).[50] After removal of the surfactant from the mesopores, the silica nanoparticles can be obtained. Then, covalent functionalization of the amino groups with the gold(III)-dithiocarbamato derivative bearing an active ester moiety generated the desired MSNs by forming an amide linkage (**Scheme 7.6**).

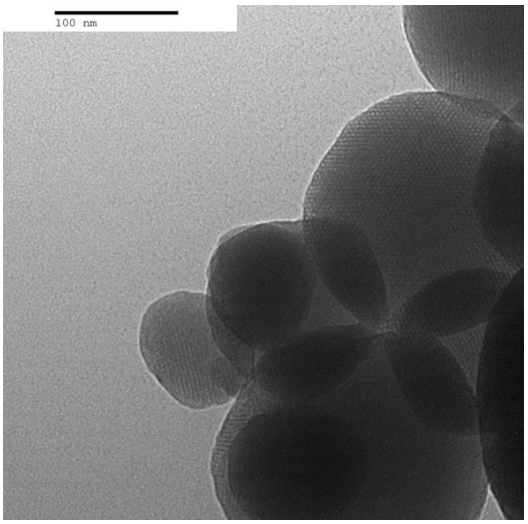

Figure 7.11. TEM image of a mesoporous silica nanoparticle MCM-41 (image obtained by Dr. Fabio Cucinotta).

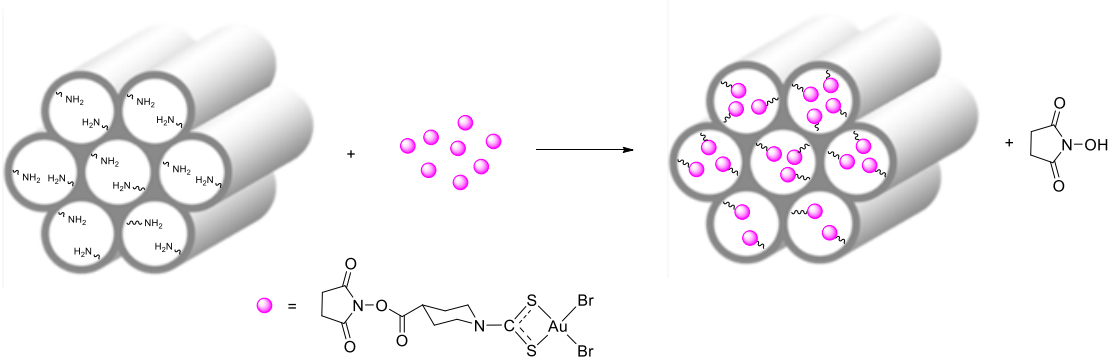

Scheme 7.6. General synthetic route for the obtainment of Au(III)-functionalized MSNs via post-grafting.

These constructs can be achieved either through a sequential grafting of the reagents to the nanoparticles, or through a one-pot co-condensation. By measuring the absorbance of the mother solution, no starting complex was detected, meaning that the loading in the silica was achieved quantitatively. SEM images showed that particles possessed a uniform size distribution and morphology, with diameter around 200-250 nm, while TEM images showed the typical honeycomb-like structure (**Figures 7.12,13**).

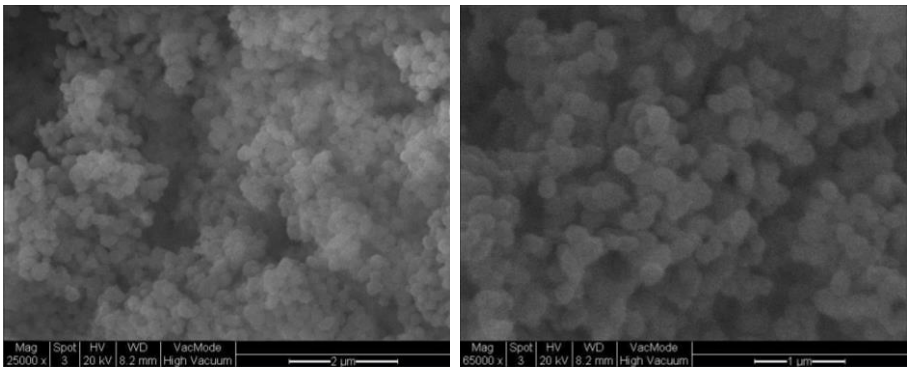

Figure 7.12. SEM images of silica nanoparticles covalently functionalized with gold(III)-dithiocarbamato complexes obtained by post-synthetic grafting (left), and by co-condensation (right) (images obtained by Dr. Fabio Cucinotta).

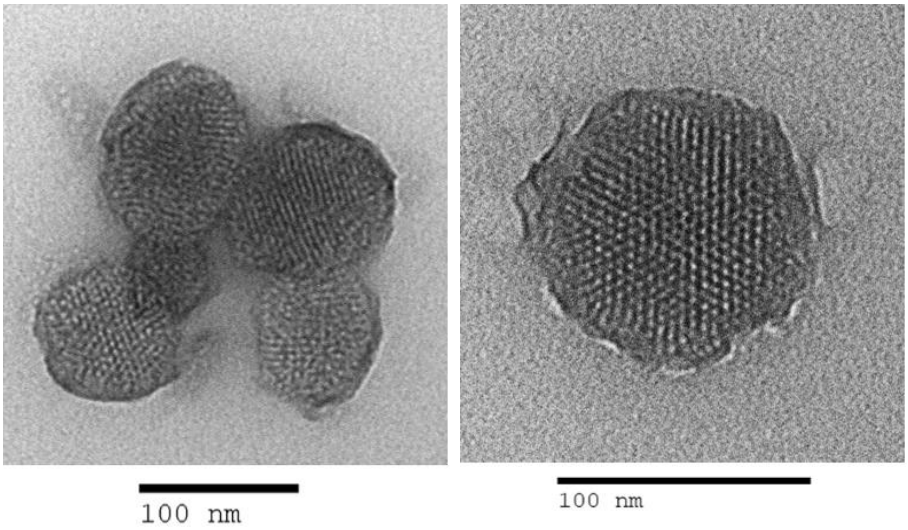

Figure 7.13. TEM images of silica nanoparticles covalently functionalized with Au(III)-dithiocarbamato complexes obtained by post-synthetic grafting (a), and by co-condensation (b) (images obtained by Dr. Fabio Cucinotta).

The release of the drug was studied by measuring the absorbance at different pH. Unfortunately, the release was very low (<1%), suggesting that cleavage of the amide bond takes place at a very low extent. Anyway, the antiproliferative activity on a panel of human tumour cell lines will be still evaluated in order to assess any biological activity of such nanocarriers.

Owing to the lack of released drug in covalently-functionalized MSNs, non-covalent incorporation of the gold(III) complex into the silica nanocarriers was also accomplished. The compound [$AuBr_2$(dtc-Inp-OSu)] (**Au6**) was encapsulated via two different approaches, either through chemical adsorption or co-encapsulation into the pores (>8 nm) of ordered mesoporous silica COK-12. The use of a surfactant like the micellar swelling agent pluronic® F127, a polyethylene glycol polymer commonly used as a templating agent, allows to form micelles with desired size for the subsequent grafting of sodium silicate to obtain the silica. In this case, the percentage of loading was around 6-8% in weight. Studies of release in aqueous buffer at pH 7 by UV-Vis showed that the release was nearly quantitative.

The next studies will involve the generation of silica carriers non-covalently functionalized with the gold(III)-dithiocarbamato complex [$AuBr_2$(dtc-Inp-OEt)] (**Au1**), whose cytotoxicity in the submicromolar range (see section 7.2) makes it an attractive substrate for further studies of drug delivery. As done with the complex [$AuBr_2$(dtc-Inp-OSu)] (**Au6**), the release will be then studied in order to assess the amount of drug released. On a later stage, cytotoxicity studies will be carried out on a panel of human

tumour cell lines in order to assess any advantage on the functionalization of these type of compounds with the silica carrier.

7.5 Concluding remarks and future work

The research work here reported and discussed focused on the design of metal-dithiocarbamato glycoconjugates which can combine the antitumor properties and the favourable toxicological profile of the metal-dithiocarbamato scaffold, along with an improved selectivity and cellular uptake provided by the glucose-containing ligands coordinated to the metal center, through the exploitation of the glucose-mediated cellular internalization facilitated by glucose transporters (GLUTs).

Novel gold(I/III)-, manganese(I)-, platinum(II)-, ruthenium(II)- and osmium(II)-dithiocarbamato glycoconjugates were generated *via* an innovative synthetic approach in good yields, and were fully characterized by NMR, IR, UV-Vis spectroscopy and elemental analysis. This method exploits a ligand exchange reaction between preformed zinc(II)-dithiocarbamato glycoconjugates (described in Chapter 2) and the corresponding metal precursors, referred to as transmetallation.

Amongst the various gold(III) complexes generated, the organometallic derivatives bearing a C^N tethered benzylpyridine ligand (Chapter 4) displayed remarkably higher *in vitro* cytotoxic activity and increased stability in physiological-like medium compared to the inactive dihalogenido derivatives (Chapter 3). In addition, it seems that the organometallic glycoconjugates do not show GLUT-mediated cell internalization in U2OS cells. The future work on these series of compounds will be aimed at assessing the *in vitro* cytotoxic activity against further tumour and non-tumour cell lines and the intracellular content of gold.

The gold(I)-carbene derivatives (Chapter 5) showed *in vitro* cytotoxic activity in the micromolar range, although no intracellular gold was detected *via* cell uptake studies, thus suggesting an extracellular mode of action. The future work will focus on live-cell imaging studies, and on the evaluation of the anticancer activity of the gold(I)-phosphino series, in order to highlight any possible comparison with the carbene derivatives.

As concerns to the carbonyl manganese(I) derivatives (Chapter 6), they showed CO-releasing properties with the myoglobin assay. The rate of CO release was fast, although the number of molecules of CO was lower compared to the reference complex CORM-401. The future work will be aimed at evaluating the *in vitro* anticancer activity, or other pharmacological properties such as anti-inflammatory properties.

Finally, other platinum(II)-, ruthenium(II)-, and osmium(II)-glycoconjugates were obtained (Chapter 7), but their anticancer activity is yet to be evaluated. Additional side-projects, not strictly related to the synthesis of metal-glycoconjugates, returned some interesting preliminary results (Chapter 7), namely on platinum(IV)-gold(III) heterobimetallic derivatives, and the incorporation of gold(III)-dithiocarbamato complexes in nucleic acid nanocapsules or in mesoporous silica nanoparticle carriers.

7.6 References

[1] G. Faraglia, D. Fregona, S. Sitran, L. Giovagnini, C. Marzano, F. Baccichetti, U. Casellato, R. Graziani, *J. Inorg. Biochem.* **2001**, *83*, 31–40.

[2] C. Marzano, D. Fregona, F. Baccichetti, A. Trevisan, L. Giovagnini, F. Bordin, *Chem. Biol. Interact.* **2002**, *140*, 215–229.

[3] C. Marzano, F. Bettìo, F. Baccichetti, A. Trevisan, L. Giovagnini, D. Fregona, *Chem. Biol. Interact.* **2004**, *148*, 37–48.

[4] C. Marzano, A. Trevisan, L. Giovagnini, D. Fregona, *Toxicol. In Vitro* **2002**, *16*, 413–419.

[5] P. Cristofori, E. Zanetti, D. Fregona, A. Piaia, A. Trevisan, *Toxicol. Pathol.* **2007**, *35*, 270–275.

[6] A. Pettenuzzo, D. Montagner, P. McArdle, L. Ronconi, *Dalton Trans.* **2018**, *47*, 10721-10736.

[7] D. C. Onwudiwe, J. N. Mugo, M. Hrubaru, E. Hosten, *J. Sulfur Chem.* **2015**, *36*, 36–47.

[8] G. A. Heath, D. C. R. Hockless, P. D. Prenzler, *Acta Cryst. C* **1996**, *52*, 537–539.

[9] M. J. Abrams, C. M. Giandomenico, J. F. Vollano, D. A. Schwartz, *Inorg. Chim. Acta* **1987**, *131*, 3–4.

[10] L. Zhang, H. Wei, Y. Zhang, Z. Guo, L. Zhu, *Spectrochim. Acta. A. Mol. Biomol. Spectrosc.* **2002**, *58*, 217–223.

[11] G. Raudaschl, B. Lippert, J. D. Hoeschele, H. E. Howard-Lock, C. J. L. Lock, P. Pilon, *Inorg. Chim. Acta* **1985**, *106*, 141–149.

[12] M. K. Amir, Z-. Rehman, F. Hayat, S. Z. Khan, G. Hogarth, T. Kondratyuk, J. M. Pezzuto, M. N. Tahir, *RSC Adv.* **2016**, *6*, 110517–110524.

[13] G. Süss-Fink, *Dalton Trans.* **2010**, *39*, 1673–1688.

[14] G. Lümmen, H. Sperling, H. Luboldt, T. Otto, H. Rübben, *Cancer Chemother. Pharmacol.* **1998**, *42*, 415–417.

[15] N. Kröger, U. R. Kleeberg, K. Mross, L. Edler, D. K. Hossfeld, *Onkologie* **2000**, *23*, 60–62.

[16] P. Köpf-Maier, *Anticancer Res.* **1999**, *19*, 493–504.

[17] G. Jaouen, A. Vessières, S. Top, *Chem. Soc. Rev.* **2015**, *44*, 8802–8817.

[18] P. J. Dyson, *Chimia* **2007**, 61, 698–703.

[19] S. J. Dougan, P. J. Sadler, *Chimia* **2007**, 61, 704–715.

[20] S. Chatterjee, S. Kundu, A. Bhattacharyya, C. G. Hartinger, P. J. Dyson, *J. Biol. Inorg. Chem.* **2008**, *13*, 1149–1155.

[21] C. Scolaro, A. Bergamo, L. Brescacin, R. Delfino, M. Cocchietto, G. Laurenczy, T. J. Geldbach, G. Sava, P. J. Dyson, *J. Med. Chem.* **2005**, *48*, 4161–4171.

[22] Y. K. Yan, M. Melchart, A. Habtemariam, P. J. Sadler, *Chem. Commun.* **2005**, *0*, 4764–4776.

[23] Y.-H. Dou, S.-D. Xu, Y. Chen, X.-H. Wu, *Phosphorus Sulfur Silicon Relat. Elem.* **2017**, *192*, 1219–1223.

[24] N. J. Wheate, S. Walker, G. E. Craig, R. Oun, *Dalton Trans.* **2010**, *39*, 8113–8127.

[25] A. Bhargava, U. N. Vaishampayan, *Expert Opin. Investig. Drugs* **2009**, *18*, 1787–1797.

[26] D. Gibson, *Dalton Trans.* **2016**, *45*, 12983–12991.

[27] S. Dhar, S. J. Lippard, *Proc. Natl. Acad. Sci.* **2009**, *106*, 22199–22204.

[28] X. Xue, S. You, Q. Zhang, Y. Wu, G. Zou, P. C. Wang, Y. Zhao, Y. Xu, L. Jia, X. Zhang, X.-J. Liang, *Mol. Pharm.* **2012**, *9*, 634–644.

[29] E. Petruzzella, R. Sirota, I. Solazzo, V. Gandin, D. Gibson, *Chem. Sci.* **2018**, *9*, 4299–4307.

[30] V. Novohradsky, I. Zanellato, C. Marzano, J. Pracharova, J. Kasparkova, D. Gibson, V. Gandin, D. Osella, V. Brabec, *Sci. Rep.* **2017**, *7*, 3751.

[31] E. Petruzzella, J. P. Braude, J. R. Aldrich-Wright, V. Gandin, D. Gibson, *Angew. Chem. Int. Ed Engl.* **2017**, *56*, 11539–11544.

[32] D. S. Pal, D. K. Mondal, R. Datta, *Antimicrob. Agents Chemother.* **2015**, *59*, 2144–2152.

[33] D. Peer, J. M. Karp, S. Hong, O. C. Farokhzad, R. Margalit, R. Langer, *Nat. Nanotechnol.* **2007**, *2*, 751–760.
[34] M. F. Tomasello, C. Nardon, V. Lanza, G. Di Natale, N. Pettenuzzo, S. Salmaso, D. Milardi, P. Caliceti, G. Pappalardo, D. Fregona, *Eur. J. Med. Chem.* **2017**, *138*, 115–127.
[35] R. W.-Y. Sun, M. Zhang, D. Li, Z.-F. Zhang, H. Cai, M. Li, Y.-J. Xian, S. W. Ng, A. S.-T. Wong, *Chem. Eur. J.* **2015**, *21*, 18534–18538.
[36] P. Ringhieri, R. Iannitti, C. Nardon, R. Palumbo, D. Fregona, G. Morelli, A. Accardo, *Int. J. Pharm.* **2014**, *473*, 194–202.
[37] C. Nardon, G. Boscutti, L. Dalla Via, P. Ringhieri, V. Di Noto, G. Morelli, A. Accardo, D. Fregona, *MedChemComm* **2015**, *6*, 155–163.
[38] J. I. Cutler, E. Auyeung, C. A. Mirkin, *J. Am. Chem. Soc.* **2012**, *134*, 1376–1391.
[39] D. A. Giljohann, D. S. Seferos, A. E. Prigodich, P. C. Patel, C. A. Mirkin, *J. Am. Chem. Soc.* **2009**, *131*, 2072–2073.
[40] C. A. Mirkin, R. L. Letsinger, R. C. Mucic, J. J. Storhoff, *Nature* **1996**, *382*, 607–609.
[41] D. Bousmail, L. Amrein, J. J. Fakhoury, H. H. Fakih, J. C. C. Hsu, L. Panasci, H. F. Sleiman, *Chem. Sci.* **2017**, *8*, 6218–6229.
[42] J. K. Awino, S. Gudipati, A. K. Hartmann, J. J. Santiana, D. F. Cairns-Gibson, N. Gomez, J. L. Rouge, *J. Am. Chem. Soc.* **2017**, *139*, 6278–6281.
[43] J. J. Santiana, B. Sui, N. Gomez, J. L. Rouge, *Bioconjug. Chem.* **2017**, *28*, 2910–2914.
[44] A. K. Hartmann, D. F. Cairns-Gibson, J. J. Santiana, M. Q. Tolentino, H. M. Barber, J. L. Rouge, *ChemBioChem* **2018**, *19*, 1734–1739.
[45] Z. Li, J. C. Barnes, A. Bosoy, J. F. Stoddart, J. I. Zink, *Chem. Soc. Rev.* **2012**, *41*, 2590–2605.
[46] I. I. Slowing, J. L. Vivero-Escoto, C.-W. Wu, V. S.-Y. Lin, *Adv. Drug Deliv. Rev.* **2008**, *60*, 1278–1288.
[47] C. Bharti, U. Nagaich, A. K. Pal, N. Gulati, *Int. J. Pharm. Investig.* **2015**, *5*, 124–133.
[48] J. L. Vivero-Escoto, I. I. Slowing, B. G. Trewyn, V. S.-Y. Lin, *Small* **2010**, *6*, 1952–1967.
[49] E. Gianotti, B. Martins Estevão, F. Cucinotta, N. Hioka, M. Rizzi, F. Renò, L. Marchese, *Chem. Eur. J.* **2014**, *20*, 10921–10925.
[50] M. Manzano, V. Aina, C. O. Areán, F. Balas, V. Cauda, M. Colilla, M. R. Delgado, M. Vallet-Regí, *Chem. Eng. J.* **2008**, *137*, 30–37.

Chapter 8

Experimental

Chapter 8. Experimental

8.1 General experimental conditions

Materials

2-benzylpyridine, α-D-glucose, BaO, D-cellobiose, CS_2, $(Et_4N)Cl{\cdot}xH_2O$, ethanolamine, KI, KPF_6, $[MnBr(CO)_5]$, NaCl, NaN_3, *N*,*N*-diisoproprylethylamine, *N*,*N*-dimethylformamide, PBS (pH 7.4), Pd/C 10%$_w$, $(Ph_4P)Cl$, triethylamine, $[Zn(OAc)_2]{\cdot}2H_2O$, $ZnCl_2$ (Sigma Aldrich), (α,β)-D-glucosamine hydrochloride, β-glucosidase from sweet almond, boron trifluoride diethyletherate, ethyl 4-piperidinecarboxylate, isonipecotamide, isonipecotic acid, methyl α-D-glucopyranoside, *N*-bromosuccinimide, PPh_3 (TCI), $K_2[PtCl_4]$, *n*-octanol, NH_4Cl, (ACROS), *N*-acetyl-(α,β)-D-glucosamine, *N,N,N',N'*-tetramethyl-*O*-(*N*-succinimidyl)uronium tetrafluoroborate (Carbosynth), CD_3OD, $CDCl_3$, D_2O, DMSO-d_6, *N*,*N*-dimethylformamide-d_7 (Deutero), $AgNO_3$, amberlite IR120 (H^+ form) resin (Merck), $K[AuBr_4]{\cdot}2H_2O$, $K[AuCl_4]{\cdot}2H_2O$ (Alfa Aesar), $[AuCl(PPh_3)]$ (STREM) were of reagent grade or comparable purity and were used as supplied. Chlorido-(1,3-diethylbenzimidazol-2-ylidene)gold(I) ([Au(BImEt$_2$)Cl]), was synthesized in Ingo Ott's lab following a reported procedure.[1,2] Dry dichloromethane was prepared by distilling over CaH_2 and storing over 4 Å activated molecular sieves. Dry methanol and dry DMF were prepared by passing the solvent through a column of alumina and storing over, respectively, 3 Å and 4 Å activated molecular sieves. All other reagents and solvents were used as purchased without any further purification.

Instrumentation

Melting points. Melting points were recorded on a Stuart SMP10 digital melting point apparatus and are uncorrected.

Chromatography. Thin layer chromatography (TLC) was performed on silica gel Merck $60F_{254}$ precoated aluminum sheets. Spots were visualized by direct UV irradiation at 254 nm or developed by exposure to either *p*-anisaldehyde or potassium permanganate staining solutions as appropriate. Flash column chromatography was performed on Sigma Aldrich 60 Å silica gel (40-63 μm, 230-400 mesh) as stationary phase using the appropriate eluent.

Elemental analyses. Elemental analyses (carbon, hydrogen and nitrogen) were performed with a Perkin Elmer 2400 CHNS/O Series II analyzer.

IR Spectroscopy. FT-IR spectra of the carbohydrate precursors were recorded from thin films at room temperature on a Perkin Elmer Spectrum 100 FT-IR spectrophotometer equipped with a UATR accessory in the range 4000-650 cm^{-1} (32 scans, resolution 4 cm^{-1}). FT-IR spectra of the metal complexes were recorded from CsI disks at room temperature on a Perkin Elmer Frontier FT-IR/FIR spectrophotometer in the range 4000-600 cm^{-1} (32 scans, resolution 4 cm^{-1}) and in the range 600-200 cm^{-1} (32 scans, resolution 2 cm^{-1}). Data processing was carried out using OMNIC version 5.1 (Nicolet Instrument Corporation).

UV-Vis Spectroscopy. UV-Vis spectra were recorded in the appropriate solvent at room temperature or 37°C (when specified) in the range 190-840 nm using a Thermo Scientific NanoDrop 2000c UV-Vis spectrophotometer. Data processing was carried out with the software OriginPro 8.

NMR Spectroscopy. All NMR spectra were acquired in the appropriate deuterated solvent at room temperature on a JEOL 400 MHz NMR ECX-400 spectrometer equipped with *z*-field gradients. ^{1}H and ^{13}C chemical shifts were referenced to TMS at 0.00 ppm *via* internal referencing to the residual peak of the deuterated solvent employed. ^{31}P chemical shifts were referenced to an external standard of 85% H_3PO_4 at 0 ppm. ^{1}H and $^{13}C\{^{1}H\}$ signals were assigned with the aid of [^{1}H,^{1}H] COSY, ^{13}C DEPT, [^{1}H,^{13}C] HSQC and [^{1}H,^{13}C] HMBC experiments. Typical acquisition parameters for 1D ^{1}H NMR spectra (^{1}H: 399.78 MHz): 16 transients, spectral width 6.0 kHz, 16k data points, relaxation delay 1.0 s. Spectra were processed using exponential weighting with a resolution of 0.5 Hz and a line-broadening threshold of 0.1 Hz. Typical acquisition parameters for 2D [^{1}H,^{1}H] COSY NMR spectra (^{1}H: 399.78 MHz): 512 transients of 2 scans per block, spectral width 3.8/3.8 kHz, 640/256 data points, relaxation delay 1.0 s. Spectra were processed using sine weighting with a resolution of 4.8/9.8 Hz and a line-broadening threshold of 0.8/1.5 Hz. Typical acquisition parameters for 1D $^{13}C\{^{1}H\}$ NMR spectra (^{13}C: 100.53 MHz): 512 transients, spectral width 25.1 kHz, 32k data points, relaxation delay 2.0 s. The pulse sequence was optimized for proton-decoupling at $^{1}J(^{13}C,^{1}H)$ = 145 Hz. Spectra were processed using exponential weighting with a resolution of 2.0 Hz and a line-broadening threshold of 2.5 Hz. Typical acquisition parameters for 2D [^{1}H,^{13}C] HMQC NMR spectra (^{1}H: 399.78/^{13}C: 100.53 MHz): 1k transients of 4 scans per block, spectral width 4.8/7.7 kHz, 1k/1k data points, relaxation delay 1.0 s. The pulse sequence was optimized for proton-decoupling at $^{1}J(^{13}C,^{1}H)$ = 145 Hz. Spectra were processed using cosine-square weighting with a resolution of 1.0/3.0 Hz and a line-broadening threshold of 0.3/1.0 Hz.

Typical acquisition parameters for 2D [^{1}H,^{13}C] HMBC NMR spectra (^{1}H: 399.78/^{13}C: 100.53 MHz): 1.2k transients of 4 scans per block, spectral width 8.0/25.1 kHz, 2k/2k data points, relaxation delay 1.0 s. The pulse sequences was optimized for proton-decoupling at $^{1}J(^{13}C,^{1}H)$ = 145 Hz and for long-range coupling at $^{n}J(^{13}C,^{1}H)$ = 5 Hz. Spectra were processed using sine-square weighting with a resolution of 0.3/1.0 Hz and a line-broadening threshold of 0.3/1.0 Hz. Whenever specified, NMR spectra were acquired in the appropriate deuterated solvent at room temperature on a Varian VNMRS 500 MHz AR spectrometer or on a Agilent DD2 NMR 600 MHz ASC spectrometer (equipped with cold probe), equipped with *z*-field gradients. ^{1}H and ^{13}C chemical shifts were referenced to TMS at 0.00 ppm *via* internal referencing to the residual peak of the deuterated solvent employed. Data processing was carried out using MestReNova version 12.0 (Mestrelab Research S.L.).

MS analysis. Electrospray ionization mass spectrometry (ESI-MS) analysis was carried out on solutions of the samples in acetonitrile/water (1:1) by means of an Agilent G6540B MS Q-TOF mass spectrometer coupled with a Dual AJS ESI ion source interface.

Single crystal X-ray diffraction analyses. Single crystal X-ray diffraction data of Na(dtc-Inp-OEt)·CH_3OH, (PPh_4)(dtc-Sar-OEt), **Zn1** and **Au1** were collected using an Oxford Diffraction Xcalibur system at room temperature. The crystal structures were solved using ShelxT[3] and refined by least-square minimization using ShelxL,[4] both of which were driven by the Oscail package.[5] Single crystal X-ray diffraction data of **Au10**, **Au11**, [Au(BimEt2)(dtc-Inp-NH2)], [Au(BimEt2)(dtc-Sar-OEt)] were collected using a Bruker D8 Venture PhotonII diffractometer at 200 K. The crystal structures were solved by Intrinsic Phasing using ShelxT[3] and refined by least-square minimization using ShelxL,[4] both of which were driven by the Olex2 package.[6]

List of compounds synthesized in this research work

Carbohydrates

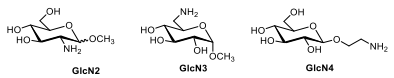

GlcN2 **GlcN3** **GlcN4**

Free dithiocarbamato ligands

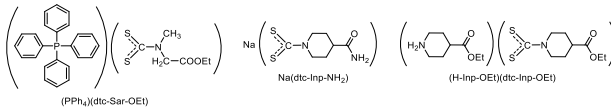

(PPh$_4$)(dtc-Sar-OEt) Na(dtc-Inp-NH$_2$) (H-Inp-OEt)(dtc-Inp-OEt)

Metal-dithiocarbamato complexes

Zinc(II)

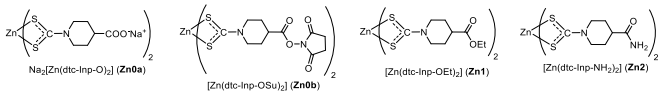

Na$_2$[Zn(dtc-Inp-O)$_2$] (**Zn0a**) [Zn(dtc-Inp-OSu)$_2$] (**Zn0b**) [Zn(dtc-Inp-OEt)$_2$] (**Zn1**) [Zn(dtc-Inp-NH$_2$)$_2$] (**Zn2**)

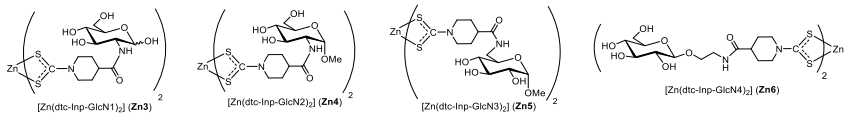

[Zn(dtc-Inp-GlcN1)$_2$] (**Zn3**) [Zn(dtc-Inp-GlcN2)$_2$] (**Zn4**) [Zn(dtc-Inp-GlcN3)$_2$] (**Zn5**) [Zn(dtc-Inp-GlcN4)$_2$] (**Zn6**)

Gold(III)

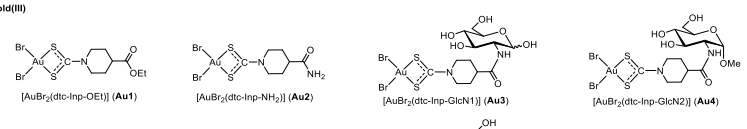

[AuBr$_2$(dtc-Inp-OEt)] (**Au1**) [AuBr$_2$(dtc-Inp-NH$_2$)] (**Au2**) [AuBr$_2$(dtc-Inp-GlcN1)] (**Au3**) [AuBr$_2$(dtc-Inp-GlcN2)] (**Au4**)

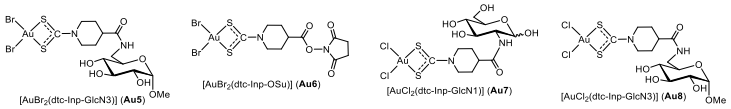

[AuBr$_2$(dtc-Inp-GlcN3)] (**Au5**) [AuBr$_2$(dtc-Inp-OSu)] (**Au6**) [AuCl$_2$(dtc-Inp-GlcN1)] (**Au7**) [AuCl$_2$(dtc-Inp-GlcN3)] (**Au8**)

Organometallic gold(III)

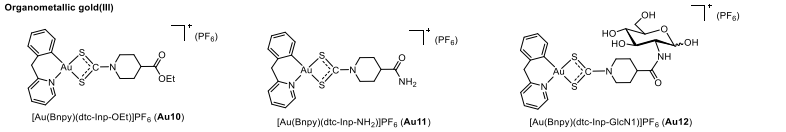

[Au(Bnpy)(dtc-Inp-OEt)]PF$_6$ (**Au10**) [Au(Bnpy)(dtc-Inp-NH$_2$)]PF$_6$ (**Au11**) [Au(Bnpy)(dtc-Inp-GlcN1)]PF$_6$ (**Au12**)

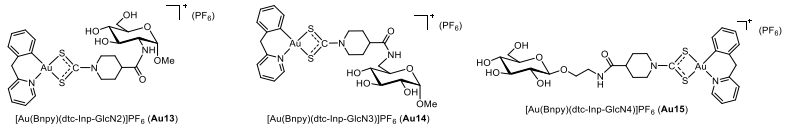

[Au(Bnpy)(dtc-Inp-GlcN2)]PF$_6$ (**Au13**) [Au(Bnpy)(dtc-Inp-GlcN3)]PF$_6$ (**Au14**) [Au(Bnpy)(dtc-Inp-GlcN4)]PF$_6$ (**Au15**)

Gold(I)-carbene

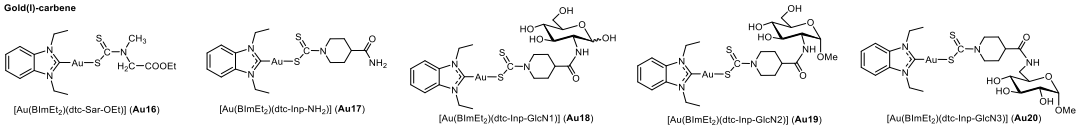

[Au(BImEt$_2$)(dtc-Sar-OEt)] (**Au16**) [Au(BImEt$_2$)(dtc-Inp-NH$_2$)] (**Au17**) [Au(BImEt$_2$)(dtc-Inp-GlcN1)] (**Au18**) [Au(BImEt$_2$)(dtc-Inp-GlcN2)] (**Au19**) [Au(BImEt$_2$)(dtc-Inp-GlcN3)] (**Au20**)

Gold(I)-phosphine

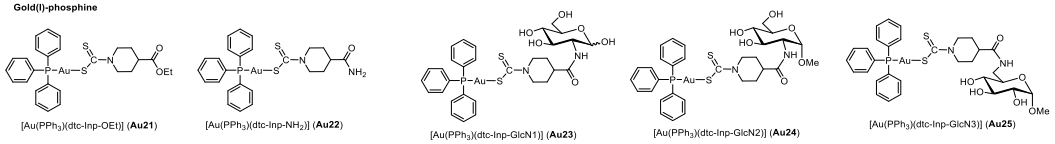

[Au(PPh$_3$)(dtc-Inp-OEt)] (**Au21**) [Au(PPh$_3$)(dtc-Inp-NH$_2$)] (**Au22**) [Au(PPh$_3$)(dtc-Inp-GlcN1)] (**Au23**) [Au(PPh$_3$)(dtc-Inp-GlcN2)] (**Au24**) [Au(PPh$_3$)(dtc-Inp-GlcN3)] (**Au25**)

Manganese(I)-tetracarbonyl

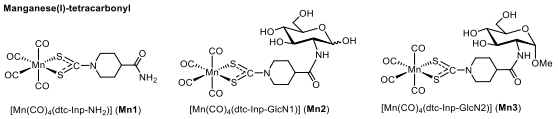

[Mn(CO)$_4$(dtc-Inp-NH$_2$)] (**Mn1**) [Mn(CO)$_4$(dtc-Inp-GlcN1)] (**Mn2**) [Mn(CO)$_4$(dtc-Inp-GlcN2)] (**Mn3**)

Platinum(II)

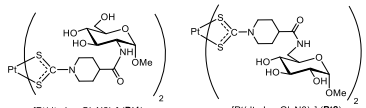

[Pt(dtc-Inp-GlcN2)$_2$] (**Pt1**) [Pt(dtc-Inp-GlcN3)$_2$] (**Pt2**)

8.2 Chapter 2 – Experimental

1-*O*-methyl-2-acetamido-2-deoxy-(α,β)-D-glucopyranoside

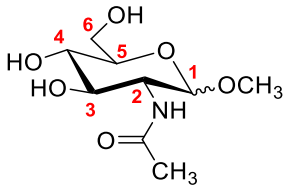

Amberlite IR120 (H^+ form) resin (5.2 g) was added to a methanol suspension (70 mL) of *N*-acetyl-(α,β)-D-glucosamine (3.15 g, 14.24 mmol). The mixture was stirred under reflux for 18 h. The mixture was then allowed to cool down to room temperature and the resin was filtered off. The resulting clear solution was evaporated to dryness to give an off-white residue which was washed with diethyl ether and dried under vacuum over P_2O_5, yielding the title compound as a white solid (2.39 g, 72% yield). FT-IR (ATR, $\tilde{\nu}_{max}$, cm^{-1}): 3350/3293 (br, ν, OH + NH overlapped), 1646 (s, ν, C=O (amide I)), 1548 (s, δ_{ip}, CNH (amide II)), 1021 (vs, ν, C–OH + C^1–O–CH_3 overlapped). ^{1}H NMR (400 MHz, DMSO-d_6, 298 K, *δ*, ppm): *δ* 7.76 (d, J_{HH} = 8.3 Hz, 1H, N*H* $_\alpha$), 7.68 (d, J_{HH} = 8.9 Hz, 0.3H, N*H* $_\beta$), 4.67 (br, 4H, O*H*), 4.51 (d, J_{HH} = 3.4 Hz, 1H, C^1H $_\alpha$), 4.16 (d, J_{HH} = 8.4 Hz, 0.3H, C^1H $_\beta$), 3.69-3.40 (m, ~5.2H, C^3H $_{\alpha+\beta}$ + C^5H $_{\alpha+\beta}$ + C^6H $_{\alpha+\beta}$ + C^6H' $_{\alpha+\beta}$), 3.31 (s, 0.9H, OCH_3 $_\beta$), 3.23 (s, 3H, OCH_3 $_\alpha$), 3.11 (dd, J_{HH} = 9.7, 8.7 Hz, 1.3H, C^4H $_{\alpha+\beta}$), 3.07-3.05 (m, 1.2H, C^2H $_{\alpha+\beta}$), 1.82 (s, 3H, C(O)CH_3 $_\alpha$), 1.79 (s, 1H, C(O)CH_3 $_\beta$). $^{13}C\{^1H\}$ NMR (100 MHz, DMSO-d_6, 298 K, *δ*, ppm): *δ* 169.48 (*C*=O $_\alpha$), 169.12 (*C*=O $_\beta$), 101.88 (C^1 $_\beta$), 97.96 (C^1 $_\alpha$), 77.03 (C^3 $_\beta$), 74.46 (C^5 $_\beta$), 72.74 (C^3 $_\alpha$), 70.88 (C^5 $_\alpha$), 70.79 (C^4 $_\alpha$), 70.64 (C^4 $_\beta$), 61.09 (C^6 $_\beta$), 60.96 (C^6 $_\alpha$), 55.66 (O*C*H$_3$ $_\beta$), 55.19 (C^2 $_\beta$), 54.28 (O*C*H$_3$ $_\alpha$), 53.76 (C^2 $_\alpha$), 23.18 (C(O)*C*H$_3$ $_\beta$), 22.68 (C(O)*C*H$_3$ $_\alpha$). Experimental data are consistent with those reported in the literature.[7,8] Solution α:β anomers ratio ≈ 3:1 (based on the ^{1}H NMR spectrum).

1-*O*-methyl-2-amino-2-deoxy-(α,β)-D-glucopyranoside (GlcN2) acetic acid

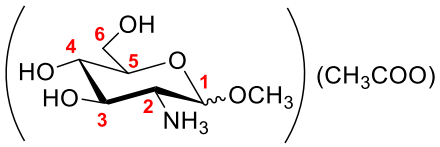

GlcN2

1-*O*-methyl-2-acetamido-2-deoxy-(α,β)-D-glucopyranoside (1.00 g, 4.25 mmol) was dissolved in water (70 mL), and BaO was added batchwise under stirring to give pH 13-14. The mixture was stirred under reflux for 6 d, during which small portions of BaO were added over time until the reaction had gone to completion (as monitored by TLC).

The mixture was then allowed to cool down to room temperature, filtered to remove insoluble barium salts, treated with dry ice, and filtered again to remove the insoluble $BaCO_3$ formed. The filtered solution (pH 6-7) was evaporated to dryness at low temperature (<30°C), and the resulting viscous residue was dried under vacuum over P_2O_5, yielding the title compound as a pale yellow syrup (0.78 g, 72% yield). FT-IR (ATR, $\tilde{\nu}_{max}$, cm^{-1}): 3205 (br, ν, OH + NH_3^+ overlapped), 2844 (br, ν_s, NH_3^+), 1628 (sh, δ_a, NH_3^+), 1546 (s, ν_a, COO^-), 1039 (vs, ν, C–OH + C^1–O–CH_3 overlapped). ^{1}H NMR (400 MHz, DMSO-d_6, 298 K, δ, ppm): 4.55 (d, J_{HH} = 3.7 Hz, 1H, C^1H_α), 4.07 (br, 3.6H, $C^3OH_{\alpha+\beta}$ + $C^4OH_{\alpha+\beta}$ + $C^6OH_{\alpha+\beta}$), 3.98 (d, J_{HH} = 8.1 Hz, 0.2H, C^1H_β), 3.68-3.64 (m, 0.2H, C^6H_β), 3.62 (dd, J_{HH} = 11.7 Hz, 1.9 Hz, 1H, C^6H_α), 3.45 (dd, J_{HH} = 11.7 Hz, 5.7 Hz, 1.2H, $C^6H'_\alpha$ + $C^6H'_\beta$ overlapped), 3.38 (s, 0.6H, $OCH_{3\,\beta}$), 3.31 (ddd, J_{HH} = 10.1 Hz, 5.7 Hz, 1.9 Hz, 1H, C^5H_α), 3.26 (s, 3H, $OCH_{3\,\alpha}$), 3.22 (dd (app t), J_{HH} = 9.2 Hz, 1H, C^3H_α, C^3H_β), 3.07-3.00 (m, 1.6H, C^3H_β + $C^4H_{\alpha+\beta}$ + C^5H_β), 2.45 (dd, J_{HH} = 9.5 Hz, 3.7 Hz, 1H, C^2H_α), 2.40-2.36 (m, 0.2H, C^2H_β), 1.79 (s, 3.2 H, CH_3COO^-). ^{13}C{^{1}H} NMR (100 MHz, DMSO-d_6, 298 K, δ, ppm): 174.4 (CH_3COO^-), 104.47 (C^1_β), 99.59 (C^1_α), 77.18 (C^3_β), 76.13 (C^5_β), 74.40 (C^3_α), 73.15 (C^5_α), 70.36 (C^4_α), 70.13 (C^4_β), 61.12 (C^6_β), 60.96 (C^6_α), 57.25 (C^2_β), 56.11 ($OCH_{3\,\beta}$), 56.01 (C^2_α), 54.38 ($OCH_{3\,\alpha}$), 23.1 (CH_3COO^-). Experimental data are consistent with those reported in the literature.[9] Solution α:β anomers ratio ≈ 5:1 (based on the ^{1}H NMR spectrum).

1-*O*-methyl-6-azido-6-deoxy-α-D-glucopyranoside

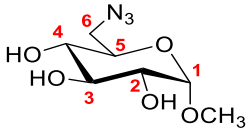

Methyl-α-D-glucopyranoside (4.69 g, 24.18 mmol) and PPh_3 (12.48 g, 47.58 mmol) were transferred into an oven-dry round-bottom flask, dissolved with dry DMF (85 mL), and kept under inert atmosphere by bubbling $N_{2\,(g)}$ into the solution. The mixture was cooled down to 0°C, treated with *N*-bromosuccinimide (8.85 g, 49.72 mmol), and stirred for 20 min at 0°C and for 3 h at 55°C. Methanol (5.2 mL) and NaN_3 (9.46 g, 145.52 mmol) were subsequently added in this order, and the resulting mixture was stirred at 85°C for 4 h. The solvent was evaporated by heating at 75°C with a stream of N_2, and the remaining residue was redissolved in water (90 mL) and treated with dichloromethane (3×90 mL). The aqueous fractions were recovered, filtered and evaporated to dryness. The resulting yellowish residue was purified by column chromatography (eluent: EtOAc/MeOH 9:1;

R_f = 0.53) and dried under vacuum over P_2O_5, yielding the title compound as a white solid (2.08 g, 39% yield).

FT-IR (ATR, $\tilde{\nu}_{max}$, cm^{-1}): 3356 (br, ν, OH), 2094 (vs, ν_{oop}, N_3), 1048/1026 (vs, ν, C–OH + C^1–O–CH_3 overlapped). ^1H NMR (400 MHz, $CDCl_3$, 298 K, δ, ppm): 4.77 (d, J_{HH} = 3.6 Hz, 1H, C^1H), 4.37 (br, 3H, C^2OH + C^3OH + C^4OH), 3.74-3.70 (m, 2H, C^3H + C^5H), 3.57-3.53 (m, 2H, C^2H + C^6H), 3.49-3.39 (m, 2H, C^4H + C^6H') 3.46 (s, 3H, OCH_3). $^{13}C\{^1H\}$ NMR (100 MHz, $CDCl_3$, 298 K, δ, ppm): 99.50 (C^1), 74.22 (C^3), 72.01 (C^2), 70.90 (C^5), 70.81 (C^4), 55.58 (OCH_3), 51.39 (C^6). Experimental data are consistent with those reported in the literature and confirm the presence of the α anomer only,[10] including the $^3J_{1,2}$ value within the 1-4 Hz range.[11]

1-*O*-methyl-6-amino-6-deoxy-α-D-glucopyranoside (GlcN3)

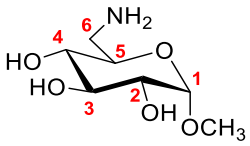

GlcN3

Pd/C 10%$_w$ (0.35 g) was added to a methanol solution (60 mL) of 1-*O*-methyl-6-azido-6-deoxy-α-D-glucopyranoside (2.05 g, 9.35 mmol). $H_{2(g)}$ was bubbled into the solution and stirred for 6 h until the reaction had gone to completion (as monitored by TLC). The catalyst was then filtered off on celite and the resulting clear solution was evaporated to dryness. The residue was dried under vacuum over P_2O_5, yielding the title compound as a white solid (1.61 g, 89% yield).

FT-IR (ATR, $\tilde{\nu}_{max}$, cm^{-1}): 3356/3299 (br, ν, OH + NH_2 overlapped), 1591 (w, δ, NH_2), 1033/1007 (vs, ν, C–OH + C^1–O–CH_3 overlapped). ^1H NMR (400 MHz, DMSO-d_6, 298 K, δ, ppm): 4.75 (br, 3H, C^2OH + C^3OH + C^4OH), 4.51 (d, J_{HH} = 3.6 Hz, 1H, C^1H), 3.35 (d, J_{HH} = 9.2 Hz, 1H, C^3H), 3.26 (s, 3H, OCH_3), 3.22 (dd, J_{HH} = 6.9 Hz, 3.2 Hz, 1H, C^5H), 3.17 (m, J_{HH} = 9.6 Hz, 3.6 Hz, 1H, C^2H), 2.99 (dd, J_{HH} = 9.6 Hz, 8.7 Hz, 1H, C^4H), 2.81 (dd, J_{HH} = 13.2 Hz, 3.2 Hz, 1H, C^6H), 2.57 (dd, J_{HH} = 13.2 Hz, 6.9 Hz, 1H, C^6H'). $^{13}C\{^1H\}$ NMR (100 MHz, DMSO-d_6, 298 K, δ, ppm): 99.72 (C^1), 73.22 (C^3), 72.42 (C^5), 72.04/72.01 (C^2 + C^4), 54.28 (OCH_3), 43.16 (C^6). Experimental data are consistent with those reported in the literature and confirm the presence of the α anomer only,[12] including the $^3J_{1,2}$ value within the 1-4 Hz range.[11]

_N_-(Benzyloxycarbonyl)ethanolamine

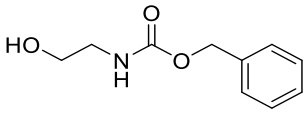

Trimethylamine (2.28 mL, 16.37 mmol) and *N*-(Benzyloxycarbonyl)succinimide (Z-OSu, 4.08 g, 16.37 mmol) were added under stirring to a THF/dichloromethane (1:1) (40 mL) solution of ethanolamine (0.98 mL, 16.37 mmol). The mixture was stirred at r.t. for 16 h, then it was evaporated to dryness. The resulting residue was redissolved in dichloromethane (30 mL), and washed with sat. $NaHCO_{3\,(aq)}$ (3×30 mL) and brine (3×30 mL). The organic fractions were recovered, dried over anhydrous Na_2SO_4, filtered and evaporated to dryness, yielding the title compound as a colourless oil (2.79 g, 91% yield). The compound was recrystallized by slow evaporation of an ethyl acetate/petroleum ether solution, affording colourless needles.

FT-IR (ATR, $\tilde{\nu}_{max}$, cm^{-1}): 3319 (br, ν, OH + NH overlapped), 1691 (vs, ν, C=O (amide I)), 1541 (vs, δ_{ip}, CNH (amide II)), 1453 (m, δ_{ip}, CNH conformer (amide II') + ν, C=C phenyl), 1266 (vs, amide III), 1032 (vs, ν_{oop}, C–C–O), 907 (m, ν_{ip}, C–C–O). ^{1}H NMR (400 MHz, $CDCl_3$, 298 K, δ, ppm): 7.32 (m, 5H, C*H* $_{arom}$), 5.30 (br, 1H, N*H*), 5.07 (s, 2H, C$H_{2\ Cbz}$), 3.64 (m, 2H, CH_2OH), 3.30 (m, 2H, CH_2NH). ^{13}C{^{1}H} NMR (100 MHz, $CDCl_3$, 298 K, δ, ppm): 157.21 (*C*=O), 136.42 (*C* $_{arom\ ipso}$), 128.61 (*C* $_{arom\ meta}$), 128.25 (*C* $_{arom\ para}$), 128.16 (*C* $_{arom\ ortho}$), 66.98 (*C*$H_{2\ Cbz}$), 62.03 (*C*H_2OH), 43.59 (*C*H_2NH). Experimental data are consistent with those reported in the literature.[13]

2-(Benzyloxycarbonyl)aminoethyl 2,3,4,6-tetra-*O*-acetyl-β-D-glucopyranoside

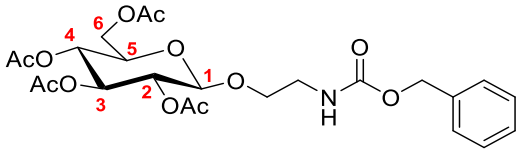

Pentaacetyl β-D-glucose (3.12 g, 8.00 mmol) and *N*-(Benzyloxycarbonyl)ethanolamine (1.56 g, 8.00 mmol) were transferred into an oven-dry round-bottom flask, dissolved with dry dichloromethane (50 mL), and kept under inert atmosphere by bubbling $N_{2\,(g)}$ into the solution. Powdered 4 Å molecular sieves were added to the mixture. The mixture was cooled down to 0°C, treated with $BF_3{\cdot}Et_2O$ (2 mL, 16.20 mmol), and stirred for 2 h at 0°C and for 14 h at r.t. Triethylamine was cautiously added to quench the reaction. The molecular sieves were filtered off and the solution was evaporated to dryness.

The resulting residue was purified by column chromatography (eluent:

dichloromethane/MeOH 96:4; R_f = 0.43) and dried under vacuum over P_2O_5, yielding the title compound as a brown oil (3.40 g, crude). Although experimental data are consistent with those reported in the literature,[14] they confirm the presence of a non-isolatable mixture of the title compound and 2,3,4,6-tetra-*O*-acetyl-D-glucose (mixture of α and β anomers). The mixture was therefore used as crude for the next step without any further purification.

2-(Benzyloxycarbonyl)aminoethyl β-D-glucopyranoside

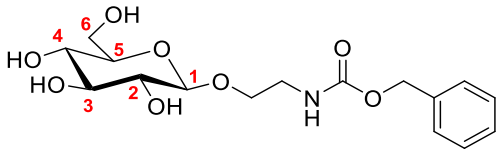

A dry methanol solution (5 mL) of sodium methoxide (66.0 mg, 1.22 mmol) was dropwise added to a dry methanol mixture (20 mL) of 2-(Benzyloxycarbonyl)aminoethyl 2,3,4,6-tetra-*O*-acetyl-β-D-glucopyranoside and 2,3,4,6-tetra-*O*-acetyl-D-glucose (1.84 g, 3.54 mmol). The mixture was stirred at r.t. for 3 h until the reaction had gone to completion (as monitored by TLC). Amberlite IR-120 (H^+ form) was added to neutralize the base. The resin was then filtered off and the solution was evaporated to dryness. The resulting colourless oily residue was purified by column chromatography (eluent: EtOAc/MeOH 8:2; R_f = 0.43) and dried under vacuum over P_2O_5, yielding the title compound as a colourless sticky foam (0.48 g, 17% yield after two steps). FT-IR (ATR, $\tilde{\nu}_{max}$, cm^{-1}): 3328 (br, ν, OH + NH_2 overlapped), 1693 (s, ν, C=O (amide I)), 1532 (m, δ_{ip}, CNH (amide II)), 1455 (w, δ_{ip}, CNH conformer (amide II') + ν, C=C phenyl), 1255 (s, amide III), 1070/1015 (br, ν, C–OH + C–O–C overlapped), 899 (w, ν_{ip}, C–C–O). ^{1}H NMR (400 MHz, D_2O, 298 K, δ, ppm): 7.39 (m, 5H, C*H* $_{arom}$), 5.08 (s, 2H, $CH_{2\ Cbz}$), 4.39 (d, J_{HH} = 8.2 Hz, 1H, C^1H), 3.92-3.83 (m, 2H, C^6H + $CH_aH_bCH_2NH$), 3.71 (ddd, J_{HH} = 10.9 Hz, 6.2 Hz, 4.4 Hz, 1H, $CH_aH_bCH_2NH$), 3.64 (dd, J_{HH} = 12.4 Hz, 5.9 Hz, 1H, C^6H'), 3.43 (dd, J_{HH} = 9.1 Hz, 1H, C^3H), 3.38-3.29 (m, 4H, C^4H + C^5H + CH_2NH), 3.21 (dd, J_{HH} = 9.1 Hz, 8.2 Hz, 1H, C^2H). $^{13}C\{^1H\}$ NMR (100 MHz, D_2O, 298 K, δ, ppm): 158.50 (*C*=O), 136.53 ($C_{\ arom\ ipso}$), 128.81 ($C_{\ arom\ meta}$), 128.41 ($C_{\ arom\ para}$), 127.74 ($C_{\ arom\ ortho}$), 102.50 (C^1), 75.92/75.65 (C^3 + C^4), 73.12 (C^2), 69.63 (C^5), 69.04 (CH_2CH_2NH), 66.98 ($CH_{2\ Cbz}$), 60.73 (C^6), 40.50 (CH_2NH). Experimental data are consistent with those reported in the literature and confirm the presence of the β anomer only, including the $^3J_{1,2}$ value within the 7-8 Hz range.[15]

1-Aminoethyl β-D-glucopyranoside (GlcN4)

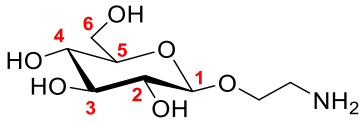

GlcN4

Pd/C 10%$_w$ (0.15 g) was added to a methanol solution (20 mL) of 2-(Benzyloxycarbonyl)aminoethyl β-D-glucopyranoside (0.48 g, 1.34 mmol). $H_{2(g)}$ was bubbled into the solution and stirred for 2 h until the reaction had gone to completion (as monitored by TLC). The catalyst was then filtered off on celite and the resulting clear solution was evaporated to dryness. The residue was dried under vacuum over P_2O_5, yielding the title compound as a colourless oil (0.28 g, 94% yield). FT-IR (ATR, $\tilde{\nu}_{max}$, cm^{-1}): 3294 (br, ν, OH + NH_2 overlapped), 1591 (w, δ, NH_2), 1072/1015 (vs, ν, C–OH + C–O–C overlapped). ^1H NMR (400 MHz, CD_3OD, 298 K, δ, ppm): 4.27 (d, J_{HH} = 7.8 Hz, 1H, C^1H), 3.93 (ddd, J_{HH} = 10.4 Hz, 7.7 Hz, 5.9 Hz, 1H, C$H_aH_bCH_2NH_2$), 3.86 (dd, J_{HH} = 11.5 Hz, 1.2 Hz, 1H, C^6H), 3.68-3.60 (m, 2H, C^6H' + CH_aH_bCH_2NH_2), 3.35 (m, 1H, C^3H), 3.27 (m, 2H, C^4H + C^5H), 3.20 (dd, J_{HH} = 9.1 Hz, 7.8 Hz, 1H, C^2H), 2.85-2.82 (m, 2H, CH_2NH_2). $^{13}C\{^1H\}$ NMR (100 MHz, CD_3OD, 298 K, δ, ppm): 104.54 (C^1), 77.99 (C^4), 77.95 (C^3), 75.15 (C^2), 72.06 (C^5), 71.64 (CH_2CH_2NH_2), 62.74 (C^6), 42.22 (CH_2NH_2). Experimental data are consistent with those reported in the literature and confirm the presence of the β anomer only, including the $^3J_{1,2}$ value within the 7-8 Hz range.[14]

(PPh_4)(dtc-Sar-OEt)

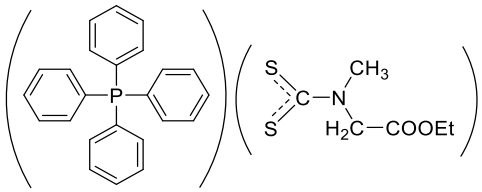

An aqueous solution (4 mL) of NaOH (260.7 mg, 6.51 mmol) and, subsequently, CS_2 (400 µL, 6.62 mmol) were added dropwise under stirring to an aqueous solution (2 mL) of ethylsarcosine hydrochloride (996.3 mg, 6.49 mmol) at 0°C. The mixture was stirred at 0°C for 3 h (pH turned from 9 to 6). The mixture was then treated with an aqueous solution (10 mL) of PPh_4Cl (1.22 g, 3.25 mmol), leading to the sudden precipitation of a yellow solid. The precipitate was centrifuged and the bulk of supernatant discarded. The residue was subsequently washed with cold water (2×5 mL) and then dried under vacuum over P_2O_5, yielding the title compound as a yellow powder (1.09 g, 32% yield). Yellow

crystals suitable for X-ray crystallography were obtained by slow evaporation of an aqueous solution of the compound.

M.p.: 155-160 °C (dec.). Anal. (%) calcd. for $C_{30}H_{30}NO_2PS_2$ (MW = 531.67 g mol^{-1}): C, 67.77; H, 5.69; N, 2.63; found: C, 68.04; H, 5.55; N, 2.46. FT-IR (CsI disk, $\tilde{\nu}_{max}$, cm^{-1}): 1732 (s, ν, C=O), 1434 (s, ν, N–CSS), 1194/1106 (vs, $\nu_{a/s}$, C–OEt), 722 (vs, ν, P–Ph), 527 (vs, δ_{oop}, PPh_4). ^{1}H NMR (400 MHz, $CDCl_3$, 298 K, δ, ppm): 7.91-7.87 (m, 4H, C*H* arom *para*), 7.80-7.75 (m, 8H, C*H* arom *meta*), 7.64-7.59 (m, 4H, C*H* arom *ortho*), 5.12 (s, 2H, NCH_2), 4.07 (q, J_{HH} = 7.2 Hz, 2H, CH_2 ethyl), 3.54 (s, 3H, NCH_3), 1.17 (t, J_{HH} = 7.2 Hz, 3H, CH_3 ethyl). ^{13}C{^{1}H} NMR (100 MHz, $CDCl_3$, 298 K, δ, ppm): 217.23 (N*C*SS), 170.30 (*C*=O), 135.85 (d, J_{PC} = 3.1 Hz, *C* arom *para*), 134.47 (d, J_{PC} = 10.8 Hz, *C* arom *ortho*), 130.78 (d, J_{PC} = 12.4 Hz, *C* arom *meta*), 117.46 (d, J_{PC} = 89.1 Hz, *C* arom *ipso*), 60.34 (*C*H_2 ethyl), 57.53 (N*C*H_2), 42.83 (N*C*H_3), 14.31 (*C*H_3 ethyl). UV-Vis (MeOH, 298 K, nm (ε, M^{-1} cm^{-1})): 230 (26900), 254 (9900), 267 (sh, 7200), 277 (6900), 291 (9500).

Na(dtc-Inp-NH$_2$)·CH$_3$OH

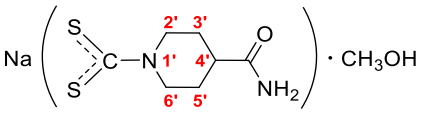

A methanol solution (5 mL) of NaOH (340.0 mg, 8.58 mmol) and, subsequently, CS_2 (1.07 mL, 17.76 mmol) were added dropwise under stirring to a methanol solution (5 mL) of isonipecotamide (1.09 g, 8.50 mmol) at 0°C. The mixture was stirred at 0°C for 3 h (pH turned from 10 to 8), treated with further CS_2 (536.0 µL, 8.88 mmol), and stored at 4°C for 16 h (pH further dropped to ~7). The mixture was then treated with diethyl ether (20 mL) at room temperature, leading to the sudden precipitation of a white solid. The precipitate was filtered off, washed with diethyl ether (3×10 mL) and then dried under vacuum over P_2O_5, yielding the title compound as a white solid (1.75 g, 80% yield). Colourless needle-shaped crystals suitable for X-ray crystallography were obtained upon storing a methanol/diethyl ether solution of the compound at 4°C. M.p. 260-268°C (dec.). Anal. (%) calcd. for $C_8H_{15}N_2NaO_2S_2$ (MM = 258.33 g mol^{-1}): C, 37.20; H, 5.85; N, 10.84; found: C, 37.45; H, 5.77; N, 10.64. FT-IR (CsI disk, $\tilde{\nu}_{max}$, cm^{-1}): 3390 (br, ν, O–H methanol), 3361 (br, ν_a, NH_2), 3198 (br, ν_s, NH_2), 1643 (vs, ν, C=O (amide I)), 1625 (s, δ_{ip}, CNH_2 (amide II)), 1472 (s, ν, N–CSS), 1203 (s, ν, C–O methanol), 1004 (s, ν_a, SCS), 545 (w, ν_s, SCS). ^{1}H NMR (400 MHz, DMSO-d_6, 298 K, δ, ppm): 7.25 (s, 1H, N*H* cis), 6.72 (s, 1H, N*H* trans), 5.78 (app d, J_{HH} = 12.4 Hz, 2H, $C^{2',6'}H_{eq}$), 4.11 (q, J_{HH} = 5.2 Hz, 1H, O*H* methanol),

3.16 (d, J_{HH} = 5.2 Hz, 3H, C$H_{3\ methanol}$), 2.82 (td, J_{HH} = 12.4 Hz, 2.3 Hz, 2H, C$^{2',6'}H_{\ ax}$), 2.29 (tt, J_{HH} = 11.5 Hz, 4.0 Hz, 1H, C$^{4'}H$), 1.60 (app dd, J_{HH} = 12.8 Hz, 2.8 Hz, 2H, C$^{3',5'}H_{\ eq}$), 1.40 (qd, J_{HH} = 12.4 Hz, 3.6 Hz, 2H, C$^{3',5'}H_{\ ax}$). ^{13}C{^{1}H} NMR (100 MHz, DMSO-d$_6$, 298 K, δ, ppm): 213.35 (N*C*SS), 176.56 (*C*=O), 48.68 (*C*$^{2',6'}$H$_2$), 48.62 (*C*H$_{3\ methanol}$), 41.97 (*C*$^{4'}$H), 28.55 (*C*$^{3',5'}$H$_2$). UV-Vis (MeOH, 298 K, nm (ε, M^{-1} cm^{-1})): 260 (13400), 290 (13100).

(H-Inp-OEt)(dtc-Inp-OEt)

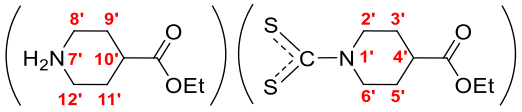

An ethanol solution (5 mL) of CS_2 (1.2 mL, 19.87 mmol) was added dropwise under stirring to a diethyl ether solution (50 mL) of ethyl isonipecotate (1.54 g, 9.80 mmol) at 0°C, leading to the sudden precipitation of a white solid. The mixture was allowed reaching r.t. and stirred for 3 h. The precipitate was filtered off, washed with diethyl ether (3×10 mL) and then dried under vacuum over P_2O_5, yielding the title compound as a white solid (1.74 g, 91% yield). M.p. 144-148°C (dec.). Anal. (%) calcd. for $C_8H_{15}N_2NaO_2S_2$ (MM = 390.56 g mol^{-1}): C, 52.28; H, 7.74; N, 7.17; found: C, 52.64; H, 7.81; N, 7.66. FT-IR (CsI disk, $\tilde{\nu}_{max}$, cm^{-1}): 2902 (br, ν, CH + NH_2^+ overlapped), 1721 (vs, ν, C=O), 1407 (vs, ν, N–CSS), 1192/1177 (s, ν, C–OEt), 1035 (s, ν, O–Et), 989 (m, ν_a, SCS). ^{1}H NMR (400 MHz, DMSO-d$_6$, 298 K, δ, ppm): 8.93 (br, 2H, NH_2^+), 5.50 (m, J_{HH} = 12.8 Hz, 2H, C$^{2',6'}H_{\ eq}$), 4.11-4.03 (2 overlapped q, J_{HH} = 7.3 Hz, 6.9 Hz, 4H, OC$H_{2\ dtc\ +\ counterion}$), 3.31 (m, J_{HH} = 12.8 Hz, 2H, C$^{8',12'}H_{\ eq}$), 3.13 (m, 2H, C$^{2',6'}H_{\ ax}$), 2.95 (m, 2H, C$^{8',12'}H_{\ ax}$), 2.70 (tt, J_{HH} = 11.1 Hz, 3.7 Hz, 1H, C$^{10'}H$), 2.58 (tt, J_{HH} = 10.9 Hz, 4.0 Hz, 1H, C$^{4'}H_{\ dtc}$), 2.00-1.96 (m, 2 H, C$^{9',11'}H_{\ eq}$), 1.81-1.71 (m, 4H, C$^{3',5'}H_{\ eq}$ + C$^{9',11'}H_{\ ax}$), 1.50-1.40 (m, 2H, C$^{3',5'}H_{\ ax}$), 1.20-1.16 (2 overlapped t, J_{HH} = 7.3 Hz, 6.9 Hz, 6H, C$H_{3\ dtc\ +\ counterion}$). ^{13}C{^{1}H} NMR (100 MHz, DMSO-d$_6$, 298 K, δ, ppm): 212.11 (N*C*SS), 174.29/173.20 (*C*=O $_{dtc\ +\ counterion}$), 60.25/59.86 (O*C*H$_{2\ dtc\ +\ counterion}$), 48.48 (*C*$^{2',6'}$H$_2$), 42.27 (*C*$^{8',12'}$H$_2$), 40.37 (*C*$^{4'}$H), 37.74 (*C*$^{10'}$H), 27.93 (*C*$^{3',5'}$H$_2$), 24.62 (*C*$^{9',11'}$H$_2$), 14.09/14.05 (*C*H$_{3\ dtc\ +\ counterion}$). UV-Vis (MeOH, 298 K, nm (ε, M^{-1} cm^{-1})): 260 (10400), 291 (10300).

$Na_2[Zn(dtc\text{-}Inp\text{-}O)_2]\cdot 2H_2O$ (Zn0a)

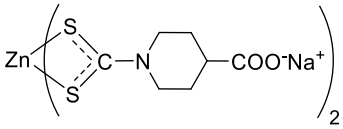

This zinc(II) intermediate was synthesized according to a modified literature procedure.[16]

Method A: NaOH (2.81 g, 70.15 mmol) was dissolved in water (70 mL) and added under stirring to a methanol solution (140 mL) of isonipecotic acid (4.50 g, 34.88 mmol). The mixture was cooled down to 0°C, treated dropwise with CS_2 (2.45 mL, 40.58 mmol), and stirred for 2 h and then at r.t. overnight (pH turned from 12 to 6). An aqueous solution (35 mL) of $[Zn(OAc)_2]\cdot 2H_2O$ (3.80 g, 17.5 mmol) was added dropwise under stirring to the solution of the ligand over a period of 2 h, leading to the sudden precipitation of a white solid. The mixture was stored at 4 °C overnight. The resulting precipitate was filtered, washed with methanol (100 mL), Et_2O (100 mL), and then dried under vacuum over P_2O_5, yielding the title compound as a white solid (2.13 g, 22% yield). More compound was obtained by evaporating of the collected mother and washing solutions, resuspending the residue in water/methanol 1:2 (60 mL), filtering and washing with methanol (100 mL) and Et_2O (100 mL) the resulting with solid (0.77 g, 8% yield).

Method B: NaOH (620.0 mg, 15.50 mmol) was dissolved in methanol (7 mL) and added under stirring to a methanol solution (10 mL) of isonipecotic acid (1.00 g, 7.74 mmol). The mixture was cooled down to 0°C, treated dropwise with CS_2 (480 µL, 7.94 mmol), and stirred for 6 h. The resulting solution was then added dropwise under stirring to a methanol solution (7 mL) of $[Zn(OAc)_2]\cdot 2H_2O$ (850.0 mg, 3.87 mmol), leading to the sudden precipitation of a white solid. The precipitate was centrifuged and the bulk of supernatant discarded. The residue was subsequently washed with methanol (3×20 mL) and then dried under vacuum over P_2O_5, yielding the title compound as a white solid (1.47 g, 68% yield). M.p. 295-297°C (dec.). Anal. (%) calcd. for $C_{14}H_{22}N_2NaO_6S_4Zn$ (MM = 553.94 g mol^{-1}): C, 30.36; H, 4.00; N, 5.06; found: C, 30.48; H, 4.08; N, 5.04. FT-IR (CsI disk, $\tilde{\nu}_{max}$, cm^{-1}): 1555 (vs, ν_a, COO^-), 1487 (vs, ν, N–CSS), 1409 (s, ν_s, COO^-), 1002 (m, ν_a, SCS), 566 (w, ν_s, SCS), 397 (w, ν_a, ZnS_4). ^1H NMR (400 MHz, DMSO-d_6, 298 K, δ, ppm): 4.93 (m, J_{HH} = 13.0 Hz, 4H, $C^{2',6'}H_{eq}$), 3.31 (br td, J_{HH} = 13.0 Hz, 2.7 Hz, 4H, $C^{2',6'}H_{ax}$), 2.46 (tt, J_{HH} = 11.2 Hz, 3.9 Hz, 2H, $C^{4'}H$), 1.95 (m, 4H, $C^{3',5'}H_{eq}$), 1.66 (m, 4H, $C^{3',5'}H_{ax}$). $^{13}C\{^1H\}$ NMR (100 MHz, DMSO-d_6,

298 K, δ, ppm): 201.66 (N*C*SS), 183.14 (*C*O), 51.81 ($C^{2',6'}H_2$), 42.80 ($C^{4'}H$), 28.83 ($C^{3',5'}H_2$). UV-Vis (H_2O, 298 K, nm (ε, M^{-1} cm^{-1})): 259 (27000), 275 (22500).

[Zn(dtc-Inp-OSu)$_2$] (Zn0b)

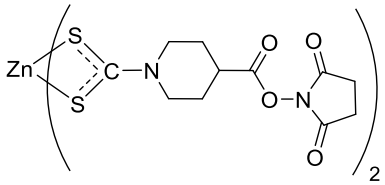

This zinc(II) intermediate was synthesized according to a literature procedure.[16] *N,N,N',N'*-tetramethyl-*O*-(*N*-succinimidyl)uronium tetrafluoroborate (TSTU, 3.07 g, 10.20 mmol) was added under stirring to an anhydrous DMF mixture (12 mL) of $Na_2[Zn(dtc\text{-}Inp\text{-}O)_2]\cdot 2H_2O$ (Zn0a) (2.51 g, 4.52 mmol) and *N*,*N*-diisopropylethylamine (DIPEA, 160 µL, 0.92 mmol). The mixture was stirred at r.t. under inert atmosphere (N_2) for 16 h, and then treated with a 1:1 water/ethanol solution (1.2 L). The resulting white solid was filtered, washed with ethanol (3×20 mL) and diethyl ether (3×20 mL), and then dried under vacuum over P_2O_5, yielding the title compound as a white solid (2.81 g, 93% yield). M.p. 220-222°C (dec.). Anal. (%) calcd. for $C_{22}H_{26}N_4O_8S_4Zn$ (MM = 668.09 g mol^{-1}): C, 39.55; H, 3.92; N, 8.39; found: C, 39.31; H, 3.98; N, 8.28. FT-IR (CsI disk, $\tilde{\nu}_{max}$, cm^{-1}): 1817 (m, ν_{ip}, C=O succinimidyl), 1784 (s, ν_{oop}, C=O succinimidyl), 1737 (vs, ν, C=O ester), 1496 (s, ν, N–CSS), 1206 (s, ν, C–OSu), 990 (vs, ν_a, SCS), 562 (w, ν_s, SCS), 397 (w, ν_a, ZnS_4). ^{1}H NMR (400 MHz, DMSO-d_6, 298 K, δ, ppm): 4.72 (m, J_{HH} = 13.0 Hz, 4H, $C^{2',6'}H_{eq}$), 3.52 (m, J_{HH} = 13.4 Hz, 11.0 Hz, 4H, $C^{2',6'}H_{ax}$), 3.26-3.19 (m, 2H, $C^{4'}H$), 2.82 (br s, 8H, $CH_{2\ succ}$), 2.10 (m, 4H, $C^{3',5'}H_{eq}$), 1.70 (m, 4H, $C^{3',5'}H_{ax}$). $^{13}C\{^1H\}$ NMR (100 MHz, DMSO-d_6, 298 K, δ, ppm): 203.30 (N*C*SS), 170.17 (C=O $_{succ}$), 169.90 (C=O $_{ester}$), 49.87 ($C^{2',6'}H_2$), 36.33 ($C^{4'}H$), 27.56 ($C^{3',5'}H_2$), 25.49 ($CH_{2\ succ}$). UV-Vis (DMSO, 298 K, nm (ε, M^{-1} cm^{-1})): 266 (28800), 278 (23100), 298 (sh, ~10900).

[Zn(dtc-Inp-OEt)$_2$] (Zn1)

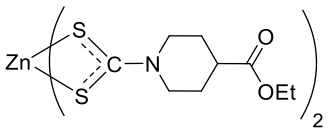

CS_2 (400 µL, 6.63 mmol) was added dropwise under stirring to a water/ethanol solution (7:3, 10 mL) of ethyl isonipecotate (1.03 g, 6.53 mmol) at 0°C. The mixture was stirred at 0°C for 3 h (pH turned from 12 to 6), and then added to an aqueous solution (3 mL) of

$ZnCl_2$ (220.0 mg, 1.63 mmol), leading to the sudden precipitation of a white solid. The precipitate was centrifuged and the bulk of supernatant discarded. The residue was subsequently washed with water (2×10 mL), acetone (2×10 mL) and diethyl ether (2×10 mL), and then dried under vacuum over P_2O_5, yielding the title compound as a white solid (620.1 mg, 72 % yield). Small colourless plate-shaped crystals suitable for X-ray crystallography were obtained upon slow evaporation of an acetonitrile/ethanol solution of the compound. M.p. 200-202°C. Anal. (%) calcd. for $C_{18}H_{28}N_2O_4S_4Zn$ (MM = 530.05 g mol^{-1}): C, 40.79; H, 5.32; N, 5.29; found: 40.57; H, 5.39; N, 5.10. FT-IR (CsI disk, $\tilde{\nu}_{max}$, cm^{-1}): 1733 (vs, ν, C=O), 1494 (vs, ν, N–CSS), 1176 (s, ν, C–OEt), 1042 (s, ν, O–Et), 1007 (m, ν_a, SCS), 568 (w, ν_s, SCS), 398 (w, ν_a, ZnS_4). ^{1}H NMR (400 MHz, DMSO-d_6, 298 K, δ, ppm): 4.72 (m, J_{HH} = 13.1 Hz, 4H, $C^{2',6'}H_{eq}$), 4.08 (q, J_{HH} = 7.1 Hz, 4H, OCH_2), 3.39 (m, 4H, $C^{2',6'}H_{ax}$), 2.68 (tt, J_{HH} = 10.5 Hz, 4.1 Hz, 2H, $C^{4'}H$), 1.95 (m, 4H, $C^{3',5'}H_{eq}$), 1.57 (m, 4H, $C^{3',5'}H_{ax}$), 1.19 (t, J_{HH} = 7.1 Hz, 6H, CH_3). $^{13}C\{^1H\}$ NMR (100 MHz, DMSO-d_6, 298 K, δ, ppm): 202.62 (N*C*SS), 173.59 (*C*=O), 60.15 (OCH_2), 50.37 ($C^{2',6'}H_2$), 38.88 ($C^{4'}H$), 27.78 ($C^{3',5'}H_2$), 14.08 (CH_3). UV-Vis (DMSO, 298 K, nm (ε, M^{-1} cm^{-1})): 267 (28900), 276 (24500), 297 (sh, ~9600).

[Zn(dtc-Inp-NH_2)$_2$] (Zn2)

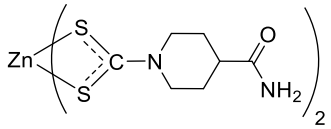

Method A: NaOH (310.0 mg, 7.80 mmol) was dissolved in methanol (10 mL) and added under stirring to a methanol solution (10 mL) of isonipecotamide (1.00 g, 7.80 mmol). The mixture was cooled down to 0°C, treated dropwise with CS_2 (470 μL, 7.80 mmol), stirred for 3 h (pH turned from 12 to 8), treated with further CS_2 (470 μL, 7.80 mmol), and stored at 4C overnight. The mixture was then added to an aqueous solution (2 mL) of $[Zn(OAc)_2]\cdot 2H_2O$ (860.0 mg, 3.90 mmol) at r.t., leading to the sudden precipitation of a white solid. The solid was centrifuged and the bulk of supernatant discarded. The precipitate was centrifuged and the bulk of supernatant discarded. The residue was subsequently washed with water (2×15 mL) and then dried under vacuum over P_2O_5, yielding the title compound as a white solid (1.77 g, 96% yield).

Method B: An aqueous solution (18 mL) of Na(dtc-Inp-NH_2)·CH_3OH (900.0 mg, 3.48 mmol), was added under stirring to an aqueous solution (2 mL) of $[Zn(OAc)_2]\cdot 2H_2O$ (379.4 mg, 1.73 mmol) at r.t., leading to the sudden precipitation of a white solid. The

precipitate was centrifuged and the bulk of supernatant discarded. The residue was subsequently washed with water (2×15 mL) and then dried under vacuum over P_2O_5, yielding the title compound as a white solid (810.4 mg, 99% yield). M.p. 293-294°C (dec.). Anal. (%) calcd. for $C_{14}H_{22}N_4O_2S_4Zn$ (MM = 471.98 g mol^{-1}): C, 35.63; H, 4.70; N, 11.87; found: C, 35.74; H, 4.89; N, 11.76. FT-IR (CsI disk, $\tilde{\nu}_{max}$, cm^{-1}): 3439/3208 (br, $\nu_{a/s}$, NH_2), 1667 (vs, ν, C=O (amide I)), 1649 (s, δ_{ip}, CNH_2 (amide II)), 1492 (s, ν, N–CSS), 1007 (m, ν_a, SCS), 531 (m, ν_s, SCS), 391 (w, ν_a, ZnS_4). ^{1}H NMR (400 MHz, DMSO-d_6, 298 K, δ, ppm): 7.36 (s, 2H, N*H* $_{cis}$), 6.87 (s, 2H, N*H* $_{trans}$), 4.82 (app d, J_{HH} = 12.5 Hz, 4H, $C^{2',6'}H_{eq}$), 3.26 (m, J_{HH} = 12.5 Hz, 1.7 Hz, 4H, $C^{2',6'}H_{ax}$), 2.40 (tt, J_{HH} = 11.2 Hz, 3.9 Hz, 2H, $C^{4'}H$), 1.80 (m, 4H, $C^{3',5'}H_{eq}$), 1.55 (m, 4H, $C^{3',5'}H_{ax}$). ^{13}C{^{1}H} NMR (100 MHz, DMSO-d_6, 298 K, δ, ppm): 202.29 (N*C*SS), 175.60 (*C*=O), 50.72 ($C^{2',6'}H_2$), 40.12 ($C^{4'}H$), 28.35 ($C^{3',5'}H_2$). UV-Vis (DMSO, 298 K, nm (ε, M^{-1} cm^{-1})): 268 (28600), 276 (25000), 296 (sh, ~9500).

[Zn(dtc-Inp-GlcN1)$_2$] (Zn3)

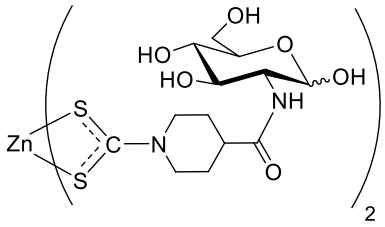

A mixture of (α,β)-D-glucosamine (**GlcN1**) hydrochloride (392.0 mg, 1.82 mmol) and *N*,*N*-diisopropylethylamine (DIPEA, 925 μL, 5.31 mmol) in anhydrous DMF (3 mL) was added under stirring to a suspension of [Zn(dtc-Inp-OSu)$_2$] (**Zn0b**) (473.3 mg, 0.71 mmol) in anhydrous DMF (2 mL). The mixture was stirred at r.t. under inert atmosphere (N_2) for 16 h and then treated with methanol (60 mL). The resulting precipitate was filtered, washed with methanol (3×20 mL), and then dried under vacuum over P_2O_5, yielding the title compound as a white solid (341.6 mg, 61% yield). M.p. 220-222°C (dec.). Anal. (%) calcd. for $C_{26}H_{42}N_4O_{12}S_4Zn$ (MM = 796.26 g mol^{-1}): C, 39.22; H, 5.32; N, 7.04; found: C, 39.18; H, 5.19; N, 6.91. FT-IR (CsI disk, $\tilde{\nu}_{max}$, cm^{-1}): 3293 (br, ν, OH + NH overlapped), 1638 (s, ν, C=O (amide I)), 1547 (m, δ_{ip}, CNH (amide II)), 1487 (s, ν, N–CSS), 1060/1025 (vs, ν, C-OH), 959 (m, ν_a, SCS), 570 (w, ν_s, SCS), 374 (w, ν_a, ZnS_4). ^{1}H NMR (400 MHz, DMSO-d_6, 298 K, δ, ppm): 7.70 (d, J_{HH} = 8.7 Hz, 0.5H, N*H* $_{\beta}$), 7.66 (d, J_{HH} = 7.8 Hz, 2H, N*H* $_{\alpha}$), 6.49 (d, J_{HH} = 6.4 Hz, 0.5H, C^1OH_{β}), 6.42 (d, J_{HH} = 4.4 Hz, 2H, C^1OH_{α}), 4.94-4.90 (m, 4H, C^1H_{α} + C^3OH_{α}), 4.82 (m, 5H, $C^{2',6'}H_{eq\,\alpha+\beta}$), 4.61 (d, J_{HH}

= 4.4 Hz, 2H, C^4OH_{α}), 4.53 (dd, J_{HH} = 5.9 Hz, 0.5H, C^6OH_{β}), 4.44 (m, 2.5H, C^1H_{β} + C^6OH_{α}), 3.69-3.39 (m, 11.5H, C^2H_{α} + $C^4H_{\alpha+\beta}$ + C^5H_{α} + $C^6H_{\alpha+\beta}$ + $C^6H'_{\alpha+\beta}$), 3.31-3.22 (m, 6H, $C^{2',6'}H_{ax\,\alpha+\beta}$ + C^2H_{β} + C^3H_{β}), 3.18-3.02 (m, 2.5H, C^3H_{α} + C^5H_{β}), 2.56 (m, 2.5H, $C^{4'}H_{\alpha+\beta}$), 1.81-1.75 (m, 5H, $C^{3',5'}H_{eq\,\alpha+\beta}$), 1.62-1.56 (m, 5H, $C^{3',5'}H_{ax\,\alpha+\beta}$). C^3OH_{β} and C^4OH_{β} could not be undoubtedly assigned: those peaks are probably overlapped with other peaks in the 4.92-4.42 ppm range. $^{13}C\{^1H\}$ NMR (100 MHz, DMSO-d_6, 298 K, δ, ppm): 202.33 (N*C*SS), 173.74 (*C*=O), 95.43 (C^1_{β}), 90.49 (C^1_{α}), 76.87 (C^5_{β}), 74.23 (C^3_{β}), 72.12 (C^5_{α}), 71.09 (C^3_{α}), 70.85 (C^4_{β}), 70.40 (C^4_{α}), 61.12 ($C^6_{\alpha+\beta}$), 57.06 (C^2_{β}), 54.31 (C^2_{α}), 50.71 ($C^{2',6'}H_2$), 40.03 ($C^{4'}H$), 28.50 ($C^{3',5'}H_2$). No differentiation of the ^{13}C signals of the isonipecotic moiety due to the presence of both α and β anomers could be detected. Solution α:β anomers ratio ≈ 4:1 (based on the ^1H NMR spectrum). UV-Vis (DMSO, 298 K, nm (ε, M^{-1} cm^{-1})): 267 (26300), 276 (22600), 298 (sh, ~9000).

[Zn(dtc-Inp-GlcN2)$_2$] (Zn4)

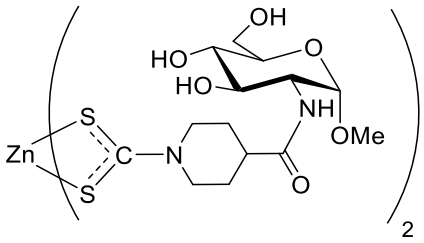

A mixture of 1-*O*-methyl-2-amino-2-deoxy-(α,β)-D-glucopyranoside (**GlcN2**) acetic acid (266.1 mg, 1.05 mmol) and *N*,*N*-diisopropylethylamine (DIPEA, 76 µL, 0.44 mmol) in anhydrous DMF (2 mL) was added under stirring to a suspension of [Zn(dtc-Inp-OSu)$_2$] (**Zn0b**) (292.8 mg, 0.44 mmol) in anhydrous DMF (2 mL). The mixture was stirred at r.t. under inert atmosphere (N_2) for 16 h and then treated with methanol (30 mL), leading to the formation of a white precipitate that was filtered off and discarded. The resulting clear pale yellow solution was allowed to slowly concentrate under the fume hood at room temperature for two days, leading to the formation of a white solid. The precipitate was resuspended in methanol (50 mL), filtered, washed with methanol (3×20 mL), and then dried under vacuum over P_2O_5, yielding the title compound as a white solid (464.6 mg, 35%). M.p. 268-272°C (dec.). Anal. (%) calcd. for $C_{28}H_{46}N_4O_{12}S_4Zn$ (MM = 824.31 g mol^{-1}): C, 40.80; H, 5.63; N, 6.80; found: C, 40.65; H, 5.74; N, 6.81. FT-IR (CsI disk, $\tilde{\nu}_{max}$, cm^{-1}): 3319 (br, ν, OH + NH overlapped), 1645 (s, ν, C=O (amide I)), 1557 (m, δ_{ip}, CNH (amide II)), 1494 (s, ν, N–CSS), 1062/1040 (vs, ν, C–OH + C^1–O–CH_3 overlapped), 950 (s, ν_a, SCS), 576 (m, ν_s, SCS), 382 (w, ν_a, ZnS_4). ^1H NMR (400 MHz,

DMSO-d_6, 298 K, δ, ppm): 7.80 (d, J_{HH} = 7.8 Hz, 2H, N*H*), 5.00 (d, J_{HH} = 5.6 Hz, 2H, C^4O*H*), 4.82 (m, J_{HH} = 12.7 Hz, 4H, $C^{2',6'}H_{eq}$), 4.73 (d, J_{HH} = 5.9 Hz, 2H, C^3O*H*), 4.56-4.52 (m, 4H, C^1*H* + C^6O*H*), 3.67-3.62 (m, 4H, C^2*H* + C^6*H*), 3.49-3.42 (m, 4H, C^3*H* + C^6*H*'), 3.33-3.24 (m, 6H, C^5*H* + $C^{2',6'}H_{ax}$), 3.24 (s, 6H, OCH_3), 3.15-3.09 (m, 2H, C^4*H*), 2.55 (m, 2H, $C^{4'}$*H*), 1.81-1.76 (m, 4H, $C^{3',5'}H_{eq}$), 1.62-1.53 (m, 4H, $C^{3',5'}H_{ax}$). The ^{1}H NMR signals refer to the α anomer. Signals related to the β anomer were barely detectable, and only a very few were observed and could be undoubtedly assigned (such as δ(N*H*) = 7.68, δ(C^3O*H*) = 4.91, δ(C^1*H*) = 4.19 ($^3J_{1,2}$ = 8.4 Hz), δ(OCH_3) = 3.58 ppm). $^{13}C\{^1H\}$ NMR (100 MHz, DMSO-d_6, 298 K, δ, ppm): 202.23 (N*C*SS), 173.91 (*C*=O), 97.88 (C^1), 72.81 (C^5), 70.80 (C^3), 70.69 (C^4), 60.85 (C^6), 54.48 (OCH_3), 53.77 (C^2), 50.80 ($C^{2',6'}H_2$), 40.00 ($C^{4'}H_2$), 28.52 ($C^{3',5'}H_2$). No $^{13}C\{^1H\}$ NMR signals assignable to the β anomer were detected. Solution α:β anomers ratio ≈ 25:1 (based on the ^{1}H NMR spectrum). UV-Vis (DMSO, 298 K, nm (ε, M^{-1} cm^{-1})): 268 (27700), 278 (22800), 295 (sh, ~9500).

[Zn(dtc-Inp-GlcN3)$_2$] (Zn5)

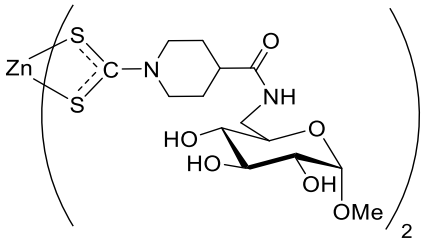

A mixture of 1-*O*-methyl-6-amino-6-deoxy-α-D-glucopyranoside (**GlcN3**) (760.0 mg, 3.93 mmol) and *N*,*N*-diisopropylethylamine (DIPEA, 1.50 mL, 8.64 mmol) in anhydrous DMF (4 mL) was added under stirring to a suspension of [Zn(dtc-Inp-OSu)$_2$] (**Zn0b**) (1.05 g, 1.57 mmol) in anhydrous DMF (4 mL). The mixture was stirred at r.t. under inert atmosphere (N_2) for 16 h and then treated with ethanol (80 mL), leading to the sudden precipitation of a white solid. The precipitate was filtered, washed with methanol (3×15 mL), and then dried under vacuum over P_2O_5, yielding the title compound as a white solid (980.0 mg, 76% yield). M.p. 245-248°C. Anal. (%) calcd. for $C_{28}H_{46}N_4O_{12}S_4Zn$ (MM = 824.31 g mol^{-1}): C, 40.80; H, 5.63; N, 6.80; found: C, 40.91; H, 5.83; N, 6.76. FT-IR (CsI disk, $\tilde{\nu}_{max}$, cm^{-1}): 3392 (br, ν, OH + NH overlapped), 1637 (s, ν, C=O (amide I)), 1543 (m, δ_{ip}, CNH (amide II)), 1494 (s, ν, N–CSS), 1049 (vs, ν, C–OH + C^1–O–CH_3 overlapped), 1010 (s, ν_a, SCS), 564 (w, ν_s, SCS), 366 (w, ν_a, ZnS_4). ^{1}H NMR (400 MHz, DMSO-d_6, 298 K, δ, ppm): 7.97 (dd, J_{HH} = 5.9 Hz, 2H, N*H*), 4.97 (d, J_{HH} = 5.5 Hz, 2H, C^4O*H*), 4.83 (m, 4H, $C^{2',6'}H_{eq}$), 4.82 (d, J_{HH} = 5.5 Hz, 2H, C^3O*H*), 4.75 (d, J_{HH} = 6.5 Hz, 2H, C^2O*H*),

4.51 (d, J_{HH} = 3.6 Hz, 2H, C^1H), 3.55 (m, 2H, C^6H), 3.36 (m, 4H, C^3H + C^5H), 3.24 (s, 6H, OCH_3), 3.24-3.19 (m, 6H, C^2H + $C^{2',6'}H_{ax}$), 3.01 (m, 2H, C^6H'), 2.90 (m, 2H, C^4H), 2.57-2.53 (m, 2H, $C^{4'}H$), 1.78-1.75 (m, 4H, $C^{3',5'}H_{eq}$), 1.62-1.53 (m, 4H, $C^{3',5'}H_{ax}$). $^{13}C\{^1H\}$ NMR (100 MHz, DMSO-d_6, 298 K, δ, ppm): 202.22 (N*C*SS), 173.78 (*C*=O), 99.64 (C^1), 72.95 (C^3), 72.09 (C^4), 71.97 (C^2), 70.30 (C^5), 54.27 (O*C*H_3), 50.74 ($C^{2',6'}H_2$), 40.14 ($C^{4'}H_2$), 40.09 (C^6), 28.42 ($C^{3',5'}H_2$). UV-Vis (DMSO, 298 K, nm (ε, M^{-1} cm^{-1})): 268 (29100), 279 (sh, ~23300), 295 (sh, ~9900).

[Zn(dtc-Inp-GlcN4)$_2$] (Zn6)

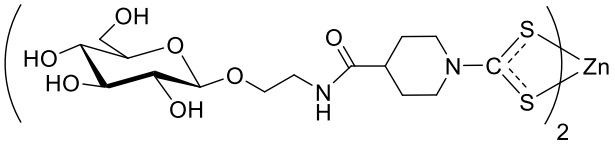

A mixture of 2-aminoethyl β-D-glucopyranoside (**GlcN4**) (91.7 mg, 0.41 mmol) and *N*,*N*-diisopropylethylamine (DIPEA, 180 µL, 1.03 mmol) in anhydrous DMF (3 mL) was added under stirring to a suspension of [Zn(dtc-Inp-OSu)$_2$] (**Zn0b**) (133.5 mg, 0.20 mmol) in anhydrous DMF (1 mL). The mixture was stirred at r.t. under inert atmosphere (N_2) for 16 h and then treated with diethyl ether (60 mL), leading to the sudden precipitation of a white solid. The precipitate was filtered, washed with ethanol (3×10 mL), and then dried under vacuum over P_2O_5, yielding the title compound as a white solid (135.3 mg, 77% yield). M.p. 194-198°C. Anal. (%) calcd. for $C_{30}H_{50}N_4O_{14}S_4Zn$ (MM = 884.36 g mol^{-1}): C, 40.74; H, 5.60; N, 6.34; found: C, 40.50; H, 5.51; N, 6.66. FT-IR (CsI disk, $\tilde{\nu}_{max}$, cm^{-1}): 3392 (br, ν, OH + NH overlapped), 1647 (s, ν, C=O (amide I)), 1556 (m, δ_{ip}, CNH (amide II)), 1494 (s, ν, N–CSS), 1264 (m, amide III), 1078/1035 (vs, ν, C–OH + C^1–O–CH_2), 1004 (sh, ν_a, SCS), 563 (w, ν_s, SCS), 386 (w, ν_a, ZnS_4). ^1H NMR (400 MHz, DMSO-d_6, 298 K, δ, ppm): 7.89 (dd, J_{HH} = 5.6 Hz, 2H, N*H*), 5.01 (d, J_{HH} = 4.2 Hz, 2H, C^2OH), 4.98 (d, J_{HH} = 4.5 Hz, 2H, C^3OH), 4.85 (d, J_{HH} = 5.1 Hz, 2H, C^4OH), 4.83 (m, 4H, $C^{2',6'}H_{eq}$), 4.56 (dd, J_{HH} = 5.7 Hz, 2H, C^6OH), 4.13 (d, J_{HH} = 7.8 Hz, 2H, C^1H), 3.75-3.64 (m, 4H, C^6H + $CH_aH_bCH_2NH$), 3.53-3.47 (m, 2H, C^6H'), 3.42 (m, 2H, $CH_aH_bCH_2NH$), 3.29-3.20 (m, 8H, $C^{2',6'}H_{ax}$ + CH_2NH), 3.17-3.08 (m, 4H, C^3H + C^5H), 3.03 (m, 2H, C^4H), 2.95 (m, 2H, C^2H), 2.45 (m, 2H, $C^{4'}H$), 1.80-1.77 (m, 4H, $C^{3',5'}H_{eq}$), 1.61-1.52 (m, 4H, $C^{3',5'}H_{ax}$). $^{13}C\{^1H\}$ NMR (100 MHz, DMSO-d_6, 298 K, δ, ppm): 202.65 (N*C*SS), 173.69 (*C*=O), 103.17 (C^1), 76.90 (C^3), 76.51 (C^5), 73.47 (C^2), 70.04 (C^4), 67.91 (C^6), 61.08 (CH_2CH_2NH), 50.54 ($C^{2',6'}H_2$), 40.37 ($C^{4'}H_2$), 38.72 (CH_2NH), 28.34 ($C^{3',5'}H_2$). UV-Vis (DMSO, 298 K, nm (ε, M^{-1} cm^{-1})): 268 (20200), 276 (sh,

~18200), 297 (sh, ~11100).

8.3 Chapter 3 – Experimental

[AuBr$_2$(dtc-Inp-OEt)] (Au1)

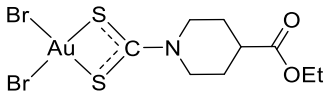

A DMF solution (2 mL) of [Zn(dtc-Inp-OEt)$_2$] (76.5 mg, 0.15 mmol) was added dropwise under stirring to a DMF solution (2 mL) of K[AuBr$_4$]·H$_2$O (170.5 mg, 0.30 mmol) at r.t. The mixture was stirred for 3 h, after which the colour of the solution turned from dark red to orange. Addition of a diethyl ether/*n*-hexane 2:1 solution (60 mL) resulted in the formation of a light orange precipitate. The precipitate was centrifuged and the bulk of supernatant discarded. The residue was subsequently washed with ethanol (15 mL), water/ethanol (1:1, 2×15 mL), and then dried under vacuum with P_2O_5, yielding the title compound as an orange solid (132.2 mg, 78% yield). Orange shiny plate-shaped crystals suitable for X-ray crystallography were obtained upon slow evaporation of an acetone solution of the compound. M.p. 243-246°C (dec.). Anal. (%) calcd. for $C_9H_{14}AuBr_2NO_2S_2$ (MW = 589.11 g mol^{-1}): C, 18.35; H, 2.40; N, 2.38; found: C, 18.27; H, 2.39; N, 2.25. FT-IR (CsI disk, $\tilde{\nu}_{max}$, cm^{-1}): 1729 (vs, ν, C=O), 1571 (vs, ν, N–CSS), 1183 (m, ν, C–OEt), 1040 (m, ν, O–Et), 1002 (w, ν_a, SCS), 536 (w, ν_s, SCS), 413 (w, ν_a, SAuS), 398 (w, ν_s, SAuS), 249 (w, ν_a, BrAuBr), 228 (w, ν_s, BrAuBr). ^{1}H NMR (400 MHz, DMSO-d$_6$, 298 K, δ, ppm): 4.09 (q, J_{HH} = 7.1 Hz, 2H, OCH_2), 4.06 (m, 2H, C$^{2',6'}H_{eq}$), 3.61 (m, 2H, C$^{2',6'}H_{ax}$), 2.90 (tt, J_{HH} = 10.6 Hz, 3.2 Hz, 1H, C$^{4'}H$), 2.08 (m, 2H, C$^{3',5'}H_{eq}$), 1.75 (m, 2H, C$^{3',5'}H_{ax}$), 1.19 (t, J_{HH} = 7.1 Hz, 3H, CH_3). ^{13}C{^{1}H} NMR (100 MHz, DMSO-d$_6$, 298 K, δ, ppm): 187.86 (N*C*SS), 173.16 (*C*=O), 60.92 (O*C*H$_2$), 48.64 (*C*$^{2',6'}$H$_2$), 39.01 (*C*$^{4'}$H), 27.33 (*C*$^{3',5'}$H$_2$), 14.59 (*C*H$_3$). UV-Vis (DMSO, 298 K, nm (ε, M^{-1} cm^{-1})): 273 (26000), 283 (27700), 372 (3900).

[AuBr$_2$(dtc-Inp-NH$_2$)] (Au2)

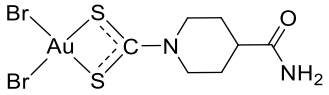

A DMF suspension (8 mL) of [Zn(dtc-Inp-NH$_2$)$_2$] (42.0 mg, 0.09 mmol) was added dropwise under stirring to a DMF solution (2 mL) of K[AuBr$_4$]·H$_2$O (105.4 mg, 0.18 mmol) at r.t. The mixture was stirred for 1.5 h, after which the suspension dissolved completely and the colour of the solution turned from dark red to orange. Addition of

diethyl ether (100 mL) resulted in the formation of an orange precipitate. The precipitate was centrifuged and the bulk of supernatant discarded. The residue was subsequently washed with methanol (3×15 mL) and then dried under vacuum over P_2O_5, yielding the title compound as an orange solid (69.3 mg, 70% yield). M.p. 268-272°C (dec.). Anal. (%) calcd. for $C_7H_{11}AuBr_2N_2OS_2$ (MM = 560.07 g mol^{-1}): C, 15.01; H, 1.98; N, 5.00; found: C, 15.06; H, 2.09; N, 4.96. FT-IR (CsI disk, $\tilde{\nu}_{max}$, cm^{-1}): 3408/3176 (br, $\nu_{a/s}$, NH_2), 1660 (vs, ν, C=O (amide I)), 1620 (w, δ_{ip}, CNH_2 (amide II)), 1565 (s, ν, N–CSS), 1019 (w, ν_a, SCS), 534 (w, ν_s, SCS), 411 (w, ν_a, SAuS), 397 (w, ν_s, SAuS), 232 (w, ν_a, BrAuBr), 227 (w, ν_s, BrAuBr). ^{1}H NMR (400 MHz, DMSO-d_6, ppm): 7.40 (s, 1H, N*H* *cis*), 6.97 (s, 1H, N*H* *trans*), 4.11 (m, J_{HH} = 13.5 Hz, 2H, $C^{2',6'}H_{eq}$), 3.57 (m, 2H, $C^{2',6'}H_{ax}$), 2.62 (tt, J_{HH} = 10.6 Hz, 3.9 Hz, 1H, $C^{4'}H$), 1.97 (m, 2H, $C^{3',5'}H_{eq}$), 1.66 (m, 2H, $C^{3',5'}H_{ax}$). ^{13}C{^{1}H} NMR (100 MHz, DMSO-d_6, 298 K, δ, ppm): 186.90 (N*C*SS), 174.50 (*C*=O), 48.42 ($C^{2',6'}H_2$), 40.33 ($C^{4'}H$), 27.53 ($C^{3',5'}H_2$). UV-Vis (DMSO, 298 K, nm (ε, M^{-1} cm^{-1})): 268 (14200), 272 (14500), 281 (15100), 360 (2600).

[AuBr$_2$(dtc-Inp-GlcN1)] (Au3)

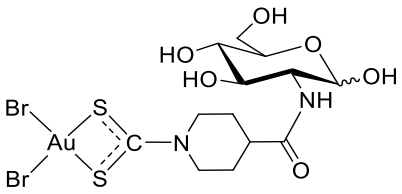

A DMF solution (2 mL) of [Zn(dtc-Inp-glucosamine)$_2$] (74.3 mg, 0.09 mmol) was added dropwise under stirring to a DMF solution (2 mL) of K[$AuBr_4$]·$2H_2O$ (110.5 mg, 0.19 mmol) at r.t. The mixture was stirred for 3 h, after which the colour of the solution turned from dark red to orange. Addition of diethyl ether (40 mL) resulted in the formation of an orange precipitate. The precipitate was centrifuged and the bulk of supernatant discarded. The residue was subsequently washed with methanol (3×10 mL) and then dried under vacuum over P_2O_5, yielding the title compound as an orange solid (100.9 mg, 75% yield). M.p. 210-211°C (dec.). Anal. (%) calcd. for $C_{13}H_{21}AuBr_2N_2O_6S_2$ (MM = 722.21 g mol^{-1}): C, 21.62; H, 2.93; N, 3.88; found: C, 21.78; H, 3.03; N, 3.78. FT-IR (CsI disk, $\tilde{\nu}_{max}$, cm^{-1}): 3306 (br, ν, OH + NH overlapped), 1636 (s, ν, C=O (amide I)), 1561 (vs, ν, N–CSS + δ_{ip}, CNH (amide II)), 1060 (m, ν, C–OH), 1008 (sh, ν_a, SCS), 575 (w, ν_s, SCS), 412 (w, ν_a, SAuS), 392 (w, ν_s, SAuS), 244 (w, ν_a, BrAuBr), 227 (m, ν_s, BrAuBr). ^{1}H NMR (400 MHz, DMSO-d_6, 298 K, δ, ppm): 7.75 (overlapped d, 0.4H, N*H* $_\beta$), 7.73 (d, J_{HH} = 8.1 Hz, 1H, N*H* $_\alpha$), 6.45 (br, 1.4H, $C^1OH_{\alpha+\beta}$), 4.91 (d, 1H, J_{HH} = 3.1 Hz, C^1H_α), 4.45 (d,

0.4H, J_{HH} = 7.8 Hz, C^1*H* $_\beta$), 4.12 (m, 2.8H, C$^{2',6'}$*H* $_{eq\ \alpha+\beta}$), ~4.00 (br, 4.2H, C^{3}O*H* $_{\alpha+\beta}$ + C^{4}O*H* $_{\alpha+\beta}$ + C^{6}O*H* $_{\alpha+\beta}$), 3.69-3.39 (m, 9H, C^2*H* $_\alpha$ + C^4*H* $_{\alpha+\beta}$ + C^5*H* $_\alpha$ + C^6*H* $_{\alpha+\beta}$ + C^6*H*‘ $_{\alpha+\beta}$ + C$^{2',6'}$*H* $_{ax\ \alpha+\beta}$), 3.37-3.23 (m, 0.8H, C^2*H* $_\beta$ + C^3*H* $_\beta$), 3.11-3.04 (m, 1.4H, C^3*H* $_\alpha$ + C^5*H* $_\beta$), 2.75 (m, 1H, C$^{4'}$*H* $_\alpha$), 2.63 (m, 0.4H, C$^{4'}$*H* $_\beta$), 1.98-1.91 (m, 2.8H, C$^{3',5'}$*H* $_{eq\ \alpha+\beta}$), 1.75-1.67 (br m, 2.8H, C$^{3',5'}$*H* $_{ax\ \alpha+\beta}$). ^{13}C{^{1}H} NMR (100 MHz, DMSO-d$_6$, 298 K, δ, ppm): 186.92 (N*C*SS), 172.76 (*C*=O $_\alpha$), 172.74 (*C*=O $_\beta$), 95.33 (*C*^{1} $_\beta$), 90.51 (*C*^{1} $_\alpha$), 76.89 (*C*^{5} $_\beta$), 74.20 (*C*^{3} $_\beta$), 72.12 (*C*^{5} $_\alpha$), 71.08 (*C*^{3} $_\alpha$), 70.77 (*C*^{4} $_\beta$), 70.44 (*C*^{4} $_\alpha$), 61.18 (*C*^{6} $_\beta$), 61.08 (*C*^{6} $_\alpha$), 57.03 (*C*^{2} $_\beta$), 54.26 (*C*^{2} $_\alpha$), 48.44 (*C*$^{2',6'}$H$_2$ $_\alpha$), 48.34 (*C*$^{2',6'}$H$_2$ $_\beta$), 40.45 (*C*$^{4'}$H $_\beta$), 40.13 (*C*$^{4'}$H $_\alpha$), 27.76 (*C*$^{3',5'}$H$_2$ $_\alpha$), 27.34 (*C*$^{3',5'}$H$_2$ $_\beta$). Solution α:β anomers ratio ≈ 2.5:1 (based on the ^{1}H NMR spectrum). UV-Vis (DMSO, 298 K, nm (ε, M^{-1} cm^{-1})): 277 (19700), 320 (sh, ~8100), ~365 (sh, ~2600).

[AuBr$_2$(dtc-Inp-GlcN2)] (Au4)

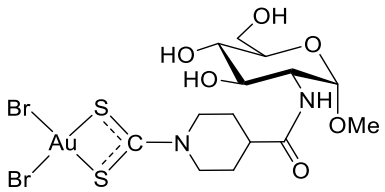

A DMF solution (2 mL) of [Zn(dtc-Inp-GlcN2)$_2$] (88.6 mg, 0.11 mmol) was added dropwise under stirring to a DMF solution (3 mL) of K[AuBr$_4$]·2H$_2$O (128.6 mg, 0.22 mmol) at r.t. The mixture was stirred for 3 h, after which the colour of the solution turned from dark red to orange. Addition of diethyl ether (50 mL) resulted in the formation of an orange precipitate. The precipitate was centrifuged and the bulk of supernatant discarded. The residue was subsequently washed with methanol (3×10 mL) and then dried under vacuum over P$_2$O$_5$, yielding the title compound as an orange solid (129.1 mg, 81% yield). M.p. 198-202°C (dec.).

Anal. (%) calcd. for C$_{14}$H$_{23}$AuBr$_2$N$_2$O$_6$S$_2$ (MM = 736.24 g mol^{-1}): C, 22.84; H, 3.15; N, 3.81; found: C, 22.85; H, 2.98; N, 3.75. FT-IR (CsI disk, $\tilde{\nu}_{max}$, cm^{-1}): 3400/3296 (br, ν, OH + NH overlapped), 1649 (s, ν, C=O (amide I)), 1561 (vs, ν, N–CSS + δ_{ip}, CNH (amide II)), 1059/1040 (vs, ν, C–OH + C^1–O–CH$_3$ overlapped), 1007 (sh, ν_a, SCS), 577 (w, ν_s, SCS), 410 (w, ν_a, SAuS), 393 (w, ν_s, SAuS), 246 (w, ν_a, BrAuBr), 220 (w, ν_s, BrAuBr). ^{1}H NMR (400 MHz, DMSO-d$_6$, 298 K, δ, ppm): 7.86 (d, J_{HH} = 8.2 Hz, 1H, N*H*), 4.97 (br, 3H, C^{3}O*H* + C^{4}O*H* + C^{6}O*H*), 4.52 (d, J_{HH} = 3.5 Hz, 1H, C^1*H*), 4.12 (m, J_{HH} = 13.5 Hz, 2H, C$^{2',6'}$*H* $_{eq}$), 3.68-3.27 (m, 7H, C^2*H* + C^3*H* + C^5*H* + C^6*H* + C^6*H*’ + C$^{2',6'}$*H* $_{ax}$), 3.24 (s, 3H, OC*H*$_3$), 3.12 (dd, J_{HH} = 9.5 Hz, 8.7 Hz, 1H, C^4*H*), 2.75 (m, 1H, C$^{4'}$*H*), 1.98-1.91 (m,

2H, $C^{3',5'}H_{eq}$), 1.76-1.66 (m, 2H, $C^{3',5'}H_{ax}$). $^{13}C\{^1H\}$ NMR (100 MHz, DMSO-d_6, 298 K, δ, ppm): 186.93 (N*C*SS), 172.89 (*C*=O), 97.83 (C^1), 72.80 (C^5), 70.77 (C^3), 70.70 (C^4), 60.80 (C^6), 54.43 (O*C*H$_3$), 53.73 (C^2), 48.44 ($C^{2',6'}H_2$), 40.34 ($C^{4'}H$), 27.70 ($C^{3',5'}H_2$). No NMR signals assignable to the β anomer were detected. UV-Vis (DMSO, 298 K, nm (ε, M^{-1} cm^{-1})): 280 (20500), 314 (12400), ~354 (sh, ~3500).

[AuBr$_2$(dtc-Inp-GlcN3)] (Au5)

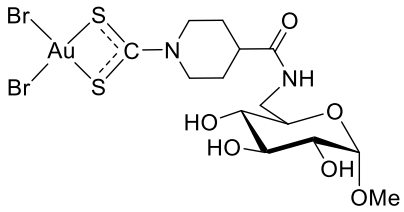

A DMF solution (2 mL) of [Zn(dtc-Inp-GlcN3)$_2$] (101.7 mg, 0.12 mmol) was added dropwise under stirring to a DMF solution (3 mL) of K[AuBr$_4$]·2H$_2$O (148.8 mg, 0.25 mmol) at r.t. The mixture was stirred for 2 h, after which the colour of the solution turned from dark red to orange. Addition of diethyl ether (60 mL) resulted in the formation of an orange precipitate. The precipitate was centrifuged and the bulk of supernatant discarded. The residue was subsequently washed with methanol (3×10 mL) and then dried under vacuum over P_2O_5, yielding the title compound as an orange solid (161.2 mg, 87% yield). M.p. 217-220 °C (dec.). Anal. (%) calcd. for $C_{14}H_{23}AuBr_2N_2O_6S_2$ (MM = 736.24 g mol^{-1}): C, 22.84; H, 3.15; N, 3.81; found: C, 22.95; H, 3.07; N, 3.78. FT-IR (CsI disk, $\tilde{\nu}_{max}$, cm^{-1}): 3400 (br, ν, OH + NH overlapped), 1650 (s, ν, C=O (amide I)), 1555 (vs, ν, N–CSS + δ_{ip}, CNH (amide II)), 1050 (vs, ν, C–OH + C^1–O–CH_3 overlapped), 1011 (m, ν_a, SCS), 570 (w, ν_s, SCS), 398 (br, $\nu_{a/s}$, SAuS), 254 (w, ν_a, BrAuBr), 227 (w, ν_s, BrAuBr). ^1H NMR (400 MHz, DMSO-d_6, 298 K, δ, ppm): 7.99 (dd, J_{HH} = 5.7 Hz, 1H, N*H*), 4.51 (d, J_{HH} = 3.6 Hz, 1H, C^1H), 4.13 (m, J_{HH} = 13.4 Hz, 2H, $C^{2',6'}H_{eq}$), ~3.60 (br, 3H, C^2OH + C^3OH + C^4OH), 3.59-3.53 (m, 3H, C^6H + $C^{2',6'}H_{ax}$), 3.37-3.30 (m, 2H, C^3H + C^5H), 3.24 (s, 3H, OC*H*$_3$), 3.19 (dd, J_{HH} = 9.6 Hz, 3.6 Hz, 1H, C^2H), 3.05-2.94 (m, 1H, C^6H'), 2.90 (dd, J_{HH} = 9.2 Hz, 1H, C^4H), 2.71 (tt, J_{HH} = 10.7 Hz, 3.8 Hz, 1H, $C^{4'}H$), 1.93 (m, 2H, $C^{3',5'}H_{eq}$), 1.75-1.66 (m, 2H, $C^{3',5'}H_{ax}$). $^{13}C\{^1H\}$ NMR (100 MHz, DMSO-d_6, 298 K, δ, ppm): 187.00 (N*C*SS), 172.74 (*C*=O), 99.65 (C^1), 72.96 (C^3), 72.07 (C^4), 71.94 (C^2), 70.30 (C^5), 54.35 (O*C*H$_3$), 48.41 ($C^{2',6'}H_2$), 40.47 ($C^{4'}H$), 40.10 (C^6), 27.67 ($C^{3',5'}H_2$). UV-Vis (DMSO, 298 K, nm (ε, M^{-1} cm^{-1})): 278 (15600), 313 (8700), 355 (sh, ~2700).

[AuBr$_2$(dtc-Inp-OSu)] (Au6)

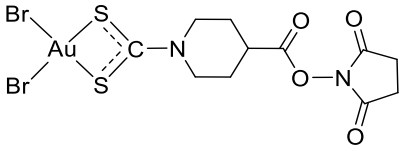

A DMF suspension (2 mL) of [Zn(dtc-Inp-OSu)$_2$] (128.0 mg, 0.19 mmol) was added dropwise under stirring to a DMF solution (4 mL) of K[AuBr$_4$]·H$_2$O (225.7 mg, 0.38 mmol) at r.t. The mixture was stirred for 1.5 h, after which the colour of the solution turned from dark red to orange. Addition of diethyl ether (60 mL) resulted in the formation of an orange precipitate. The precipitate was centrifuged and the bulk of supernatant discarded. The residue was subsequently washed with methanol (3×15 mL), and then dried under vacuum with P_2O_5, yielding the title compound as an orange solid (219.7 mg, 88% yield). M.p. 281-283°C (dec.). Anal. (%) calcd. for $C_{11}H_{13}AuBr_2N_2O_4S_2$ (MW = 658.13 g mol^{-1}): C, 20.08; H, 1.99; N, 4.26; found: C, 20.22; H, 2.31; N, 4.01. FT-IR (CsI disk, $\tilde{\nu}_{max}$, cm^{-1}): 1808 (m, ν_{ip}, C=O succinimidyl), 1779 (m, ν_{oop}, C=O succinimidyl), 1738 (vs, ν, C=O ester), 1575 (s, ν, N–CSS), 1205 (s, ν, C–OSu), 989 (m, ν_a, SCS), 573 (w, ν_s, SCS), 405 (w, ν_a, SAuS), 372 (w, ν_s, SAuS), 245 (w, ν_a, BrAuBr), 232 (w, ν_s, BrAuBr). ^{1}H NMR (400 MHz, DMSO-d$_6$, 298 K, δ, ppm): 4.12 (m, J_{HH} = 13.6 Hz, 3.7 Hz, 2H, C$^{2',6'}$*H* $_{eq}$), 3.67 (m, 2H, C$^{2',6'}$*H* $_{ax}$), 3.43 (tt, J_{HH} = 10.5 Hz, 3.9 Hz, 1H, C$^{4'}$*H*), 2.82 (br s, 4H, C*H*$_{2\ succ}$) 2.21 (m, 2H, C$^{3',5'}$*H* $_{eq}$), 1.90 (m, 2H, C$^{3',5'}$*H* $_{ax}$). ^{13}C{^{1}H} NMR (100 MHz, DMSO-d$_6$, 298 K, δ, ppm): 188.07 (N*C*SS), 170.13 (*C*=O $_{succ}$), 169.11 (*C*=O $_{ester}$) 47.65 (*C*$^{2',6'}$H$_2$), 37.01 (*C*$^{4'}$H), 26.53 (*C*$^{3',5'}$H$_2$), 25.49 (*C*H$_{2\ succ}$). UV-Vis (DMSO, 298 K, nm (ε, M^{-1} cm^{-1})): 279 (16000), 315 (sh, ~8400).

[AuCl$_2$(dtc-Inp-GlcN1)] (Au7)

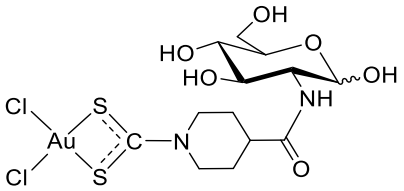

A DMF solution (2 mL) of [Zn(dtc-Inp-glucosamine)$_2$] (112.9 mg, 0.14 mmol) was added dropwise under stirring to a DMF solution (2 mL) of Na[AuCl$_4$]·2H$_2$O (112.7 mg, 0.28 mmol) at r.t. The mixture was stirred for 2 h, after which the colour of the solution turned from bright yellow to yellow-orange. Addition of diethyl ether (40 mL) resulted in the formation of a yellow precipitate. The precipitate was centrifuged and the bulk of supernatant discarded. The residue was subsequently washed with methanol (3×10 mL)

and then dried under vacuum over P_2O_5, yielding the title compound as a yellow solid (94.5 mg, 53% yield). M.p. 214-219°C (dec.). Anal. (%) calcd. for $C_{13}H_{21}AuCl_2N_2O_6S_2$ (MW = 633.31 g mol^{-1}): C, 24.66; H, 3.34; N, 4.42; found: C, 24.48; H, 3.14; N, 4.12. FT-IR (CsI disk, $\tilde{\nu}_{max}$, cm^{-1}): 3369 (br, ν, OH + NH overlapped), 1649 (s, ν, C=O (amide I)), 1554 (vs, ν, N–CSS + δ_{ip}, CNH (amide II)), 1059 (s, ν, C–OH), 1028 (m, ν_a, SCS), 575 (w, ν_s, SCS), 406 (w, $\nu_{a/s}$, SAuS), 357 (w, $\nu_{a/s}$, ClAuCl). ^{1}H NMR (400 MHz, DMSO-d_6, 298 K, δ, ppm): 7.78 (d, J_{HH} = 7.8 Hz, 1H, N*H* $_\alpha$), 7.75 (d, J_{HH} = 7.8 Hz, 0.4H, N*H* $_\beta$), 6.45 (br, 1.4H, C^{1}O*H* $_{\alpha+\beta}$), 4.92 (d, 1H, J_{HH} = 3.1 Hz, C^1*H* $_\alpha$), ~ 4.70 (br, 4.2H, C^{3}O*H* $_{\alpha+\beta}$ + C^{4}O*H* $_{\alpha+\beta}$ + C^{6}O*H* $_{\alpha+\beta}$), 4.45 (d, 0.4H, J_{HH} = 7.4 Hz, C^1*H* $_\beta$), 4.21-4.13 (m, 2.8H, C$^{2',6'}$*H* $_{eq\ \alpha+\beta}$), 3.69-3.28 (m, 9.8H, C^2*H* $_{\alpha+\beta}$ + C^3*H* $_\beta$ + C^4*H* $_{\alpha+\beta}$ + C^5*H* $_\alpha$ + C^6*H* $_{\alpha+\beta}$ + C^6*H*‘ $_{\alpha+\beta}$ + C$^{2',6'}$*H* $_{ax\ \alpha+\beta}$), 3.13-3.06 (m, 1.4H, C^3*H* $_\alpha$ + C^5*H* $_\beta$), 2.77 (m, 1H, C$^{4'}$*H* $_\alpha$), 2.66 (m, 0.4H, C$^{4'}$*H* $_\beta$), 2.03-1.91 (br m, 2.8H, C$^{3',5'}$*H* $_{eq\ \alpha+\beta}$), 1.76-1.65 (br m, 2.8H, C$^{3',5'}$*H* $_{ax\ \alpha+\beta}$). ^{13}C{^{1}H} NMR (100 MHz, DMSO-d_6, 298 K, δ, ppm): 192.52 (N*C*SS), 172.91 (*C*=O $_\alpha$), 172.83 (*C*=O $_\beta$), 95.38 (*C*^{1} $_\beta$), 90.49 (*C*^{1} $_\alpha$), 76.88 (*C*^{5} $_\beta$), 74.17 (*C*^{3} $_\beta$), 72.13 (*C*^{5} $_\alpha$), 71.05 (*C*^{3} $_\alpha$), 70.79 (*C*^{4} $_\beta$), 70.36 (*C*^{4} $_\alpha$), 61.16 (*C*^{6} $_\beta$), 61.08 (*C*^{6} $_\alpha$), 57.01 (*C*^{2} $_\beta$), 54.35 (*C*^{2} $_\alpha$), 49.05 (*C*$^{2',6'}$H$_2$ $_\beta$), 48.77 (*C*$^{2',6'}$H$_2$ $_\alpha$), 40.30 (*C*$^{4'}$H $_{\alpha+\beta}$), 27.97 (*C*$^{3',5'}$H$_2$ $_\alpha$), 27.72 (*C*$^{3',5'}$H$_2$ $_\beta$). Solution α:β anomers ratio ≈ 2.5:1 (based on the ^{1}H NMR spectrum). UV-Vis (DMSO, nm (ε, M^{-1} cm^{-1})): 277 (18800), 319 (13800).

[AuCl$_2$(dtc-Inp-GlcN3)] (Au8)

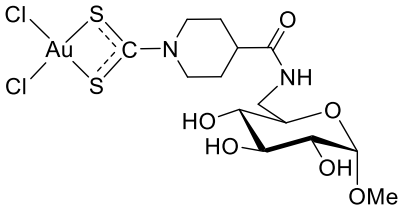

A DMF solution (2 mL) of [Zn(dtc-Inp-GlcN3)$_2$] (98.6 mg, 0.12 mmol) was added dropwise under stirring to a DMF solution (2 mL) of Na[AuCl$_4$]·2H$_2$O (97.0 mg, 0.24 mmol) at r.t. The mixture was stirred for 2 h, after which the colour of the solution turned from bright yellow to yellow-orange. Addition of diethyl ether (40 mL) resulted in the formation of a yellow precipitate. The precipitate was centrifuged and the bulk of supernatant discarded. The residue was subsequently redissolved in methanol (20 mL). The resulting yellow solution was allowed to slowly concentrate under the fume hood at room temperature to about half of the initial volume, leading to the formation of a brown solid. The mixture was filtered, the resulting filtered solution was evaporated to dryness and then dried under vacuum over P_2O_5, yielding the title compound as an orange solid

(44.4 mg, 28% yield). M.p. 218-223°C (dec.). Anal. (%) calcd. for $C_{14}H_{23}AuCl_2N_2O_6S_2$ (MW = 647.33 g mol^{-1}): C, 25.98; H, 3.58; N, 4.33; found: C, 25.86; H, 3.68; N, 4.18. FT-IR (CsI disk, $\tilde{\nu}_{max}$, cm^{-1}): 3403/3323 (br, ν, OH + NH overlapped), 1642 (s, ν, C=O (amide I)), 1552 (vs, ν, N–CSS + δ_{ip}, CNH (amide II)), 1051 (vs, ν, C–OH + C^1–O–CH_3 overlapped), 1012 (m, ν_a, SCS), 543 (w, ν_s, SCS), 394 (w, ν_a, SAuS), 376 (w, ν_s, SAuS), 342 (w, $\nu_{a/s}$, ClAuCl). ^{1}H NMR (400 MHz, DMSO-d_6, 298 K, δ, ppm): 8.05 (dd, J_{HH} = 5.7 Hz, 1H, N*H*), ~5.00/4.82 (br, 3H, C^2O*H* + C^3O*H* + C^4O*H*), 4.51 (d, J_{HH} = 3.6 Hz, 1H, C^1*H*), 4.20 (m, J_{HH} = 13.4 Hz, 2H, $C^{2',6'}H_{eq}$), 3.60-3.54 (m, 3H, C^6H + $C^{2',6'}H_{ax}$), 3.37-3.33 (m, 2H, C^3H + C^5H), 3.24 (s, 3H, OCH_3), 3.19 (dd, J_{HH} = 9.6 Hz, 3.6 Hz, 1H, C^2H), 3.04-2.97 (m, 1H, C^6H'), 2.90 (dd, J_{HH} = 9.2 Hz, 1H, C^4H), 2.76-2.69 (m, 1H, $C^{4'}H$), 2.00-1.92 (m, 2H, $C^{3',5'}H_{eq}$), 1.75-1.64 (m, 2H, $C^{3',5'}H_{ax}$). ^{13}C{^{1}H} NMR (100 MHz, DMSO-d_6, 298 K, δ, ppm): 192.61 (N*C*SS), 172.91 (*C*=O), 99.66 (C^1), 72.97 (C^3), 72.07 (C^4), 71.94 (C^2), 70.30 (C^5), 54.33 (OCH_3), 48.73 ($C^{2',6'}H_2$), 40.40 ($C^{4'}H$), 40.12 (C^6), 27.96 ($C^{3',5'}H_2$). UV-Vis (DMSO, 298 K, nm (ε, M^{-1} cm^{-1})): 278 (18400), 320 (14700).

8.4 Chapter 4 – Experimental

[Au(Bnpy)Cl$_2$] (Au9)

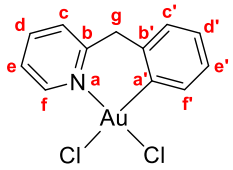

Method A: 2-benzylpyridine (102 µL, 0.63 mmol) was added dropwise under stirring to an aqueous solution (10 mL) of $Na[AuCl_4]\cdot 2H_2O$ (249.8 mg, 0.63 mmol) at r.t. The mixture was stirred for 16 h under reflux, after which the colour of the solution turned from yellow to pale yellow, with formation of an off-white precipitate. The precipitate was filtered and the bulk of supernatant discarded. The residue was subsequently washed with water (3×10 mL) and then dried under vacuum over P_2O_5. Recrystallization from a solution of the residue in dichloromethane/diethyl ether yielded the title compound as a white crystalline solid (214.6 mg, 78% yield).

Method B: 2-benzylpyridine (102 µL, 0.63 mmol) was added dropwise under stirring to an aqueous solution (10 mL) of $Na[AuCl_4]\cdot 2H_2O$ (251.4 mg, 0.63 mmol) at r.t. The mixture was heated under microwaves at 140°C for 20 min, after which the colour of the solution turned from yellow to pale yellow, with formation of an off-white precipitate. The precipitate was filtered and the bulk of supernatant discarded. The residue was subsequently washed with water (3×10 mL) and then dried under vacuum over P_2O_5.

Recrystallization from a solution of the residue in dichloromethane/diethyl ether yielded the title compound as a white crystalline solid (151.5 mg, 55% yield). FT-IR (CsI disk, $\tilde{\nu}_{max}$, cm^{-1}): 3116/3050 (w, ν, C–H aromatic), 2978/2911 (w, ν, C–H aliphatic), 1610 (m, ν, quadrant), 1566 (m, ν, quadrant), 1460 (m, ν, semicircle), 1438 (s, ν, semicircle), 1026 (s, δ_{ip}, CH rocking), 751 (vs, δ, adjacent H wagging), 359 (m, ν, Au–^{35}Cl trans to N), 350 (w, ν, Au–^{37}Cl trans to N) 294 (s, ν, Au–Cl trans to C). ^{1}H NMR (400 MHz, DMSO-d_6, 298 K, δ, ppm): 9.17 (m, J_{HH} = 6.0 Hz, 1H, $C^{f}H$), 8.26 (m, J_{HH} = 7.7 Hz, 1H, $C^{d}H$), 7.99 (m, J_{HH} = 7.9 Hz, 1H, $C^{c}H$), 7.71 (m, 1H, $C^{e}H$), 7.40 (m, J_{HH} = 7.7 Hz, 1H, $C^{f'}H$), 7.24 (m, J_{HH} = 7.2 Hz, 1.1 Hz. 1H, $C^{c'}H$), 7.18 (m, J_{HH} = 7.0 Hz, 1H, $C^{d'}H$), 7.07 (m, J_{HH} = 7.3 Hz, 1H, $C^{e'}H$), 4.61, 4.34 (m (AB pattern), $^{2}J_{HH}$ = 15.1 Hz, 2H, $C^{g}H_2$). ^{13}C{^{1}H} NMR (100 MHz, DMSO-d_6, 298 K, δ, ppm): 155.69 (C^{b}), 152.09 (C^{f}), 143.29 (C^{d}), 141.09 ($C^{b'}$), 132.72 ($C^{f'}$), 131.96 ($C^{a'}$), 128.63 ($C^{d'}$), 127.96 ($C^{e'}$), 126.94 ($C^{c'}$), 126.41 (C^{c}), 124.50 (C^{e}), 46.07 ($C^{g}H_2$).

Experimental data are consistent with those reported in the literature.[17,18]

[Au(dtc-Inp-OEt)(Bnpy)]PF_6 (Au10)

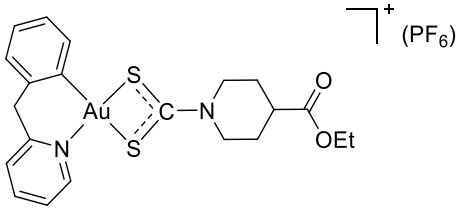

<u>*Method A*</u>: a dichloromethane solution (4 mL) of (H_2-Inp-OEt)(dtc-Inp-OEt) (44.8 mg, 0.11 mmol) was added dropwise under stirring to a dichloromethane suspension (4 mL) of [Au(Bnpy)Cl_2] (49.5 mg, 0.11 mmol) at r.t. The mixture was stirred for 15 min, during which it turned clear and the colour of the solution turned from yellow to pale yellow. The solution was evaporated to dryness at low temperature (<40°C), affording a pale yellow oily residue. The residue was redissolved in methanol (3 mL), then an aqueous solution (3 mL) of KPF_6 (43.0 mg, 0.23 mmol) was added dropwise. A light yellow precipitate formed. The mixture was stirred for 30 min, then the precipitate was centrifuged and the bulk of supernatant discarded. The residue was subsequently washed with water (3×5 mL) and then dried under vacuum over P_2O_5, yielding the title compound as a light yellow solid (74.2 mg, 88% yield).

<u>*Method B*</u>: a DMF solution (2 mL) of [Zn(dtc-Inp-OEt)$_2$] (21.3 mg, 0.04 mmol) was added dropwise under stirring to a DMF solution (1 mL) of [Au(Bnpy)Cl_2] (35.1 mg, 0.08 mmol) at r.t. The mixture was stirred for 30 min, during which it turned clear and the colour of

the solution turned from yellow to pale yellow. Solid KPF_6 (30.5 mg, 0.17 mmol) was added, and the mixture was stirred for further 30 min. The solution was evaporated to dryness at low temperature (<40°C), affording a sticky white residue. The residue was then redissolved in methanol (3 mL). Addition of water (3 mL) to the methanol solution resulted in the formation of a white precipitate. The precipitate was centrifuged and the bulk of supernatant discarded. The residue was subsequently washed with water (3×5 mL) and then dried under vacuum over P_2O_5, yielding the title compound as a white solid (46.9 mg, 78% yield).

Method C: a dichloromethane solution (2 mL) of [Zn(dtc-Inp-OEt)$_2$] (20.7 mg, 0.04 mmol) was added dropwise under stirring to a dichloromethane solution (1 mL) of [Au(Bnpy)Cl$_2$] (34.1 mg, 0.08 mmol) at r.t. The mixture was stirred for 15 min, during which it turned clear and the colour of the solution turned from yellow to pale yellow. The solution was evaporated to dryness at low temperature (<40°C), affording a pale yellow oily residue. The residue was then redissolved in methanol (3 mL). Solid KPF_6 (29.9 mg, 0.16 mmol) was added, and the mixture was stirred for further 30 min. Addition of water (3 mL) to the methanol solution resulted in the formation of a white precipitate. The precipitate was centrifuged and the bulk of supernatant discarded. The residue was subsequently washed with water (3×5 mL) and then dried under vacuum over P_2O_5, yielding the title compound as a white solid (51.5 mg, 89% yield). Colourless crystals suitable for X-ray crystallography were obtained upon slow evaporation of a dichloromethane/methanol solution of the compound. M.p. 192-193°C (dec.). Anal. (%) calcd. for $C_{21}H_{24}AuF_6N_2O_2PS_2$ (MM = 742.49 g mol^{-1}): C, 33.97; H, 3.96; N, 3.77; found: C, 34.18; H, 3.22; N, 3.92. FT-IR (CsI disk, $\tilde{\nu}_{max}$, cm^{-1}): 1728 (s, ν, C=O), 1551 (s, ν, N–CSS), 1195 (m, ν, C–OEt), 1038 (m, ν, O–Et), 1026 (m, ν_a, SCS), 842 (vs, ν_a, PF_6^-), 578 (w, ν_s, SCS), 558 (s, δ_{ip}, PF_6^- scissoring), 409 (w, $\nu_{a/s}$, SAuS). ^{1}H NMR (400 MHz, DMSO-d$_6$, 298 K, δ, ppm): 8.98 (m (app d), J_{HH} = 5.8 Hz, 1H, C^f*H*), 8.33 (m (app t), J_{HH} = 7.7 Hz, 1.4 Hz, 1H, C^d*H*), 8.09 (m (app d), J_{HH} = 7.5 Hz, 1H, C^c*H*), 7.73 (m, 1H, C^e*H*), 7.41-7.36 (m, 2H, C$^{c'}$*H* + C$^{f'}$*H*), 7.29 (m (app t), J_{HH} = 7.0 Hz, 1H, C$^{d'}$*H*), 7.15 (m (app td), J_{HH} = 7.5 Hz, 1.4 Hz, 1H, C$^{e'}$*H*), 4.54 (s, 2H, C^g*H*$_2$), 4.36/4.25 (2m, 2H, C$^{2',6'}$*H* $_{eq}$), 4.11 (q, J_{HH} = 7.1 Hz, 2H, OC*H*$_2$), 3.77/3.68 (m, 2H, C$^{2',6'}$*H* $_{ax}$), 2.93 (tt, J_{HH} = 10.5 Hz, 3.8 Hz, 1H, C$^{4'}$*H*), 2.15 (m, 2H, C$^{3',5'}$*H* $_{eq}$), 1.71 (m, 2H, C$^{3',5'}$*H* $_{ax}$), 1.21 (t, J_{HH} = 7.1 Hz, 3H, C*H*$_3$). ^{13}C{^{1}H} NMR (100 MHz, DMSO-d$_6$, 298 K, δ, ppm): 192.58 (N*C*SS), 172.86 (*C*=O), 156.06 (*C*^{b}), 151.88 (*C*^{f}), 145.30 (*C*$^{b'}$), 143.62 (*C*^{d}), 133.22 (*C*$^{a'}$), 130.61 (*C*$^{f'}$), 128.93 (*C*$^{c'}$), 128.63 (*C*$^{d'}$), 128.30 (*C*$^{e'}$), 127.00 (*C*^{c}), 125.61 (*C*^{e}), 60.42 (O*C*H$_2$),

49.94/47.99 ($C^{2',6'}H_2$), 45.99 ($C^{g}H_2$), 39.09 ($C^{4'}H$), 27.61/27.38 ($C^{3',5'}H_2$), 14.05 (CH_3). ESI(+)-MS: *m/z* calcd. for $[M\text{-}PF_6]^+$: 597.0945; found: 597.0891 (100%). UV-Vis (DMSO, 298 K, nm (ε, M^{-1} cm^{-1})): 268 (30000), ~293 (sh, ~15700).

[Au(dtc-Inp-NH$_2$)(Bnpy)]PF$_6$ (Au11)

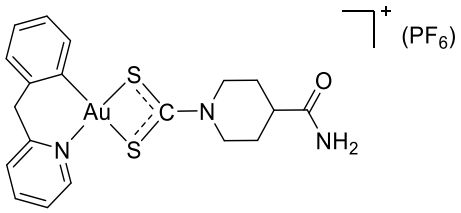

A DMF suspension (2 mL) of [Zn(dtc-Inp-NH_2)$_2$] (25.5 mg, 0.05 mmol) was added dropwise under stirring to a DMF solution (1 mL) of [Au(Bnpy)Cl_2] (47.2 mg, 0.11 mmol) at r.t. The mixture was stirred for 30 min, during which it turned clear and the colour of the solution turned from yellow to pale yellow. Solid KPF_6 (52.5 mg, 0.28 mmol) was added, and the mixture was stirred for further 30 min. The solution was evaporated to dryness at low temperature (<40°C), affording a sticky white residue. The residue was then resuspended in water (15 mL), resulting in the formation of a white precipitate. The precipitate was centrifuged and the bulk of supernatant discarded. The residue was subsequently washed with water (3×5 mL) and then dried under vacuum over P_2O_5, yielding the title compound as a white solid (60.6 mg, 79% yield). Pale yellow plate-shaped crystals suitable for X-ray crystallography were obtained upon slow evaporation of an acetonitrile solution (solvate with acetonitrile) and a dichloromethane/methanol solution (no solvate) of the compound. M.p. 194-196°C (dec.). Anal. (%) calcd. for $C_{19}H_{21}AuF_6N_3OPS_2$ (MM = 713.45 g mol^{-1}): C, 31.99; H, 2.97; N, 5.89; found: C, 31.92; H, 2.98; N, 6.24. FT-IR (CsI disk, $\tilde{\nu}_{max}$, cm^{-1}): 3455/3203 (br, $\nu_{a/s}$, NH_2), 1666 (s, ν, C=O (amide I)), 1611 (s, δ_{ip}, CNH_2 (amide II)), 1556 (s, ν, N–CSS), 1026 (m, ν_a, SCS), 842 (vs, ν_a, PF_6^-), 558 (s, δ_{ip}, PF_6^- scissoring + ν_s, SCS, overlapped), 415 (w, $\nu_{a/s}$, SAuS). ^{1}H NMR (400 MHz, DMSO-d_6, 298 K, δ, ppm): 8.98 (m (app dd), J_{HH} = 5.9 Hz, 0.9 Hz, 1H, C^fH), 8.33 (m (app td), J_{HH} = 7.8 Hz, 1.2 Hz, 1H, C^dH), 8.09 (m (app d), J_{HH} = 7.4 Hz, 1H, C^cH), 7.73 (m, 1H, C^eH), 7.46 (br s, 1H, NH_{cis}), 7.41-7.36 (m, 2H, $C^{c'}H$ + $C^{f'}H$), 7.29 (m (app td), J_{HH} = 7.3 Hz, 1.2 Hz, 1H, $C^{d'}H$), 7.17 (m (app td), J_{HH} = 7.5 Hz, 1.4 Hz, 1H, $C^{e'}H$), 7.00 (br s, 1H, NH_{trans}), 4.55 (s, 2H, C^gH_2), 4.41/4.28 (2m, 2H, $C^{2',6'}H_{eq}$), 3.73/3.62 (m, 2H, $C^{2',6'}H_{ax}$), 2.65 (tt, J_{HH} = 10.7 Hz, 3.8 Hz, 1H, $C^{4'}H$), 2.05-2.01 (m, 2H, $C^{3',5'}H_{eq}$), 1.74-1.60 (m, 2H, $C^{3',5'}H_{ax}$). ^{13}C{^{1}H} NMR (100 MHz, DMSO-d_6, 298 K, δ, ppm): 192.10 (N*C*SS), 174.70 (*C*=O), 156.08 (C^b), 151.90 (C^f), 145.32 ($C^{b'}$), 143.61 (C^d),

133.24 ($C^{a'}$), 130.62 ($C^{f'}$), 128.91 ($C^{c'}$), 128.61 ($C^{d'}$), 128.28 ($C^{e'}$), 127.00 (C^{c}), 125.60 (C^{e}), 50.32/48.33 ($C^{2',6'}H_2$), 45.98 ($C^{g}H_2$), 39.09 ($C^{4'}H$), 28.36/28.07 ($C^{3',5'}H_2$). ESI(+)-MS: *m/z* calcd. for $[M\text{-}PF_6]^+$: 568.0792; found: 568.0808 (100%). UV-Vis (DMSO, 298 K, nm (ε, M^{-1} cm^{-1})): 268 (32200), 271 (31800), ~292 (sh, ~17000), ~342 (~3200).

[Au(dtc-Inp-GlcN1)(Bnpy)]PF_6 (Au12)

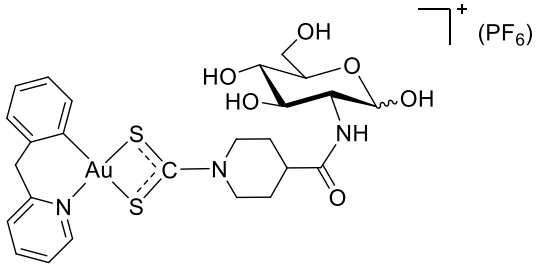

A DMF suspension (2 mL) of [Zn(dtc-Inp-GlcN1)$_2$] (45.8 mg, 0.06 mmol) was added dropwise under stirring to a DMF solution (1 mL) of [Au(Bnpy)Cl_2] (50.1 mg, 0.12 mmol) at r.t. The mixture was stirred for 30 min, during which it turned clear and the colour of the solution turned from yellow to pale yellow. Solid KPF_6 (59.8 mg, 0.32 mmol) was added, and the mixture was stirred for further 30 min. Addition of diethyl ether (30 mL) resulted in the formation of a cloudy mixture and a pale yellow sticky residue. The residue was centrifuged and the bulk of supernatant discarded. The residue was subsequently triturated with a mixture of diethyl ether/dichloromethane (1:1, 10 mL), filtered, washed with diethyl ether/dichloromethane (1:1, 3×15 mL), and then dried with a gentle stream of N_2. The residue was then resuspended in water (5 mL), resulting in the formation of a white precipitate. The precipitate was centrifuged and the bulk of supernatant discarded. The residue was subsequently washed with water (3×5 mL) and then dried under vacuum over P_2O_5, yielding the title compound as an off-white solid (34.5 mg, 34% yield). Anal. (%) calcd. for $C_{25}H_{31}AuF_6N_3O_6PS_2$ (MM = 875.89 g mol^{-1}): C, 34.29; H, 3.57; N, 4.80; found: C, 34.45; H, 3.56; N, 4.81. M.p. 177-181°C (dec.). FT-IR (CsI disk, $\tilde{\nu}_{max}$, cm^{-1}): 3414 (br, ν, OH + NH overlapped), 1659 (m, ν, C=O (amide I)), 1554 (s, ν, N–CSS + δ_{ip}, CNH (amide II)), 1065 (m, ν, C–OH), 1028 (s, ν_a, SCS), 843 (vs, ν_a, PF_6^-), 575 (w, ν_s, SCS), 559 (s, δ_{ip}, PF_6^- scissoring), 405 (w, $\nu_{a/s}$, SAuS). ^{1}H NMR (400 MHz, DMSO-d_6, 298 K, *δ*, ppm): 8.99 (m (app d), J_{HH} = 5.6 Hz, 1H, C^fH), 8.33 (m (app td), J_{HH} = 7.7 Hz, 0.9 Hz, 1H, C^dH), 8.09 (m (app d), J_{HH} = 7.7 Hz, 1H, C^cH), 7.93 (d, J_{HH} = 8.3 Hz, 1H, N*H*), 7.72 (m, 1H, C^eH), 7.41-7.37 (m, 2H, $C^{c'}H$ + $C^{f'}H$), 7.29 (m (app t), J_{HH} = 7.3 Hz, 1H, $C^{d'}H$), 7.17 (m (app t), J_{HH} = 7.3 Hz, 1H, $C^{e'}H$), 4.90 (br, 3H, C^3OH + C^4OH + C^6OH), 4.97-4.91 (m, 2H, C^1H_α + C^3OH_α), 4.54 (s, 3H, C^gH_2), 4.44-4.30 (m, 5H, C^1H_β + C^4OH

$_{\alpha+\beta}$ + C$^{2',6'}H_{\text{eq }\alpha+\beta}$), 3.78-3.28 (m, 10.5H, C$^2H_{\alpha+\beta}$ + C$^3H_{\beta}$ + C$^4H_{\alpha+\beta}$ + C$^5H_{\alpha}$ + C$^6H_{\alpha+\beta}$ + C$^6H'_{\alpha+\beta}$ + C$^{2',6'}H_{\text{ax }\alpha+\beta}$), 3.14-3.02 (m, 1.5H, C$^3H_{\alpha}$ + C$^5H_{\beta}$), 2.79 (tt, J_{HH} = 10.6 Hz, 3.6 Hz, 1H, C$^{4'}H_{\alpha}$), 2.67 (tt, J_{HH} = 10.6 Hz, 3.7 Hz, 0.5H, C$^{4'}H_{\beta}$), 2.05-1.95 (m, 3H, C$^{3',5'}H_{\text{eq }\alpha+\beta}$), 1.74-1.65 (m, 3H, C$^{3',5'}H_{\text{ax }\alpha+\beta}$). ^{13}C{^{1}H} NMR (100 MHz, DMSO-d$_6$, 298 K, δ, ppm): 192.11 (N*C*SS), 172.95 (*C*=O $_{\alpha}$), 172.81 (*C*=O $_{\beta}$), 156.11 (*C*^{b}), 151.90 (*C*^{f}), 145.35 (*C*$^{b'}$), 143.62 (*C*^{d}), 133.27 (*C*$^{a'}$), 130.65 (*C*$^{f'}$), 128.93 (*C*$^{c'}$), 128.62 (*C*$^{d'}$), 128.30 (*C*$^{e'}$), 127.01 (*C*^{c}), 125.61 (*C*^{e}), 95.37 (*C*^{1} $_{\alpha}$), 90.54 (*C*^{1} $_{\beta}$), 76.90 (*C*^{5} $_{\beta}$), 74.22 (*C*^{3} $_{\beta}$), 72.14 (*C*^{5} $_{\alpha}$), 71.11 (*C*^{3} $_{\alpha}$), 70.82 (*C*^{4} $_{\beta}$), 70.44 (*C*^{4} $_{\alpha}$), 61.19 (*C*^{6} $_{\beta}$), 61.09 (*C*^{6} $_{\alpha}$), 57.02 (*C*^{2} $_{\beta}$), 54.30 (*C*^{2} $_{\alpha}$), 50.37/50.29/48.38/48.31 (*C*$^{2',6'}$H$_{2\ \alpha+\beta}$), 46.00 (*C*^{g}H$_2$), 40.50 (*C*$^{4'}$H $_{\beta}$), 40.11 (*C*$^{4'}$H $_{\alpha}$), 28.55/28.22 (*C*$^{3',5'}$H$_{2\ \alpha+\beta}$). No differentiation of the ^{1}H and ^{13}C signals of the benzylpyridine moiety due to the presence of both α and β anomers could be detected. Solution α:β anomers ratio ≈ 2:1 (based on the ^{1}H NMR spectrum). ESI(+)-MS: *m/z* calcd. for [M-PF$_6$]$^+$: 730.1320; found: 730.1350 (100%). UV-Vis (DMSO, 298 K, nm (ε, M^{-1} cm^{-1})): 268 (44500), 271 (45100), ~294 (sh, ~24300), ~340 (~3500).

[Au(dtc-Inp-GlcN2)(Bnpy)]PF$_6$ (Au13)

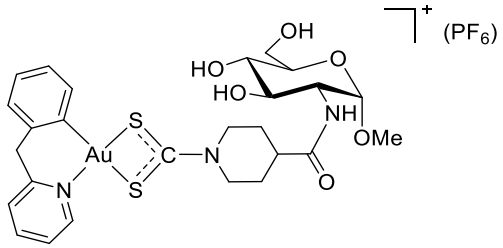

A DMF solution (2 mL) of [Zn(dtc-Inp-GlcN2)$_2$] (46.8 mg, 0.06 mmol) was added dropwise under stirring to a DMF solution (1 mL) of [Au(Bnpy)Cl$_2$] (49.5 mg, 0.11 mmol) at r.t. The mixture was stirred for 30 min, during which it turned clear and the colour of the solution turned from yellow to pale yellow. Solid KPF$_6$ (53.0 mg, 0.29 mmol) was added, and the mixture was stirred for further 90 min. The solution was evaporated to dryness at low temperature (<40°C), affording a sticky white residue. The residue was then resuspended in water (5 mL), resulting in the formation of a white precipitate. The precipitate was centrifuged and the bulk of supernatant discarded. The residue was subsequently washed with water (3×5 mL) and then dried under vacuum over P$_2$O$_5$, yielding the title compound as a white solid (91.9 mg, 91% yield). Anal. (%) calcd. for C$_{26}$H$_{33}$AuF$_6$N$_3$O$_6$PS$_2$ (MM = 889.62 g mol^{-1}): C, 35.10; H, 3.74; N, 4.72; found: C, 34.93; H, 3.84; N, 4.47. M.p. 177-180°C (dec.). FT-IR (CsI disk, $\tilde{\nu}_{max}$, cm^{-1}): 3417 (br, ν, OH + NH overlapped), 1661 (m, ν, C=O (amide I)), 1551 (s, ν, N–CSS + δ_{ip}, CNH (amide II)),

1049 (m, ν, C–OH + C^1–O–CH_3 overlapped), 1024 (m, ν_a, SCS), 844 (vs, ν_a, PF_6^-), 575 (w, ν_s, SCS), 558 (s, δ_{ip}, PF_6^- scissoring), 403 (w, $\nu_{a/s}$, SAuS). ^{1}H NMR (400 MHz, DMSO-d_6, 298 K, δ, ppm): 8.99 (m (app d), J_{HH} = 5.6 Hz, 1H, C^fH), 8.33 (m (app td), J_{HH} = 7.7 Hz, 0.9 Hz, 1H, C^dH), 8.09 (m (app d), J_{HH} = 7.7 Hz, 1H, C^cH), 7.93 (d, J_{HH} = 8.3 Hz, 1H, N*H*), 7.72 (m, 1H, C^eH), 7.41-7.37 (m, 2H, $C^{c'}H$ + $C^{f'}H$), 7.29 (m (app t), J_{HH} = 7.3 Hz, 1H, $C^{d'}H$), 7.17 (m (app t), J_{HH} = 7.3 Hz, 1H, $C^{e'}H$), 4.90 (br, 3H, C^2OH + C^3OH + C^4OH), 4.54 (s, 2H, C^gH_2), 4.53 (d, J_{HH} = 3.7 Hz, 1H, C^1H), 4.43/4.31 (2m, 2H, $C^{2',6'}H_{eq}$), 3.75-3.58 (m, 4H, C^2H + C^6H + $C^{2',6'}H_{ax}$), 3.49-3.43 (m, 2H, C^3H + C^6H'), 3.32 (m, 1H, C^5H), 3.25 (s, 3H, OCH_3), 3.13 (m, J_{HH} = 9.1 Hz, 1H, C^4H), 2.79 (tt, J_{HH} = 10.8 Hz, 3.8 Hz, 1H, $C^{4'}H$), 2.04-1.97 (m, 2H, $C^{3',5'}H_{eq}$), 1.75-1.61 (m, 2H, $C^{3',5'}H_{ax}$). ^{13}C{^{1}H} NMR (100 MHz, DMSO-d_6, 298 K, δ, ppm): 192.14 (N*C*SS), 173.08 (*C*=O), 156.10 (C^b), 151.90 (C^f), 145.34 ($C^{b'}$), 143.62 (C^d), 133.25 ($C^{a'}$), 130.63 ($C^{f'}$), 128.92 ($C^{c'}$), 128.62 ($C^{d'}$), 128.29 ($C^{e'}$), 127.01 (C^c), 125.61 (C^e), 97.84 (C^1), 72.80 (C^5), 70.78 (C^3), 70.69 (C^4), 60.79 (C^6), 54.43 (OCH_3), 53.75 (C^2), 50.35/48.36 ($C^{2',6'}H_2$), 45.98 (C^gH_2), 40.06 ($C^{4'}H$), 28.54/28.19 ($C^{3',5'}H_2$). ESI(+)-MS: *m/z* calcd. for $[M\text{-}PF_6]^+$: 744.1476; found: 744.1510 (100%). UV-Vis (DMSO, 298 K, nm (ε, M^{-1} cm^{-1})): 268 (30000), ~292 (sh, ~15800), ~340 (~1700).

[Au(dtc-Inp-GlcN3)(Bnpy)]PF_6 (Au14)

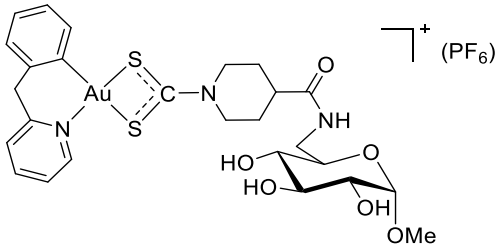

A DMF solution (2 mL) of [Zn(dtc-Inp-GlcN3)$_2$] (47.6 mg, 0.06 mmol) was added dropwise under stirring to a DMF solution (2 mL) of [Au(Bnpy)Cl_2] (50.4 mg, 0.12 mmol) at r.t. The mixture was stirred for 30 min, during which it turned clear and the colour of the solution turned from yellow to pale yellow. Solid KPF_6 (50.5 mg, 0.27 mmol) was added, and the mixture was stirred for further 90 min. Addition of diethyl ether (30 mL) resulted in the formation of a cloudy mixture and a pale yellow sticky residue. The residue was centrifuged and the bulk of supernatant discarded. The residue was subsequently triturated with a mixture of diethyl ether/dichloromethane (1:1, 10 mL), filtered, washed with diethyl ether/dichloromethane (1:1, 3×15 mL), and then dried with a gentle stream of N_2. The residue was then resuspended in water (5 mL), resulting in the formation of a

white precipitate. The precipitate was centrifuged and the bulk of supernatant discarded. The residue was subsequently washed with water (3×5 mL) and then dried under vacuum over P_2O_5, yielding the title compound as an off-white solid (31.9 mg, 31% yield). Anal. (%) calcd. for $C_{26}H_{33}AuF_6N_3O_6PS_2$ (MM = 889.62 g mol^{-1}): C, 35.10; H, 3.74; N, 4.72; found: C, 35.23; H, 3.83; N, 4.98. M.p. 146-150°C (dec.). FT-IR (CsI disk, $\tilde{\nu}_{max}$, cm^{-1}): 3432 (br, ν, OH + NH overlapped), 1659 (m, ν, C=O (amide I)), 1554 (s, ν, N–CSS + δ_{ip}, CNH (amide II)), 1051 (s, ν, C–OH + C^1–O–CH_3 overlapped), 1025 (m, ν_a, SCS), 844 (vs, ν_a, PF_6^-), 558 (s, δ_{ip}, PF_6^- scissoring + ν_s, SCS overlapped), 412 (w, $\nu_{a/s}$, SAuS). ^{1}H NMR (400 MHz, DMSO-d_6, 298 K, δ, ppm): 8.98 (m (app d), J_{HH} = 5.3 Hz, 1H, C^fH), 8.33 (m (app td), J_{HH} = 7.8 Hz, 1.4 Hz, 1H, C^dH), 8.09 (m, 2H, C^cH + N*H*), 7.72 (m, 1H, C^eH), 7.41-7.36 (m, 2H, $C^{c'}H$ + $C^{f'}H$), 7.29 (m (app t), J_{HH} = 7.2 Hz, 1H, $C^{d'}H$), 7.17 (m (app td), J_{HH} = 7.2 Hz, 1.3 Hz, 1H, $C^{e'}H$), 4.99 (br d, J_{HH} = 3.8 Hz, 1H, C^4O*H*), 4.85 (br, 1H, C^3O*H*), 4.78 (br, 1H, C^2O*H*), 4.54 (s, 2H, C^gH_2), 4.53 (d, J_{HH} = 3.5 Hz, 1H, C^1H), 4.43/4.29 (2m, 2H, $C^{2',6'}H_{eq}$), 3.71 (m, 1H, $C^{2',6'}H_{ax}$), 3.63-3.56 (m, 2H, C^6H + $C^{2',6'}H_{ax}$), 3.38-3.34 (m, 2H, C^3H + C^5H), 3.25 (s, 3H, OCH_3), 3.22 (m, 1H, C^2H), 3.02 (m, 1H, C^6H'), 2.91 (m, 1H, C^4H), 2.75 (tt, J_{HH} = 10.8 Hz, 3.8 Hz, 1H, $C^{4'}H$), 2.00-1.98 (m, 2H, $C^{3',5'}H_{eq}$), 1.74-1.62 (m, 2H, $C^{3',5'}H_{ax}$). ^{13}C{^{1}H} NMR (100 MHz, DMSO-d_6, 298 K, δ, ppm): 192.17 (N*C*SS), 172.96 (*C*=O), 156.09 (C^b), 151.90 (C^f), 145.31 ($C^{b'}$), 143.61 (C^d), 133.24 ($C^{a'}$), 130.63 ($C^{f'}$), 128.92 ($C^{c'}$), 128.61 ($C^{d'}$), 128.28 ($C^{e'}$), 127.00 (C^c), 125.60 (C^e), 99.67 (C^1), 72.97 (C^3), 72.06 (C^4), 71.95 (C^2), 70.31 (C^5), 54.33 (OCH_3), 50.32/48.34 ($C^{2',6'}H_2$), 45.98 (C^gH_2), 40.20 ($C^{4'}$H), 40.13 (C^6), 28.29/27.96 ($C^{3',5'}H_2$). ESI(+)-MS: *m/z* calcd. for $[M\text{-}PF_6]^+$: 744.1476; found: 744.1478 (100%). UV-Vis (DMSO, 298 K, nm (ε, M^{-1} cm^{-1})): 268 (31600), 271 (31000), ~293 (sh, ~16500), ~333 (~3400).

[Au(dtc-Inp-GlcN4)(Bnpy)]PF_6 (Au15)

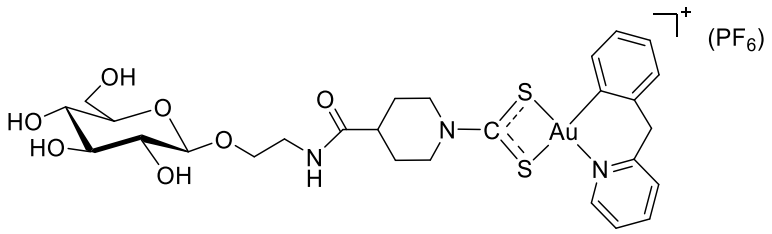

A DMF solution (2 mL) of [Zn(dtc-Inp-GlcN4)$_2$] (50.7 mg, 0.06 mmol) was added dropwise under stirring to a DMF solution (2 mL) of [Au(Bnpy)Cl_2] (50.0 mg, 0.12 mmol) at r.t. The mixture was stirred for 90 min, during which it turned clear and the colour of

the solution turned from yellow to pale yellow. Addition of diethyl ether (25 mL) resulted in the formation of a white precipitate. The precipitate was centrifuged and the bulk of supernatant discarded. The residue was washed with diethyl ether (3×10 mL) and dichloromethane (3×10 mL), and then dried under vacuum over P_2O_5. The residue was then redissolved in methanol (10 mL), solid KPF_6 (32.3 mg, 0.18 mmol) was added, and the mixture was stirred for further 60 min. Addition of diethyl ether (40 mL) resulted in the formation of a white precipitate. The precipitate was filtered, washed with diethyl ether (3×10 mL), dichloromethane (3×10 mL), and then dried under vacuum over P_2O_5, yielding the title compound as an off-white solid (95.0 mg, 90% yield). Anal. (%) calcd. for $C_{27}H_{35}AuF_6N_3O_7PS_2$ (MM = 919.64 g mol^{-1}): C, 35.26; H, 3.84; N, 4.57; found: C, 35.01; H, 3.74; N, 4.63. M.p. 165-168°C (dec.). FT-IR (CsI disk, $\tilde{\nu}_{max}$, cm^{-1}): 3400 (br, ν, OH + NH overlapped), 1650 (m, ν, C=O (amide I)), 1544 (vs, ν, N–CSS + δ_{ip}, CNH (amide II)), 1264 (w, amide III), 1076/1037 (s, ν, C–OH + C^1–O–CH_3 overlapped), 1027 (m, ν_a, SCS), 842 (vs, ν_a, PF_6^-), 559 (m, δ_{ip}, PF_6^- scissoring + ν_s, SCS overlapped), 412 (w, ν_a, SAuS), 394 (w, ν_s, SAuS). ^{1}H NMR (400 MHz, DMSO-d_6, 298 K, δ, ppm): 8.98 (m (app d), J_{HH} = 5.3 Hz, 1H, C^fH), 8.32 (m (app td), J_{HH} = 7.6 Hz, 1.4 Hz, 1H, C^dH), 8.08 (m (app d), J_{HH} = 7.8 Hz, 1H, C^cH), 8.04 (t, J_{HH} = 5.5 Hz, 1H, N*H*), 7.72 (m, 1H, C^eH), 7.40-7.36 (m, 2H, $C^{c'}H$ + $C^{f'}H$), 7.29 (m (app td), J_{HH} = 7.4 Hz, 0.8 Hz, 1H, $C^{d'}H$), 7.16 (m (app td), J_{HH} = 7.4 Hz, 1.3 Hz, 1H, $C^{e'}H$), 5.01 (d, J_{HH} = 4.3 Hz, 1H, C^2OH), 4.99 (d, J_{HH} = 4.7 Hz, 1H, C^3OH), 4.96 (d, J_{HH} = 4.9 Hz, 1H, C^4OH), 4.58 (t, J_{HH} = 5.2 Hz, 1H, C^6OH), 4.55 (s, 2H, C^gH_2), 4.41/4.28 (2m, 2H, $C^{2',6'}H_{eq}$), 4.13 (d, J_{HH} = 7.8 Hz, 1H, C^1H), 3.75-3.60 (m, 4H, C^6H + $CH_aH_bCH_2NH$ + $C^{2',6'}H_{ax}$), 3.55-3.49 (m, 1H, C^6H'), 3.46-3.41 (m, 1H, $CH_aH_bCH_2NH$), 3.29-3.23 (m, 2H, CH_2NH), 3.17-3.08 (m, 4H, C^3H + C^5H), 3.04 (ddd, J_{HH} = 9.1 Hz, 4.9 Hz, 1H, C^4H), 2.97 (ddd, J_{HH} = 8.3 Hz, 4.3 Hz 1H, C^2H), 2.72 (m, 1H, $C^{4'}H$), 2.05-1.98 (m, 2H, $C^{3',5'}H_{eq}$), 1.76-1.63 (m, 2H, $C^{3',5'}H_{ax}$). ^{13}C{^{1}H} NMR (100 MHz, DMSO-d_6, 298 K, δ, ppm): 192.18 (N*C*SS), 172.84 (*C*=O), 156.15 (C^b), 151.82 (C^f), 145.32 ($C^{b'}$), 143.44 (C^d), 133.24 ($C^{a'}$), 130.64 ($C^{f'}$), 128.92 ($C^{c'}$), 128.53 ($C^{d'}$), 128.23 ($C^{e'}$), 126.92 (C^c), 125.50 (C^e), 103.15 (C^1), 76.90 (C^3), 76.55 (C^5), 70.05 (C^2), 70.05 (C^4), 67.82 (C^6), 61.08 (CH_2CH_2NH), 50.24/48.26 ($C^{2',6'}H_2$), 45.98 (C^gH_2), 40.20 ($C^{4'}H$), 38.79 (CH_2NH), 28.42/28.12 ($C^{3',5'}H_2$). ESI(+)-MS: *m/z* calcd. for $[M\text{-}PF_6]^+$: 774.1582; found: 774.1552 (100%). UV-Vis (DMSO, 298 K, nm (ε, M^{-1} cm^{-1})): 262 (23200), 268 (26300), ~294 (sh, ~13200), ~350 (~2100).

8.5 Chapter 5 – Experimental

[Au(BImEt$_2$)(dtc-Sar-OEt)] (Au16)

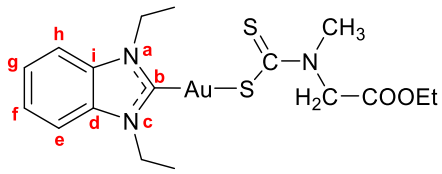

A water/acetone solution (6:1, 10 mL) of (PPh$_4$)(dtc-Sar-OEt) (119.0 mg, 0.22 mmol) was added dropwise under stirring to an acetone solution (2 mL) of [AuCl(BImEt$_2$)] (84.8 mg, 0.21 mmol) at r.t, leading to the sudden precipitation of a white solid. The mixture was stirred for 3h. The precipitate was centrifuged and the bulk of supernatant discarded. The residue was subsequently washed with water (3×15 mL) and then dried under vacuum over P_2O_5, yielding the title compound as a fluffy ivory solid (119.3 mg, 99% yield). Colourless needle-shaped crystals suitable for X-ray crystallography were obtained upon slow evaporation of a DMF solution of the compound. Anal. (%) calcd. for $C_{17}H_{24}AuN_3O_2S_2$ (MM = 563.48 g mol^{-1}): C, 36.24; H, 4.29; N, 7.46; found: C, 36.31; H, 4.23; N, 7.42. M.p. 144-146°C (dec.). FT-IR (CsI disk, $\tilde{\nu}_{max}$, cm^{-1}): 1739 (vs, ν, C=O), 1483 (s, ν, N–CSS), 1197/1103 (s, $\nu_{a/s}$, C–OEt), 1001/982 (m, ν, S=C–S), 569 (w, ν, Au–C), 556/496 (w, δ, S=C–S + ν_s, S=C–S overlapped), 346 (w, ν, Au–S). ^{1}H NMR (400 MHz, $CDCl_3$, 298 K, δ, ppm): 7.49-7.45 (m, 2H, C*H* $_{arom}$), 7.42-7.39 (m, 2H, C*H* $_{arom}$), 4.81 (s, 2H, NC*H*$_2$ $_{dtc}$), 4.61 (q, J_{HH} = 7.3 Hz, 4H, C*H*$_2$ $_{ethyl\ NHC}$), 4.24 (q, J_{HH} = 7.1 Hz, 2H, C*H*$_2$ $_{ethyl\ dtc}$), 3.58 (s, 3H, NC*H*$_3$ $_{dtc}$), 1.56 (t, J_{HH} = 7.3 Hz, 6H, C*H*$_3$ $_{ethyl\ NHC}$), 1.30 (t, J_{HH} = 7.1 Hz, 3H, C*H*$_3$ $_{ethyl\ dtc}$). ^{13}C{^{1}H} NMR (100 MHz, $CDCl_3$, 298 K, δ, ppm): 210.56 (N*C*SS), 185.60 (*C*^{b}), 168.42 (*C*=O), 133.10 (*C*^{d,i}), 124.17 (*C*^{f,g}), 111.42 (*C*^{e,h}), 61.39 (*C*H$_2$ $_{ethyl}$), 58.30 (NCH$_2$ $_{dtc}$), 44.54 (NCH$_3$ $_{dtc}$), 43.93 (CH$_2$ $_{ethyl\ NHC}$), 15.60 (CH$_3$ $_{ethyl\ NHC}$), 14.38 (CH$_3$ $_{ethyl}$). UV-Vis (DMF, 298 K, nm (ε, M^{-1} cm^{-1})): 280 (sh, ~25000), 286 (33500), 305 (12200).

[Au(BImEt$_2$)(dtc-Inp-NH$_2$)] (Au17)

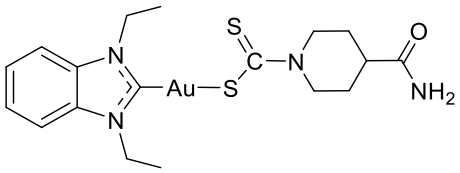

A water/acetone solution (6:1, 7 mL) of Na(dtc-Inp-NH$_2$)·CH$_3$OH (44.6 mg, 0.17 mmol) was added dropwise under stirring to an acetone solution (2 mL) of [AuCl(BImEt$_2$)] (64.8 mg, 0.16 mmol) at r.t, leading to the sudden precipitation of an off-white solid. The

mixture was stirred for 1h. The precipitate was centrifuged and the bulk of supernatant discarded. The residue was subsequently washed with water (3×10 mL) and then dried under vacuum over P_2O_5, yielding the title compound as a fluffy off-white solid (76.0 mg, 83% yield). Colourless needle-shaped crystals suitable for X-ray crystallography were obtained upon slow evaporation of a DMF solution of the compound. Anal. (%) calcd. for $C_{18}H_{25}AuN_4OS_2$ (MM = 574.51 g mol^{-1}): C, 37.63; H, 4.39; N, 9.75; found: C, 37.68; H, 4.61; N, 9.75. M.p. 202-210°C (dec.). FT-IR (CsI disk, $\tilde{\nu}_{max}$, cm^{-1}): 3343/3159 (br, $\nu_{a/s}$, NH_2), 3159 (br, ν_s, NH_2), 1684 (vs, ν, C=O (amide I)), 1623 (w, δ_{ip}, CNH_2 (amide II)), 1463 (m, ν, N–CSS), 1004/915 (m, ν, S=C–S), 593 (w, ν, C–S), 559 (w, ν, Au–C), 327 (w, ν, Au–S). ^{1}H NMR (400 MHz, DMSO-d_6, ppm): 7.84-7.82 (m, 2H, C*H* $_{arom}$), 7.48-7.46 (m, 2H, C*H* $_{arom}$), 7.35 (s, 1H, N*H* $_{cis}$), 6.86 (s, 1H, N*H* $_{trans}$), 5.08 (m (app d), J_{HH} = 12.8 Hz, 2H, C$^{2',6'}$*H* $_{eq}$), 4.58 (q, J_{HH} = 7.1 Hz, 4H, C*H*$_2$ $_{ethyl}$), 3.19 (m (app t), J_{HH} = 11.4 Hz, 2H, C$^{2',6'}$*H* $_{ax}$), 2.43 (tt, J_{HH} = 11.3 Hz, 4.0 Hz, 1H, C$^{4'}$*H*), 1.80-1.76 (m, 2H, C$^{3',5'}$*H* $_{eq}$), 1.60-1.52 (m, 2H, C$^{3',5'}$*H* $_{ax}$), 1.42 (t, J_{HH} = 7.1 Hz, 6H, C*H*$_3$ $_{ethyl}$). ^{13}C{^{1}H} NMR (100 MHz, DMSO-d_6, 298 K, δ, ppm): 204.49 (N*C*SS), 184.17 (*C*^{b}), 175.84 (*C*=O), 132.38 (*C*^{d,i}), 124.21 (*C*^{f,g}), 112.01 (*C*^{e,h}), 50.42 (*C*$^{2',6'}$H$_2$), 43.12 (*C*H$_2$ $_{ethyl}$), 40.90 (*C*$^{4'}$H$_2$), 28.39 (*C*$^{3',5'}$H$_2$), 15.51 (*C*H$_3$ $_{ethyl}$). UV-Vis (DMF, 298 K, nm (ε, M^{-1} cm^{-1})): 283 (sh, ~32800), 288 (39900), 303 (sh, ~12200).

[Au(BImEt$_2$)(dtc-Inp-GlcN1)] (Au18)

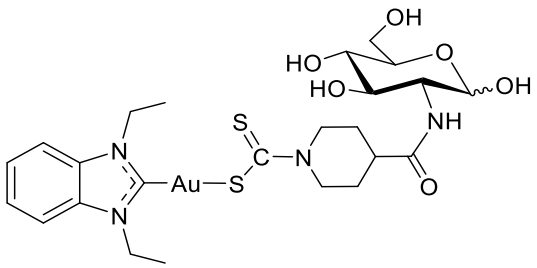

A DMF solution (2 mL) of [Zn(dtc-Inp-GlcN1)$_2$] (49.4 mg, 0.06 mmol) was added dropwise under stirring to a DMF solution (2 mL) of [AuCl(BImEt$_2$)] (50.5 mg, 0.12 mmol) at r.t., and the mixture was stirred for 5 min. Upon addition of diethyl ether (60 mL), the solution turned cloudy and a yellow solid residue formed. The precipitate was filtered, washed with diethyl ether (3×10 mL), dichloromethane (3×10 mL), and then dried under vacuum over P_2O_5, yielding the title compound as a pale yellow solid (80.2 mg, 88% yield). Anal. (%) calcd. for $C_{24}H_{35}AuN_4O_6S_2$ (MM = 736.65 g mol^{-1}): C, 39.13; H, 4.79; N, 7.61; found: C, 39.01; H, 4.65; N, 7.77. M.p. 154-157°C (dec.). FT-IR (CsI disk, $\tilde{\nu}_{max}$, cm^{-1}): 3401 (br, ν, OH + NH overlapped), 1657 (vs, ν, C=O (amide I)), 1543

(m, δ_{ip}, CNH (amide II)), 1483 (s, ν, N–CSS), 1089/1059/1041 (s, ν, C–OH + C^1–O–CH_3 overlapped), 998/914 (sh, ν, S=C–S), 566 (w, ν, C–S), 506 (w, ν, Au–C), 385 (w, ν, Au–S). ^{1}H NMR (400 MHz, DMSO-d_6, 298 K, δ, ppm): 7.84-7.82 (m, 2.8H, C*H* $_{arom}$), 7.69 (d, J_{HH} = 8.1 Hz, 0.4H, N*H* $_{\beta}$), 7.65 (d, J_{HH} = 7.7 Hz, 1H, N*H* $_{\alpha}$), 7.48-7.46 (m, 2.8H, C*H* $_{arom}$), 6.50 (d, J_{HH} = 6.3 Hz, 0.4H, C^1O*H* $_{\beta}$), 6.42 (d, J_{HH} = 4.1 Hz, 1H, C^1O*H* $_{\alpha}$), 5.10-5.07 (m, 2.8H, $C^{2',6'}$*H* $_{eq\ \alpha+\beta}$), 4.91 (m, 1.4H, C^1*H* $_{\alpha}$ + C^4O*H* $_{\beta}$), 4.82 (m, 0.4H, C^3O*H* $_{\beta}$), 4.62-4.55 (m, 7.0H, C^4O*H* $_{\alpha}$ + C^6O*H* $_{\beta}$ + C$H_{2\ ethyl}$), 4.45-4.42 (m, 1.4H, C^1*H* $_{\beta}$ + C^6O*H* $_{\alpha}$), 3.69-3.05 (m, 11.2H, C^2*H* $_{\alpha+\beta}$ + C^3*H* $_{\alpha+\beta}$ + C^4*H* $_{\alpha+\beta}$ + C^5*H* $_{\alpha+\beta}$ + C^6*H* $_{\alpha+\beta}$ + C^6*H*' $_{\alpha+\beta}$ + $C^{2',6'}$*H* $_{ax\ \alpha+\beta}$), 2.58 (m, J_{HH} = 11.1 Hz, 4.0 Hz, 1.4H, $C^{4'}$*H* $_{\alpha+\beta}$), 1.82-1.71 (m, 2.8H, $C^{3',5'}$*H* $_{eq\ \alpha+\beta}$), 1.65-1.54 (m, 2.8H, $C^{3',5'}$*H* $_{ax\ \alpha+\beta}$), 1.42 (t, J_{HH} = 7.0 Hz, 8.4H, C*H*$_{3\ ethyl}$). ^{13}C{^{1}H} NMR (100 MHz, DMSO-d_6, 298 K, δ, ppm): 204.47 (N*C*SS), 184.18 (C^b), 173.94 (*C*=O), 132.37 ($C^{d,i}$), 124.20 ($C^{f,g}$), 111.99 ($C^{e,h}$), 95.44 (C^1 $_{\beta}$), 90.49 (C^1 $_{\alpha}$), 76.86 (C^5 $_{\beta}$), 74.23 (C^3 $_{\beta}$), 72.11 (C^5 $_{\alpha}$), 71.08 (C^3 $_{\alpha}$), 70.82 (C^4 $_{\beta}$), 70.38 (C^4 $_{\alpha}$), 61.21 (C^6 $_{\beta}$), 61.00 (C^6 $_{\alpha}$), 57.00 (C^2 $_{\beta}$), 54.28 (C^2 $_{\alpha}$), 50.54 ($C^{2',6'}H_2$), 43.12 (*C*H$_{2\ ethyl}$), 40.79 ($C^{4'}$H $_{\alpha+\beta}$), 28.53/28.43 ($C^{3',5'}H_{2\ \alpha+\beta}$), 15.50 (*C*H$_{3\ ethyl}$). No differentiation of the ^{1}H and ^{13}C signals of the carbene and the isonipecotic moieties due to the presence of both α and β anomers could be detected. Solution α:β anomers ratio ≈ 2.5:1 (based on the ^{1}H NMR spectrum). UV-Vis (DMF, 298 K, nm (ε, M^{-1} cm^{-1})): 282 (sh, ~40600), 287 (50100), 302 (sh, ~17600).

[Au(BImEt$_2$)(dtc-Inp-GlcN2)] (Au19)

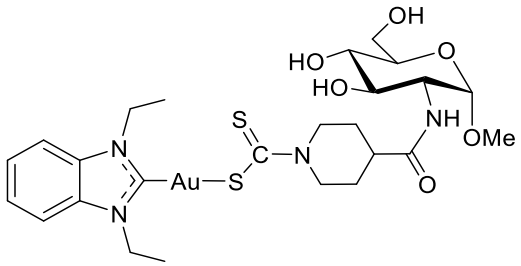

A DMF solution (2 mL) of [Zn(dtc-Inp-GlcN2)$_2$] (52.1 mg, 0.06 mmol) was added dropwise under stirring to a DMF solution (2 mL) of [Au(BImEt$_2$)Cl] (51.4 mg, 0.12 mmol) at r.t., and the mixture was stirred for 5 min. Upon addition of diethyl ether (60 mL), the solution turned cloudy and a yellow solid residue formed. The precipitate was filtered, washed with a diethyl ether/dichloromethane (1:1) mixture (3×15 mL), and then dried under vacuum over P_2O_5, yielding the title compound as a pale yellow solid (83.5 mg, 88% yield). Anal. (%) calcd. for $C_{25}H_{37}AuN_4O_6S_2$ (MM = 750.68 g mol^{-1}): C, 40.00; H, 4.97; N, 7.46; found: C, 40.23; H, 4.96; N, 7.27. M.p. 155-157°C (dec.). FT-IR (CsI disk, $\tilde{\nu}_{max}$, cm^{-1}): 3434 (br, ν, OH + NH overlapped), 1658 (s, ν, C=O (amide I)), 1542 (m,

δ_{ip}, CNH (amide II)), 1491 (s, ν, N–CSS), 1055/1042 (vs, ν, C–OH + C^1–O–CH_3 overlapped), 1000/914 (sh, ν, S=C–S), 578 (w, ν, C–S), 568 (w, ν, Au–C), 384 (w, ν, Au–S). ^{1}H NMR (400 MHz, DMSO-d_6, 298 K, δ, ppm): 7.83-7.77 (m, 3H, N*H* + C*H* $_{arom}$), 7.48-7.46 (m, 2H, C*H* $_{arom}$), 5.10-5.07 (m, 2H, $C^{2',6'}H_{eq}$), 5.01 (d, J_{HH} = 5.6 Hz, 1H, C^4O*H*), 4.72 (d, J_{HH} = 5.9 Hz, 1H, C^3O*H*), 4.61-4.53 (m, 6H, C^1H + C^6O*H* + CH_2 $_{ethyl}$), 3.68-3.62 (m, 2H, C^2H + C^6H), 3.49-3.43 (m, 2H, C^3H + C^6H'), 3.33-3.30 (m, 1H, C^5H), 3.25 (s, 3H, OCH_3), 3.22-3.07 (m, 3H, C^4H + $C^{2',6'}H_{ax}$), 2.58 (m, 1H, $C^{4'}H$), 1.80-1.72 (m, 2H, $C^{3',5'}H_{eq}$), 1.64-1.55 (m, 2H, $C^{3',5'}H_{ax}$), 1.42 (t, J_{HH} = 7.1 Hz, 6H, CH_3 $_{ethyl}$). ^{13}C{^{1}H} NMR (100 MHz, DMSO-d_6, 298 K, δ, ppm): 204.32 (N*C*SS), 184.07 (C^b), 174.12 (*C*=O), 132.38 ($C^{d,i}$), 124.24 ($C^{f,g}$), 112.02 ($C^{e,h}$), 97.87 (C^1), 72.80 (C^5), 70.79 (C^3), 70.66 (C^4), 60.83 (C^6), 54.46 (O*C*H$_3$), 53.75 (C^2), 50.50 ($C^{2',6'}H_2$), 43.14 (*C*H$_2$ $_{ethyl}$), 40.77 ($C^{4'}H_2$), 28.48 ($C^{3',5'}H_2$), 15.51 (*C*H$_3$ $_{ethyl}$). UV-Vis (DMF, 298 K, nm (ε, M^{-1} cm^{-1})): 282 (sh, ~30600), 287 (38500), 303 (sh, ~13000).

[Au(BImEt$_2$)(dtc-Inp-GlcN3)] (Au20)

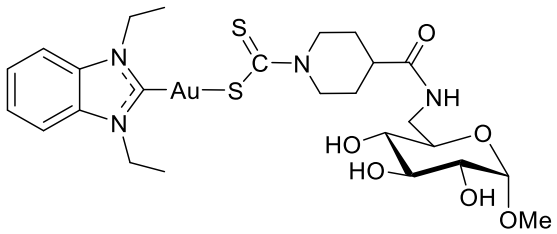

A DMF solution (2 mL) of [Zn(dtc-Inp-GlcN3)$_2$] (51.3 mg, 0.06 mmol) was added dropwise under stirring to a DMF solution (2 mL) of [AuCl(BImEt$_2$)] (50.6 mg, 0.12 mmol) at r.t., and the mixture was stirred for 5 min. Upon addition of diethyl ether (60 mL), the solution turned cloudy and a yellow solid residue formed. The precipitate was filtered, washed with a diethyl ether/dichloromethane (1:1) mixture (3×15 mL), and then dried under vacuum over P_2O_5, yielding the title compound as a pale yellow solid (82.8 mg, 89% yield). Anal. (%) calcd. for $C_{25}H_{37}AuN_4O_6S_2$ (MM = 750.68 g mol^{-1}): C, 40.00; H, 4.97; N, 7.46; found: C, 39.76; H, 4.92; N, 7.68. M.p. 151-155°C (dec.). FT-IR (CsI disk, $\tilde{\nu}_{max}$, cm^{-1}): 3401 (br, ν, OH + NH overlapped), 1656 (s, ν, C=O (amide I)), 1545 (m, δ_{ip}, CNH (amide II)), 1484 (s, ν, N–CSS), 1050 (vs, ν, C–OH + C^1–O–CH_3 overlapped), 1007/914 (sh, ν, S=C–S), 565 (w, ν, C–S), 513 (w, ν, Au–C), 384 (w, ν, Au–S). ^{1}H NMR (400 MHz, DMSO-d_6, 298 K, δ, ppm): 7.97 (dd, J_{HH} = 5.3 Hz, 1H, N*H*), 7.84-7.81 (m, 2H, C*H* $_{arom}$), 7.48-7.46 (m, 2H, C*H* $_{arom}$), 5.10-5.07 (m, 2H, $C^{2',6'}H_{eq}$), 4.98 (d, J_{HH} = 5.4 Hz, 1H, C^4O*H*), 4.82 (d, J_{HH} = 4.9 Hz, 1H, C^3O*H*), 4.76 (d, J_{HH} = 6.3 Hz, 1H, C^2O*H*),

4.61-4.55 (q, J_{HH} = 7.0 Hz, 4H, C$H_{2\ ethyl}$), 4.51 (d, J_{HH} = 3.7 Hz, 1H, C^{1}H), 3.55 (m, 1H, C^{6}H), 3.39-3.33 (m, 2H, C^{3}H + C^{5}H), 3.25 (s, 3H, OCH_3), 3.22-3.15 (m, 3H, C^{2}H + C$^{2',6'}H_{\ ax}$), 3.05-2.98 (m, 1H, C^{6}H'), 2.93-2.87 (m, 1H, C^{4}H), 2.54 (m, 1H, C$^{4'}H$), 1.78-1.70 (m, 2H, C$^{3',5'}H_{\ eq}$), 1.65-1.56 (m, 2H, C$^{3',5'}H_{\ ax}$), 1.42 (t, J_{HH} = 7.0 Hz, 6H, C$H_{3\ ethyl}$). ^{13}C{^{1}H} NMR (100 MHz, DMSO-d$_6$, 298 K, δ, ppm): 204.98 (N*C*SS), 184.62 (*C*^{b}), 174.55 (*C*=O), 132.91 (*C*^{d,i}), 124.75 (*C*^{f,g}), 112.54 (*C*^{e,h}), 100.17 (*C*^{1}), 72.95 (*C*^{3}), 72.11 (*C*^{4}), 71.97 (*C*^{2}), 70.32 (*C*^{5}), 54.27 (O*C*H$_3$), 50.51 (*C*$^{2',6'}$H$_2$), 43.15 (*C*H$_{2\ ethyl}$), 40.93 (*C*$^{4'}$H$_2$), 28.48 (*C*$^{3',5'}$H$_2$), 15.50 (*C*H$_{3\ ethyl}$). UV-Vis (DMF, 298 K, nm (ε, M^{-1} cm^{-1})): 282 (sh, ~27800), 287 (34800), 301 (sh, ~11900).

[Au(dtc-Inp-OEt)(PPh$_3$)] (Au21)

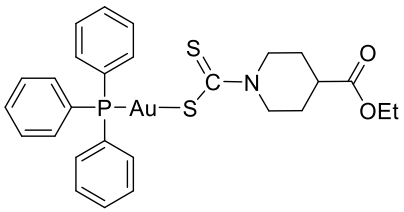

A methanol solution (4 mL) of (H$_2$-Inp-OEt)(dtc-Inp-OEt) (60.6 mg, 0.15 mmol) was added dropwise under stirring to a dichloromethane solution (2 mL) of [AuCl(PPh$_3$)] (76.6 mg, 0.15 mmol) at r.t. The mixture was stirred for 60 min, during which it turned pale yellow. The solution was evaporated to dryness at low temperature (<40°C), affording a lemon yellow residue. The residue was then resuspended in water (10 mL), resulting in the formation of a lemon yellow precipitate. The precipitate was centrifuged and the bulk of supernatant discarded. The residue was subsequently washed with water (2×10 mL), and then dried under vacuum over P_2O_5, yielding the title compound as a lemon yellow solid (97.5 mg, 91% yield). Anal. (%) calcd. for $C_{27}H_{29}AuNO_2PS_2$ (MM = 691.59 g mol^{-1}): C, 46.89; H, 4.23; N, 2.03; found: C, 46.81; H, 4.29; N, 2.18. M.p. 53-56°C (dec.). FT-IR (CsI disk, $\tilde{\nu}_{max}$, cm^{-1}): 1729 (s, ν, C=O), 1480 (s, ν, N–CSS), 1436 (vs, ν, C=C phenyl), 1190 (s, ν, C–OEt), 1101 (s, ν $_{q\text{-vib}}$, P–Ph$_3$), 1040 (m, ν, O–Et), 999/917 (m, ν, S=C–S), 749 (m, δ_{oop}, C–H phenyl), 710/694 (w, ν $_{r\text{-vib}}$, P–Ph$_3$), 558 (w, ν, C–S), 540/510/501 (vs, δ $_{y\text{-vib}}$, P–Ph$_3$), 433 (w, ν $_{t\ vib}$, P–Ph$_3$), 393 (w, ν, Au–S). ^{1}H NMR (400 MHz, CDCl$_3$, 298 K, δ, ppm): 7.62-7.57 (m, 6H, C$H_{\ arom\ ortho}$), 7.50-7.42 (m, 9H, C$H_{\ arom\ meta+para}$), 4.97 (m (app dt), J_{HH} = 13.3 Hz, 3.7 Hz, 2H, C$^{2',6'}H_{\ eq}$), 4.15 (q, J_{HH} = 7.1 Hz, 2H, OCH_2), 3.43 (m, 2H, C$^{2',6'}H_{\ ax}$), 2.59 (tt, J_{HH} = 10.2 Hz, 4.3 Hz, 1H, C$^{4'}H$), 2.03-1.98 (m, 2H, C$^{3',5'}H_{\ eq}$), 1.94-1.84 (m, 2H, C$^{3',5'}H_{\ ax}$), 1.25 (t, J_{HH} = 7.1 Hz, 3H, CH_3). ^{13}C{^{1}H} NMR (100 MHz, CDCl$_3$, 298 K, δ, ppm): 206.98 (N*C*SS), 174.34 (*C*=O), 134.33 (d, J_{PC}

= 13.9 Hz, $C_{\text{arom }ortho}$), 131.54 (d, J_{PC} = 1.7 Hz, $C_{\text{arom }para}$), 130.24 (d overlapped, $C_{\text{arom }ipso}$), 129.10 (d, J_{PC} = 11.5 Hz, $C_{\text{arom }meta}$), 60.79 (OCH$_2$), 50.96 ($C^{2',6'}$H$_2$), 40.58 ($C^{4'}$H$_2$), 28.02 ($C^{3',5'}$H$_2$), 14.34 (CH$_3$). ^{31}P{^{1}H} NMR (162 MHz, CDCl$_3$, 298 K, δ, ppm): 36.59 (AuPPh$_3$). UV-Vis (CH$_2$Cl$_2$, 298 K, nm (ε, M^{-1} cm^{-1})): 230 (22300), 237 (23500), 242 (23800), ~245 (sh, ~23200), 268 (24700), ~295 (sh, ~7700), ~316 (sh, ~5200).

[Au(dtc-Inp-NH$_2$)(PPh$_3$)] (Au22)

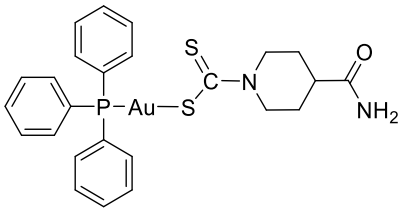

A methanol solution (4 mL) of Na(dtc-Inp-NH$_2$)·CH$_3$OH (38.7 mg, 0.15 mmol) was added dropwise under stirring to a dichloromethane solution (2 mL) of [AuCl(PPh$_3$)] (73.4 mg, 0.15 mmol) at r.t. The mixture was stirred for 30 min, during which it turned from cloudy to clear and pale yellow. The solution was evaporated to dryness at low temperature (<40°C), affording a light yellow residue. The residue was then resuspended in water (10 mL), resulting in the formation of a light yellow precipitate. The precipitate was centrifuged and the bulk of supernatant discarded. The residue was subsequently washed with water (2×10 mL), and then dried under vacuum over P_2O_5, yielding the title compound as a light yellow solid (84.5 mg, 86% yield). Yellow plate-shaped crystals suitable for X-ray crystallography were obtained upon slow evaporation of a dichloromethane/methanol solution of the compound. Anal. (%) calcd. for $C_{25}H_{26}AuN_2OPS_2$ (MM = 662.56 g mol^{-1}): C, 45.32; H, 3.96; N, 4.23; found: C, 45.63; H, 3.91; N, 4.13. M.p. 215-219°C (dec.). FT-IR (CsI disk, $\tilde{\nu}_{max}$, cm^{-1}): 3442/3162 (br, $\nu_{a/s}$, NH$_2$), 1676 (vs, ν, C=O (amide I)), 1614 (w, δ_{ip}, CNH$_2$ (amide II)), 1477 (m, ν, N–CSS), 1435 (vs, ν, C=C phenyl), 1101 (m, ν $_{q\text{-vib}}$, P–Ph$_3$), 998/914 (m, ν, S=C–S), 751 (m, δ_{oop}, C–H phenyl), 709/694 (s, ν $_{r\text{-vib}}$, P–Ph$_3$), 540/508/499 (vs, δ $_{y\text{-vib}}$, P–Ph$_3$ + ν, C–S overlapped), 420 (w, ν $_{t\text{ vib}}$, P–Ph$_3$ + ν, Au–S). ^{1}H NMR (400 MHz, CDCl$_3$, 298 K, δ, ppm): 7.63-7.57 (m, 6H, CH $_{\text{arom }ortho}$), 7.63-7.57 (m, 9H, CH $_{\text{arom }meta+para}$), 5.55 (br, 1H, NH $_{cis}$), 5.44 (br, 1H, NH $_{trans}$), 5.18 (m (app d), J_{HH} = 12.9 Hz, 2H, C$^{2',6'}H$ $_{eq}$), 3.29 (m, 2H, C$^{2',6'}H$ $_{ax}$), 2.48 (tt, J_{HH} = 10.9 Hz, 4.1 Hz, 1H, C$^{4'}H$), 2.02-1.97 (br m, 2H, C$^{3',5'}H$ $_{eq}$), 1.91-1.81 (br m, 2H, C$^{3',5'}H$ $_{ax}$). ^{13}C{^{1}H} NMR (100 MHz, CDCl$_3$, 298 K, δ, ppm): 207.15 (NCSS), 176.28 (C=O), 134.32 (d, J_{PC} = 14.1 Hz, $C_{\text{arom }ortho}$), 131.52 (d, J_{PC} = 1.7 Hz, $C_{\text{arom }para}$), 130.32 (d overlapped, $C_{\text{arom }ipso}$), 129.15 (d, J_{PC} = 11.5 Hz, $C_{\text{arom }meta}$), 51.04

($C^{2',6'}H_2$), 41.94 ($C^{4'}H_2$), 28.68 ($C^{3',5'}H_2$). $^{31}P\{^1H\}$ NMR (162 MHz, $CDCl_3$, 298 K, δ, ppm): 36.57 (Au*P*Ph_3). UV-Vis (CH_2Cl_2, 298 K, nm (ε, M^{-1} cm^{-1})): 231 (25800), 236 (26400), 240 (26800), 243 (26800), ~246 (sh, ~26000), 268 (28400), ~296 (sh, ~9000), ~316 (sh, ~6400).

[Au(dtc-Inp-GlcN1)(PPh_3)] (Au23)

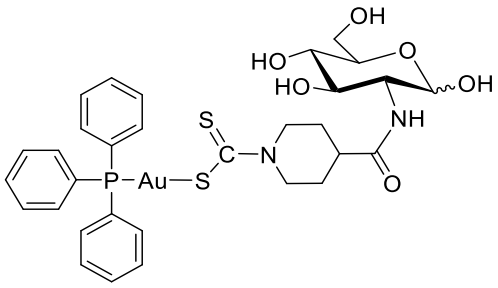

A DMF solution (2 mL) of [Zn(dtc-Inp-GlcN1)$_2$] (60.1 mg, 0.07 mmol) was added dropwise under stirring to a DMF solution (2 mL) of [AuCl(PPh_3)] (74.8 mg, 0.15 mmol) at r.t., and the mixture was stirred for 1 h. Upon addition of diethyl ether (40 mL), the solution turned cloudy and a white solid residue formed. The precipitate was centrifuged and the bulk of supernatant discarded. The sticky residue was subsequently triturated with diethyl ether (3×10 mL) and dichloromethane (3×10 mL), and then dried under vacuum over P_2O_5, yielding the title compound as a light yellow solid (85.3 mg, 68% yield). M.p. 170-172°C (dec.). Anal. (%) calcd. for $C_{31}H_{36}AuN_2O_6PS_2$ (MM = 824.70 g mol^{-1}): C, 45.15; H, 4.40; N, 3.40; found: C, 44.89; H, 4.39; N, 3.36. FT-IR (CsI disk, $\tilde{\nu}_{max}$, cm^{-1}): 3401 (br, ν, OH+ NH overlapped), 1650 (s, ν, C=O (amide I)), 1544 (m, δ_{ip}, CNH (amide II)), 1481 (m, ν, N–CSS), 1437 (vs, ν, C=C phenyl), 1101 (m, ν $_{q\text{-vib}}$, P–Ph_3), 1059 (s, ν, C–OH), 998/913 (m, ν, S=C–S), 750 (m, δ_{oop}, C–H phenyl), 710/693 (s, ν $_{r\text{-vib}}$, P–Ph_3), 578 (w, ν, C–S), 538/509 (vs, δ $_{y\text{-vib}}$, P–Ph_3), 426 (w, ν $_{t\ vib}$, P–Ph_3), 369 (w, ν, Au–S). ^1H NMR (400 MHz, DMSO-d_6, 298 K, δ, ppm): 7.70 (d, J_{HH} = 8.5 Hz, 0.25H, N*H* $_\beta$), 7.66 (d, J_{HH} = 7.8 Hz, 1H, N*H* $_\alpha$), 7.60-7.56 (m, 18.75H, C*H* $_{arom}$), 6.50 (d, J_{HH} = 6.5 Hz, 0.25H, C^1OH $_\beta$), 6.42 (d, J_{HH} = 4.6 Hz, 1H, C^1OH $_\alpha$), 4.93-4.89 (m, 4.5H, C^1H $_\alpha$ + C^3OH $_\alpha$ + $C^{2',6'}H$ $_{eq\ \alpha+\beta}$), 4.61 (d, J_{HH} = 4.4 Hz, 1H, C^4OH $_\alpha$), 4.54 (dd, J_{HH} = 5.8 Hz, 0.25H, C^6OH $_\beta$), 4.44 (m, 1.25H, C^1H $_\beta$ + C^6OH $_\alpha$), 3.70-3.39 (m, 5.75H, C^2H $_\alpha$ + C^4H $_{\alpha+\beta}$ + C^5H $_\alpha$ + C^6H $_{\alpha+\beta}$ + C^6H' $_{\alpha+\beta}$), 3.29-3.20 (m, 3H, C^2H $_\beta$ + C^3H $_\beta$ + $C^{2',6'}H$ $_{ax\ \alpha+\beta}$), 3.14-3.03 (m, 1.25H, C^3H $_\alpha$ + C^5H $_\beta$), 2.58 (tt, J_{HH} = 11.1 Hz, 4.0 Hz, 1H, $C^{4'}H$ $_\alpha$), 2.45 (m, 0.25H, $C^{4'}H$ $_\beta$), 1.81-1.75 (m, 2.5H, $C^{3',5'}H$ $_{eq\ \alpha+\beta}$), 1.64-1.54 (m, 2.5H, $C^{3',5'}H$ $_{ax\ \alpha+\beta}$). $^{13}C\{^1H\}$ NMR (100 MHz, DMSO-d_6, 298 K, δ, ppm): 204.39 (N*C*SS), 173.87 (*C*=O), 133.66 (d, J_{PC} =

15.7 Hz, $C_{\text{arom } ortho}$), 131.86 (d, J_{PC} = 2.8 Hz, $C_{\text{arom } para}$), 129.79 (d overlapped, $C_{\text{arom } ipso}$), 129.47 (d, J_{PC} = 11.9 Hz, $C_{\text{arom } meta}$), 95.44 (C^1 β), 90.50 (C^1 α), 76.88 (C^5 β), 74.24 (C^3 β), 72.13 (C^5 α), 71.10 (C^3 α), 70.85 (C^4 β), 70.41 (C^4 α), 61.13 (C^6 α+β), 57.05 (C^2 β), 54.31 (C^2 α) 50.73 ($C^{2',6'}H_2$ α+β), 41.04 ($C^{4'}H_2$ α+β), 28.54/28.45 ($C^{3',5'}H_2$ α+β). $^{31}P\{^1H\}$ NMR (162 MHz, DMSO-d_6, 298 K, δ, ppm): 36.46 (Au*P*Ph_3). No differentiation of the ^1H and ^{13}C signals of the triphenylphosphine and the isonipecotic moieties due to the presence of both α and β anomers could be detected. Solution α:β anomers ratio ≈ 4:1 (based on the ^1H NMR spectrum). UV-Vis (DMSO, 298 K, nm (ε, M^{-1} cm^{-1})): 272 (19700), ~296 (sh, ~8400), ~316 (sh, ~4900).

[Au(dtc-Inp-GlcN2)(PPh_3)] (Au24)

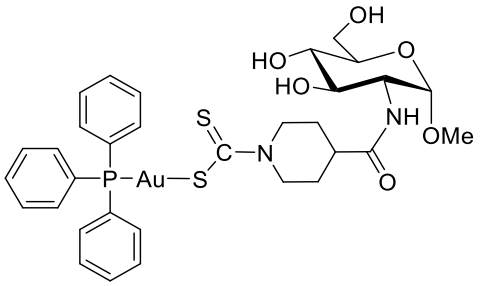

A DMF solution (2 mL) of [Zn(dtc-Inp-GlcN2)$_2$] (65.0 mg, 0.08 mmol) was added dropwise under stirring to a DMF solution (2 mL) of [AuCl(PPh_3)] (78.0 mg, 0.16 mmol) at r.t., and the mixture was stirred for 1 h. Upon addition of diethyl ether (40 mL), the solution turned cloudy and a white solid residue formed. The precipitate was centrifuged and the bulk of supernatant discarded. The sticky residue was subsequently triturated with diethyl ether (3×10 mL) and dichloromethane (3×10 mL), and then dried under vacuum over P_2O_5, yielding the title compound as a light yellow solid (80.2 mg, 60% yield). M.p. 188-190°C (dec.). Anal. (%) calcd. for $C_{32}H_{38}AuN_2O_6PS_2$ (MM = 838.72 g mol^{-1}): C, 45.83; H, 4.57; N, 3.34; found: C, 45.92; H, 4.63; N, 3.29. FT-IR (CsI disk, $\tilde{\nu}_{max}$, cm^{-1}): 3424 (br, ν, OH+ NH overlapped), 1651 (vs, ν, C=O (amide I)), 1544 (m, δ_{ip}, CNH (amide II)), 1490 (m, ν, N–CSS), 1438 (vs, ν, C=C phenyl), 1100 (m, ν $_{q\text{-vib}}$, P–Ph_3), 1056 (vs, ν, C–OH + C^1–O–CH_3), 1001/914 (m, ν, S=C–S), 752 (w, δ_{oop}, C–H phenyl), 710/694 (w, ν $_{r\text{-vib}}$, P–Ph_3), 578 (w, ν, C–S), 539/509/500 (m, δ $_{y\text{-vib}}$, P–Ph_3), 427 (w, ν $_{t\text{ vib}}$, P–Ph_3), 380 (w, ν, Au–S). ^1H NMR (400 MHz, DMSO-d_6, 298 K, δ, ppm): 7.81 (d, J_{HH} = 5.7 Hz, 1H, N*H*), 7.60-7.50 (m, 15H, C*H* $_{arom}$), 5.00 (d, J_{HH} = 5.5 Hz, 1H, C^4O*H*), 4.85 (m, 2H, $C^{2',6'}H_{eq}$), 4.73 (d, J_{HH} = 6.0 Hz, 1H, C^3O*H*), 4.54 (dd, J_{HH} = 6.0 Hz, 1H, C^6O*H*), 4.53 (d, J_{HH} = 3.1 Hz, 1H, C^1*H*), 3.68-3.62 (m, 2H, C^2*H* + C^6*H*), 3.49-3.42 (m, 2H, C^3*H* + C^6*H*'), 3.33-

3.26 (m, 3H, C^5H + $C^{2',6'}H_{ax}$), 3.24 (s, 3H, OCH_3), 3.13-3.09 (m, 1H, C^4H), 2.59-2.53 (m, 1H, $C^{4'}H$), 1.84-1.74 (m, 2H, $C^{3',5'}H_{eq}$), 1.67-1.55 (m, 2H, $C^{3',5'}H_{ax}$). $^{13}C\{^1H\}$ NMR (100 MHz, DMSO-d_6, 298 K, δ, ppm): 202.18 (NCSS), 173.88 (C=O), 133.67 (d, J_{PC} = 14.3 Hz, $C_{arom\ ortho}$), 131.86 (d, J_{PC} = 2.0 Hz, $C_{arom\ para}$), 129.79 (d overlapped, $C_{arom\ ipso}$), 129.48 (d, J_{PC} = 11.3 Hz, $C_{arom\ meta}$), 97.86 (C^1), 72.80 (C^5), 70.79 (C^3), 70.67 (C^4), 60.83 (C^6), 54.46 (OCH_3), 53.76 (C^2) 50.81 ($C^{2',6'}H_2$), 40.42 ($C^{4'}H_2$), 28.44 ($C^{3',5'}H_2$). $^{31}P\{^1H\}$ NMR (162 MHz, DMSO-d_6, 298 K, δ, ppm): 36.46 ($AuPPh_3$). UV-Vis (DMSO, 298 K, nm (ε, M^{-1} cm^{-1})): 270 (29700), ~293 (sh, ~12300), ~310 (sh, ~8400).

[Au(dtc-Inp-GlcN3)(PPh_3)] (Au25)

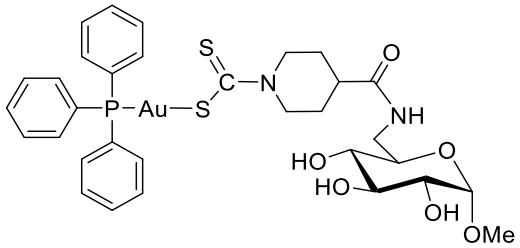

A DMF solution (2 mL) of [Zn(dtc-Inp-GlcN3)$_2$] (67.0 mg, 0.08 mmol) was added dropwise under stirring to a DMF solution (2 mL) of [AuCl(PPh_3)] (80.4 mg, 0.16 mmol) at r.t., and the mixture was stirred for 1 h. Upon addition of diethyl ether (40 mL), the solution turned cloudy and a white solid residue formed. The precipitate was centrifuged and the bulk of supernatant discarded. The sticky residue was subsequently triturated with diethyl ether (3×10 mL) and dichloromethane (3×10 mL), and then dried under vacuum P_2O_5, yielding the title compound as a light yellow solid (95.2 mg, 70% yield). M.p. 162-166°C (dec.). Anal. (%) calcd. for $C_{32}H_{38}AuN_2O_6PS_2$ (MM = 838.72 g mol^{-1}): C, 45.83; H, 4.57; N, 3.34; found: C, 45.96; H, 4.56; N, 3.39. FT-IR (CsI disk, $\tilde{\nu}_{max}$, cm^{-1}): 3429 (br, ν, OH+ NH overlapped), 1654 (s, ν, C=O (amide I)), 1544 (m, δ_{ip}, CNH (amide II)), 1483 (m, ν, N–CSS), 1437 (s, ν, C=C phenyl), 1101 (m, ν $_{q\text{-vib}}$, P–Ph_3), 1051 (vs, ν, C–OH + C^1–O–CH_3), 1000/914 (m, ν, S=C–S), 750 (m, δ_{oop}, C–H phenyl), 711/694 (m, ν $_{r\text{-vib}}$, P–Ph_3), 577 (w, ν, C–S), 539/510/500 (m, δ $_{y\text{-vib}}$, P–Ph_3), 437 (w, ν $_{t\ vib}$, P–Ph_3), 397 (w, ν, Au–S). ^1H NMR (400 MHz, DMSO-d_6, 298 K, δ, ppm): 7.98 (dd, J_{HH} = 5.7 Hz, 1H, N*H*), 7.62-7.55 (m, 15H, CH_{arom}), 4.98 (d, J_{HH} = 5.4 Hz, 1H, C^4OH), 4.89 (m, J_{HH} = 12.5 Hz, 2H, $C^{2',6'}H_{eq}$), 4.82 (d, J_{HH} = 4.6 Hz, 1H, C^3OH), 4.76 (d, J_{HH} = 6.5 Hz, 1H, C^2OH), 4.51 (d, J_{HH} = 3.7 Hz, 1H, C^1H), 3.55 (ddd, J_{HH} = 13.6 Hz, 5.7 Hz, 2.2 Hz, 1H, C^6H), 3.38-3.33 (m, 2H, C^3H + C^5H), 3.24 (s, 3H, OCH_3), 3.24-3.17 (m, 3H, C^2H + $C^{2',6'}H_{ax}$), 3.01 (m, 1H, C^6H'), 2.93-2.89 (m, 1H, C^4H), 2.55 (m, 1H, $C^{4'}H$), 1.79-1.75 (m, 2H,

$C^{3',5'}H_{eq}$), 1.65-1.56 (m, 2H, $C^{3',5'}H_{ax}$). $^{13}C\{^1H\}$ NMR (100 MHz, DMSO-d_6, 298 K, δ, ppm): 203.57 (N*C*SS), 173.85 (*C*=O), 133.66 (d, J_{PC} = 15.7 Hz, $C_{arom\ ortho}$), 131.86 (d, J_{PC} = 2.0 Hz, $C_{arom\ para}$), 129.79 (d overlapped, $C_{arom\ ipso}$), 129.48 (d, J_{PC} = 11.3 Hz, $C_{arom\ meta}$), 99.64 (C^1), 72.96 (C^3), 72.10 (C^4), 71.97 (C^2), 70.31 (C^5), 54.29 (O*C*H$_3$), 51.16 ($C^{2',6'}H_2$), 40.54 ($C^{4'}H_2$), 40.09 (C^6), 28.48 ($C^{3',5'}H_2$). $^{31}P\{^1H\}$ NMR (162 MHz, DMSO-d_6, 298 K, δ, ppm): 36.47 (Au*P*Ph$_3$). UV-Vis (DMSO, 298 K, nm (ε, M^{-1} cm^{-1})): 272 (19400), ~293 (sh, ~9300), ~313 (sh, ~5000).

8.6 Chapter 6 – Experimental

[Mn(CO)$_4$(dtc-Inp-NH$_2$)] (Mn1)

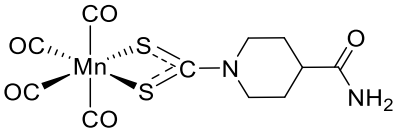

A methanol solution (2 mL) of Na(dtc-Inp-NH$_2$)·CH$_3$OH (77.9 mg, 0.30 mmol) was added dropwise under stirring to a methanol solution (10 mL) of [MnBr(CO)$_5$] (82.4 mg, 0.30 mmol), and the mixture was stirred at 40°C under inert atmosphere (N$_2$) and in the dark for 2 h. The solution darkened after some minutes, then it gradually turned yellow. The solution was evaporated to dryness, affording a red oily residue. The residue was subsequently triturated with diethyl ether (20 mL), affording a yellow solid. The solid was filtered, the bulk of supernatant discarded, then the solid was redissolved in acetone. The obtained solution was filtered to remove unsoluble NaBr salts, and the filtered solution was evaporated to dryness. The residue was subsequently triturated with diethyl ether (20 mL). The bulk of supernatant was discarded, and the resulting yellow solid was dried with a gentle stream of N$_2$ and then under vacuum with P_2O_5, yielding the title complex as an ochre yellow/light brown powder (71.1 mg, 64% yield). M.p. 164-168°C (dec.). FT-IR (CsI disk, $\tilde{\nu}_{max}$, cm^{-1}): 3441/3190 (br, $\nu_{a/s}$, NH$_2$), 2084/2030/2009/1923/1906 (vs, ν, C≡O), 1662 (vs, ν, C=O (amide I)), 1611 (m, δ_{ip}, CNH (amide II)), 1517 (s, ν, N–CSS), 1017 (m, ν_a, SCS), 671/628 (m, δ, Mn–CO), 521 (w, ν_s, SCS), 361 (w, ν_a, SMnS). ^1H NMR (400 MHz, DMSO-d_6, 298 K, δ, ppm): 7.32 (br, 1H, N*H* $_{cis}$), 6.84 (br, 1H, N*H* $_{trans}$), 4.60 (br, 2H, $C^{2',6'}H_{eq}$), 3.31 (br, 2H, $C^{2',6'}H_{ax}$), 1.83 (br, 2H, $C^{3',5'}H_{eq}$), 1.41 (br, 2H, $C^{3',5'}H_{ax}$). $C^{4'}H$ not detected due to overlap with solvent signal at *ca*. 2.50 ppm. $^{13}C\{^1H\}$ NMR (100 MHz, CD$_3$OD, 298 K, δ, ppm): 217.75/212.57 (C≡O), 207.17 (N*C*SS), 193.93 (*C*=O), 46.56 ($C^{4'}H_2$), 29.24 ($C^{3',5'}H_2$). $C^{2',6'}H_2$ not detected due to overlap with solvent signal at *ca*. 49.00 ppm. UV-Vis (DMSO, 298 K, nm (ε, M^{-1} cm^{-1})):

265 (10800), ~310 (sh, ~4800), ~385 (br, ~1300).

[Mn(CO)$_4$(dtc-Inp-GlcN1)] (Mn2)

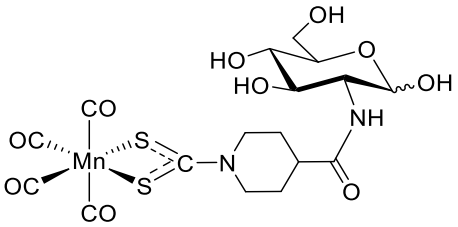

A dry DMF solution (2 mL) of **Zn3** (120.0 mg, 0.15 mmol) was added dropwise under stirring to a 1:2 dry DMF/acetone solution (3 mL) of [MnBr(CO)$_5$] (83.0 mg, 0.30 mmol), and the mixture was stirred at r.t. and in the dark for 4.5 h. Afterwards, the yellow solution was concentrated under reduced pressure to remove acetone. Then, the mixture was treated with a 1:1 Et$_2$O/*n*-hexane solution (80 mL), leading to the sudden precipitation of a yellow solid. The mixture was stored at -20°C for 1 h, centrifuged and the bulk of supernatant discarded. The residue was subsequently triturated with diethyl ether (3×10 mL) and dichloromethane (3×10 mL), and then dried under vacuum P_2O_5, yielding the title compound as a light yellow powder (142.0 mg, 89% yield). M.p. 154-157°C (dec.). FT-IR (CsI disk, $\tilde{\nu}_{max}$, cm^{-1}): 3375 (br, ν, OH+ NH overlapped), 2084/2031/2011/1926 (vs, ν, C≡O), 1647 (vs, ν, C=O (amide I)), 1546 (m, δ_{ip}, CNH (amide II)), 1496 (m, ν, N–CSS), 1060/1028 (br, ν, C–OH + ν_a, SCS overlapped), 670/629 (m, δ, Mn–CO), 520 (w, ν_s, SCS), 378 (w, ν_a, SMnS). ^{1}H NMR (400 MHz, DMSO-d$_6$, 298 K, *δ*, ppm): 7.69 (br, 0.25H, N*H* $_\beta$), 7.65 (br, 1H, N*H* $_\alpha$), 6.44 (br, 0.25H, C^{1}O*H* $_\beta$), 6.38 (br, 1H, C^{1}O*H* $_\alpha$), 4.88-4.38 (m, 7.5H, C^1*H* $_{\alpha+\beta}$ + CO*H* + C$^{2',6'}$*H* $_{eq\ \alpha+\beta}$), 3.56-3.03 (m, 10H, C^2*H* $_{\alpha+\beta}$ + C^3*H* $_{\alpha+\beta}$ + C^4*H* $_{\alpha+\beta}$ + C^5*H* $_{\alpha+\beta}$ + C^6*H* $_{\alpha+\beta}$ + C^6*H*' $_{\alpha+\beta}$ + C$^{2',6'}$*H* $_{ax\ \alpha+\beta}$), 2.61 (br m, 1H, C$^{4'}$*H* $_\alpha$), 2.35 (br m, 1H, C$^{4'}$*H* $_\beta$), 1.88-1.76 (br m, 2.5H, C$^{3',5'}$*H* $_{eq\ \alpha+\beta}$), 1.60-1.40 (br m, 2.5H, C$^{3',5'}$*H* $_{ax\ \alpha+\beta}$). ^{13}C{^{1}H} NMR (100 MHz, CD$_3$OD, 298 K, *δ*, ppm, only α anomer): 217.54/212.26 (C≡O), 206.81 (N*C*SS), 173.89 (*C*=O), 92.18 (*C*^{1}), 72.80-72.25 (*C*^{3} + *C*^{4} + *C*^{5}), 62.57 (*C*^{6}), 55.37 (*C*^{2}), 46.33 (*C*$^{4'}$H), 29.07 (*C*$^{3',5'}$H$_2$). *C*$^{2',6'}$H$_2$ not detected due to overlap with solvent signal at *ca*. 49.00 ppm. No differentiation of the ^{1}H and ^{13}C signals of the isonipecotic and carbonyl moieties due to the presence of both α and β anomers could be detected. Solution α:β anomers ratio ≈ 4:1 (based on the ^{1}H NMR spectrum). UV-Vis (DMSO, 298 K, nm (ε, M^{-1} cm^{-1})): 265 (10500), ~310 (sh, ~3500), ~385 (br, ~800).

[Mn(CO)$_4$(dtc-Inp-GlcN2)] (Mn3)

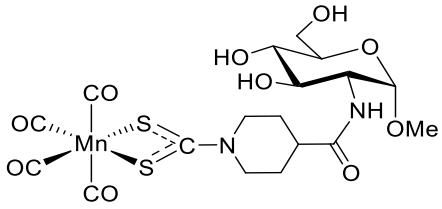

A dry DMF solution (2 mL) of **Zn4** (83.2 mg, 0.10 mmol) was added dropwise under stirring to a 1:2 dry DMF/acetone solution (3 mL) of [MnBr(CO)$_5$] (55.5 mg, 0.20 mmol), and the mixture was stirred at r.t. and in the dark for 4.5 h. Afterwards, the yellow solution was concentrated under reduced pressure to remove acetone. Then, the mixture was treated with a 1:1 Et$_2$O/*n*-hexane solution (80 mL), leading to the sudden precipitation of a yellow solid. The mixture was stored at -20°C for 1 h, centrifuged and the bulk of supernatant discarded. The residue was subsequently triturated with diethyl ether (3×10 mL) and dichloromethane (3×10 mL), and then dried under vacuum P_2O_5, yielding the title compound as an ochre yellow powder. M.p. 176-180°C (dec.). FT-IR (CsI disk, $\tilde{\nu}_{max}$, cm^{-1}): 3420 (br, ν, OH+ NH overlapped), 2084/2031/2010/1924 (vs, ν, C≡O), 1654 (vs, ν, C=O (amide I)), 1538/1516 (m, δ_{ip}, CNH (amide II) + ν, N–CSS overlapped), 1056/1034 (br, ν, C–OH + ν_a, SCS overlapped), 672/629 (m, δ, Mn–CO), 529 (w, ν_s, SCS), 379 (w, ν_a, SMnS). ^{1}H NMR (400 MHz, DMSO-d$_6$, 298 K, *δ*, ppm): 7.79 (br, 1H, N*H*), 4.97-4.50 (br m, 6H, C^1*H* + CO*H* + C$^{2',6'}$*H* $_{eq}$), 3.62-3.10 (br m, 8H, C^2*H*+ C^3*H* + C^4*H* + C^5*H* + C^6*H* + C^6*H*' + C$^{2',6'}$*H* $_{ax}$), 3.22 (br s, 3H, OC*H*$_3$), 2.61 (br, 1H, C$^{4'}$*H*), 1.87-1.75 (br m, 2H, C$^{3',5'}$*H*), 1.58-1.39 (br m, 2H, C$^{3',5'}$*H* $_{ax}$). ^{13}C{^{1}H} NMR (100 MHz, DMSO-d$_6$, 298 K, *δ*, ppm): 202.91 (N*C*SS), 173.40 (*C*=O), 97.54 (*C*^{1}), 72.47 (*C*^{5}), 70.47 (*C*^{3}), 70.36 (*C*^{4}), 62.57 (*C*^{6}), 55.37 (*C*^{2}), 46.33 (*C*$^{4'}$H), 29.07 (*C*$^{3',5'}$H$_2$). *C*≡O signals not detected; *C*$^{4'}$H not detected due to overlap with solvent signal at *ca*. 40.00 ppm. UV-Vis (DMSO, 298 K, nm (ε, M^{-1} cm^{-1})): 261 (8400), ~311 (sh, ~2400), ~385 (br, ~700).

8.7 Chapter 7 – Experimental

(PPh$_4$)[PtCl$_3$(NH$_3$)]

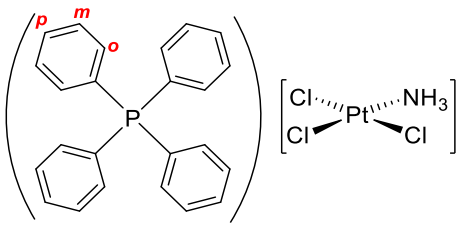

$(PPh_4)[PtCl_3(NH_3)]$ was synthesized according to a literature procedure.[19] $(Et_4N)Cl{\cdot}xH_2O$ (220.0 mg, 1.33 mmol) was added under stirring at r.t. to an *N*,*N*-dimethylacetamide (25 mL) solution of cisplatin (338.0 mg, 1.13 mmol). The reaction mixture was kept under inert atmosphere by bubbling N_2 into the solution and stirred at 100°C for 6 h, after which the colour of the solution turned from yellow to orange and the volume reduced to ~20 mL (***note***: prolonged heating above 105°C results in extensive decomposition of the reaction mixture). The mixture was then cooled down to r.t. and treated with a 1:1 ethyl acetate/*n*-hexane solution (300 mL). The resulting cloudy reaction mixture was stored at -10°C overnight, leading to the formation of a thick orange oil. The bulk of clear colourless supernatant was discarded, the orange oil dissolved in water (10 mL), and the remaining insoluble residue (*i.e.* unreacted cisplatin) was filtered off and discarded. The resulting clear orange solution was then treated with $(PPh_4)Cl$ (475.0 mg, 1.27 mmol), stirred at room temperature for 1 h and stored at 4°C overnight, leading to the formation of a light orange solid. The precipitate was filtered off, washed with cold water (2×10 mL), and then dried under vacuum over P_2O_5, yielding the title compound as a pale yellow solid (389.0 mg, 52%). Anal. (%) calcd. for $C_{24}H_{23}Cl_3NPPt$ (MM = 657.86 g mol^{-1}): C, 43.82; H, 3.52; N, 2.16; found: C, 44.02; H, 3.48; N, 2.16. FT-IR (CsI disk, $\tilde{\nu}_{max}$, cm^{-1}): 3250 (ν_a, NH_3), 3173 (ν_s, NH_3), 1638 (δ_a, NH_3), 1291 (δ_s, NH_3), 1108 ($\nu_{q\text{-vib}}$, P–Ph_4), 780 (ρ, NH_3), 721 ($\nu_{r\text{-vib}}$, P–Ph_4), 527 ($\delta_{y\text{-vib}}$, P–Ph_4 + ν, Pt–N overlapped), 456/437 ($\nu_{t\text{-vib}}$, P–Ph_4), 337/327 ($\nu_{a/s}$, $PtCl_3$), 260 ($\delta_{x\text{-vib}}$, P–Ph_4). ^{1}H NMR (400 MHz, DMSO-d_6, 298 K, δ, ppm): 7.97 (m, 4H, C*H* arom *para*), 7.84-7.79 (m, 8H, C*H* arom *meta*), 7.77-7.71 (m, 8H, C*H* arom *ortho*), 3.97 (br, 3H, N*H*$_3$). ^{13}C{^{1}H} NMR (100 MHz, DMSO-d_6, 298 K, δ, ppm): 135.36 (d, J_{PC} = 2.7 Hz, $C_{arom\ para}$), 134.58 (d, J_{PC} = 10.6 Hz, $C_{arom\ ortho}$), 130.47 (d, J_{PC} = 13.3 Hz, $C_{arom\ meta}$), 117.70 (d, J_{PC} = 89.3, $C_{arom\ ipso}$), ^{31}P{^{1}H} NMR (162 MHz, DMSO-d_6, 298 K, δ, ppm): 23.5 (PPh_4^+). The main IR bands, ^{1}H, ^{13}C and ^{31}P NMR peaks are in agreement with literature data.[19–21]

[Pt(dtc-Inp-GlcN2)$_2$] (Pt1)

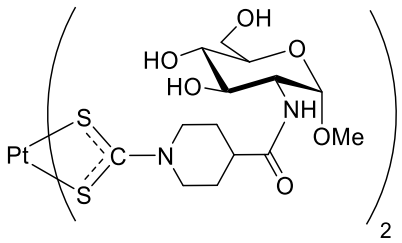

A DMF solution (2 mL) of [Zn(dtc-Inp-GlcN2)$_2$] (15.2 mg, 0.02 mmol) was added dropwise under stirring to a DMF solution (2 mL) of (PPh_4)[$PtCl_3(NH_3)$] (24.4 mg, 0.04 mmol) at room temperature. The mixture was stirred for 16 h and then treated with diethyl ether (40 mL). The resulting cloudy solution was stored at 4°C for 1 h, leading to the formation of a yellow precipitate. The precipitate was centrifuged and the bulk of supernatant discarded. The residue was subsequently washed with a 1:1 methanol/dichloromethane solution (3×10 mL), and then dried under vacuum over P_2O_5, yielding the title compound as a yellow solid (12.2 mg, 35%). M.p. 195-198°C (dec.). Anal. (%) calcd. for $C_{28}H_{46}N_4O_{12}PtS_4$ (MM = 954.02 g mol^{-1}): C, 35.25; H, 4.86; N, 5.87; found: C, 35.14; H, 4.95; N, 5.81. FT-IR (CsI disk, $\tilde{\nu}_{max}$, cm^{-1}): 3401/3314 (br, ν, OH + NH overlapped), 1650 (m, ν, C=O (amide I)), 1523 (vs, ν, N–CSS + δ_{ip}, CNH (amide II) overlapped), 1055 (vs, ν, C–OH + C^1–O–CH_3 overlapped), 1005 (m, ν_a, SCS), 576 (w, ν_s, SCS), 365 (w, ν_a, PtS_4). ^{1}H NMR (400 MHz, DMSO-d_6, 298 K, *δ*, ppm): 7.84 (d, J_{HH} = 7.7 Hz, 2H, N*H*), 5.01 (d, J_{HH} = 5.7 Hz, 2H, C^4O*H*), 4.73 (d, J_{HH} = 5.7 Hz, 2H, C^3O*H*), 4.53 (m, 4H, C^1*H* + C^6O*H*), 4.18 (m, J_{HH} = 13.3 Hz, 4H, $C^{2',6'}H_{eq}$), 3.67-3.62 (m, 4H, C^2*H* + C^6*H*), 3.49-3.42 (m, 4H, C^6*H*' + C^3*H*), 3.33-3.24 (m, 6H, C^5*H* + $C^{2',6'}H_{ax}$), 3.24 (s, 6H, OC*H*$_3$), 3.15-3.09 (m, 2H, C^4*H*), 2.64 (m, 2H, $C^{4'}$*H*), 1.90-1.83 (m, 4H, $C^{3',5'}H_{eq}$), 1.60-1.51 (m, 4H, $C^{3',5'}H_{ax}$). ^{13}C{^{1}H} NMR (100 MHz, DMSO-d_6, 298 K, *δ*, ppm): 207.19 (N*C*SS), 173.39 (*C*=O), 97.83 (C^1), 72.80 (C^5), 70.77 (C^3), 70.66 (C^4), 60.81 (C^6), 54.43 (O*C*H$_3$), 53.75 (C^2), 46.11 ($C^{2',6'}H_2$), 40.44 ($C^{4'}H_2$), 27.95 ($C^{3',5'}H_2$). No NMR signals assignable to the β anomer were detected. UV-Vis (DMF, nm (ε, M^{-1} cm^{-1})): 270 (17400), 276 (16800), 323 (sh, ~8500).

[Pt(dtc-Inp-GlcN3)$_2$] (Pt2)

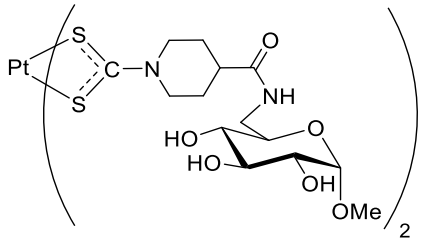

Method A: a DMF solution (2 mL) of [Zn(dtc-Inp-GlcN3)$_2$] (34.8 mg, 0.04 mmol) was added dropwise under stirring to a DMF solution (2 mL) of (PPh_4)[$PtCl_3(NH_3)$] (55.6 mg, 0.08 mmol) at room temperature. The mixture was stirred for 16 h and then treated with diethyl ether (40 mL). The resulting cloudy solution was stored at 4°C for 1 h, leading to the formation of an oily yellow residue. The residue was centrifuged and the bulk of

supernatant discarded. The oily residue was subsequently triturated with dichloromethane (10 mL) to obtain a yellow solid which was filtered off, washed with dichloromethane (3×10 mL), and then dried under vacuum over P_2O_5, yielding the title compound as a yellow solid (40.0 mg, 49%).

Method B: a methanol suspension (5 mL) of [Zn(dtc-Inp-GlcN3)$_2$] (21.7 mg, 0.026 mmol) was added dropwise under stirring to a methanol solution (5 mL) of (PPh_4)[$PtCl_3(NH_3)$] (34.7 mg, 0.053 mmol). The mixture was stirred for 16 h, after which a yellow solid precipitated. The solid was centrifuged and the bulk of supernatant discarded. The solid was subsequently washed with dichloromethane (3×10 mL), and then dried under vacuum over P_2O_5, yielding the title compound as a yellow solid (25.7 mg, 49%). M.p. 217-220 °C (dec.). Anal. (%) calcd. for $C_{28}H_{46}N_4O_{12}PtS_4$ (MW = 954.02 g mol^{-1}): C, 35.25; H, 4.86; N, 5.87; found: C, 35.04; H, 5.06; N, 5.84. FT-IR (CsI disk, $\tilde{\nu}_{max}$, cm^{-1}): 3392/3324 (br, ν, OH + NH overlapped), 1647 (s, ν, C=O (amide I)), 1553 (m, ν, N–CSS + δ_{ip}, CNH (amide II) overlapped), 1048 (vs, ν, C–OH + C^1–O–CH_3 overlapped), 1007 (m, ν_a, SCS), 566 (w, ν_s, SCS), 349 (w, ν_a, PtS_4). ^{1}H NMR (400 MHz, DMSO-d_6, 298 K, δ, ppm): 7.99 (dd, J_{HH} = 5.2 Hz, 2H, N*H*), 4.98 (d, J_{HH} = 5.5 Hz, 2H, C^4O*H*), 4.83 (d, J_{HH} = 4.7 Hz, 2H, C^3O*H*), 4.76 (d, J_{HH} = 5.9 Hz, 2H, C^2O*H*), 4.51 (d, J_{HH} = 3.3 Hz, 2H, C^1*H*), 4.18 (m, J_{HH} = 12.7 Hz, 4H, $C^{2',6'}H_{eq}$), 3.55 (m, 2H, C^6*H*), 3.37-3.34 (m, 4H, $C^3H + C^5H$), 3.24 (s, 6H, OCH_3), 3.24-3.19 (m, 6H, $C^2H + C^{2',6'}H_{ax}$), 3.05-2.95 (m, 2H, C^6H'), 2.90 (m, 2H, C^4*H*), 2.60 (m, 2H, $C^{4'}H$), 1.86-1.83 (m, 4H, $C^{3',5'}H_{eq}$), 1.57-1.52 (m, 4H, $C^{3',5'}H_{ax}$). ^{13}C{^{1}H} NMR (100 MHz, DMSO-d_6, 298 K, δ, ppm): 207.20 (N*C*SS), 173.28 (*C*=O), 99.64 (C^1), 72.96 (C^3), 72.09 (C^4), 71.95 (C^2), 70.29 (C^5), 54.30 (OCH_3), 46.09 ($C^{2',6'}H_2$), 40.61 ($C^{4'}H_2$), 40.10 (C^6), 27.97 ($C^{3',5'}H_2$). UV-Vis (DMF, nm (ε, M^{-1} cm^{-1})): 270 (15600), 277 (sh, ~14000), 349 (6800).

8.8 Miscellaneous

Docking studies with GLUT1

Molecular docking was performed by the software AutoDock Vina 1.1.2.[22] The Protein Data Bank file PDB ID: 4PYP was used as model of the human glucose transporter GLUT1. The geometries of compounds **Au3**, **Au5** and [$AuBr_2$(dtc-Sar-OEt)] (AUL12**)**, were fully optimized by DFT calculations implemented in the Gaussian09 program package,[23] using the B3LYP functional,[24–26] the Lanl2dz pseudopotential basis set for gold,[27] and the 6-31G* basis set for the other atoms.[28,29] The Autodock Tools 1.5.6 software was used to add and merge non-polar hydrogens to the receptors and to assign

the rotatable bonds to the ligands.[30] Grid size for 4PYP was set to 20Å × 30Å × 24Å points with grid spacing of 1.0 Å and a grid center of 586.801, -25.349 and 207.404. Exhaustiveness was set to 20. Figures were rendered using Chimera software.[31]

Cell culture

HT-29 (colon carcinoma), MDA-MB-231 (breast adenocarcinoma), MCF7 (breast adenocarcinoma) and U2OS (osteosarcoma) cells were maintained in Dulbecco's modified Eagle medium (4.5 g L^{-1} D-glucose, L-glutamine, pyruvate), which was supplemented with gentamycin (50 mg L^{-1}) and fetal bovine serum superior, standardized (Biochrom GmbH) (10% v/v), and were passaged once a week. HeLa (human cervix adenocarcinoma) cells were grown in Nutrient Mixture F-12 [HAM] (Sigma Chemical Co.); A2780 (human ovarian carcinoma cells) and A2780cis (human ovarian carcinoma cisplatin-resistant cells) were grown in RPMI 1640 (Sigma Chemical Co.), which was supplemented with $NaHCO_3$ (1.5g L^{-1}), heat-inactivated fetal calf serum (Invitrogen) (10% v/v), penicillin (100 U/mL), streptomycin (100 mg L^{-1}), and amphotericin B (Sigma Chemical Co.) (0.25 mg L^{-1}). The cells were incubated at 37°C in a moist atmosphere of 5% carbon dioxide in air.

RC-124 healthy human kidney cells were maintained in McCoy's 5A (modified, with L-glutamine) medium which was supplemented with gentamycin (50 mg L^{-1}) and fetal bovine serum superior, standardized (Biochrom GmbH, Berlin) (10% v/v), and were also passaged once a week. For experiments with RC-124 cells, microtiter plates had been pretreated in the following way: 30 µL of a sterilized gelatine solution (1.5% w/v) were added to each well of flat bottom 96-well plates, the plates were covered with their lids and incubated for 1 h at 37 °C, the excess solution was removed, the wells were washed with PBS pH 7.4, and the new cell-culture medium was added.

Antiproliferative assay in tumorigenic (HT-29, MDA-MB-231, MCF7) and non-tumorigenic (RC124) cells

The antiproliferative effects were determined according to a recently used method with minor modifications.[1,32] Briefly, 100 mL of HT-29 cells (2500 cells mL^{-1}), MDA-MB-231 cells (4000 cells mL^{-1}), MCF7 cells (4800 cells mL^{-1}), or RC-124 cells (1400 cells mL^{-1}) were transferred into 96-well plates (note: for RC-124, pretreated plates were used, see above) and incubated at 37°C under 5% CO_2 for 72 h (MCF7, MDA-MB-231, RC-124) or 48 h (HT-29). Stock solutions of the compounds in *N*,*N*-dimethylformamide

(DMF) were freshly prepared and diluted with the respective cell culture medium to graded concentrations (final concentration of DMF: 0.1% v/v). After 72 h (HT-29) or 96 h (MCF7, MDA-MB-231, RC-124) of exposure, the cell biomass was determined by crystal violet staining, and the IC_{50} value was determined as the concentration that caused 50% inhibition of cell proliferation compared to an untreated control. Results were calculated as the mean values of three independent experiments.

Cell proliferation studies in U2OS cells

1 mL of U2OS cells (10000 cells mL^{-1}) were transferred into 24-well plates and incubated at 37°C under 5% CO_2 for 24 h. Stock solutions of the compounds in dimethyl sulfoxide (DMSO) were freshly prepared and diluted with the respective cell culture medium to graded concentrations (final concentration of DMSO: 0.1% v/v). After 72 h (compounds **Au2-8**) or 48 h (compounds **Au10-15**) of exposure, a resazurin (compounds **Au2-8**) or crystal violet (compounds **Au10-14**) assay was performed to determine cell viability.

For cytotoxicity assays using the GLUT1 inhibitor 4,6-*O*-ethylidene-α-D-glucose (EDG), U2OS cells (10000 cells in 1000 µL medium/well) were seeded on a 24 well-plate in 1000 µL DMEM. After incubation at 37°C for 24 h, the medium was replaced with fresh medium (1000 µL medium/well) containing EDG and solutions of the compounds in DMSO (final concentration of DMSO: 0.1% v/v), diluted with medium to the desired concentration (final concentration 75 mM EDG, 15 µM **Au11** and 50 µM **Au12-14**). The cell viability was evaluated after 24 h by using the crystal violet assay

Cell proliferation studies in HeLa, A2780, A2780cis cells

Cells (5×10^4) were seeded into each well of a 24-well cell culture plate. After incubation for 24 h, various concentrations of the test agents were added to the complete medium and incubated for a further 48 h. Stock solutions of new complexes were made in dimethylsulfoxide at 20 mM concentration and then diluted with complete medium in such a way that the final amount of solvent in each well did not exceed 0.5%. Cisplatin was dissolved in 0.9% NaCl. A Trypan blue assay was performed to determine cell viability.

Cell uptake studies in MCF-7 cells

The cellular metal uptake was determined according to previously described methods.[33,34] Two different cell culture media were used. Dulbecco's modified Eagle medium as described above and Dulbecco's modified Eagle medium (L-glutamine), which was also supplemented with gentamycin (50 mg L^{-1}) and fetal bovine serum superior, standardized (Biochrom GmbH, Berlin) (10% v/v).

In short: MCF-7 human breast carcinoma cells were grown until at least 75–80% confluency in 175 cm^2 cell-culture flasks. Stock solutions of the compounds and cytochalasin B in DMF were freshly prepared and diluted with the relevant cell-culture medium to a final concentration of 10.0 μM and for cytochalasin B 50.0 μM immediately before use (final DMF concentration: 0.1% v/v). The cell culture medium of the flasks was replaced with the medium that contained the metal compound (10 mL) and the flasks were incubated at 37 °C/5% CO_2 up to 6 h. After the desired incubation period the uptake was stopped by removing the cell culture medium. The cells were washed with PBS (10 mL), the washing solution was removed, and the cells were isolated in PBS (10mL) with a scratcher by centrifugation (5 min, 3500 rpm). The obtained cell pellets were stored at −20 °C for further use. For metal and protein quantification the pellets were resuspended in demineralized water (200 μL) and lysed for 30 min by ultra-sonication.

AAS measurements

For the gold measurements a contrAA 700 high resolution continuum-source atomic absorption spectrometer (Analytik Jena AG) was used. Pure samples of the respective complexes were used as standards and calibration was performed in a matrix-matched manner (meaning that all samples and standards were adjusted to the same protein concentration by dilution with distilled water). Triton-X 100 (1%, 10 μL) as well as ascorbic acid (1%, 10 μL) were added to each standard sample (100 μL). Samples were injected (25 μL) into coated standard graphite tubes (Analytik Jena AG) and thermally processed as previously described in more detail.[33] Gold was quantified at a wavelength of 242.79 nm. The mean integrated absorbance of triple injections was used throughout the studies. The final results of gold concentrations were calculated from the data obtained in two independent experiments and are expressed as nmol of metal per mg of cellular protein and as cellular molar concentration [mM].

Measurement of lipophilicity (Log$D_{7.4}$)

The *n*-octanol-water partition coefficients (Log*D*) of compounds **Au10-15** were determined with the shake-flask method.[35,36] PBS buffered milliQ water (100 mL, pH 7.4) and analytical grade *n*-octanol (100 mL) were mutually saturated and mechanically shaken for 72 h (Stuart rotator drive STR4). A solution of the complex in *n*-octanol-saturated PBS was prepared at a concentration of 25 μM by diluition of a stock solution 5 mM of the complex in DMSO (final content of DMSO in solution 0.5% v/v). 5 mL of this stock solution was added to 5 mL of PBS-saturated *n*-octanol and mechanically shaken for 1 h. The biphasic solution was centrifuged at 3000 rpm for 5 min to allow separation of the phases.

For complex [Au(Bnpy)(dtc-Inp-OEt)]PF_6 (**Au15**), the absorbance of the solution of the complex in *n*-octanol before and after partitioning was measured by means of UV-Vis spectrophotometry at 265 nm, while for the other complexes the absorbance of the solution of the complex in PBS before and after partitioning was measured at 261 nm. Measurements were carried out in triplicate for each complex. For complex [Au(Bnpy)(dtc-Inp-OEt)]PF_6 (**Au10**), Log$D_{7.4}$ was calculated using the following equation, modified by taking into account the different employed volumes:[37]

$$\mathrm{Log}D = \log\frac{C_{oct}}{C_w} \cong \log\left(\frac{A_{oct}}{A_w}\cdot\frac{V_w}{V_{oct}}\right) = \log\left(\frac{A_{oct}}{A_0 - A_{oct}}\cdot\frac{V_w}{V_{oct}}\right)$$

Where A_{oct} is the absorbance of the octanolic solution after partitioning, A_0 is the absorbance of the stock solution, and V_w and V_{oct} are, respectively, the volumes of water and *n*-octanol. When same volumes are employed, the equation simplifies as:

$$\mathrm{Log}D = \log\left(\frac{A_{oct}}{A_0 - A_{oct}}\right)$$

For the other complexes, Log$D_{7.4}$ was calculated using the following formula:

$$\mathrm{Log}D = \log\frac{C_{oct}}{C_w} \cong \log\left(\frac{A_{oct}}{A_w}\right) = \log\left(\frac{A_0 - A_w}{A_w}\right)$$

β-glucosidase activity assay

The activity of β-glucosidase on the C1-β glycosylated conjugate **Au15** was assessed by means of ^{1}H NMR spectroscopy following a modified reported protocol.[38]

Compound **Au15** (5.0 mg) was dissolved in buffer acetate pH 5 in deuterium oxide (D_2O, 1 mL) (prepared by mixing 714 μL sodium acetate 0.1 M in D_2O with 1286 μL acetic acid 0.1 M in D_2O). This solution of the complex was then split in two different aliquots (500 μL each) and transferred in two different NMR tubes. The two test solutions

contained, respectively, only complex, and complex with enzyme (obtained by adding 50 μL of β-glucosidase 5U/mL in buffer acetate in D_2O). The ^1H NMR spectra were recorded, then the samples were heated in a water bath at 37°C. The samples were taken at different intervals after 1 and 3 h to record the ^1H NMR spectra. After 3 h, more enzyme was added (50 μL), and the spectra recorded again after 5 h the first addition. After 24 h, DMSO-d_6 was added (30 μL) as internal reference and the ^1H NMR spectra recorded again. For comparison, the ^1H NMR spectra of D-glucose in buffer acetate pH 5 in D_2O + DMSO-d_6 (30 μL) was recorded.

CO-release test with myoglobin assay

The release of CO in the Mn(I)-carbonyl complexes **Mn1-3** was measured spectrophotometrically by monitoring the conversion of deoxy-myoglobin (deoxy-Mb) to carboxy-myoglobin (Mb-CO) over the time, according to the procedure reported by Schatzschneider.[39] In a quartz cuvette, a fresh solution of horse skeletal muscle myoglobin (60 μM final concentration) in phosphate buffered saline (PBS, pH = 7.4, 500 μL), previously bubbled with $N_{2\,(g)}$, was diluted with degassed PBS (400 μL). A fresh solution of sodium dithionite (100 mM) in degassed PBS was then added (100 μL) to reach a total volume of 1000 μL and to convert the Mb solution to deoxy-Mb. The UV-Vis spectrum of reduced deoxy-Mb was recorded at 37 °C, and the real concentration of deoxy-Mb was calculated by measuring the absorbance at 560 nm. To the solution of deoxy-Mb, 2 mM stock solution of the CORM in DMSO was added (5 μL) in order to reach a final concentration of CORM of 10 μM. The cuvette was mixed and overlaid with paraffin oil (500 μL) to prevent CO escaping or myoglobin being oxygenated. UV-Vis spectra at different times were recorded at 37 °C. All measurements were carried out in triplicate. The UV-Vis spectra were processed with Origin 8.0 and then data were plotted with Graphpad Prism software. The correction method proposed by Atkin for the UV-Vis spectra was applied to intersect all the spectra at the isosbestic point at 510 nm.[40] The concentration of Mb-CO was calculated by measuring the absorbance at 540 nm and applying the equation reported by Schatzschneider.[41]

8.9 References

[1] R. Rubbiani, I. Kitanovic, H. Alborzinia, S. Can, A. Kitanovic, L. A. Onambele, M. Stefanopoulou, Y. Geldmacher, W. S. Sheldrick, G. Wolber, A. Prokop, S. Wölfl, I. Ott, *J. Med. Chem.* **2010**, *53*, 8608–8618.
[2] H. M. J. Wang, C. Y. L. Chen, I. J. B. Lin, *Organometallics* **1999**, *18*, 1216–1223.
[3] G. M. Sheldrick, *Acta Cryst A*, **2015**, *71*, 3–8.
[4] G. M. Sheldrick, *Acta Cryst C*, **2015**, *71*, 3–8.

[5] P. McArdle, *J. Appl. Cryst.* **2017**, *50*, 320–326.

[6] O. V. Dolomanov, L. J. Bourhis, R. J. Gildea, J. A. K. Howard, H. Puschmann, *J. Appl. Cryst.* **2009**, *42*, 339–341.

[7] F. Gao, X. Yan, T. Shakya, O. M. Baettig, S. Ait-Mohand-Brunet, A. M. Berghuis, G. D. Wright, K. Auclair, *J. Med. Chem.* **2006**, *49*, 5273–5281.

[8] G. E. Whitworth, M. S. Macauley, K. A. Stubbs, R. J. Dennis, E. J. Taylor, G. J. Davies, I. R. Greig, D. J. Vocadlo, *J. Am. Chem. Soc.* **2007**, *129*, 635–644.

[9] X. Hu, W. Zhang, I. Carmichael, A. S. Serianni, *J. Am. Chem. Soc.* **2010**, *132*, 4641–4652.

[10] A. Blaskó, C. A. Bunton, S. Bunel, C. Ibarra, E. Moraga, *Carbohydr. Res.* **1997**, *298*, 163–172.

[11] L. Wiebe, J. Diakur, **2007**, US20070021380A1.

[12] T. Muhizi, S. Grelier, V. Coma, *J. Agric. Food Chem.* **2009**, *57*, 8770–8775.

[13] M. L. Di Gioia, A. Gagliardi, A. Leggio, V. Leotta, E. Romio, A. Liguori, *RSC Adv.* **2015**, *5*, 63407–63420.

[14] R. Šardzík, G. T. Noble, M. J. Weissenborn, A. Martin, S. J. Webb, S. L. Flitsch, *Beilstein J. Org. Chem.* **2010**, *6*, 699–703.

[15] S. Hanessian, M. Tremblay, A. Kornienko, N. Moitessier, *Tetrahedron*, **2001**, *57*, 3255–3265.

[16] J. Lecina, A. Carrer, A. Álvarez-Larena, U. Mazzi, L. Melendez-Alafort, J. Suades, *Organometallics*, **2012**, *31*, 5884–5893.

[17] B. Bertrand, S. Spreckelmeyer, E. Bodio, F. Cocco, M. Picquet, P. Richard, P. Le Gendre, C. Orvig, M. A. Cinellu, A. Casini, *Dalton Trans.* **2015**, *44*, 11911–11918.

[18] A. P. Shaw, M. Tilset, R. H. Heyn, S. Jakobsen, *J. Coord. Chem.* **2011**, *64*, 38–47.

[19] M. J. Abrams, C. M. Giandomenico, J. F. Vollano, D. A. Schwartz, *Inorg. Chim. Acta*, **1987**, *131*, 3–4.

[20] G. B. Deacon, R. A. Jones, P. E. Rogasch, *Aust. J. Chem.* **1963**, *16*, 360–370.

[21] D. Weber, S. H. Hausner, A. Eisengräber-Pabst, S. Yun, J. A. Krause-Bauer, H. Zimmer, *Inorg. Chim. Acta*, **2004**, *357*, 125–134.

[22] O. Trott, A. J. Olson, *J. Comput. Chem.* **2010**, *31*, 455–461.

[23] M. J. Frisch, G. W. Trucks, H. B. Schlegel, G. E. Scuseria, M. A. Robb, J. R. Cheeseman, G. Scalmani, V. Barone, B. Mennucci, G. A. Petersson, H. Nakatsuji, M. Caricato, X. Li, H. P. Hratchian, A. F. Izmaylov, J. Bloino, G. Zheng, J. L. Sonnenberg, M. Hada, M. Ehara, K. Toyota, R. Fukuda, J. Hasegawa, M. Ishida, T. Nakajima, Y. Honda, O. Kitao, H. Nakai, T. Vreven, J. A. Montgomery Jr., J. E. Peralta, F. Ogliaro, M. Bearpark, J. J. Heyd, E. Brothers, K. N. Kudin, V. N. Staroverov, R. Kobayashi, J. Normand, K. Raghavachari, A. Rendell, J. C. Burant, S. S. Iyengar, J. Tomasi, M. Cossi, N. Rega, J. M. Millam, M. Klene, J. E. Knox, J. B. Cross, V. Bakken, C. Adamo, J. Jaramillo, R. Gomperts, R. E. Stratmann, O. Yazyev, A. J. Austin, R. Cammi, C. Pomelli, J. W. Ochterski, R. L. Martin, K. Morokuma, V. G. Zakrzewski, G. A. Voth, P. Salvador, J. J. Dannenberg, S. Dapprich, A. D. Daniels, Ö. Farkas, J. B. Foresman, J. V Ortiz, J. Cioslowski, D. J. Fox, Gaussian 09, Gaussian, Inc., Wallingford CT, **2009**.

[24] A. D. Becke, *J. Chem. Phys.* **1993**, *98*, 5648–5652.

[25] C. Lee, W. Yang, R. G. Parr, *Phys. Rev. B*, **1988**, *37*, 785–789.

[26] P. J. Stephens, F. J. Devlin, C. F. Chabalowski, M. J. Frisch, *J. Phys. Chem.* **1994**, *98*, 11623–11627.

[27] P. J. Hay, W. R. Wadt, *J. Chem. Phys.* **1985**, *82*, 270–283.

[28] P. C. Hariharan, J. A. Pople, *Theoret. Chim. Acta*, **1973**, *28*, 213–222.

[29] M. M. Francl, W. J. Pietro, W. J. Hehre, J. S. Binkley, M. S. Gordon, D. J. DeFrees, J. A. Pople, *J. Chem. Phys.* **1982**, *77*, 3654–3665.

[30] G. M. Morris, R. Huey, W. Lindstrom, M. F. Sanner, R. K. Belew, D. S. Goodsell, A. J. Olson, *J. Comput. Chem.* **2009**, *30*, 2785–2791.

[31] E. F. Pettersen, T. D. Goddard, C. C. Huang, G. S. Couch, D. M. Greenblatt, E. C. Meng, T. E. Ferrin, *J. Comput. Chem.* **2004**, *25*, 1605–1612.

[32] R. Rubbiani, L. Salassa, A. de Almeida, A. Casini, I. Ott, *ChemMedChem*, **2014**, *9*, 1205–1210.

[33] C. Schmidt, B. Karge, R. Misgeld, A. Prokop, R. Franke, M. Brönstrup, I. Ott, *Chem. Eur. J.* **2017**, *23*, 1869–1880.

[34] H. Scheffler, Y. You, I. Ott, *Polyhedron*, **2010**, *29*, 66–69.

[35] *OECD Guidelines for the Testing of Chemicals, Test No. 107: Partition Coefficient (n-Octanol/Water): Shake Flask Method*, Organization for Economic Cooperation and Development, Paris, **1995**.

[36] A. Andrés, M. Rosés, C. Ràfols, E. Bosch, S. Espinosa, V. Segarra, J. M. Huerta, *Eur. J. Pharm. Sci.* **2015**, *76*, 181–191.

[37] I. V. Tetko, H. P. Varbanov, M. Galanski, M. Talmaciu, J. A. Platts, M. Ravera, E. Gabano, *J. Inorg. Biochem.* **2016**, *156*, 1–13.

[38] G. R. Periyannan, B. A. Lawrence, A. E. Egan, *J. Chem. Educ.* **2015**, *92*, 1244–1249.

[39] S. Pai, M. Hafftlang, G. Atongo, C. Nagel, J. Niesel, S. Botov, H.-G. Schmalz, B. Yard, U. Schatzschneider, *Dalton Trans.* **2014**, *43*, 8664–8678.
[40] A. J. Atkin, J. M. Lynam, B. E. Moulton, P. Sawle, R. Motterlini, N. M. Boyle, M. T. Pryce, I. J. S. Fairlamb, *Dalton Trans.* **2011**, *40*, 5755–5761.
[41] C. Bischof, T. Joshi, A. Dimri, L. Spiccia, U. Schatzschneider, *Inorg. Chem.* **2013**, *52*, 9297–9308.

Appendix. Crystal structure information

Crystal structure of (PPh_4)(dtc-Sar-OEt)

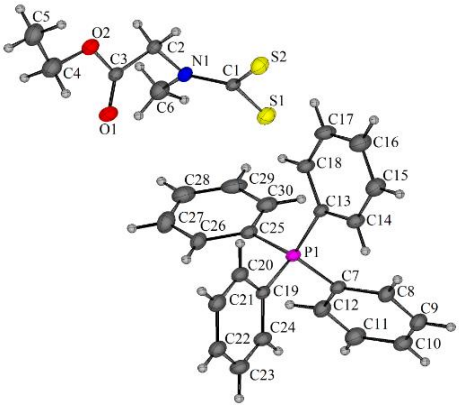

Crystal data and structure refinement.

Identification code	ap_1	
Empirical formula	C30 H30 N O2 P S2	
Formula weight	531.64	
Temperature	297.0(1) K	
Wavelength	0.71073 Å	
Crystal system	Triclinic	
Space group	P-1	
Unit cell dimensions	a = 10.1305(6) Å	a= 83.631(4)°.
	b = 11.0650(5) Å	b= 71.711(5)°.
	c = 13.6416(6) Å	g = 74.528(5)°.
Volume	1398.67(13) $Å^3$	
Z	2	
Density (calculated)	1.262 Mg/m^3	
Absorption coefficient	0.275 mm^{-1}	
F(000)	560	
Crystal size	0.50 x 0.40 x 0.35 mm^3	
Theta range for data collection	3.441 to 29.185°.	
Index ranges	-13<=h<=12, -14<=k<=13, -17<=l<=18	
Reflections collected	11765	
Independent reflections	6352 [R(int) = 0.0223]	
Completeness to theta = 25.242°	99.7 %	
Absorption correction	Semi-empirical from equivalents	
Max. and min. transmission	1.00000 and 0.94941	
Refinement method	Full-matrix least-squares on F^2	
Data / restraints / parameters	6352 / 0 / 327	
Goodness-of-fit on F^2	1.016	
Final R indices [I>2sigma(I)]	R1 = 0.0500, wR2 = 0.1223	
R indices (all data)	R1 = 0.0796, wR2 = 0.1439	
Extinction coefficient	n/a	
Largest diff. peak and hole	0.495 and -0.346 e.$Å^{-3}$	

Crystal structure of Na(dtc-Inp-NH_2)·CH_3OH (CCDC 1835869)

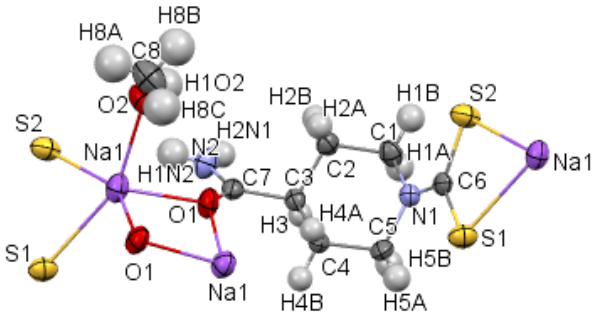

Na^+ coordination sphere

Crystal data and structure refinement.

Identification code	and_1	
Empirical formula	C8 H15 N2 Na O2 S2	
Formula weight	258.33	
Temperature	300.0(1) K	
Wavelength	0.71073 Å	
Crystal system	Monoclinic	
Space group	I2/a	
Unit cell dimensions	a = 15.2035(17) Å	α= 90°
	b = 11.0876(11) Å	β= 111.081(13)°
	c = 15.0618(15) Å	γ = 90°
Volume	2369.0(5) $Å^3$	
Z	8	
Density (calculated)	1.449 Mg/m^3	
Absorption coefficient	0.468 mm^{-1}	
F(000)	1088	
Crystal size	0.50 x 0.30 x 0.20 mm^3	
Theta range for data collection	3.675 to 29.001°	
Index ranges	-16<=h<=20, -11<=k<=14, -19<=l<=11	
Reflections collected	5411	
Independent reflections	2706 [R(int) = 0.0280]	
Completeness to theta = 25.242°	99.6 %	
Absorption correction	Semi-empirical from equivalents	
Max. and min. transmission	1.00000 and 0.66852	
Refinement method	Full-matrix least-squares on F^2	
Data / restraints / parameters	2706 / 0 / 149	
Goodness-of-fit on F^2	1.037	
Final R indices [I>2sigma(I)]	R1 = 0.0500, wR2 = 0.0873	
R indices (all data)	R1 = 0.0840, wR2 = 0.1005	
Extinction coefficient	n/a	
Largest diff. peak and hole	0.378 and -0.236 $e.Å^{-3}$	

Crystal structure of [Zn(dtc-Inp-OEt)$_2$] (Zn1) (CCDC 1835870)

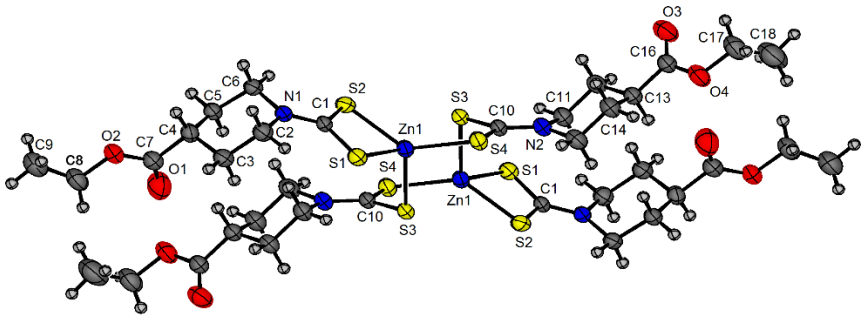

Crystal data and structure refinement.

Identification code	ap226	
Empirical formula	C18 H28 N2 O4 S4 Zn	
Formula weight	530.03	
Temperature	299.0(2) K	
Wavelength	0.71073 Å	
Crystal system	Triclinic	
Space group	P-1	
Unit cell dimensions	a = 9.4775(7) Å	α= 81.181(6)°
	b = 10.8781(8) Å	β= 72.125(6)°
	c = 12.1158(9) Å	γ = 81.757(6)°
Volume	1168.58(16) Å^3	
Z	2	
Density (calculated)	1.506 Mg/m^3	
Absorption coefficient	1.435 mm^{-1}	
F(000)	552	
Crystal size	0.50 x 0.40 x 0.20 mm^3	
Theta range for data collection	3.558 to 29.223°.	
Index ranges	-12<=h<=11, -14<=k<=14, -16<=l<=15	
Reflections collected	9243	
Independent reflections	5332 [R(int) = 0.0363]	
Completeness to theta = 25.242°	99.7 %	
Absorption correction	Semi-empirical from equivalents	
Max. and min. transmission	1.00000 and 0.87706	
Refinement method	Full-matrix least-squares on F^2	
Data / restraints / parameters	5332 / 0 / 264	
Goodness-of-fit on F^2	0.857	
Final R indices [I>2sigma(I)]	R1 = 0.0470, wR2 = 0.0984	
R indices (all data)	R1 = 0.0950, wR2 = 0.1211	
Extinction coefficient	n/a	
Largest diff. peak and hole	0.537 and -0.307 e.Å^{-3}	

Crystal structure of [AuBr$_2$(dtc-Inp-OEt)] (Au1) (CCDC 1835871)

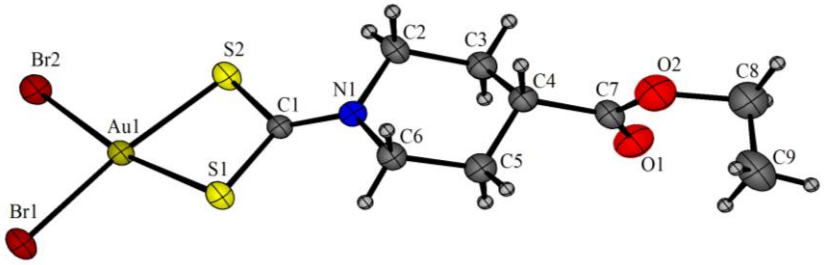

Crystal data and structure refinement.

Identification code	ap228	
Empirical formula	C9 H14 Au Br2 N O2 S2	
Formula weight	589.12	
Temperature	298.0(1) K	
Wavelength	0.71073 Å	
Crystal system	Monoclinic	
Space group	$P2_1/c$	
Unit cell dimensions	a = 8.0665(4) Å	α= 90°
	b = 16.5901(11) Å	β= 102.529(5)°
	c = 11.7403(6) Å	γ = 90°
Volume	1533.72(15) Å^3	
Z	4	
Density (calculated)	2.551 Mg/m^3	
Absorption coefficient	15.064 mm^{-1}	
F(000)	1088	
Crystal size	0.50 x 0.40 x 0.20 mm^3	
Theta range for data collection	3.555 to 25.350°.	
Index ranges	-9<=h<=9, -19<=k<=11, -14<=l<=14	
Reflections collected	6113	
Independent reflections	2814 [R(int) = 0.0306]	
Completeness to theta = 25.242°	99.8 %	
Absorption correction	Semi-empirical from equivalents	
Max. and min. transmission	1.00000 and 0.30787	
Refinement method	Full-matrix least-squares on F^2	
Data / restraints / parameters	2814 / 0 / 155	
Goodness-of-fit on F^2	1.059	
Final R indices [I>2sigma(I)]	R1 = 0.0392, wR2 = 0.0669	
R indices (all data)	R1 = 0.0667, wR2 = 0.0777	
Extinction coefficient	n/a	
Largest diff. peak and hole	0.816 and -0.908 e.Å^{-3}	

Crystal structure of [Au(Bnpy)(dtc-Inp-OEt)]PF_6 (Au10)

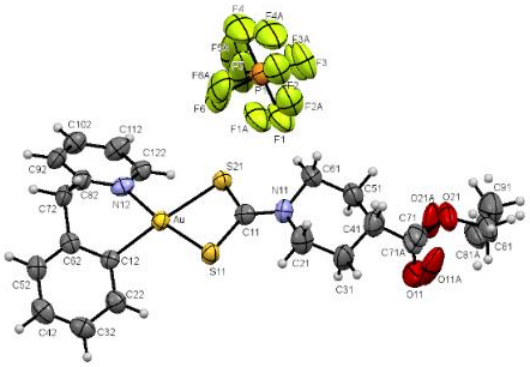

Crystal data and structure refinement.

Identification code	ap295ronc_0m
Empirical formula	$C_{21}H_{24}AuF_6N_2O_2PS_2$
Formula weight	742.48
Temperature/K	199.98
Crystal system	monoclinic
Space group	$P2_1/c$
a/Å	10.6007(5)
b/Å	23.2714(10)
c/Å	11.2065(5)
α/°	90
β/°	115.9010(10)
γ/°	90
Volume/$Å^3$	2486.87(19)
Z	4
$\rho_{calc}g/cm^3$	1.983
μ/mm^{-1}	6.216
F(000)	1440.0
Crystal size/mm^3	0.16 × 0.14 × 0.06
Radiation	MoKα (λ = 0.71073)
2Θ range for data collection/°	4.616 to 51.428
Index ranges	-12 ≤ h ≤ 12, -28 ≤ k ≤ 28, -13 ≤ l ≤ 13
Reflections collected	34990
Independent reflections	4714 [R_{int} = 0.0589, R_{sigma} = 0.0349]
Data/restraints/parameters	4714/46/360
Goodness-of-fit on F^2	1.062
Final R indexes [I>=2σ (I)]	R_1 = 0.0429, wR_2 = 0.1036
Final R indexes [all data]	R_1 = 0.0641, wR_2 = 0.1190
Largest diff. peak/hole / e $Å^{-3}$	2.23/-1.54

Crystal structure of [Au(Bnpy)(dtc-Inp-NH_2)]PF_6 (Au11)

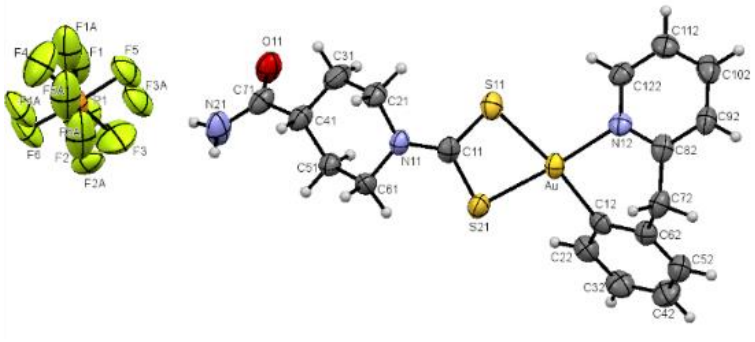

Crystal data and structure refinement.

Identification code	ap307dmronc_0m
Empirical formula	$C_{19}H_{21}AuF_6N_3OPS_2$
Formula weight	713.44
Temperature/K	200.0
Crystal system	monoclinic
Space group	$P2_1/c$
a/Å	14.5240(4)
b/Å	8.7052(2)
c/Å	19.7955(6)
α/°	90
β/°	109.3320(10)
γ/°	90
Volume/$Å^3$	2361.71(11)
Z	4
$\rho_{calc}g/cm^3$	2.007
μ/mm^{-1}	6.539
F(000)	1376.0
Crystal size/mm^3	0.21 × 0.2 × 0.16
Radiation	MoKα (λ = 0.71073)
2Θ range for data collection/°	5.946 to 52.784
Index ranges	$-18 \leq h \leq 18$, $-10 \leq k \leq 10$, $-24 \leq l \leq 24$
Reflections collected	27625
Independent reflections	4813 [R_{int} = 0.0403, R_{sigma} = 0.0285]
Data/restraints/parameters	4813/12/329
Goodness-of-fit on F^2	1.046
Final R indexes [I>=2σ (I)]	R_1 = 0.0304, wR_2 = 0.0662
Final R indexes [all data]	R_1 = 0.0401, wR_2 = 0.0721
Largest diff. peak/hole / e $Å^{-3}$	1.33/-1.26

Crystal structure of [Au(BImEt$_2$)(dtc-Sar-OEt)] (Au16)

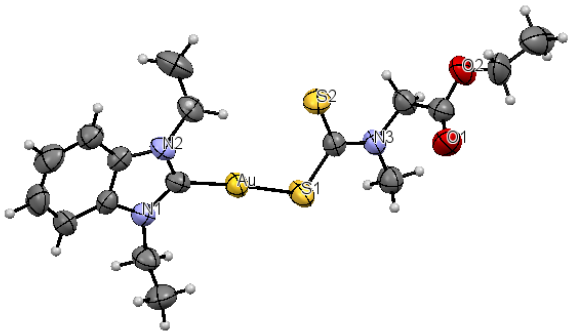

Crystal data and structure refinement.

Identification code	shelx	
Empirical formula	C17 H24 Au N3 O2 S2	
Formula weight	563.48	
Temperature	293(2) K	
Wavelength	0.71073 Å	
Crystal system	Monoclinic	
Space group	P n	
Unit cell dimensions	a = 4.971(3) Å	α= 90°
	b = 11.096(8) Å	β= 90.727(10)°
	c = 18.762(10) Å	γ = 90°
Volume	1034.8(11) Å^3	
Z	2	
Density (calculated)	1.808 Mg/m^3	
Absorption coefficient	7.325 mm^{-1}	
F(000)	548	
Crystal size	0.32 x 0.14 x 0.13 mm^3	
Theta range for data collection	1.835 to 26.572°.	
Index ranges	-6<=h<=6, -13<=k<=13, -23<=l<=23	
Reflections collected	12120	
Independent reflections	4289 [R(int) = 0.0487]	
Completeness to theta = 25.242°	100.0 %	
Absorption correction	Semi-empirical from equivalents	
Max. and min. transmission	0.754 and 0.422	
Refinement method	Full-matrix least-squares on F^2	
Data / restraints / parameters	4289 / 60 / 256	
Goodness-of-fit on F^2	0.997	
Final R indices [I>2sigma(I)]	R1 = 0.0358, wR2 = 0.0656	
R indices (all data)	R1 = 0.0472, wR2 = 0.0697	
Absolute structure parameter	0.020(10)	
Extinction coefficient	n/a	
Largest diff. peak and hole	0.902 and -0.461 e.Å^{-3}	

Crystal structure of [Au(BImEt$_2$)(dtc-Inp-NH$_2$)] (Au17)

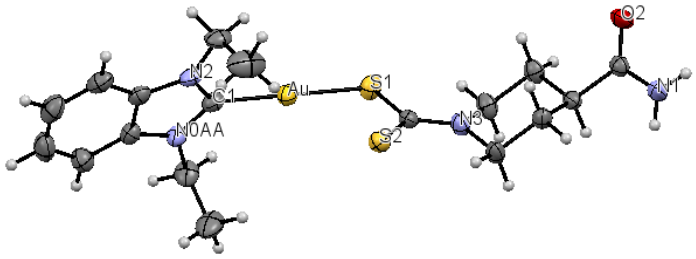

Crystal data and structure refinement.

Identification code	mo_AP270_0m
Empirical formula	$C_{18}H_{25}AuN_4OS_2$
Formula weight	574.51
Temperature/K	200
Crystal system	monoclinic
Space group	$P2_1/n$
a/Å	16.3371(5)
b/Å	7.3801(2)
c/Å	17.3336(5)
α/°	90
β/°	97.1320(10)
γ/°	90
Volume/Å^3	2073.73(10)
Z	4
ρ_{calc}g/cm^3	1.840
μ/mm^{-1}	7.310
F(000)	1120.0
Crystal size/mm^3	0.22 × 0.12 × 0.04
Radiation	MoKα (λ = 0.71073)
2Θ range for data collection/°	6.008 to 52.064
Index ranges	$-20 \leq h \leq 20$, $-9 \leq k \leq 9$, $-21 \leq l \leq 20$
Reflections collected	25889
Independent reflections	4050 [R_{int} = 0.0360, R_{sigma} = 0.0229]
Data/restraints/parameters	4050/0/237
Goodness-of-fit on F^2	1.014
Final R indexes [I>=2σ (I)]	R_1 = 0.0175, wR_2 = 0.0593
Final R indexes [all data]	R_1 = 0.0242, wR_2 = 0.0825
Largest diff. peak/hole / e Å^{-3}	1.35/-1.61

Crystal structure of [Au(PPh$_3$)(dtc-Inp-NH$_2$)] (Au22)

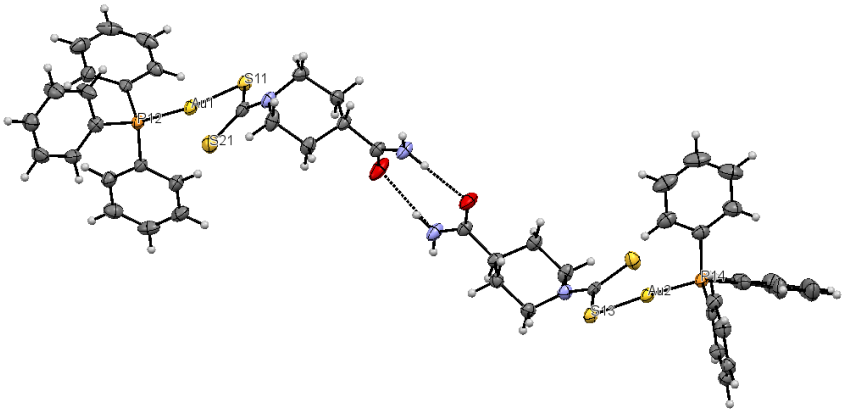

Crystal data and structure refinement.

Identification code	ap320dmronc_0m
Empirical formula	$C_{25}H_{26}AuN_2OPS_2$
Formula weight	662.53
Temperature/K	200.01
Crystal system	monoclinic
Space group	$P2_1$
a/Å	9.8812(3)
b/Å	16.9091(4)
c/Å	15.5657(5)
α/°	90
β/°	107.2230(10)
γ/°	90
Volume/Å^3	2484.13(13)
Z	4
ρ_{calc}g/cm^3	1.772
μ/mm^{-1}	6.175
F(000)	1296.0
Crystal size/mm^3	0.22 × 0.18 × 0.18
Radiation	MoKα (λ = 0.71073)
2Θ range for data collection/°	5.544 to 54.38
Index ranges	-12 ≤ h ≤ 12, -21 ≤ k ≤ 21, -19 ≤ l ≤ 19
Reflections collected	81310
Independent reflections	10854 [R_{int} = 0.0381, R_{sigma} = 0.0315]
Data/restraints/parameters	10854/1/577
Goodness-of-fit on F^2	1.027
Final R indexes [I>=2σ (I)]	R_1 = 0.0177, wR_2 = 0.0407
Final R indexes [all data]	R_1 = 0.0189, wR_2 = 0.0413
Largest diff. peak/hole / e Å^{-3}	0.83/-1.18
Flack parameter	0.016(2)

Acknowledgements

This manuscript is the product of ideas and work of a lot of different people, whose contribution to its realization is priceless. What I can really do at first instance is to give them my sincere and greatest acknowledgements.

First I would like to thank my supervisor, Dr. Luca Ronconi, for its guidance and support all over this four years. Coming in Ireland has been a great challenge and it's thanks to you if I succeeded to "survive" during my first days here.

This research work has been also done owing to the collaboration of a lot of great people, without their passion, time and dedication nothing would have been possible. Therefore, I need to thank Seamus Collier and Dr. Roisin Doohan for the NMR assistance (I know, Seamus, I won't piss you off with my requests, but I'll also miss you for your jokes about the Italians) and all the NUIG technical staff: I really appreciated your constant help. Thanks to Prof. Ingo Ott and Jessica for the genuine collaboration we established, Prof. Pat McArdle and Dr. Luciano Marchiò for the X-ray crystallography (even if most of times crystals were useless, sorry for that), Dr. Diego Montagner for the elemental analysis, Dr. Alessio Terenzi for the computational studies, Prof. Olivier Thomas and Hiren for mass spec analysis, Prof. Lisa Dalla Via and Aida García and her whole group for the biological studies, Prof. Ullrich Schatzschneider, Dr. Fabio Cucinotta, Prof. Jessica Rouge and her group, Dr. Nicolas Barry, Prof. Dani Gibson, Dr. Emanuele Petruzzella and Prof. Viktor Brabec.

A special thank goes to Prof. Corrado Santocanale from the Biomedical Science Building, where I could spend a short period to carry out some cell studies. In particular, I have to thank Oliviano and Veronica for their patience and time they dedicated assisting me.

I'd like to thank my colleagues, Eirini, Iannis and Roberta, not just labmates but true friends, and also Niccolò, Francesco and Adele. Hope to get a proper Italy *vs*. Greece kitchen contest soon!

Thanks also to my family, my parents, my brother and my grandmother Maria. I know that now we are far but still close with the thoughts. Thanks also to my friends in Italy, Jacopo, Peo, Bius, Nice and Francesco to make this distance from Ireland not so big.

Last, but not the least, I have to say a great THANK YOU to the person who supported and gave me strength, motivation and inspiration to strive during this path. Thank you very much, Sara.